

EFFECT OF MECHANICAL VIBRATION ON THE MICROSTRUCTURE AND
THE MECHANICAL PROPERTIES OF 7075 ALUMINUM ALLOY PRODUCED
BY SEMI-SOLID MELTING METHOD

A THESIS SUBMITTED TO
THE GRADUATE SCHOOL OF NATURAL AND APPLIED SCIENCES
OF
MIDDLE EAST TECHNICAL UNIVERSITY

BY

CEMRE METİN POYRAZ

IN PARTIAL FULFILLMENT OF THE REQUIREMENTS
FOR
THE DEGREE OF MASTER OF SCIENCE
IN
METALLURGICAL AND MATERIALS ENGINEERING

AUGUST 2019

Approval of the thesis:

**EFFECT OF MECHANICAL VIBRATION ON THE MICROSTRUCTURE
AND THE MECHANICAL PROPERTIES OF 7075 ALUMINUM ALLOY
PRODUCED BY SEMI-SOLID MELTING METHOD**

submitted by **CEMRE METİN POYRAZ** in partial fulfillment of the requirements
for the degree of **Master of Science in Metallurgical and Materials Engineering**
Department, Middle East Technical University by,

Prof. Dr. Halil Kalıpçılar
Dean, Graduate School of **Natural and Applied Sciences**

Prof. Dr. C. Hakan Gür
Head of Department, **Met. and Mat. Eng.**

Prof. Dr. Ali Kalkanlı
Supervisor, **Met. and Mat. Eng., METU**

Prof. Dr. Ekrem Selçuk
Co-Supervisor, **Met. And Mat. Eng., METU**

Examining Committee Members:

Prof. Dr. C. Hakan Gür
Met. And Mat. Eng., METU

Prof. Dr. Ali Kalkanlı
Met. and Mat. Eng., METU

Prof. Dr. Arcan F. Dericioğlu
Met. And Mat. Eng., METU

Prof. Dr. Özgül Keleş
Met. And Mat. Eng., İstanbul Technical University

Assist. Prof. Dr. M. Bilge İmer
Met. And Mat. Eng., METU

Date: 06.08.2019

I hereby declare that all information in this document has been obtained and presented in accordance with academic rules and ethical conduct. I also declare that, as required by these rules and conduct, I have fully cited and referenced all material and results that are not original to this work.

Name, Surname: Cemre Metin Poyraz

Signature:

ABSTRACT

EFFECT OF MECHANICAL VIBRATION ON THE MICROSTRUCTURE AND THE MECHANICAL PROPERTIES OF 7075 ALUMINUM ALLOY PRODUCED BY SEMI-SOLID MELTING METHOD

Poyraz, Cemre Metin
Master of Science, Metallurgical and Materials Engineering
Supervisor: Prof. Dr. Ali Kalkanlı
Co-Supervisor: Prof. Dr. Ekrem Selçuk

August 2019, 201 pages

This study aims to understand the effect of the semi-solid melting process parameters such as casting temperature and vibration frequency on the mechanical, thermal and microstructural properties. For this purpose, rheocasting of 7075 aluminum alloy with and without B₄C as 7075 matrix composite were carried out at various temperatures in between 620-635°C under different vibration frequencies in the range of 15-35 Hz. For this purpose, rheocasting experiments were carried out successfully. Microstructure, thermal and mechanical properties of both rheocast 7075 alloys and 7075 matrix composites were investigated. Optimum microstructure was achieved as globular grain structure in the plain matrix of rheocast 7075 alloy with average grain size below 40 µm and the same rheocast alloy with B₄C addition yielded finer average grain size of 20 µm. Examination of microstructures of sand and rheocast specimen produced by using squeeze casting unit revealed that the amount of porosity decreased below 1% after conditioning by applying mechanical vibration frequency of 25 at delivery temperature at 635°C SSM temperature then solidification under pressure of 208 MPa. The highest UTS and flexural strength values were obtained as 483 MPa and 1020 MPa, respectively for the plain rheocast 7075 alloy. The highest mechanical property value of flexural strength was in the range of 960-1030 MPa for 10wt. %

7075/B₄C metal matrix composite prepared and hot rolled at 475°C. The highest hardness values of plain 7075 rheocast alloy was measured as 145 HB and the hardness of the same alloy with 10wt.% B₄C addition was measured as 190 HB.

This study revealed that the optimum processing condition for rheocasting of 7075 alloy without and with B₄C addition stands for 635°C SSM temperature and 25 Hz mechanical vibration frequency.

Keywords: High strength aluminum alloys, 7075 series, Aluminum matrix composites, Semi-solid melting method

ÖZ

MEKANİK TİTREŞİMİN, YARI KATI DÖKÜM TEKNİĞİ İLE ÜRETİLEN 7075 ALÜMİNYUM ALAŞIMLARI MİKRO YAPISI VE MEKANİK ÖZELLİKLERİ ÜZERİNDEKİ ETKİSİ

Poyraz, Cemre Metin
Yüksek Lisans, Metalurji ve Malzeme Mühendisliği
Tez Danışmanı: Prof. Dr. Ali Kalkanlı
Ortak Tez Danışmanı: Prof. Dr. Ekrem Selçuk

Ağustos 2019, 201 sayfa

Bu çalışmada yar katı döküm sıcaklığı ve titreşim frekansı gibi değişkenlerin, 7075 alaşımının iç yapısı, ısıl ve mekanik özellikleri üstündeki etkilerinin incelenmesi hedeflenmiştir. Bu hedef doğrultusunda 620-635°C arasında değişen sıcaklıklarda ve 15-35 Hz titreşim frekans aralığında, karıştırımlı döküm yöntemiyle 7075 alaşımı ve bor karbür (B₄C) takviyeli 7075 matris kompozit üretimi gerçekleştirilmiştir. Bu amaçla karıştırımlı döküm deneyleri başarı ile gerçekleştirilmiştir. Dökülen 7075 alaşımları ve 7075 matrisli kompozitlerin iç yapısı, ısıl ve mekanik özellikleri incelenmiştir. En etkin küresel mikro yapı, karıştırımlı döküm ile üretilen 7075 alaşımlarda elde edilmiş ve ortalama tane boyutu 40 µm altında ölçülmüştür. Aynı alaşım B₄C takviye edilerek döküldüğünde ise daha ince taneli bir iç yapı oluşmuş ve ortalama tane boyutu 20 µm olarak ölçülmüştür. Kum kalıba döküm yöntemi ve sıkıştırımlı döküm yöntemiyle üretilen numunelerin iç yapıları incelendiğinde, 25 Hz frekansında titreşim verilen ve 635°C'de 208MPa basınç altında katılaştıran numunelerin gözenek oranının %1 in altına düştüğü görülmüştür. Karıştırımlı dökümle üretilen 7075 alaşımlarında en yüksek çekme mukavemeti 483 MPa ve en yüksek bükülme mukavemeti 1020 MPa olarak bulunmuştur. 475°C' de sıcak haddeden geçmiş 10% B₄C içeren 7075 matrisli kompozitlerin en yüksek bükülme

mukavemetine sahip olduđu ve bu deęerin 960-1030 MPa aralıęında olduđu grlmştr. 7075 alaşımlarının en yksek sertlik deęeri 145 HB, B₄C ieren 7075 matrisli kompozitlerin sertlik deęeri ise 190 HB olarak lmştr.

Bu alıřma, 7075 alařımı ve B₄C takviyeli 7075 matrisli kompozitler iin en uygun karıřtırımlı dkm kořullarının 25 Hz mekanik titreřim frekansı ve 635°C dkm sıcaklıęı olduęunu gstermiřtir.

Anahtar Kelimeler: Yksek mukavemetli alminyum alaşımları, 7075 serisi, Alminyum matris kompozitler, Yarı katı eritme yntemi

To My Family

ACKNOWLEDGEMENTS

First of all, all praise belongs to Allah whose help and guidance allow me to complete my thesis study with determination and strong will.

I would like to express my sincere thanks to my supervisor Prof. Dr. Ali Kalkanlı for his support, guidance, encouragement and insight throughout my master of science education. It was an honor to work with Professor Kalkanlı in the casting which is a core field of metallurgy and I wish to speak out my deepest gratitude to him.

I am also very thankful to Yusuf Yıldırım, Cemal Yanardağ, Süha Tirkeş and most especially Ali Osman Atik, without his technical and mental support I would not have written these quotes and finished my thesis. I hope that I will always be able to work with colleagues that are patient, honest, hardworking and friendly just like Ali Osman Atik.

I would like to share the names of my close friends; Taha Yasin Eken and Şahin Gören who had precious helps in my thesis journey.

The last and the most important special thanks to my family; my beloved wife ‘Ayşenur Poyraz’, my dear mother and father ‘Dilek Poyraz’ and ‘Mehmet Poyraz’, and my brother ‘Emre Poyraz’. I could not have continued within this whole period without my wife’s and family’s support, faith and love.

TABLE OF CONTENTS

ABSTRACT	v
ÖZ	vii
ACKNOWLEDGEMENTS	x
TABLE OF CONTENTS	xi
LIST OF TABLES	xvi
LIST OF FIGURES	xx
CHAPTERS	
1. INTRODUCTION	1
2. BASIC KNOWLEDGE	3
2.1. Semi-Solid Melting (SSM).....	5
2.2. Rheocasting	12
2.2.1. Slurry preparation step.....	16
2.2.2. Forming/shaping step.....	18
2.2.2.1. High pressure die casting (HPDC).....	19
2.2.2.2. Squeeze casting	22
2.3. Aluminum Alloy Selection.....	25
2.3.1. Aluminum alloy series	25
2.3.2. Mechanical and thermal properties of aluminum alloys.....	26
2.3.3. Heat treatment of aluminum alloys.....	33
2.3.3.1. Solutionizing	34
2.3.3.2. Quenching	38
2.3.3.3. Age hardening	39

2.3.4. High strength 7075 aluminum alloy	43
2.3.4.1. Phase transformations and solidification characteristics	44
2.3.4.2. Microstructural evolution and characterization	46
2.3.5. Calculation of solid fraction for SSM process	49
3. LITERATURE REVIEW	51
3.1. Rheocasting of 7075 Alloy	52
3.2. Rheocasting of 7075 Matrix Composite	63
4. AIM OF THE STUDY	67
4.1. Motivation of The Study	67
4.2. Main Contribution to The Literature.....	68
5. EXPERIMENTAL PROCEDURE.....	69
5.1. Rheocasting Experiments.....	71
5.1.1. Sand casting.....	73
5.1.2. Squeeze casting	75
5.1.2.1. Squeeze casting of 7075 alloy	76
5.1.2.2. Squeeze casting of aluminum matrix composite	83
5.1.2.3. Post processing of aluminum matrix composites	85
5.2. Production of Tensile Test Specimens.....	85
5.3. Production of 3-Point Bending Test Specimens	88
5.4. Heat Treatment.....	89
5.5. Characterization Techniques.....	90
5.5.1. Optical emission spectroscopy	91
5.5.2. Thermal analysis.....	92
5.5.3. Metallographic specimen preparation	94

5.5.4. Optical microscopy	96
5.5.5. Scanning electron microscopy	97
5.5.6. X-Ray diffraction	98
5.6. Mechanical Testing	99
5.6.1. Tensile testing	99
5.6.2. Hardness testing	100
5.6.3. 3-Point bending testing	101
6. RESULTS AND DISCUSSIONS	103
6.1. Chemical Analysis Results	103
6.2. Thermal Analysis Results	105
6.2.1. Solidus & liquidus temperature calculation	105
6.2.2. Calculation of solid fraction	109
6.3. Optical Micrographs and Microstructural Analysis	111
6.3.1. Microstructure under optical microscopy	112
6.3.1.1. Sand casting	112
6.3.1.2. Squeeze casting of 7075 alloy	117
6.3.1.3. Squeeze casting of 7075/B ₄ C composites	122
6.3.1.4. Hot rolling of 7075/B ₄ C composites	124
6.3.2. Grain size measurement	127
6.3.2.1. Sand casting	127
6.3.2.2. Squeeze casting of 7075 alloy	130
6.3.2.3. Squeeze casting and hot rolling of 7075/B ₄ C composite	133
6.3.3. Porosity measurement	135
6.3.3.1. Sand casting	135

6.3.3.2. Squeeze casting.....	138
6.4. X-Ray diffraction results.....	141
6.4.1.1. Sand casting	141
6.4.1.2. Squeeze casting of 7075 alloy	142
6.4.1.3. Squeeze casting of 7075/B ₄ C composite	143
6.5. Microstructure Under Scanning Electron Microscopy	144
6.5.1. Sand casting.....	144
6.5.2. Squeeze casting	146
6.5.3. Squeeze casting and hot rolling of 7075/B ₄ C composite	153
6.6. Mechanical Testing	156
6.6.1. Hardness test.....	156
6.6.1.1. Sand casting	156
6.6.1.2. Squeeze casting of 7075 alloy	159
6.6.1.3. Squeeze casting and hot rolling of 7075/B ₄ C composites	162
6.6.2. Tensile Test	164
6.6.2.1. Sand casting	164
6.6.2.2. Squeeze casting.....	167
6.6.3. 3-Point bending test.....	171
6.6.3.1. Squeeze casting of 7075 alloy	171
6.6.3.2. Squeeze casting of 7075/B ₄ C composite	174
6.6.3.3. Hot rolled 7075/B ₄ C composite.....	175
7. CONCLUSIONS.....	179
REFERENCES	181
APPENDICES	187

A. Thermal Analysis	187
B. Microstructures	190
C. Grain Size Measurements	192
D. XRD Results	196
E. Tensile Test Results	198
F. 3- Point Bending Test Results	200

LIST OF TABLES

TABLES

Table 2-1 Different worldwide companies using various rheocasting processes [11]	12
Table 2-2 Typical viscosities of common materials and viscosity range of semi solid slurries [5].....	16
Table 2-3 Classification of wrought aluminum alloys [1].....	26
Table 2-4 Strengthening method and tensile strength of various wrought Al alloys [1]	27
Table 2-5 General temper designations for aluminum alloys.....	28
Table 2-6 Subdivision of strain hardened ‘H’ aluminum alloys [18].....	29
Table 2-7 Subdivision of solution heat treated ‘T’ aluminum alloys [18]	30
Table 2-8 Typical mechanical properties of widely used aerospace aluminum alloys produced by extrusion[19].....	32
Table 2-9 Approximate melting range and temper designation of various aluminum alloys [18].....	32
Table 2-10 Solutionizing and theoretical eutectic temperature of 2xxx series alloys	35
Table 2-11 Typical solution heat treatment temperature of 2xxx, 6xxx and 7xxx series alloys [35].....	36
Table 2-12 Soaking time and maximum quench delay for wrought aluminum alloys [35].....	37
Table 2-13 Typical precipitation heat treatment temperature of 2xxx, 6xxx and 7xxx series alloys.....	42
Table 2-14 Chemical composition of 7075 alloy in wt.% [16]	43
Table 2-15 Various 7xxx series aluminum alloy parts used in aerospace industry [17]	43

Table 2-16 Phase transformations during solidification with different cooling rates [36]	45
Table 3-1 Rheocasting casting temperature and injection pressure information [20]	53
Table 3-2 Tensile test results of as-cast and T6 heat treated 7075 alloy produced by conventional HPDC and rheocasting with different casting temperatures [20].....	55
Table 3-3 Chemical compositions of three commercial wrought aluminum alloys (weight %) [21]	56
Table 3-4 Calculated liquidus, solidus temperatures and deduced rheocasting parameters for three wrought aluminum alloys [21].....	57
Table 3-5 T6 heat treatment parameters for rheocast aluminum alloys [21]	57
Table 3-6 Tensile properties of rheocast and T6 heat treated alloys [21].....	58
Table 3-7 Chemical composition of each batch of grain refined 7075 alloys [42]....	59
Table 3-8 Tensile properties of rheocast 7075 alloys with different grade of grain refinement in T6 condition [42]	60
Table 5-1 Rheocasting experiment parameters information	70
Table 5-2 Specifications of standard tensile test specimen for wrought and cast aluminum alloys [48]	86
Table 5-3 T6 Heat treatment process information for rheocast 7075 alloy tensile specimens and 7075/B ₄ C composite 3-point bending specimens	89
Table 6-1 Spectral analysis results of different type of supplied scrap 7075 alloys	104
Table 6-2 Spectral analysis results of sand cast samples produced under three different vibration frequencies	104
Table 6-3 Spectral analysis results of squeeze cast samples produced under three different vibration frequencies	105
Table 6-4 Calculated solidus and liquidus temperatures of rheocast 7075 alloys produced under three different vibration frequency at four different SSM temperatures	107
Table 6-5 Solid fraction values of 7075 alloy at critical temperatures	111
Table 6-6 Grain size measurements of sand cast 7075 alloys produced under three different vibration frequencies and four different SSM temperatures	128

Table 6-7 Grain size measurements of sand cast and T6-treated 7075 alloys produced under three different vibration frequencies and four different SSM temperatures..	128
Table 6-8 Grain size measurements of squeeze cast 7075 alloys produced under three different vibration frequencies and three different SSM temperatures	131
Table 6-9 Grain size measurements of squeeze cast and T6 treated 7075 alloys produced under three different vibration frequencies and three SSM temperatures	131
Table 6-10 Grain size measurements of T6-treated squeeze cast and hot-rolled 7075/B ₄ C composites with different % B ₄ C addition.....	134
Table 6-11 Porosity measurement results of sand cast 7075 alloys produced under three different vibration frequencies and four different SSM temperatures.....	136
Table 6-12 Porosity results of sand cast and T6-treated 7075 alloys produced under three different vibration frequencies and four different SSM temperatures.....	136
Table 6-13 Porosity results of as-squeeze cast 7075 alloys under three different vibration frequencies and four different SSM temperatures.....	139
Table 6-14 Porosity results of as-squeeze cast and T6 treated 7075 alloys under three different vibration frequencies and four different SSM temperatures.....	139
Table 6-15 Hardness test results of sand cast 7075 alloys produced under three different vibration frequencies and four different SSM temperatures.....	156
Table 6-16 Hardness test results of sand cast and T6-treated 7075 alloys produced under three different vibration frequencies and four different SSM temperatures..	157
Table 6-17 Hardness test results of squeeze cast 7075 alloys produced under three different vibration frequencies and three different SSM temperatures	159
Table 6-18 Hardness test results of squeeze cast and T6-treated 7075 alloys produced under three different vibration frequencies and three different SSM temperatures	159
Table 6-19 Hardness test results of T6-treated squeeze cast and hot rolled 7075/B ₄ C composites with different % B ₄ C addition	162
Table 6-20 Fracture stress values of tensile test results of sand cast as-cast and T6-treated 7075 alloys produced under three different vibration frequencies and four different SSM temperatures	164

Table 6-21 UTS values of tensile test results of squeeze cast and T6-treated 7075 alloys produced under three different vibration frequencies and three different SSM temperatures	167
Table 6-22 Flexural strength values of 3-point bending test results of squeeze cast as-cast and T6-treated 7075 alloys produced under three different vibration frequencies	171
Table 6-23 Flexural strength values of 3-point bending test results of squeeze cast and T6-treated 7075/B ₄ C composites produced 25Hz and 635°C	174
Table 6-24 Flexural strength values of 3-point bending test results of hot-rolled and T6-treated 7075/B ₄ C composites	176

LIST OF FIGURES

FIGURES

Figure 2.1 Dendritic grain structure in solidifying metal castings	3
Figure 2.2 Scheil model of (a) dendritic structure, (b) part of phase diagram, (c) liquid composition vs distance from interface and (d) solid fraction at any distance from interface [3].....	4
Figure 2.3 Different models to calculate solid fraction at a given temperature [4].....	4
Figure 2.4 Representation of mass feeding (left) and inter-dendritic feeding (right) stages [5].....	5
Figure 2.5 Isothermal shear strength of semi-solid Sn-15Pb alloys and simple experimental set-up used in the study [7]	6
Figure 2.6 Radiography of Al-10Cu alloy filled with hot tears [8]	7
Figure 2.7 Transformation of solidifying particles during solidification under shearing (a) initial dendrite (b) dendritic growth (c) rosette (d) grown rosette (e) spherical [5]	8
Figure 2.8 Viscosity and shear stress vs solid fraction graph for Sn-15Pb alloy with a shear rate of 200s^{-1} and cooling rate of 0.006 Ks^{-1} in Spencer's experiments [7].....	8
Figure 2.9 The effect of increasing shear rate/ intensity of turbulence and increasing solidification on the morphology of solidifying nuclei [10].....	9
Figure 2.10 Sn-15wt% Pb alloy continuously cooled with 0.006 Ks^{-1} cooling rate (a) low shear rate and low solid fraction (b) low shear rate and higher solid fraction (c) high shear rate and high solid fraction [7]	10
Figure 2.11 Schematic illustration of comparison of two types of SSM methods [2]	11
Figure 2.12 Rheocast thin walled structural parts in doors AUDI A3 [2].....	13
Figure 2.13 Rear door hinge AUDI A2 produced by rheocasting [2]	13

Figure 2.14 Rear seat cover BMW R 1200 C motor bike (left) and a component for AUDI A6 V8 energy management system for bumpers produced by rheocasting [2]	14
.....	
Figure 2.15 Schematic illustration of gas induced stirring for slurry preparation [12]	15
.....	
Figure 2.16 Schematic illustration of high pressure die casting of gas induced semi-solid slurry [12].....	15
Figure 2.17 Schematic diagram of different stirring techniques used (a) batch rheocaster, (b) continuous, (c) electromagnetic	17
Figure 2.18 Schematic illustration of initial pouring stage, metal filling stage and final solidification stages followed by extraction of solid metal in conventional HPDC [29]	19
.....	
Figure 2.19 Schematic illustration of basic parts of cold chamber HPDC machine [30]	19
.....	
Figure 2.20 Velocity of HPDC piston with respect to the position of plunger or the piston and the real experimental result showing pressure variation during the phases of HPDC [28].....	20
Figure 2.21 Various HPDC aluminum alloy products used in aerospace and automotive industries [32].....	22
Figure 2.22 Schematic illustration of direct and indirect squeeze casting machines [24]	23
.....	
Figure 2.23 Schematic illustration of stages of direct squeeze casting method [24].	23
Figure 2.24 As cast microstructures of LM24 Al-Si alloy produced by.....	24
Figure 2.25 Various squeeze casting products.....	25
Figure 2.26 Schematic temperature vs time graph showing solution	34
Figure 2.27 Cooling curves for 7075-T6 sheets for quenching [35].....	39
Figure 2.28 Aging characteristics of sheet aluminum alloys at various temperatures [35].....	40
Figure 2.29 Tensile strength variation of 6061 alloy sheets during aging at different temperatures [35]	41

Figure 2.30 Liquid fraction of 7075 alloy vs temperature curve estimated by DSC heating curves [41]	46
Figure 2.31 SEM images of Al ₂ Cu precipitates [38].....	47
Figure 2.32 EDX spectrometry results of Al ₂ Cu precipitates in figure 28 [38]	47
Figure 2.33 XRD peaks of squeeze cast and T6 heat treated 7075 alloy [38].....	48
Figure 2.34 TEM images of solution heat treated and multi- directionally forged 7075 alloy artificially aged in the left and naturally aged in the right side [39].....	48
Figure 2.35 TEM images of 7075 alloy (a) as-received (b) T6 treated (c) RRA [40]	48
Figure 2.36 Comparison of polynomial and linear Newtonian and Fourier base lines for Al-7%Si alloy [46]	50
Figure 2.37 Comparison of solid fractions by Fourier and Newtonian methods [46]50	
Figure 3.1 Schematic illustration of ISPC process followed by HPDC [20].....	53
Figure 3.2 As cast microstructure of 7075 alloy produced by; (a) conventional HPDC, (b) ISPC process with 630°C casting temperature and 60 MPa injection pressure, (c) ISPC process with 628°C casting temperature and 60 MPa injection pressure, (d) ISPC process with 626°C casting temperature and 60 MPa injection pressure, (e) ISPC process with 624°C casting temperature and 60 MPa injection pressure, (f) ISPC process with 626°C casting temperature and 90 MPa injection pressure, (g) ISPC process with 626°C casting temperature and 120 MPa injection pressure [20]	54
Figure 3.3 Optical micrographs of 7075 alloy; (a) as-cast F-condition, (b) T6 heat treated, (c) eutectic area in F condition, (d) eutectic area in T6 condition [21]	58
Figure 3.4 Optical micrographs of rheocast 7075 alloys in F-condition with grain refinement value of (a) 0.03% Ti, (b) 0.13% Ti, (c) 0.29% Ti [42]	60
Figure 3.5 SEM micrographs of rheocast samples; (a) as-cast, (b) SHT at 450°C for 1h, (c) SHT at 450°C for 4h, (d) SHT at 450°C for 8h, (e) SHT at 480°C for 1h [43]	61
Figure 3.6 Tensile strength and elongation % of rheocast 7075 alloys in T6-condition with different aging temperatures and times [43].....	62
Figure 3.7 Hardness vs time graph for different aging temperatures [43].....	62

Figure 3.8 Production route of rheocast SiC _p /Al composites [50].....	64
Figure 3.9 Rheocast cylindrical SiC _p /Al composite parts; a) outside surface, b) inside surface [50].....	64
Figure 3.10 Microstructure and XRD result of ultrasonic-assisted rheocast SiC _p /Al composites; a) microstructure b) XRD pattern [50].....	65
Figure 3.11 Microstructure of rheocast SiC _p /Al composite under TEM (left) and SEM (right) [50].....	65
Figure 3.12 Mechanical properties of rheocast 7075 composites with different hydraulic pressure [50].....	66
Figure 3.13 Mechanical properties of rheocast 7075 composites with different SiC vol. % [50].....	66
Figure 5.1 Flow chart showing overall experimental steps	72
Figure 5.2 Whole experimental set-up used in sand-casting experiments consisting of electrical resistance furnace, vibration machine, sand mold and thermocouple recorder	74
Figure 5.3 Transferring of liquid 7075 alloy and casting into the sand mold.....	74
Figure 5.4 Temperature recording during solidification and the application of vibration	75
Figure 5.5 Induction furnace (25 kg steel capacity) where 7075 alloy was prepared.....	76
Figure 5.6 Vibration machine and thermal analysis set-up connected to each other.....	77
Figure 5.7 Detailed technical drawing of the squeeze casting machine and the metal die.....	77
Figure 5.8 Detailed technical drawing of the mechanical vibration machine.....	78
Figure 5.9 Pre-heating of metal mold by torch	79
Figure 5.10 Transferring of liquid 7075 alloy and application of vibration in the ladle	79
Figure 5.11 The application of vibration inside the ladle for conditioning	80
Figure 5.12 Casting of the semi-solid slurry into the die cavity just before pressure application.....	80
Figure 5.13 Early stage of pressure application before upper punch movement.....	81

Figure 5.14 Final stage of pressure application before ejection	81
Figure 5.15 The removal of the rheocast product.....	82
Figure 5.16 Semi-solid squeeze cast 7075 samples at different SSM temperatures .	82
Figure 5.17 Single sample of 7075 alloy produced by squeeze casting	83
Figure 5.18 The stages of 7075/B ₄ C mixture during composite making; a)initial addition of B ₄ C powder after mixing of; b)5 minutes; c) 15 minutes; d)30 minutes	84
Figure 5.19 LAMASAN Twin roller which post-processing was carried out.....	85
Figure 5.20 2-D Technical drawing of tensile test specimen of rheocast products...	87
Figure 5.21 As machined tensile test specimen of squeeze casting experiment	87
Figure 5.22 As machined 7075 alloy 3-point bending test specimen of squeeze casting experiment	88
Figure 5.23 Tensile test specimens' placement in the electrical resistance furnace before solutionizing	90
Figure 5.24 WAS Foundry Master optical emission spectroscopy used for chemical analysis	91
Figure 5.25 K-type cable thermocouple	93
Figure 5.26 K-type thermocouple with metal casing.....	93
Figure 5.27 Thermocouple data logger.....	93
Figure 5.28 METACUT 251 Specimen cutter (right) and the mounting device (left)	94
Figure 5.29 Rotating disc type grinder	95
Figure 5.30 Rotating disc type polisher with 6 μ by 1 μ diamond solutions.....	95
Figure 5.31 HUVITZ optical microscopy and the computer interface.....	96
Figure 5.32 SOIF XJP-6A optical microscopy and DeWinter Material Plus.....	97
Figure 5.33 NOVA NANOSEM 430 Scanning electron microscopy setup.....	98
Figure 5.34 Bruker brand XRD device setup	98
Figure 5.35 Instron Electromechanical Testing Device	100
Figure 5.36 Hardness Machine used.....	100
Figure 5.37 3-Point Bending Test on Instron Electromechanical Testing Device ..	101

Figure 6.1 Example cooling curve with 0.25°C/sec cooling rate (15Hz frequency with 620°C SSM Temperature sample).....	106
Figure 6.2 Example first derivative (15Hz frequency with 620°C SSM Temperature sample) on which local maximum points were marked.....	106
Figure 6.3 Solidus temperature variation at three different vibration frequencies (15, 25, 35 Hz) as SSM temperature decreases	108
Figure 6.4 Liquidus temperature variation at three different vibration frequencies (15, 25, 35 Hz) as SSM temperature decreases	108
Figure 6.5 First Derivative of cooling curve of 7075 alloy with 0.05°C/sec cooling rate and its polynomial fit	109
Figure 6.6 Solid fraction of 7075 alloy in the solidification temperature range (450-650°C) obtained by Newtonian method used in this study	110
Figure 6.7 Solid fraction vs temperature graph of 7075 alloy on which four critical temperatures are marked, obtained by Newtonian method used in this study	111
Figure 6.8 Microstructure of sand cast and T6 treated 7075 alloy produced under 15Hz frequency and 635°C SSM temperature obtained by optical microscopy (200x)	113
Figure 6.9 Microstructure of sand cast and T6 treated 7075 alloy produced under 15Hz frequency at 630°C SSM temperature obtained by optical microscopy (200x).....	113
Figure 6.10 Microstructure of sand cast and T6 treated 7075 alloy produced under 15Hz frequency at 625°C SSM temperature obtained by optical microscopy (200x)	114
Figure 6.11 Microstructure of sand cast and T6 treated 7075 alloy produced under 15Hz frequency and 620°C SSM temperature obtained by optical microscopy (200x)	114
Figure 6.12 Microstructure of sand cast 7075 alloy produced under 15Hz frequency 635°C SSM temperature obtained by optical microscopy (50x).....	115
Figure 6.13 Microstructures of sand cast 7075 alloy under 15Hz frequency and 630°C SSM temperature obtained by optical microscopy (50x).....	115

Figure 6.14 Microstructures of sand cast 7075 alloy produced under 15Hz frequency and 625°C SSM temperature obtained by optical microscopy (50x) 116

Figure 6.15 Microstructure of sand cast 7075 alloy produced under 15Hz frequency and 620°C SSM temperature obtained by optical microscopy (50x) 116

Figure 6.16 Microstructure of squeeze cast 7075 alloy produced under 25Hz frequency at 635°C SSM temperature obtained by optical microscopy (200x) 118

Figure 6.17 Microstructure of squeeze cast 7075 alloy under produced under 25Hz frequency at 630°C SSM temperature obtained by optical microscopy (200x) 118

Figure 6.18 Microstructure of squeeze cast 7075 alloy under produced under 25Hz frequency at 625°C SSM temperature obtained by optical microscopy (200x) 119

Figure 6.19 Microstructure of squeeze cast and T6-treated 7075 alloy produced under 25Hz frequency at 635°C SSM temperature obtained by optical microscopy (200x) 119

Figure 6.20 Microstructure of squeeze cast and T6-treated 7075 alloy produced under 25Hz frequency at 630°C SSM temperature obtained by optical microscopy (200x) 120

Figure 6.21 Microstructure of T6- squeeze cast and T6-treated 7075 alloy produced under 25Hz frequency at 625°C SSM temperature obtained by optical microscopy (200x)..... 120

Figure 6.22 Microstructure of squeeze cast 7075 alloy produced with no-vibration at 670°C obtained by optical microscopy (200x) 121

Figure 6.23 Microstructures of squeeze cast and T6-treated 7075 alloy produced with no-vibration at 670°C obtained by optical microscopy (200x)..... 121

Figure 6.24 Microstructures of squeeze cast and T6-treated 8wt.% 7075/B₄C composite produced under 25Hz frequency at 635°C SSM temperature (200x)..... 123

Figure 6.25 Microstructures of squeeze cast and T6-treated 10wt.% 7075/B₄C composite produced under 25Hz frequency at 635°C SSM temperature (200x)..... 123

Figure 6.26 Microstructures of squeeze cast and T6-treated 10wt.% 7075/B₄C composite produced under 25Hz frequency at 635°C SSM temperature (200x).... 124

Figure 6.27 Microstructures of hot rolled and T6-treated 8wt.% 7075/B ₄ C composite (200x).....	125
Figure 6.28 Microstructures of hot rolled and T6-treated 10wt.% 7075/B ₄ C composite (200x).....	126
Figure 6.29 Microstructures of hot rolled and T6-treated 12wt.% 7075/B ₄ C composite (200x).....	126
Figure 6.30 Grain size measurement on the microstructure of sand cast 7075 alloy produced under 15Hz frequency and 635°C SSM temperature (200x).....	127
Figure 6.31 Grain size measurement on the microstructure of sand cast and T6 treated 7075 alloy under 15Hz frequency and 635°C SSM temperature (200x)	127
Figure 6.32 Grain size variation of sand cast 7075 alloy produced under three different vibration frequency as SSM temperature decreases.....	129
Figure 6.33 Grain size variation of sand cast and T6-treated 7075 alloy produced under three different vibration frequency as SSM temperature decreases.....	129
Figure 6.34 Grain size measurement on the microstructure of squeeze cast 7075 alloy produced under 15Hz frequency and 635°C SSM temperature (200x).....	130
Figure 6.35 Grain size measurement on the microstructure of squeeze cast and T6 treated 7075 alloy produced under 15Hz frequency at 635°C SSM temperature (200x)	130
Figure 6.36 Grain size variation of squeeze cast 7075 alloy produced under three different vibration frequency as SSM temperature decreases.....	132
Figure 6.37 Grain size variation of squeeze cast and T6-treated 7075 alloy produced under three different vibration frequency as SSM temperature decreases.....	132
Figure 6.38 Example grain size measurement on the microstructure of T6-treated squeeze cast 10wt.% 7075/B ₄ C composite	133
Figure 6.39 Example grain size measurement on the microstructure of T6-treated hot-rolled 10wt.% 7075/B ₄ C composite.....	133
Figure 6.40 Grain size variation of T6-treated squeeze cast and hot-rolled 7075/B ₄ C composites as % B ₄ C addition	134

Figure 6.41 Porosity (red) in the microstructure of sand cast 7075 alloy produced under 15Hz frequency and 635°C SSM temperature (100x)	135
Figure 6.42 Porosity (red) in the microstructure of sand cast and T6-treated 7075 alloy produced under 15Hz frequency at 635°C SSM temperature (100x)	135
Figure 6.43 Porosity variation of sand cast 7075 alloy produced under three different vibration frequency as SSM temperature decreases	137
Figure 6.44 Porosity variation of sand cast and T6-treated 7075 alloy produced under three different vibration frequency as SSM temperature decreases	137
Figure 6.45 Porosity (red) in the microstructure of as-squeeze cast 7075 alloy produced under 15Hz frequency at 635°C SSM temperature (100x)	138
Figure 6.46 Porosity (red) in the microstructure of squeeze cast and T6-treated 7075 alloy produced by 15Hz frequency at 635°C SSM temperature (100x)	138
Figure 6.47 Porosity variation of squeeze cast 7075 alloy produced under three different vibration frequency as SSM temperature decreases	140
Figure 6.48 Porosity variation of squeeze cast and T6-treated 7075 alloy produced under three different vibration frequency with decreasing SSM temperature.....	140
Figure 6.49 XRD Patterns of sand cast 7075 alloy produced under 15Hz vibration frequency with four different SSM temperatures	141
Figure 6.50 XRD Patterns of sand cast and T6-treated 7075 alloy produced under 15Hz vibration frequency with four different SSM temperatures	141
Figure 6.51 XRD Patterns of squeeze cast 7075 alloy produced under 15Hz vibration frequency with four different SSM temperatures	142
Figure 6.52 XRD Patterns of squeeze cast and T6-treated 7075 alloy produced under 15Hz vibration frequency with four different SSM temperatures (left) and focused area on the sample produced at 635°C SSM temperature (right)	142
Figure 6.53 XRD Patterns of powder B ₄ C used for the production of 7075/B ₄ C ...	143
Figure 6.54 XRD Patterns of squeeze cast and T6-treated 7075/B ₄ C composites and peaks of 10wt.% 7075/B ₄ C composite between 37-40° angles	143
Figure 6.55 SEM image of sand cast and T6-treated 7075 alloy produced under 35Hz frequency and 630°C SSM temperature	144

Figure 6.56 SEM image of sand cast and T6-treated 7075 alloy produced under 35Hz frequency and 635°C SSM temperature	145
Figure 6.57 SEM image of needle-like phases in sand cast and T6-treated 7075 alloy produced under 35Hz frequency and 625°C SSM temperature	145
Figure 6.58 SEM image of dendrite structure mixed with globular grains in squeeze cast 7075 alloy produced under 15Hz frequency and 625°C SSM temperature	146
Figure 6.59 SEM image of eutectic phase in dendrite boundaries in squeeze cast 7075 alloy produced under 15Hz frequency at 625°C SSM temperature	147
Figure 6.60 EDX analysis result of dendrite boundary phase in squeeze cast 7075 alloy produced under 15Hz frequency at 625°C SSM temperature	147
Figure 6.61 SEM image of globular alpha grains in squeeze cast 7075 alloy produced under 15Hz frequency and 635°C SSM temperature	148
Figure 6.62 EDX analysis results of globular grain boundary in squeeze cast 7075 alloy produced under 15Hz frequency at 635°C SSM temperature	148
Figure 6.63 SEM image of white precipitates in squeeze cast and T6-treated 7075 alloy produced under 25Hz frequency and 635°C SSM temperature	149
Figure 6.64 EDX analysis results of white precipitates in squeeze cast and T6-treated 7075 alloy produced under 15Hz frequency at 635°C SSM temperature	149
Figure 6.65 SEM image of finest precipitates in squeeze cast and T6-treated 7075 alloy produced under 25Hz frequency at 635°C SSM temperature	150
Figure 6.66 SEM image of finest precipitates in squeeze cast and T6-treated 7075 alloy produced under 35Hz frequency at 635°C SSM temperature	150
Figure 6.67 SEM image of finest precipitates in squeeze cast and T6-treated 7075 alloy produced under 35Hz frequency at 635°C SSM temperature	151
Figure 6.68 SEM image of cleavage planes in the fracture surface of squeeze cast and T6-treated 7075 alloy produced under 35Hz frequency at 625°C SSM temperature	152
Figure 6.69 SEM image of the crack in the fracture surface of squeeze cast and T6-treated 7075 alloy produced under 35Hz frequency at 625°C SSM temperature	152

Figure 6.70 SEM image of B ₄ C particulate powder used for squeeze casting of 7075/B ₄ C composites.....	153
Figure 6.71 SEM image of black particle in squeeze cast 8wt.% 7075/B ₄ C composite	154
Figure 6.72 EDX analysis results of black agglomerate in squeeze cast 8wt.% 7075/B ₄ C composite	154
Figure 6.73 SEM image of white precipitates along the grain boundaries in hot-rolled 10wt.% 7075/B ₄ C composite.....	155
Figure 6.74 EDX analysis results of white precipitates along the grain boundaries in hot-rolled 10wt.% 7075/B ₄ C composite	155
Figure 6.75 Hardness variation of sand cast 7075 alloy produced under three different vibration frequency as SSM temperature decreases	158
Figure 6.76 Hardness variation of sand cast and T6-treated 7075 alloy produced under three different vibration frequency as SSM temperature decreases	158
Figure 6.77 Hardness variation of squeeze cast 7075 alloy produced under three different vibration frequency as SSM temperature decreases	160
Figure 6.78 Hardness variation of squeeze cast and T6-treated 7075 alloy produced under three different vibration frequency as SSM temperature decreases	160
Figure 6.79 Comparison of average hardness values of squeeze cast 7075 alloy produced under different vibration frequencies at 635°Cf	161
Figure 6.80 Comparison of average hardness values of squeeze cast and T6-treated 7075 alloy produced under different vibration frequencies at 635°C.....	161
Figure 6.81 Hardness variation of T6 treated squeeze cast and hot-rolled 7075/B ₄ C composites as % B ₄ C addition.....	163
Figure 6.82 Comparison of average hardness values of T6-treated squeeze cast 7075 alloy, squeeze cast 10wt.% 7075/B ₄ C composite and hot-rolled 10wt.% 7075/B ₄ C	163
Figure 6.83 Tensile stress vs tensile strain curves for as-cast and T6-treated sand cast 7075 alloy produced under 15Hz frequency at 635°C SSM temperature.....	165

Figure 6.84 Stress at fracture variation of sand cast 7075 alloy produced under three different vibration frequency as SSM temperature decreases	166
Figure 6.85 Stress at fracture variation of sand cast and T6-treated 7075 alloy produced under three different vibration frequency as SSM temperature decreases	166
Figure 6.86 Tensile stress vs tensile strain curves for as-cast and T6 treated squeeze cast 7075 alloy produced under 15Hz frequency at 635°C SSM temperature.....	168
Figure 6.87 UTS variation of squeeze cast 7075 alloy produced under three different vibration frequency as SSM temperature decreases.....	169
Figure 6.88 UTS variation of squeeze cast and T6-treated 7075 alloy produced under three different vibration frequency as SSM temperature decreases.....	169
Figure 6.89 Comparison of average UTS values of squeeze cast 7075 alloy produced under different vibration frequencies at 635°C and with non-vibrated sample at 670°C	170
Figure 6.90 Comparison of average UTS values of squeeze cast and T6-treated 7075 alloy produced under different vibration frequencies at 635°C and with non-vibrated sample at 670°C	170
Figure 6.91 Flexural stress vs flexural strain curves for as-cast and Sand cast and T6 treated 7075 alloy produced under 15Hz frequency and 635°C SSM temperature .	172
Figure 6.92 Flexural strength variation of squeeze cast T6-treated and as-cast 7075 alloy produced under three different vibration frequency as SSM temperature decreases	173
Figure 6.93 Comparison of average flexural strength values of squeeze cast and T6-treated 7075 alloy produced under different vibration frequencies at 635°C and with non-vibrated sample at 670°C	173
Figure 6.94 Flexural stress vs flexural strain curves of T6-treated squeeze cast 7075/B ₄ C composites produced under 25Hz frequency at 635°C SSM temperature	174

Figure 6.95 Comparison of average flexural strength values of squeeze cast and T6-treated 7075/B₄C composites produced under 25Hz vibration frequencies at 635°C 175

Figure 6.96 Flexural stress vs flexural strain curves of hot-rolled and T6-treated 7075/B₄C composites produced under 25Hz frequency at 635°C SSM temperature 176

Figure 6.97 Comparison of average flexural strength values of hot-rolled and T6-treated 7075/B₄C composites..... 177

Figure 6.98 Overall comparison of average flexural strength values of T6-treated squeeze cast 7075 alloys, squeeze cast 7075/B₄C composite and hot-rolled 7075/B₄C composites 177

CHAPTER 1

INTRODUCTION

Production of high strength aluminum alloys and aluminum matrix composites have been significantly studied in recent years and gained importance in many application fields such as military, defense and aerospace industries since they offer low density, high specific strength, high ductility, high corrosion resistance and various production methods. 7000 series aluminum alloys, especially 7075 aluminum alloys, are one of the most commonly used aluminum alloy type due to their high strength capability and many available production methods such as forging, extrusion, rolling and so on. Since some of the common production methods have drawbacks like high production (tool) cost in forging, significant amount of metal waste in extrusion and restricted shaping capacity in rolling processes, the requirement for a production method of high strength 7000 series (especially 7075) aluminum alloys have been much more critical in order to supply the huge demand of high strength and low density 7075 aluminum alloys in defense, military, aerospace and automotive industries. Thus, casting which is one of the easiest, fastest and most economical process of forming/shaping may be considered as a good candidate method to produce high strength 7075 aluminum alloy.

However, conventional casting methods like sand-casting and high pressure die casting are incapable of obtaining high strength alloy with desired microstructure. The main reason is that the solidifying liquids grow in the form of dendrites in conventional casting methods where initial metal is casted in fully liquid phase. Dendritic growth of the first solid phase leads to formation of porous microstructure which is detrimental for mechanical properties. Fortunately, the developments in casting technology made possible to obtain pore-free microstructure with minimum amount of shrinkage and gas voids by modern casting methods such as semi-solid melting method where initial metal is casted in partially liquid phase.

Semi-solid casting methods such as rheocasting became quite suitable for the production of high strength low porosity 7075 Series aluminum alloys and aluminum matrix composites. The priority in production of high strength 7075 Series aluminum alloys and aluminum matrix composites is minimizing the porosity content and optimization of the grain refinement with favorable heat treatment (generally homogenization and aging) process. Production of high strength 7075 Series aluminum alloy or aluminum matrix composites with sustainable methods is going to be able to meet the demand in the main fields of aerospace, automotive and defense industry.

It has been mentioned earlier that the application field of 7000 Series high strength aluminum alloys expanded from automotive and aerospace to defense and military industries. Especially, the parts used in aerospace industry with high strength and low density requirements are generally produced especially by 7075 alloy. In addition to use of 7075 aluminum alloys in aerospace industry, these high strength aluminum alloys have been significantly used in automotive industry.

It has been clearly pointed out that rheocasting which is a semi-solid melting production method is well worth to study by taking the capability of producing high strength 7075 aluminum alloy in easier, more effective and faster way into consideration. Therefore, this study aims to determine the effect of rheocasting parameters on the 7075 aluminum alloy and also it is aimed to determine the optimal process parameters for the production of high strength 7075 Alloy by semi-solid melting which might be used instead of solid phase forming methods.

CHAPTER 2

BASIC KNOWLEDGE

During solidification, metals and alloys have tendency to form in the shape of dendritic grain structure generally. The reason for the dendritic solidification morphology of the grains is the sudden release of heat and solute atoms during solidification due to the thermodynamic and kinetic reasons. The dendritic structure could either be columnar or equiaxed as seen in figure 2.1. [3]

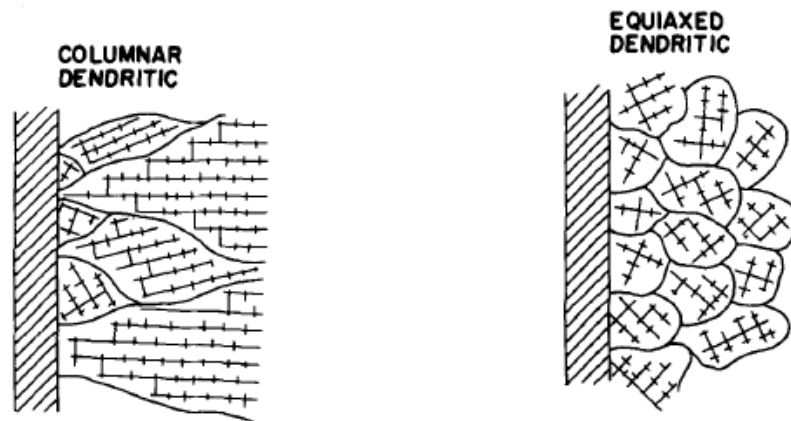


Figure 2.1 Dendritic grain structure in solidifying metal castings

Equilibrium is maintained during solidification just at the solid-liquid interface and the solid fraction at a given distance from interface can be determined by well-known

Scheil equation; $f_L = \left(\frac{c_L}{c_0}\right)^{-1/1-k}$

c_L =concentration liquid, c_0 =initial concentration, k =partition ratio

where it is driven by simple mass balance and the diffusion in the solid phase is neglected. By the help of Scheil model, it is possible to determine the solid fraction at any distance from the solid/liquid interface as seen in figure 2.2. [3]

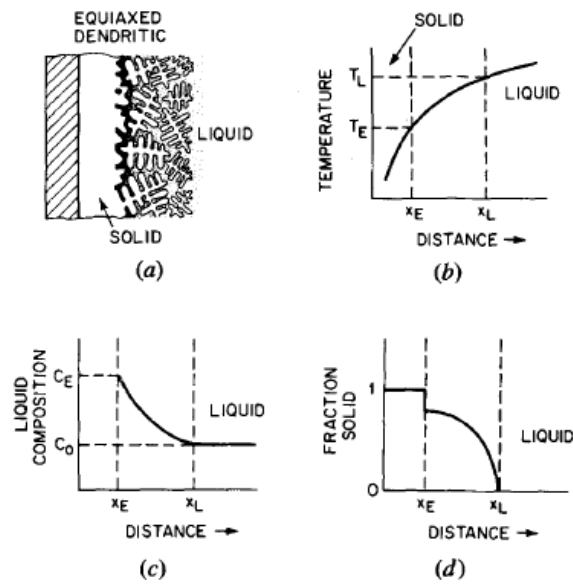


Figure 2.2 Scheil model of (a) dendritic structure, (b) part of phase diagram, (c) liquid composition vs distance from interface and (d) solid fraction at any distance from interface [3]

For better and more realistic models have been introduced to calculate the solid fraction of solidifying metal in order to consider the diffusion in the solid phase and the ripening of solid particles. As the cooling/solidification rate decreases, diffusion in the solid rises apparently (see in figure 2.3). [4]

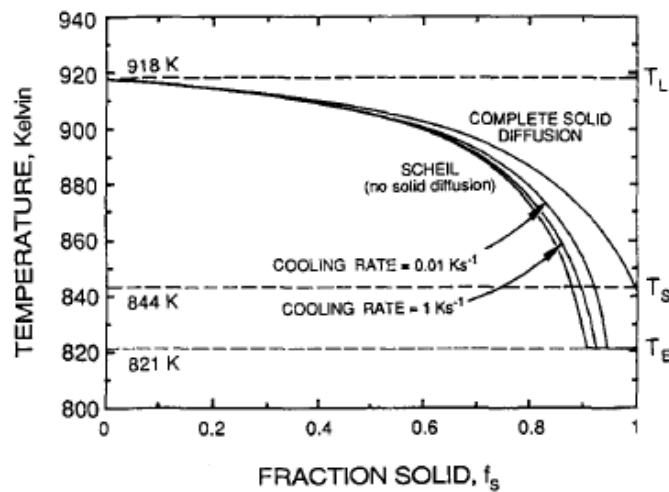


Figure 2.3 Different models to calculate solid fraction at a given temperature [4]

2.1. Semi-Solid Melting (SSM)

As mentioned earlier, the general behavior of solidifying metals is the formation of dendritic grain morphology either in equiaxed or columnar manner. Newly formed solid nuclei begin to grow in a dendritic manner. In the initial stages of the solidification, these growing dendrites are quite free to move inside the partial solid/liquid metal due to the high liquid fraction earlier which was called as ‘mass feeding’. However, in progress of solidification time, the dendritic structure keeps growing up to a point at which dendrite network forms and it is called ‘inter-dendritic feeding’ in the corresponding literature works as seen in figure 2.4. [5]

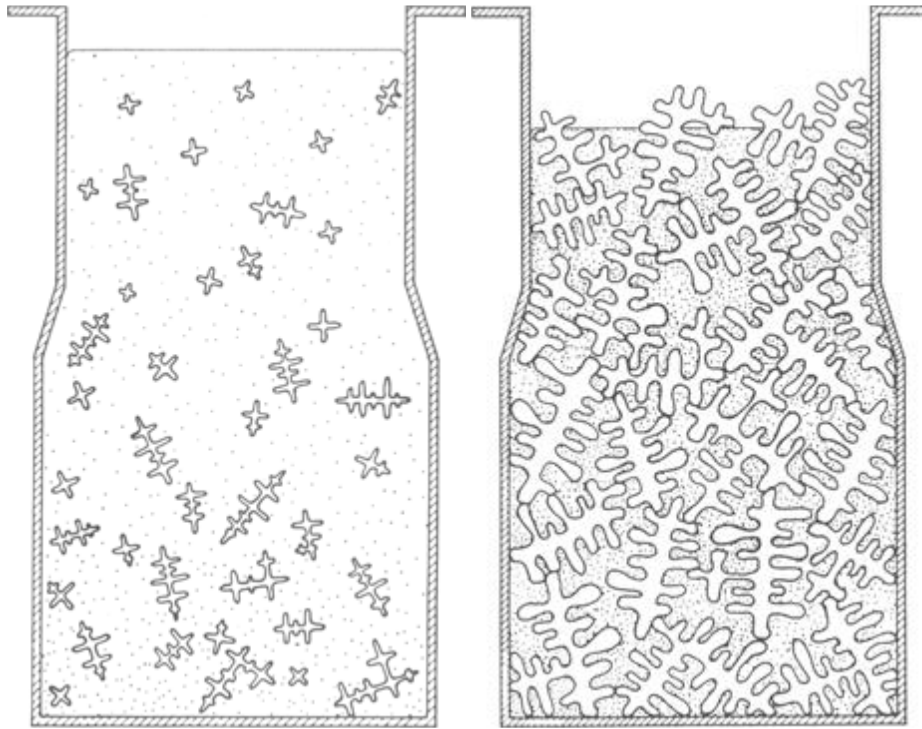


Figure 2.4 Representation of mass feeding (left) and inter-dendritic feeding (right) stages [5]

After reaching this critical solid fraction, measurable strength develops within the dendrite network. Many studies reported in similar results about this critical point beyond which the partial solid alloy can be deformed, 0.2 solid fraction value have

been found to be this critical point for both aluminum alloys [6] and also Lead-Tin alloys [7]. After this point shear strength measurements said to be increased when the solid fraction rises as well. Literature studies in the relationship between shear strength and solid fraction in the solidifying metals were focused on the idea of applying isothermal shear stress to the partial solid/liquid slurries. [6,7]

One of the important study about the isothermal shearing of Sn-15wt%Pb alloys carried out by Spencer et al. [7] They used a device composed of counter rotating discs in which molten Sn-Pb alloys were sheared isothermally. In this study, similarly measurable strength has been observed at about 0.2 solid fraction and reached up to 200 kPa at about 0.4 solid fraction as seen in figure 2.5 and increases so rapidly after this point due to the impingement or intersection of growing solid dendrite arms. At low solid fractions, deformations of some dendrites took place and the resulting opening filled with the liquid. However, at sufficiently high solid fractions, remaining liquid can no longer compensate the shear stresses and internal openings which are called ‘hot tears’ are formed [8] as seen in figure 2.6.

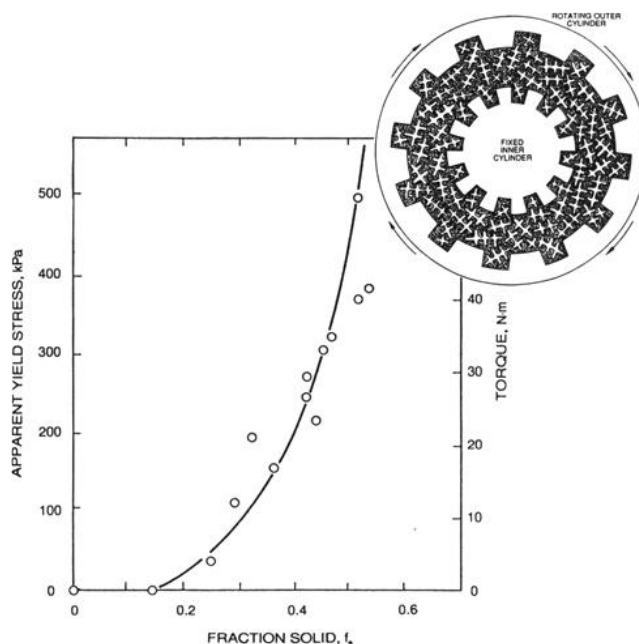


Figure 2.5 Isothermal shear strength of semi-solid Sn-15Pb alloys and simple experimental set-up used in the study [7]



Figure 2.6 Radiography of Al-10Cu alloy filled with hot tears [8]

Therefore, the origin of Semi Solid Melting (SSM) could be said to base upon the study of Spencer and colleagues in Massachusetts Institute of Technology in 1970's. The study was related to hot tearing behavior of Sn-Pb alloys [7]. One of the most important and interesting observation in this study was that application of continuous shearing above the liquidus temperature of the alloy, instead of isothermal shearing of partial liquid alloy, followed by slow cooling reduced the maximum shear stress dramatically that was required to deform the dendrites. For Sn-15Pb alloys, maximum shear stress drops from 200 kPa (see in figure 2.8) to 0.2 kPa (see in figure 2.8) for solid fraction value of 0.4 by applying continuous shearing was the significant outcome of Spencer's study. This dramatic decrease in the maximum shear stress was actually originated from the fundamental changes in the microstructure. Rather than the conventional dendritic grain structure of metals/alloys, these Sn-Pb alloys showed different type of morphology. Figure 2.7 shows the transformation of solidifying particles from dendrite to rosette like shape to even spherical [5], by applying external shearing classical dendrite morphology could be successfully transformed into finer and spherical grain structure which is called 'globular structure'. Spencer and

colleagues (MIT researchers) called this new process as ‘Rheocasting’ which emphasizes the importance of rheological behavior of solidifying metals.

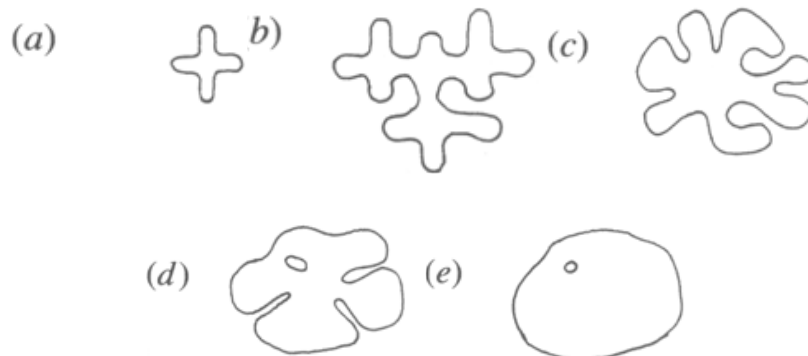


Figure 2.7 Transformation of solidifying particles during solidification under shearing (a) initial dendrite (b) dendritic growth (c) rosette (d) grown rosette (e) spherical [5]

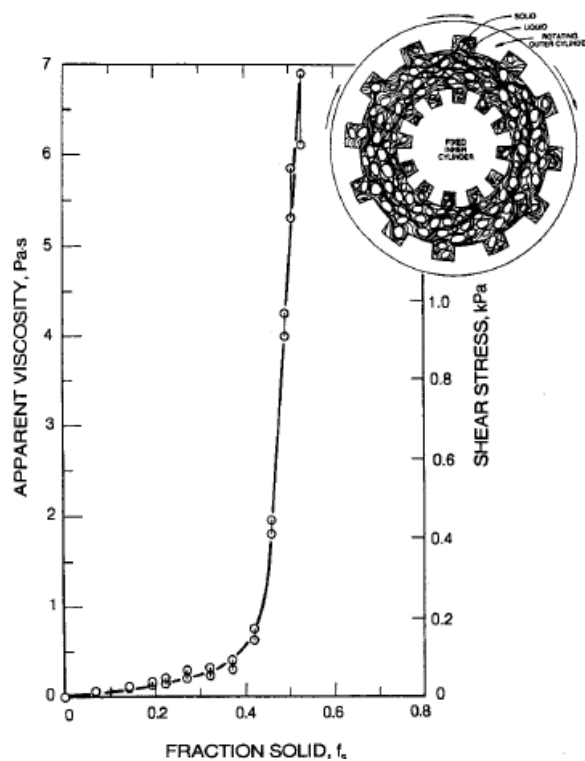


Figure 2.8 Viscosity and shear stress vs solid fraction graph for Sn-15Pb alloy with a shear rate of 200s^{-1} and cooling rate of 0.006 Ks^{-1} in Spencer’s experiments [7]

The external shearing could be applied by either actual shear forces in the case of Spencer's study or vibration could also be used to shear the semi-solid metals and transform microstructure. There were two explanations to morphology transformation from classical dendrite to globular shape in the solidifying metals; the very first one was that vibration is actually able to promote heterogeneous or even homogenous nucleation and resulted in grain refinement which was not fully accepted then. [9] The other explanation of this mechanisms have been relatively more accepted in the literature which indicates, the transformation and the grain refinement by shearing or vibration is actually by fragmentation of dendrite arms as seen in figure 2.7 [10].

Spencer's results about the microstructural transformation during solidification by means of external force such as vibration were substantial. Figure 2.9 summarizes the microstructural change that Spencer's have observed during his experiments [10]. By increasing shearing or intensity of turbulence, growing nuclei in the form of dendrite as conventional could be changed into spherical or 'globular' in shape which was very crucial finding at that time since fine and spherical grain microstructure is actually able to obtain by an effective and easy method in the case of conventional solidification processes such as castings, without using any nucleation agents or post processes.

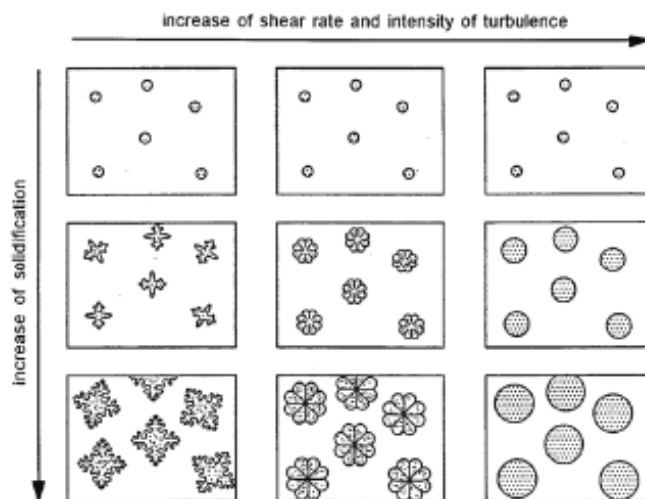


Figure 2.9 The effect of increasing shear rate/ intensity of turbulence and increasing solidification on the morphology of solidifying nuclei [10]

Figure 2.10 shows the effect of increasing shear rate and solid fraction on the microstructure of Sn-15Pb alloys during solidification experiments of Spencer. [7] In figure 2.10 (a), the solidification with low shear rate and low solid fraction resulted a microstructure consists of fully conventional dendritic morphology. In figure 2.10 (b) on the other hand, increasing shear rate changed dendritic microstructure to cellular. In addition to high solid fraction, increasing shear rate, in the case of figure 2.10 (c) transformed successfully the initial dendrites into globular grain structure. Spencer's experiments clearly showed that increasing shearing by means of mechanical external forces and increasing solid fraction during solidification promote the fragmentation of dendrites and globular grain formation.

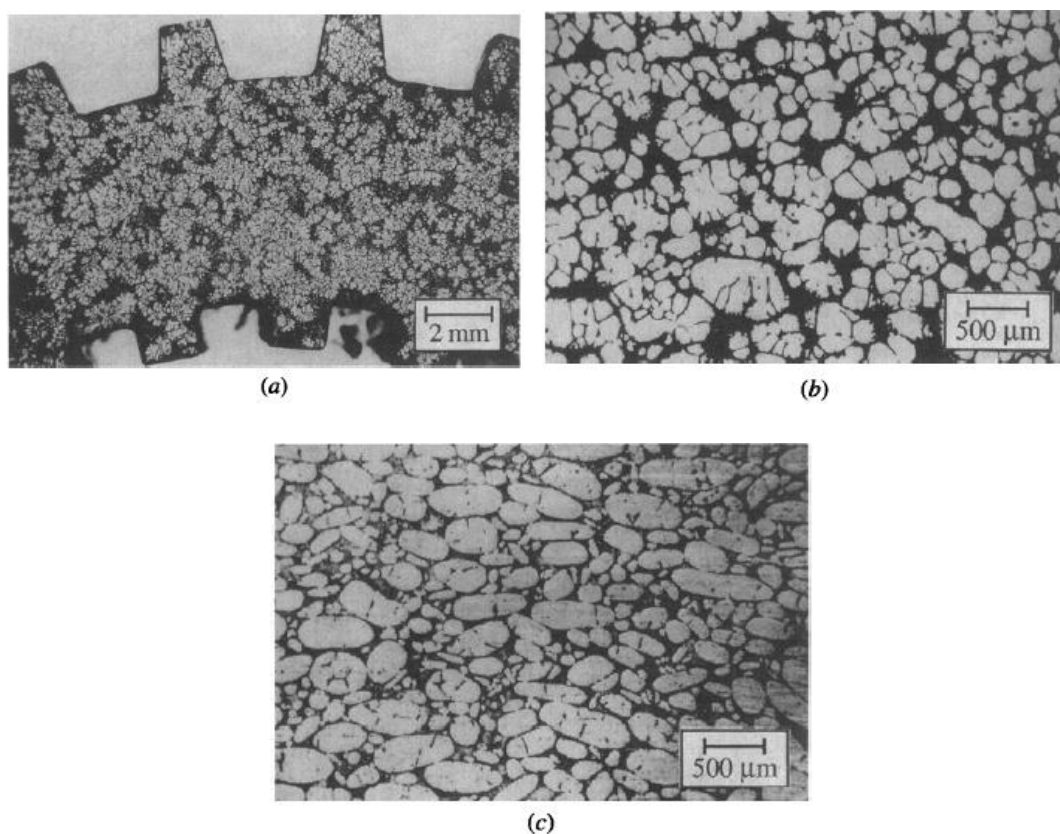


Figure 2.10 Sn-15wt% Pb alloy continuously cooled with 0.006 K s^{-1} cooling rate (a) low shear rate and low solid fraction (b) low shear rate and higher solid fraction (c) high shear rate and high solid fraction [7]

There are basically two types of semi solid melting (SSM) method which has been developed and used for mass production in various industries. The first SSM method is thixocasting in which production of solid billets having globular grain structure takes place initially, then the billet is heated up above the solidus temperature in order to obtain semi solid metal or rather partial solid metal, thixocasting process finalizes with the shaping or forming processes which may be forging, extrusion, rolling, etc. Therefore, some type of thixocasting process is also known as ‘thixoforging’, ‘thixoextrusion’, etc. The second SSM method is rheocasting in which liquid alloy in desired chemical composition is melted initially, then this fully liquid alloy is cooled below liquidus temperature down to a temperature where partial solid slurry is formed and shaped easily. The next and the final step of rheocasting process is the forming which might be high pressure die casting (HPDC), squeeze casting or solid state forming methods like extrusion and forging [2]. By considering practical way of production of metal parts by SSM methods, rheocasting becomes prominent compared to thixocasting which requires more advance starting materials and somewhat similar to the solid phase forming methods mentioned in previous sections.

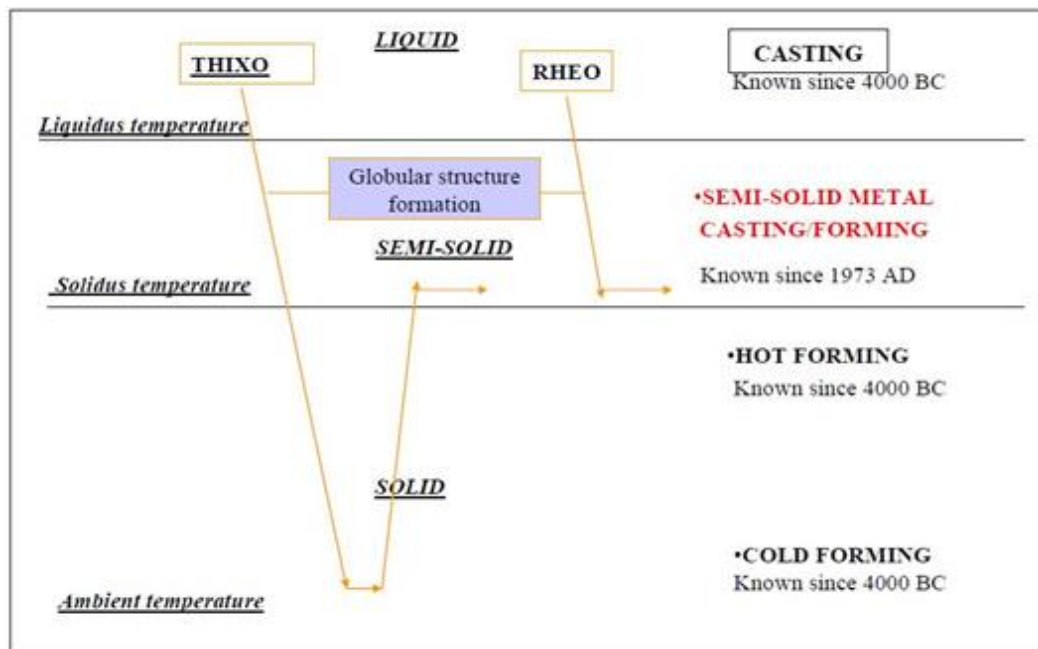


Figure 2.11 Schematic illustration of comparison of two types of SSM methods [2]

2.2. Rheocasting

Rheocasting is a semi solid melting (SSM) method which is composed of two stages as described beforehand, i.e. preparation of slurry and the shaping stages. Table 2.1 summarizes various worldwide companies that has been using rheocasting as production method. This SSM technique is commonly used in the production of light-weight alloys such as aluminum alloys by many famous European, USA and Japanese companies. [11]

Table 2-1 Different worldwide companies using various rheocasting processes [11]

Process Name	Company	Location	Slurry Technique
Gibbs	Gibbs Die Casting	USA	Stirring
Hitachi	Hitachi Metals	Japan	Stirring
Honda	Honda	Japan	Stirring
Induction Stirring	CSIR	South Africa	Stirring
SEED Process	Alcan	Canada	Stirring
Slurry on Demand	Mercury Marine	USA	Stirring
Rheo-Diecasting	Brunel University	England	Dendrite Fragmentation
Semi-solid Rheocasting	Idra Prince	USA	Numerous Nuclei
ATM	CSIRO	Australia	Numerous Nuclei
Buhler	Buhler	Switzerland	Numerous Nuclei
Direct Thermal Method	University College Dublin	Ireland	Numerous Nuclei
New Rheocasting	Ube	Japan	Numerous Nuclei

The importance of rheocasting process have been realized more and more day by day especially among many application fields, especially in automotive industry. There is a huge demand of many metal/alloy products requiring high strength with low cost and novel production methods should be cost effective, efficient and faster compared to conventional ones in order to supply this huge demands. Giant automotive companies such as BMW and AUDI have been using rheocast products in their cars and motor bikes more frequently and increasing the number of these products. [2] Figure 2.12, 2.13 and 2.14 show some of these products manufactured by rheocasting method.



Figure 2.12 Rheocast thin walled structural parts in doors AUDI A3 [2]



Figure 2.13 Rear door hinge AUDI A2 produced by rheocasting [2]



Figure 2.14 Rear seat cover BMW R 1200 C motor bike (left) and a component for AUDI A6 V8 energy management system for bumpers produced by rheocasting [2]

Rheocasting process simply includes two stages; the preparation of semi-solid slurry and the shaping or forming of the slurry. In the preparation of slurry stage, fragmentation of dendrites takes place by applying external shear forces or building up shear forces within the slurry. Initially, the alloy with determined chemical composition is melted, then this melted is decreased to a specified temperature after which it is kept at that temperature for a while. The critical step of slurry making comes after, stirring of the slurry is carried out by mechanically [12], magnetically or ultrasonically, gas induced [13] stirring is also optional process which is relatively a new approach. Whatever stirring process is used for the preparation of slurry, the objective is the fragmentation of dendrite arms and formation of globular grain structure effectively as mentioned previously.

In figure 2.15 and 2.16, schematic illustration of gas induced stirring of semi-solid slurry for slurry preparation step followed by HPDC of this slurry for shaping step is shown [14], which are the fundamental steps for the most cases in the rheocasting of nowadays products in the industry

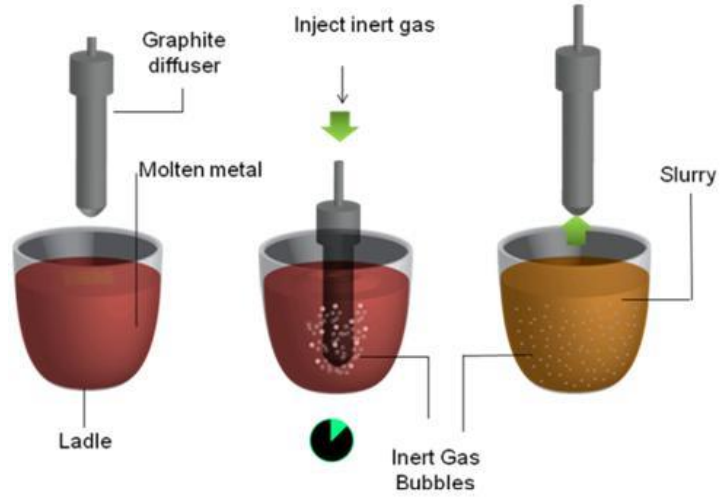


Figure 2.15 Schematic illustration of gas induced stirring for slurry preparation [12]

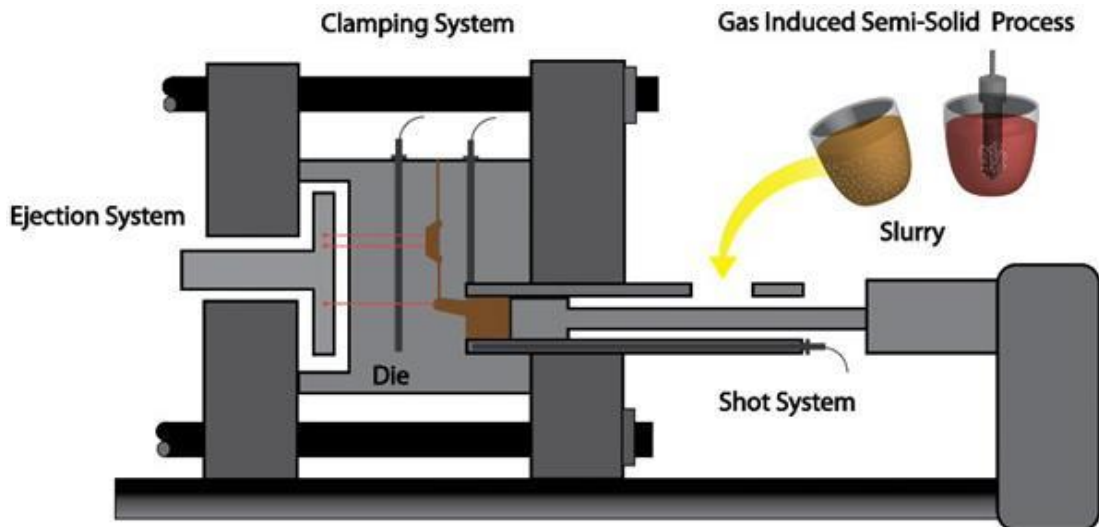
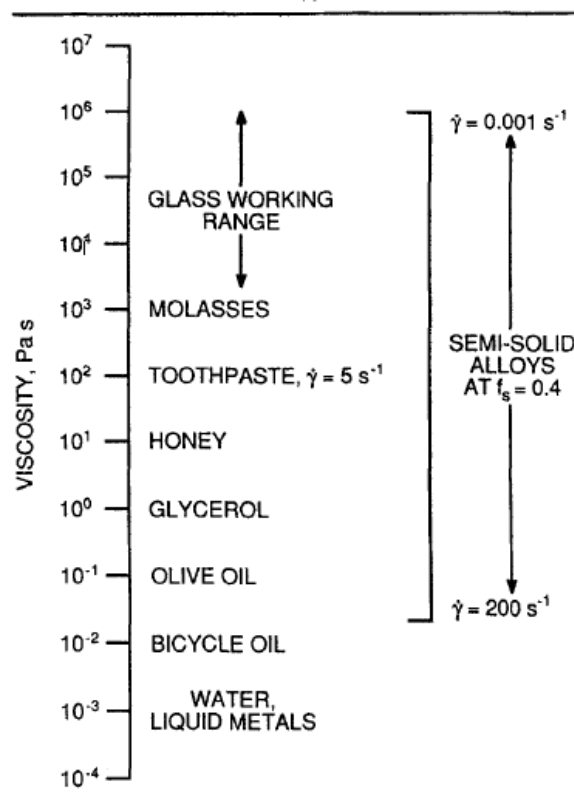


Figure 2.16 Schematic illustration of high pressure die casting of gas induced semi-solid slurry [12]

2.2.1. Slurry preparation step

The first step in rheocasting process is the preparation of semi solid slurry. Slurry is mud like suspension of partially liquid and partially solid alloy whose viscosity is close to viscosity of oil and below than viscosity of glass working range (see in Table 2.2). Initially, liquid alloy is melted from solid charge materials, even the scrap metals could be used as starting materials, with intended chemical compositions. After obtaining fully liquid melt, the temperature is decreased down to a temperature at which slurry has reasonable viscosity, i.e. temperature at which it is not considered as solid yet. At such low viscosities the slurry or semi solid alloy can flow even under gravity of itself. When the viscosity of slurry reaches above 10^6 Pa.s value, it begins to act as solid metal and limited amount of deformation can be observed under loading. This viscosity value corresponds to solid fraction between 0.4 and 0.5. [5]

Table 2-2 Typical viscosities of common materials and viscosity range of semi solid slurries [5]



In order to obtain the semi-solid slurry before final forming operations, the partial liquid alloy having relatively low viscosity values ($<10^6$ Pa.s) or low solid fractions ($<0.4-0.5$) is exposed to shear forces by means of different methods and equipment. There are many methods in which the slurry is exposed to shearing for dendrite fragmentation and thus forming globular grain microstructure. The earliest and simplest way was mechanical mixing of solidifying metal during cooling by using batch rheocaster as seen in figure 2.17 (a). The idea was to break dendrite arms by mechanical stirring which forms internal turbulence and shearing. The another type of stirring process is carried out by continuous rheocaster as seen in figure 2.17 (b). This time higher shear forces with limited amount of gas entrapment could be achieved since the stirring actually takes place beneath the surface of the slurry. Another important process route is electromagnetic stirring of semi solid slurry which enables the continuous production of large scale castings as seen in figure 2.17 (c). [5] There are also recently developed and used stirring techniques in the literature such as gas induced stirring [12] (see in figure 2.15), inverted cone shaped pouring channel method in which fully liquid alloy is poured into a channel in which falling of liquid metal through a zig zag channel forms mechanical shear forces. [20]. Induction stirring with simultaneous forced air cooling is also another new method [21]. The details of these methods will be discussed in literature review section.

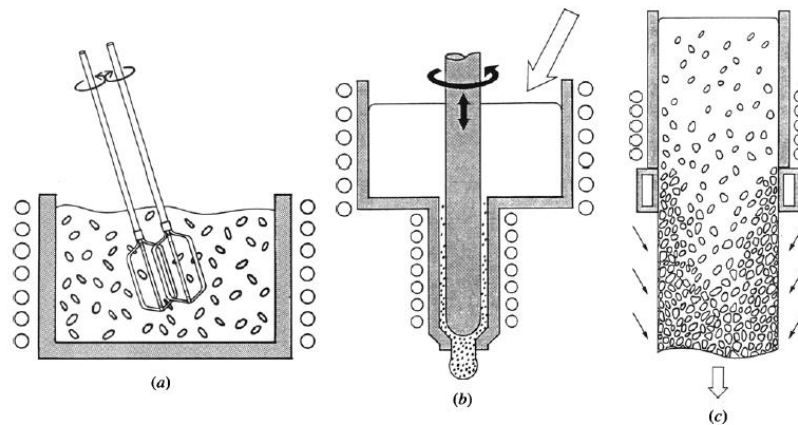


Figure 2.17 Schematic diagram of different stirring techniques used (a) batch rheocaster, (b) continuous, (c) electromagnetic

2.2.2. Forming/shaping step

After the slurry preparation step is complete, the semi-solid slurry with reasonable viscosity values is required to be formed into the final shape by means of different techniques. In the literature studies of rheocasting of mainly aluminum alloys, the most common technique is high pressure die casting (HPDC). Almost all of the studies in this topic focused on HPDC of semi-solid slurries prepared by different methods [20] [21]. On the other hand, it is quite possible to integrate any solid phase forming techniques like extrusion or thixocasting Al-Zn-Mg-Cu alloy in the case of study of Fang et al [22], or forging as in the case of semi-solid thixo-forming study of 6061 aluminum alloy by Zhi-ming et al [23]. As indicated by their names the studies related to forming operations rather than HPDC such as extrusion, forging, rolling, etc. are categorized as thixo-forming operations rather than rheocasting. The reason behind this categorization is simply the working temperature of these shaping operations. When the temperature is not high enough to work in the range of solid fraction above 0.5, the process simply named or categorized into thixo-forming. However, it is possible to decrease the solid fraction and perform other methods rather than HPDC. All in all, HPDC is the most common method for the final forming operation of semi-solid slurries. In this part, two possible methods will be mentioned, one of which is HPDC. The other candidate method for final forming operation is squeeze casting.

Both HPDC and squeeze casting techniques are pressure assisted castings methods where liquid or semi-liquid metal is poured into a re-usable die or die cavity followed by pressure assisted solidification. [24] [25] Advancement of introducing pressure during solidification actually has been reported to yield better surface quality, less casting defects like shrinkage and better mechanical properties in the final products and have been used for the mass production of light-weight aluminum and magnesium alloys extensively. Use of pressure assisted casting methods have been gaining importance in fact. [25]

2.2.2.1. High pressure die casting (HPDC)

High pressure die casting (HPDC) method is pressure assisted casting method where typically cold chamber die casting machines with high capacities (hundreds of tons) is used [26] to carry out the casting process. There are several steps in conventional HPDC method; initially liquid alloy is maintained and kept in holding furnaces at predetermined temperatures, then the filling or pouring of the liquid metal into shot sleeve by a container or ladle takes place, the final step of HPDC is the injection of liquid metal into the dies and rapid solidification of pressured metal, three basic steps could be seen in figure 18. The parts of conventional HPDC machine is schematically represented in figure 2.19.

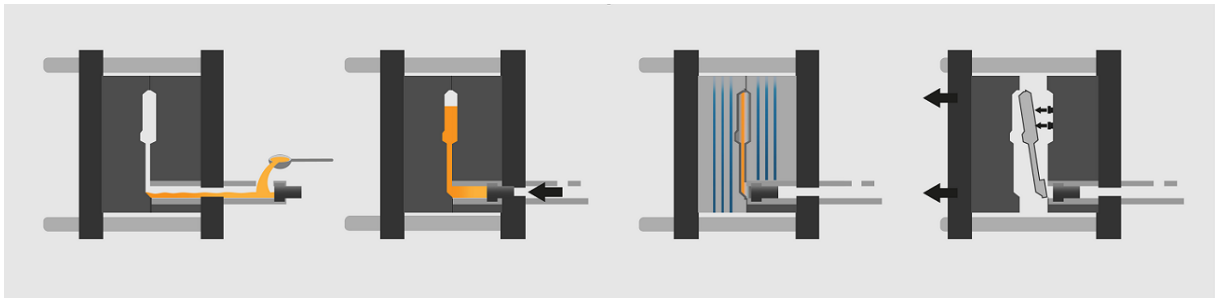


Figure 2.18 Schematic illustration of initial pouring stage, metal filling stage and final solidification stages followed by extraction of solid metal in conventional HPDC [29]

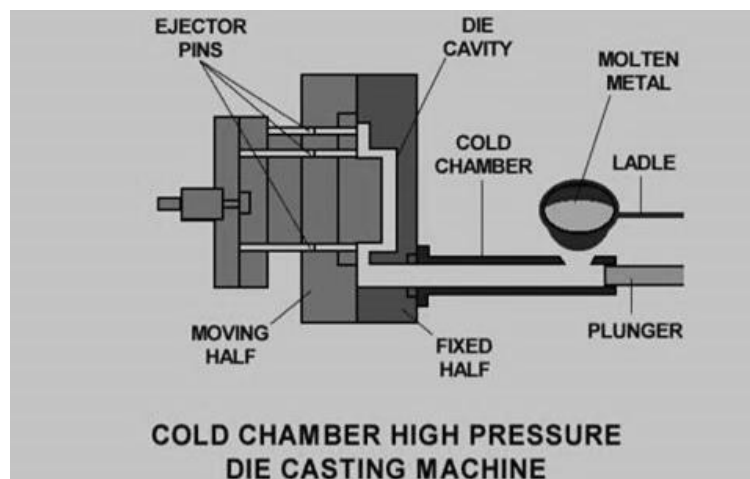


Figure 2.19 Schematic illustration of basic parts of cold chamber HPDC machine [30]

Due to characteristics of HPDC method such as high production rate, highly automation systems, excellent surface quality and dimensional consistency; it has become the most popular and world-wide used production method in the manufacturing of light-weight non-ferrous alloys such as aluminum, magnesium and zinc. Almost 60% of light-weight alloy castings in world-wide is being carried out by HPDC method. Although the method is quite advantageous in terms of high production rate of good quality products, it has certain drawbacks. [27] It is crucial to understand the working principle of HPDC, in fact filling of liquid metal. The metal in the shot sleeve is injected by hydraulic pistons into HPDC dies to complete filling and solidification. There several stages of movement of piston during filling of liquid metal. The velocity of piston is rather low at the initial stages, on the other hand the pressure and the speed of the piston becomes extremely high at the final stages of metal filling, example case of sudden jump in the piston velocity after some critical point during mold filling can be seen in figure 2.20. This sudden increase in the velocity of piston and the filling metal simply leads to formation of turbulent flow. A real example of pressure change during three different phase/stage of HPDC experiment was shown in figure 2.20 [28]

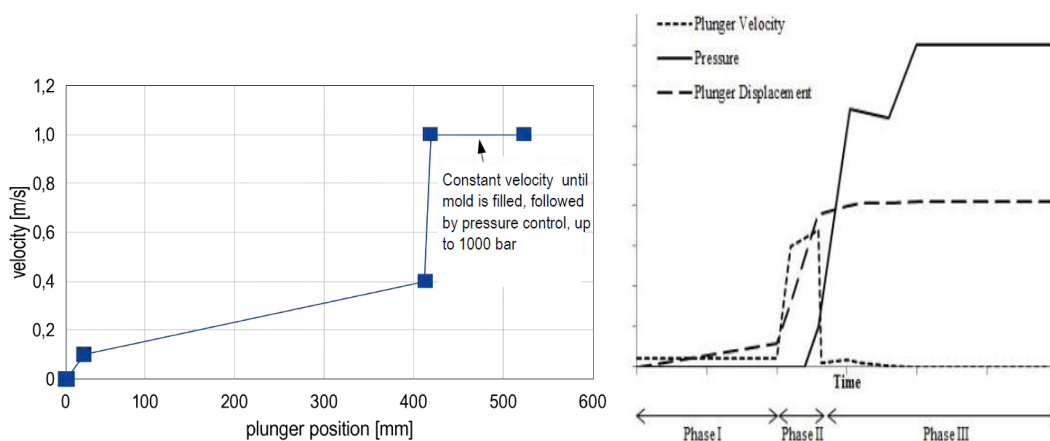


Figure 2.20 Velocity of HPDC piston with respect to the position of plunger or the piston and the real experimental result showing pressure variation during the phases of HPDC [28]

Unfortunately, turbulent flow in HPDC promotes the dissolution or entrapment of gas molecules during filling of metal. Therefore, the outcomes of turbulent flow are shown in the microstructure of HPDC products as gas porosities, voids or inclusions. In addition, these casting defects in the microstructure of conventional HPDC products makes post heat treatment is impossible since gas porosities could easily turn into blisters by heat activation. In order to minimize the casting defects in HPDC and optimize the mechanical properties of final products, it is crucial to carefully control the process parameters such as pressing speed or load applied by the piston, mold filling time, mold temperature and the temperature of liquid metal.

The application fields of HPDC products are vast, as stated previously the major use of HPDC is in the automotive industry, especially in the production of light-weight alloys such as aluminum alloys. Al-Si-Mg alloys are one of the most common light-weight alloys produced by HPDC method, some of which are A360, A380 alloys and so on [31]. Various products produced by HPDC methods which are used in different application fields are shown in figure 2.21. [32] The importance of HPDC method in conventional castings of high quality aluminum alloy products are incontrovertible reality. In accordance with the extensive use of HPDC technique by conventional methods, it is clear that semi-solid melting, especially rheocasting of aluminum alloys by HPDC as final forming method is worth to study and has great capacity of improvement in conventional methods. Studies related to rheocasting of aluminum alloys by using HPDC method will be discussed later on.



Figure 2.21 Various HPDC aluminum alloy products used in aerospace and automotive industries [32]

2.2.2.2. Squeeze casting

Squeeze casting is a pressure assisted casting method, as the name suggests, where squeezing of liquid metal takes place until complete solidification, usually even after the solidification. Similar to HPDC method, liquid metal is pressed within a re-usable metal dies which basically a combination of forging and permanent mold casting. Compared to other conventional pressure assisted methods like HPDC, squeeze casting is relatively current technique mainly commercialized in Europe and Japan in order to produce high quality light-weight alloys. The final products generally require minor post-process or are used directly, therefore squeeze casting is accepted as near net shape production method. [24] Squeeze cast products possess excellent surface finish, variety of shape and size design and superior mechanical properties. As well as

the better properties of final products, the metal loss is also limited or non-existent in squeeze casting process since there is no feeding or runner system requirements. The very basic reason behind these excellent outcomes of squeeze casting products are originated by the application of pressure during whole process even after solidification is completed. Squeeze casting process consists of several stages; initially pre-determined amount of liquid metal is poured into a die cavity on which hydraulic press system is located, then the sudden increase in pressure is applied to close the die and pressurize the molten metal, finally pressure slowly is applied to the liquid metal until the end of solidification. Figure 2.22 shows the parts of direct and indirect squeeze casting systems where open dies and pressure application could be seen.

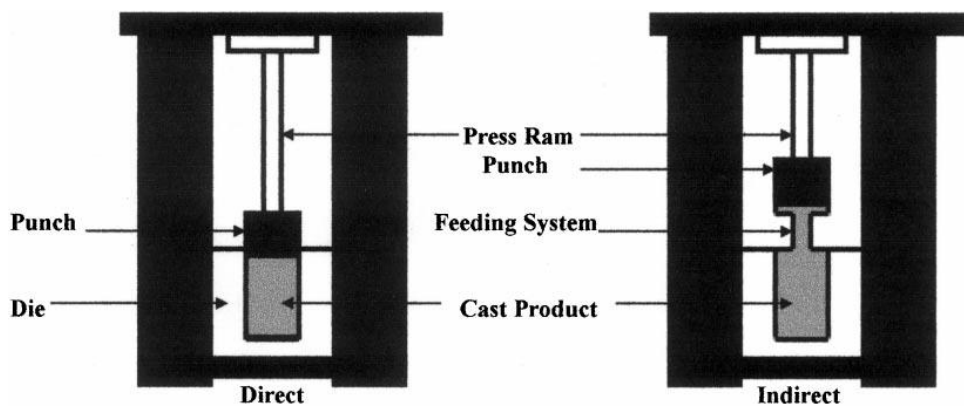


Figure 2.22 Schematic illustration of direct and indirect squeeze casting machines [24]

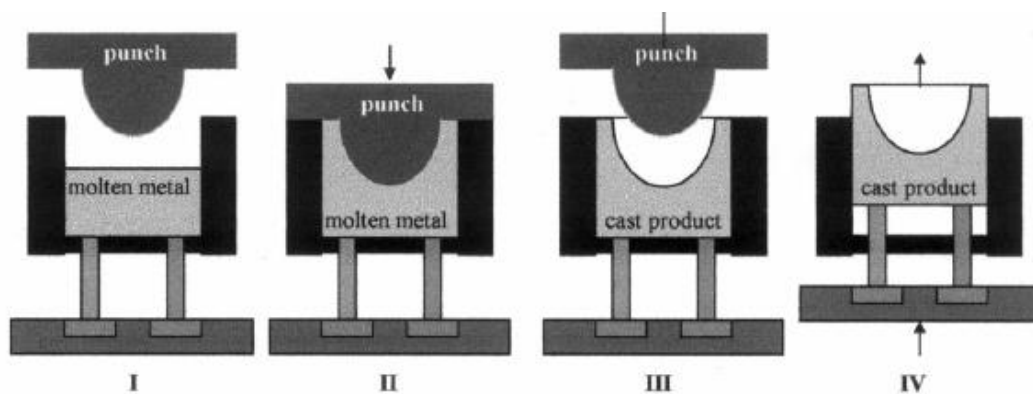


Figure 2.23 Schematic illustration of stages of direct squeeze casting method [24]

Figure 2.23 shows the application of squeeze casting to molten metal and all the stages during direct squeeze casting. Application of high pressures slowly and constantly until the end of solidification have beneficial effects in microstructure of the final product. Unlike conventional HPDC method, turbulent flow is avoided in this case and micro-shrinkage and gas porosities can be effectively eliminated, almost completely, in the microstructure which is the most crucial benefit of squeeze casting method, lower amount of porosity in squeeze cast Al-Si alloys compared to conventional casting methods is seen in figure 2.24. [24]

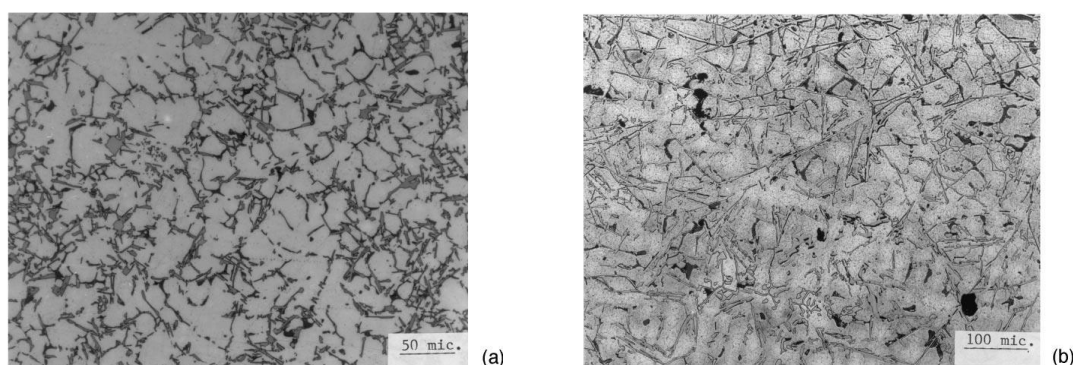


Figure 2.24 As cast microstructures of LM24 Al-Si alloy produced by
(a) squeeze casting, (b) conventional casting [24]

Squeeze casting are being used mainly in the production of mainly light-weight aluminum and magnesium alloys and the application field has been expanding thanks to many advantages that the method provides. Especially the production of metal matrix composites has been gaining importance, squeeze casting became the most popular and common method in metal matrix composite production. Various type of products used in automotive, aerospace and many other industries are being produced by squeeze casting method, some of which are seen in figure 2.25. On the basis of the information about beneficial outcomes and practicality of squeeze casting method, the process might be a good candidate for the production of semi-solid melting, i.e.

rheocasting. Although, it is commercialized in order to apply pressure onto fully molten metals, it is quite possible to use squeeze casting in the forming of semi-solid slurries which might be highly beneficial and more suitable compared to HPDC.



Figure 2.25 Various squeeze casting products

2.3. Aluminum Alloy Selection

2.3.1. Aluminum alloy series

Industrially used aluminum alloys are specified according to their series number varied from 1xxx to 8xxx series. There are various types of alloying elements within the chemical composition of different aluminum series. Table 2.3 shows aluminum series starting from 1xxx to 8xxx and the main alloying elements of these series. [1] In table 2.4, strengthening mechanism and tensile strength range of wrought aluminum alloy series are shown.

Table 2-3 Classification of wrought aluminum alloys [1]

Alloy System	Aluminum Series
Work-hardenable Alloys	
Pure Al	1xxx
Al-Mn	3xxx
Al-Si	4xxx
Al-Mg	8xxx
Al-Fe	8xxx
Precipitation-hardenable	
Al-Cu	2xxx
Al-Cu-Mg	2xxx
Al-Cu-Li	2xxx
Al-Mg-Si	6xxx
Al-Zn	7xxx
Al-Zn-Mg	7xxx
Al-Zn-Mg-Cu	7xxx
Al-Li-Cu-Mg	8xxx

2.3.2. Mechanical and thermal properties of aluminum alloys

Conventional casting methods such as gravity sand casting and high pressure die casting are thought to be detrimental for the production of wrought aluminum alloy series and therefore are not widely used for the manufacturing of these alloys. Because

of the common casting defects like hot tearing, casting of wrought aluminum alloys are generally avoided. [15] On the other hand, among all series of aluminum alloys from 1xxx to 8xxx, wrought aluminum alloy series such as 7xxx alloys are well-known and have been used due to their excellent mechanical properties, high specific strength, low density and high corrosion resistant. As mentioned previously these superior properties of such aluminum series have been successfully obtained by the solid phase forming methods like forging, extrusion, rolling, etc. Semi-solid forming of these high strength wrought alloy series, especially 7xxx, is promising since one of the important outcome of SSM of alloys is prohibiting dendritic growth and by that way decreasing casting defects.

Table 2-4 Strengthening method and tensile strength of various wrought Al alloys [1]

Aluminum Series	Alloy System	Strengthening Method	Tensile Strength Range (MPa)
1xxx	Al	Cold work	70-175
2xxx	Al-Cu-Mg (1-2.5%Cu)	Heat Treat	170-310
2xxx	Al-Cu-Mg-Si (3-6%Cu)	Heat Treat	380-520
3xxx	Al-Mn-Mg	Cold work	140-280
4xxx	Al-Si	Cold work	105-350
5xxx	Al-Mg (1-2.5%Mg)	Cold work	140-280
5xxx	Al-Mg-Mn	Cold work	280-380

	(3-6%Mg)		
6xxx	Al-Mg-Si	Heat treat	150-380
7xxx	Al-Zn-Mg	Heat treat	380-520
7xxx	Al-Zn-Mg-Cu	Heat treat	520-620
8xxx	Al-Li-Cu-Mg	Heat treat	280-560

Thermal and mechanical processing of aluminum alloys are quite essential for the mechanical and other properties. Various type of thermal and/or mechanical processes have been applied to different type of aluminum alloys, for example: 2xxx and 7xxx series are generally strengthened by post heat treatments, etc. (see in table 2.4). For international usage purposes of wrought and cast aluminum alloys, temper designation system has been developed to obtain general information about thermal and/or mechanical processes applied.

General temper designation can be seen in table 2.5. The letters such as F, O and H are used for the temper designation of aluminum alloys. The explanations of each designation letter can be seen in table 2.5.

Table 2-5 General temper designations for aluminum alloys

Temper Designation	Explanation
F (as fabricated)	F applies to products shaped by cold working, hot working, or casting processes where there is no special control over thermal conditions or strain hardening.
O (annealed)	O applies to wrought products that are annealed to obtain lowest-strength temper and to cast products that are annealed to improve ductility and dimensional stability.

H (strain hardened)	H indicates products strengthened by strain hardening, followed with or without thermal treatment to obtain some reduction in strength. H is always followed by two or more digits.
W (solution heat treated)	This is an unstable temper applicable only to alloys whose strength naturally changes at room temperature over a duration of months or even years after solution heat treatment. The designation is specific only when the period of natural aging is indicated (for example, W 12h)
T (solution heat treated)	This applies to alloys whose strength is stable within a few weeks of solution heat treatment. The T is always followed by one or more digits, as discussed in the section "System for Heat-Treatable Alloys" in this article.

Wrought aluminum alloys which are strengthened only by strain hardening is designated by H letter. When H letter is followed by two or more digits, the designation is stated as subdivision of H (see in table 2.6). First digit refers to basic operations and second digit refers to the degree of strain hardening. Wrought and cast aluminum alloys which are strengthened by heat treatment to obtain stable tempers rather than W, O or H tempers. The letter T is followed by numbers from 1 to 10 (see in table 2.7) referring specific sequence of heat treatments and the second digit refers to variation of basic heat treatment. [18]

Table 2-6 Subdivision of strain hardened ‘H’ aluminum alloys [18]

Temper Designation	Explanation
H1 (only strain hardened)	H1 applies to products that are strain hardened to obtain the desired strength without following thermal treatment.

	The digit following the H1 indicates the degree of strain hardening
H2 (strain hardened and partially annealed)	H2 indicates that the products that are strain-hardened more than the desired final amount and then reduced in strength to the desired level by partial annealing. The digit following the H2 indicates the degree of strain hardening remaining after the product has been partially annealed
H3 (strain hardened and stabilized)	H3 indicates that the products that are strain-hardened and whose mechanical properties are stabilized by a low-temperature thermal treatment or as a result of heat introduced during fabrication. Stabilization usually improves ductility. This designation applies only to those alloys that, unless stabilized, gradually age soften at room temperature. The digit following the H3 indicates the degree of strain hardening remaining after stabilization.

Table 2-7 Subdivision of solution heat treated ‘T’ aluminum alloys [18]

Temper Designation	Explanation
T1 (Cooled From an Elevated-Temperature Shaping Process and Naturally Aged to Substantially Stable Condition)	This designation applies to products that are not cold worked after an elevated-temperature shaping process such as casting or extrusion and for which mechanical properties have been stabilized by room-temperature aging.

<p>T2</p> <p>(Cooled From an Elevated-Temperature Shaping Process, Cold Worked, and Naturally Aged to a Substantially Stable Condition)</p>	<p>This variation refers to products that are cold worked specifically to improve strength after cooling from a hot-working process such as rolling or extrusion and for which mechanical properties have been stabilized by room-temperature aging.</p>
<p>T3</p> <p>(Solution Heat Treated, Cold Worked, and Naturally Aged to a Substantially Stable Condition)</p>	<p>T3 applies to products that are cold worked specifically to improve strength after solution heat treatment and for which mechanical properties have been stabilized by room-temperature aging.</p>
<p>T4</p> <p>(Solution Heat Treated and Naturally Aged to a Substantially Stable Condition)</p>	<p>This signifies products that are not cold worked after solution heat treatment and for which mechanical properties have been stabilized by room-temperature aging.</p>
<p>T5</p> <p>(Cooled From an Elevated-Temperature Shaping Process and Artificially Aged)</p>	<p>T5 includes products that are not cold worked after an elevated-temperature shaping process such as casting or extrusion and for which mechanical properties have been substantially improved by precipitation heat treatment..</p>
<p>T6</p> <p>(Solution Heat Treated and Artificially Aged)</p>	<p>This group encompasses products that are not cold worked after solution heat treatment and for which mechanical properties or dimensional stability/ have been substantially improved by precipitation heat treatment.</p>

Table 2-8 Typical mechanical properties of widely used aerospace aluminum alloys produced by extrusion[19]

Alloy	Temper	Density	Elastic Modulus	Tensile Properties		
				Yield Strength (MPa)	UTS (MPa)	% Elongation
AA2014	T6	2.80	72.4	415	485	13
AA2219	T62	2.84	73.8	290	415	10
AA2024	T4	2.77	72.4	325	470	20
AA7050	T74	2.83	70.3	450	510	13
AA7075	T6	2.80	71	505	570	11

Table 2-9 Approximate melting range and temper designation of various aluminum alloys [18]

Alloy	Approximate Melting Range		Temper Designation
	°C	°F	
1060	645-655	1195-1215	O, H18
2011	540-643	1005-1190	T3, T8
2024	500-638	935-1180	O, T3/T4, T6/T81
2618	550-638	1020-1180	T6
3004	630-655	1165-1210	All
4045	575-600	1065-1100	All
4343	577-613	1070-1135	All

5050	625-650	1155-1250	All
6005	610-655	1125-1210	T1, T5
6070	565-650	1050-1200	T6
7075	475-635	890-1175	T6
8030	645-655	1190-1215	H12 H212

2.3.3. Heat treatment of aluminum alloys

There are two types of classifications of aluminum alloys; the first classification is made according to production method. There two types of aluminum alloys depending on production method which are wrought aluminum alloys (see in table 2.3) and cast aluminum alloys. The second classification is according to heat treatability of the alloys. In this classification, there are two types of aluminum alloys which are heat treatable and non-heat treatable. Heat treatable alloys could be found in both wrought and cast aluminum series. Some wrought aluminum alloy series could also be strengthened by mechanical or thermo-mechanical processes such as strain hardening, for example: cold rolling, drawing, stretching, etc. However, cast aluminum alloys cannot be work-hardenable. That is why heat treatment process is quite essential for the strengthening of aluminum alloy castings. 1xxx, 3xxx, 4xxx and 5xxx aluminum alloy series are classified as non-heat treatable series whereas 2xxx, 6xxx and 7xxx series are heat treatable aluminum alloy series. Heat treatment of aluminum alloys consists of several heating and cooling procedures that yields to formation of stable fine precipitates in the microstructure of final products. This strengthening mechanism is called as precipitation hardening. There are several stages of precipitation hardening heat treatments for aluminum alloys; initially the alloy is heated up to a certain temperature at which solute solubility is maximized, this stage is called as solutionizing. The second stage comes just after solutionizing which is very rapid cooling of solutionized alloy, this stage is called quenching. The final stage is the

heating of alloy up to relatively lower temperatures and keeping it for definite time in order to form stable precipitates in the microstructure, the final stage is called as aging (see all in figure 2.26). [18]

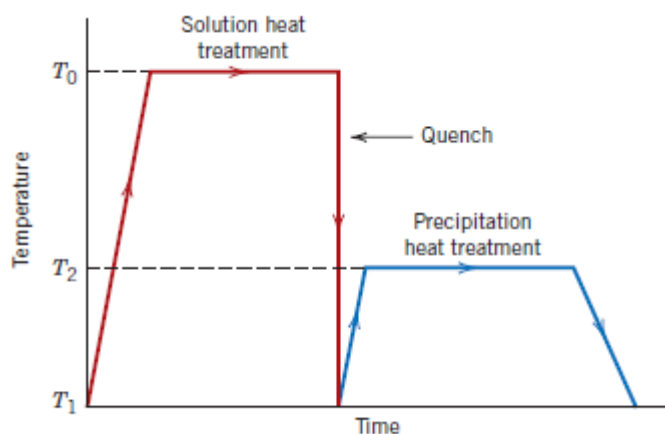


Figure 2.26 Schematic temperature vs time graph showing solution and precipitation heat treatment sequences [34]

2.3.3.1. Solutionizing

Solutionizing or solution heat treatment is a heat treatment process where the metal is heated up to a certain temperature in order to maximize the solute solubility of aluminum. Solutionizing temperature is determined in order to obtain maximum solid solubility of solute atoms in aluminum matrix. Maximum solid solubility of eutectic aluminum alloys is seen at the temperatures just below the eutectic temperatures, binary or ternary. The time duration of solution heat treatment is a critical factor that affects the formation of complete solute solution in aluminum matrix homogeneously. [18]

Solutionizing temperature of aluminum alloys has to be chosen in order not to give rise to formation of any liquid phase in the solid product. For the narrow solutionizing range aluminum alloys such as Al-Cu alloys the solution heat treatment temperature

determination is crucial, little variation in that specific temperature could result in local melting of the product. Moreover, if solutionizing temperatures are not high enough to form maximum solid solubility in aluminum matrix, the heat treatment would be inadequate and wastage. Commercial selection of solutionizing temperatures are determined by eutectic temperatures and left some margin for the safety of solid products, the differences between eutectic and solutionizing temperatures of commercial 2xxx series aluminum alloys can be seen in table 2.10. For the complex Al systems such as ternary and quaternary in the case of 7xxx series, the effects of other solute atoms are taken into consideration and ternary or quaternary eutectic points should be determined in this case. [35]

Table 2-10 Solutionizing and theoretical eutectic temperature of 2xxx series alloys

Alloy	Solutionizing Temperature (°C)	Eutectic Temperature (°C)
2014	496-507	510
2017	496-507	513
2024	488-499	502

Table 2.11 summarizes the solution heat treatment temperatures of commercial heat treatable aluminum alloy series which are 2xxx, 6xxx and 7xxx [35]. Solutionizing temperatures are varied with respect to the type of the alloy which is actually related to the chemical composition and eutectic temperatures of the alloys.

Table 2-11 Typical solution heat treatment temperature of 2xxx, 6xxx and 7xxx series alloys [35]

Alloy	Product Form	Solution Heat Treatment	
		Temp (°C)	Temper Designation
2011	Rolled rod and bar	525	T3
2025	Die forgings	515	T4
2018	Die forgings	510	T4
2024	Flat Sheet	495	T3
2024	Plate	495	T351
2024	Extruded rod, bar, tubes	495	T3
6005	Extruded rod, bar, tubes	530	T1
6061	Sheet	530	T4
6061	Drawn Tube	530	T4
6262	Rolled rod, wire and bar	540	T4
6262	Extruded rod, bar, tubes	540	T4
7050	Extrusions	475	W510
7050	Die and hand forgings	475	W511
7075	Rolled rod, wire and bar	490	W511
7075	Extruded rod, bar, tubes	465	W510
7075	Die forgings	470	W52
7175	Rolled rings	470	W
7175	Die forgings	470	W

The dimensions of the heat treated products are also important parameter in the selection of heat treatment duration or soaking time. Solution heat treatment time is key factor for the homogeneity of microstructure before quenching and the prevention of defect formation during solutionizing treatment at relatively high temperatures. Increasing the soaking time might seem to be beneficial for homogeneity of solute distribution in aluminum matrix, however the solubility of gas molecules also increases at that relatively high temperatures (400-600°C), that is why optimum amount of soaking time is required for solution heat treatment of aluminum alloys in order to prevent dissolution of any gas molecules which has negative effect on mechanical properties of final product. Especially dissolution of Hydrogen gas molecules is detrimental for 7xxx series aluminum alloys. As seen in table 2.12, soaking time gets the maximum value of 75 minutes for relatively thick samples and beyond that duration it will be detrimental for the final product. [18]

Table 2-12 Soaking time and maximum quench delay for wrought aluminum alloys [35]

Thickness (mm)	Soaking Time (minutes)				Maximum quench delay
	Air Furnace		Salt Bath		
	min	max	min	max	
<0.41	20	25	10	15	5
0.51	20	30	10	20	7
0.64	25	35	15	25	7
0.81	25	35	15	25	7
1.02	30	40	20	30	10
1.27	30	40	20	30	10

1.35	30	40	20	30	10
1.80	35	45	25	35	10
2.03	35	45	25	35	10
2.29	35	45	25	35	10
2.54	40	55	30	45	15
3.18	40	55	30	45	15
4.06	50	60	35	45	15
4.57	50	60	35	45	15
6.35	55	65	35	45	15
>6.35	65	75	45	55	15

2.3.3.2. Quenching

Quenching is one of the most important heat treatment stage of aluminum alloys. Quenching can be described as sudden cooling of samples by means of materials having high heat transfer coefficients. The quenching medium could be water, oil or salt, or the combination of different materials with these medium. By rapid cooling down to low temperatures as room temperature basically retards the diffusion of solute atoms and preserves the solution of aluminum having maximum solute solubility at high temperatures which is named as supersaturated solid solution. Quenching not only preserves high temperature solid solution, but also leads to formation of vacant sites at which helps solute atoms to nucleate and form precipitates at relatively low temperatures. [18] [35] Quenching stage just follows the solution heat treatment. aluminum alloys at solutionizing temperatures is quenched generally to room temperature. The quenching must be carried out rapid enough that yields to

supersaturated solid solution at room temperature which is the optimal condition for following heat treatment ‘aging’. The time passes as solutionized alloy contacts with the quench medium is called the delay time. The delay time is another important parameter for obtaining well-quenched super saturated solid solution. In the case of elapsing maximum delay time for the quenching of aluminum alloys, there is a risk of formation of undesired precipitates at medium temperatures. [18] Delay time also varies with the thickness of the sample and increases as the thickness increases as seen in table 2.12. Some practical cooling curves for different medium in quenching of 7075 alloy is seen in figure 2.27. [35]

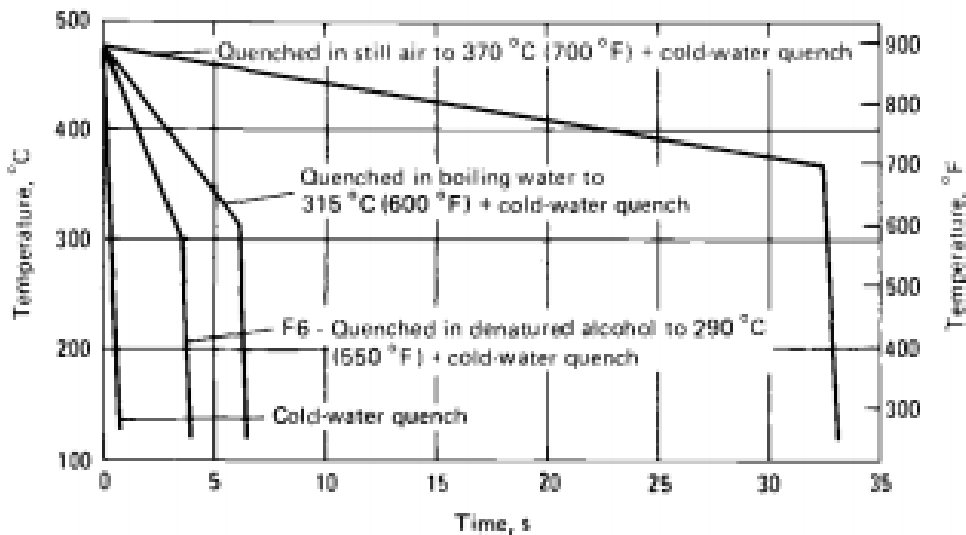


Figure 2.27 Cooling curves for 7075-T6 sheets for quenching [35]

2.3.3.3. Age hardening

After quenching stages of heat treatment, hardening of the alloy is promoted by two ways. Either the hardening takes place at room temperature, in this case it is called as ‘natural aging’, or it can be hardened by precipitation treatment at relatively lower temperatures which is called as ‘artificial aging’. For some aluminum alloys such as 2xxx series, precipitation occurs at room temperatures within a few days which result

in commercially usable stable products. Thus, there is a risk of premature hardening of 2xxx alloys, i.e. these alloys have the risk to harden and increase their strength before any shaping process which is undesirable for industrial applications. In order to prevent undesired hardening before forming operations take place 2xxx series aluminum alloys are kept at -18°C , even down to -40°C , which delays the aging process and provides safety until complete manufacturing of the product. Figure 2.28 shows the tensile strength change of 3 different aluminum alloys in time; 2024, 6061 and 7075. Among them 2024 requires quite shorter period to get harden and strong at low temperatures. [35]

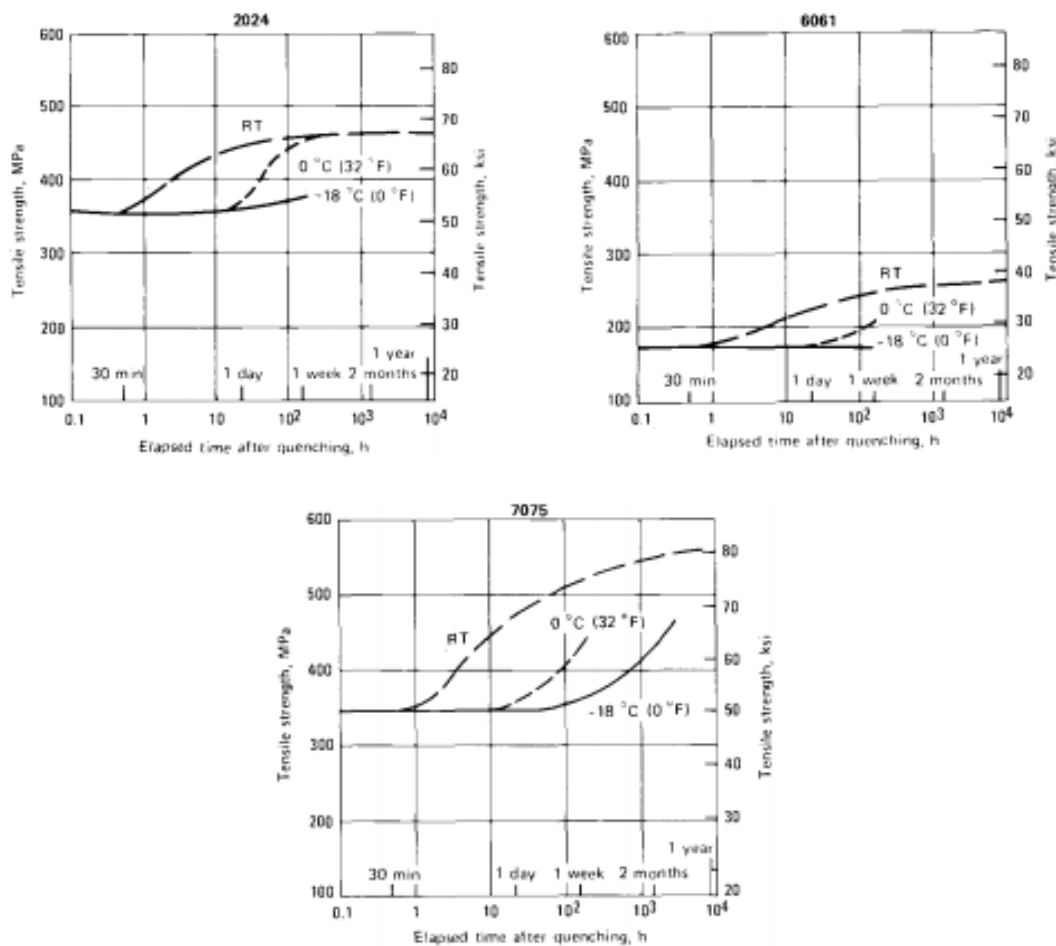


Figure 2.28 Aging characteristics of sheet aluminum alloys at various temperatures [35]

On the other hand, some aluminum alloys are required to be heat treated by precipitation hardening at relatively lower temperatures within long terms. After quenching, supersaturated solution is heated up to temperatures between 115°C-190°C for about 5 to 48 hours. At that temperatures solute atoms have tendency to diffuse and form clusters at grain boundaries, dispersoids or vacancies. The diffusion of solute atoms into these clusters forms GP zones which are metastable. In progress of time, GP zones turn into coherent precipitates with little lattice mismatch forming strain fields around them and by that way dislocation movement is hindered. Therefore, formation of coherent or semi-coherent precipitates in long period of time results in the increase in strength and hardness of aluminum alloys which is called precipitation hardening. In addition to aging temperature, other important parameter is the aging time. Excess amount of aging process or over-aging of aluminum alloys actually causes to decrease in both strength and hardness due to growth of semi-coherent precipitates and ineffective dislocation hindering of larger precipitates. After reaching critical time at defined aging temperature, aluminum alloys start to lose hardness and strength as seen in figure 2.29 for 6061 aluminum alloy strength variation in different temperatures [35] Optimum temperatures and aging times for precipitation heat treatment is seen in table 2.13 [35] for different heat treatable aluminum alloy series.

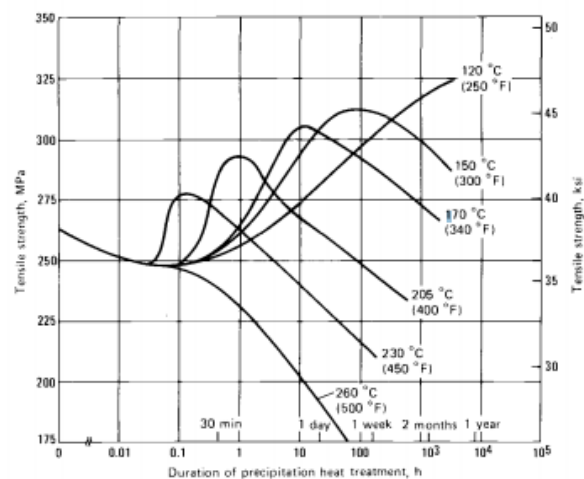


Figure 2.29 Tensile strength variation of 6061 alloy sheets during aging at different temperatures [35]

Table 2-13 Typical precipitation heat treatment temperature of 2xxx, 6xxx and 7xxx series alloys

Alloy	Product Form	Precipitation Heat Treatment		
		Temp (°C)	Time	Temper Designation
2011	Rolled rod and bar	160	14	T8
2025	Die forgings	170	10	T6
2018	Die forgings	170	10	T61
2024	Flat Sheet	190	9	T62
2024	Plate	190	12	T851
2024	Extruded rod, bar, tubes	190	12	T81
6005	Extruded rod, bar, tubes	175	8	T5
6061	Sheet	170	10	T6
6061	Drawn Tube	175	8	T62
6262	Rolled rod, wire and bar	170	8	T6
6262	Extruded rod, bar, tubes	175	12	T651
7001	Extruded rod, bar, tubes	120	24	T62
7005	Extruded rod, bar, tubes	120	24	T53
7075	Rolled rod, wire and bar	120	24	T6
7075	Extruded rod, bar, tubes	120	24	T6
7075	Die forgings	120	24	T6
7175	Rolled rings	120	24	T6

2.3.4. High strength 7075 aluminum alloy

7075 alloys are 7xxx series aluminum alloys having 3 main alloying elements which are zinc (5-6%), magnesium (2-3%) and copper (1-2%), there are several alloying elements in addition as seen in table 2.14. [16] 7075 alloys are heat treatable wrought alloys having superior mechanical properties among all series of aluminum alloys. As it can be seen in table 2.8, high strength of heat treated 7075 alloy could reach up to 600 MPa which is quite high even among aluminum alloys. Thanks to their superior mechanical properties, i.e. high specific strength, low density and corrosion resistance 7075 alloys are widely used in automotive, defense and aerospace industries generally in structural parts. Some of these structural parts such as fuselage stringers, frames and seat rails which require high strength and low density are produced by extrusion of 7075 alloy (see in table 2.15). [17]

Table 2-14 Chemical composition of 7075 alloy in wt.% [16]

Element	Si	Fe	Cu	Mn	Mg	Cr
wt. %	0.40	0.50	1.2-2.0	0.30	2.1-2.9	0.18-0.28
Element	Zn	Ti	Al			
wt. %	5.1-6.1	0.20	Remainder			

Table 2-15 Various 7xxx series aluminum alloy parts used in aerospace industry [17]

Production Method	Strength Level	Alloy/Temper	Application
Extrusions	Medium/High Strength	7075-T73511	Fuselage stringers and frames, upper wing stringers
		7075-T79511	
		7150-T6511	

7175-T79511	floor beams, seat
7055-T77511	rails
7055-T79511	

As stated in previous chapters rheocasting, a SSM method, became suitable for the production of high strength light-weight alloys in an effective way. For the selection of the material and production routes for rheocasting method, slurry preparation and forming, it is quite essential to determine the alloy with favorable mechanical and thermal properties. 7075 aluminum alloys provide both excellent mechanical properties, having yield strength up to 600 MPa for wrought alloys (see in table 2.8), and thermal properties such as wide freezing range (475-635°C) compared to other aluminum alloys having narrow freezing range (see in table 2.9). Besides, T6 heat treatment processes which consist of solution heat treatment followed by quenching and artificial aging applied to wrought 7075 alloys are quite suitable for the casting of these alloys. Therefore, rheocasting of 7075 alloy is the main focus of this study and the thermal, mechanical and microstructural characteristics of 7075 alloy in addition to characterization will be informed in the scope of this study.

2.3.4.1. Phase transformations and solidification characteristics

Phase formations and precipitation are quite essential for wrought 7075 aluminum alloys since the most important strengthening mechanism is the precipitation hardening. The size and the morphology of the phases are mainly affected by solidification and heat treatment processes. 7075 alloy is relatively complex quaternary system having 3 alloying element which are Zinc, Magnesium and Copper, in addition to these elements the alloy also contains Chromium, Silicon, Iron and Manganese which makes difficult to determine the phase transformations. [36] By several thermal analysis and EDS analysis methods, Backerud et al. [37] have

conducted a study related to phase transformations during solidification of commercial 7075 alloy with different cooling rates. The observation in the study was that after the formation of aluminum dendritic matrix starting from 630°C to 620°C, intermetallic compounds Al_3Fe and Mg_2Si transform. At the end of the solidification eutectic reaction takes place from very little amount of liquid present at about 470°C and Al_2Cu and MgZn_2 precipitates transform (see in table 2.16). There are also trace amount of phases such as $\text{Al}_{18}\text{Mg}_3\text{Cr}_2$ (called E-phase) and $\text{Al}_2\text{Mg}_3\text{Zn}_3$ (called T-phase). [36] The fine precipitates of Al_2Cu and MgZn_2 are quite essential for obtaining high strength 7075 alloy after T6 heat treatment which will be discussed later on.

Table 2-16 Phase transformations during solidification with different cooling rates [36]

Phase Transformation		Cooling rates (K/s)		
		0.3	0.7	2.3
1st reaction	$\text{Liq} \rightarrow \text{Al Dendrites}$	630-623 °C	630-622 °C	628 °C
2nd reaction	$\text{Liq} \rightarrow \text{Al} + \text{Al}_3\text{Fe}$	618-615 °C	606-601 °C	
3rd reaction	$\text{Liq} \rightarrow \text{Al} + \text{Mg}_2\text{Si}$	568-563 °C	566-561 °C	558-550 °C
4th reaction	$\text{Liq} \rightarrow \text{Al} + \text{Al}_2\text{Cu} + \text{MgZn}_2$	469 °C	470 °C	466 °C

Figure 2.30 shows the liquid fraction as temperature changes derived from DSC heating curve results in the study of Bolouri et al. [41]. Liquid fraction change curve

gives crucial information about the working range of semi-solid melting of 7075 alloy. It will be discussed in the next chapters in detail that the amount of solid fraction during forming stage of rheocasting process plays important role on final microstructure and mechanical properties. Moreover, there is also a common value of optimum solid fraction for the highest mechanical properties for semi-solid slurry shaping which is accepted by many studies in the literature.

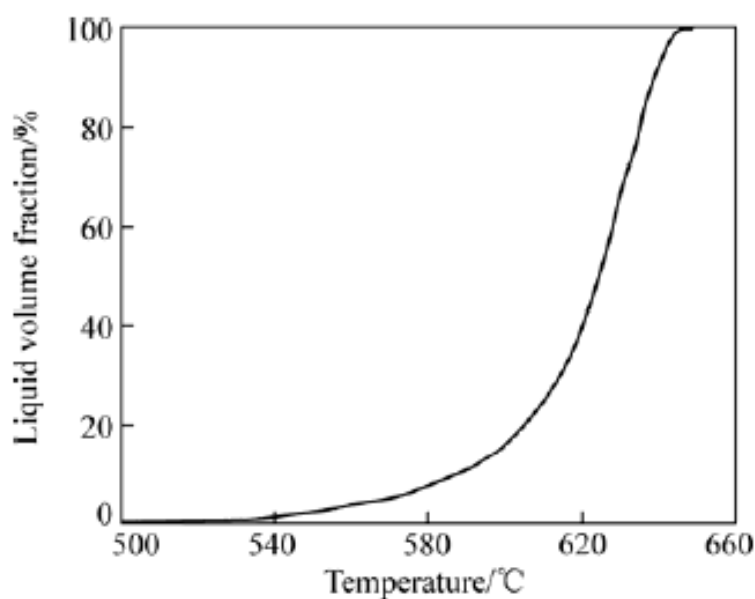


Figure 2.30 Liquid fraction of 7075 alloy vs temperature curve estimated by DSC heating curves [41]

2.3.4.2. Microstructural evolution and characterization

In microstructural evolution of 7075 alloy, many characterization methods should be used, in fact XRD, SEM, EDX and TEM are some of these characterization method to reveal the microstructure. As stated before, fine precipitates Al_2Cu and MgZn_2 plays important role on the high strength of the alloy. In a thesis study of Durmaz [38] Al_2Cu precipitates in 7075 alloy could be detected by EDX spectroscopy in scanning electron microscope as seen in figure 2.31. SEM images of the precipitates are about in the order of several micro meters (see in figure 2.31). On the other hand, in the same

study, $MgZn_2$ precipitates could not be detected neither by SEM-EDX method nor by XRD measurements as seen in figure 2.33 and 2.34. The reason is addressed in the literature to the sub-micron, even under 100 nano meter, particle size of $MgZn_2$ precipitates. Thus, characterization of 7075 alloy under transmission electron microscopy plays important role here for the detection of $MgZn_2$ precipitates. There are various attempts on TEM study of 7075 alloy in the literature.

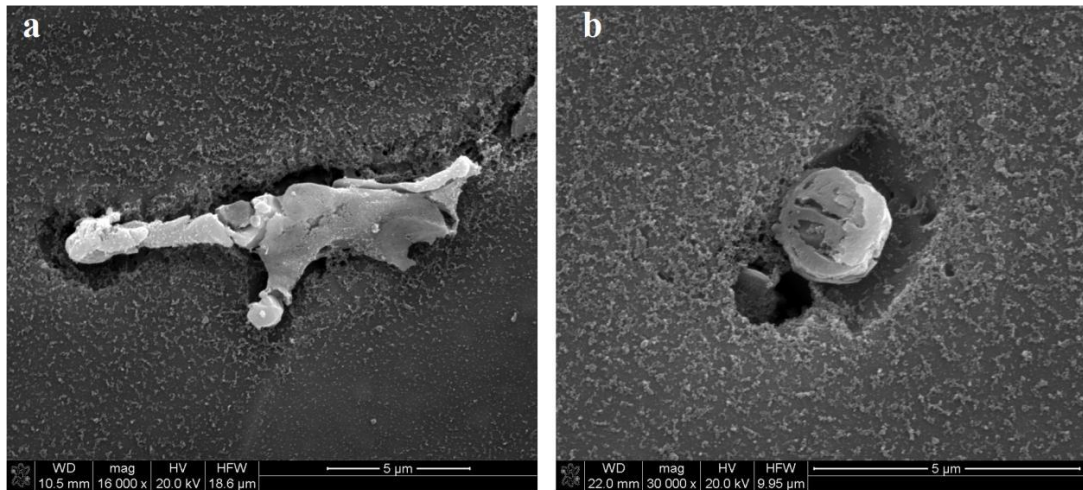


Figure 2.31 SEM images of Al_2Cu precipitates [38]

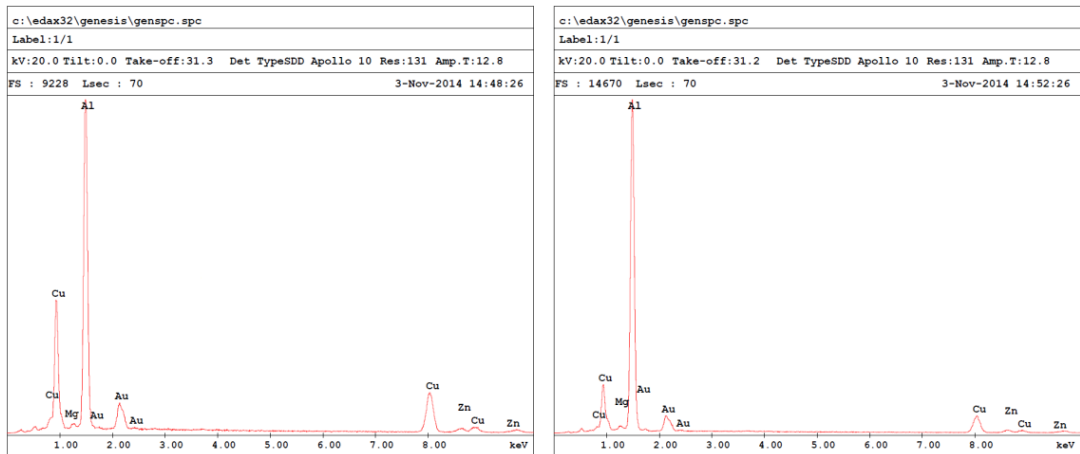


Figure 2.32 EDX spectrometry results of Al_2Cu precipitates in figure 28 [38]

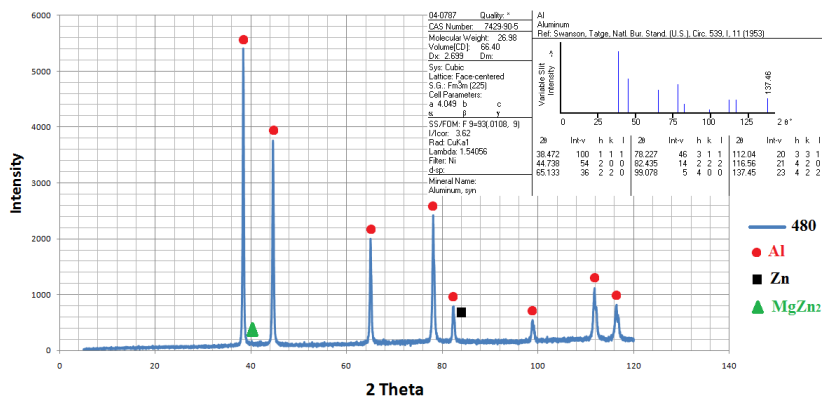


Figure 2.33 XRD peaks of squeeze cast and T6 heat treated 7075 alloy [38]

One of the research related to microstructural observation of $MgZn_2$ precipitates was conducted by Aoba et al. [39], they applied solution heat treatment and multi-directional forging to conventional 7075 alloy and characterized under TEM. They determined the size of semi-coherent $MgZn_2$ precipitate, generally named as η' in the literature, even below 10nm for the artificially aged samples as seen in figure 2.34. In another study related to friction stir welding of 7075 alloy, Kumar et al. [40] detected fine $MgZn_2$ precipitates under TEM as seen in figure 2.35. The particles size of the precipitates in T6 heat treated alloy is between 10-30 nano meter in this study.

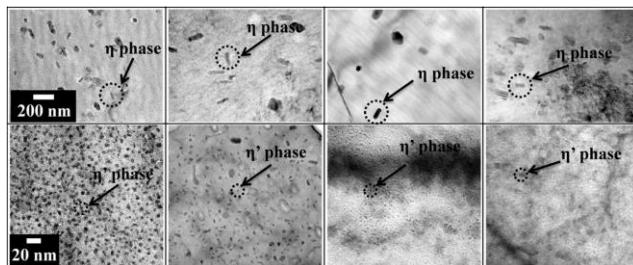


Figure 2.34 TEM images of solution heat treated and multi- directionally forged 7075 alloy artificially aged in the left and naturally aged in the right side [39]

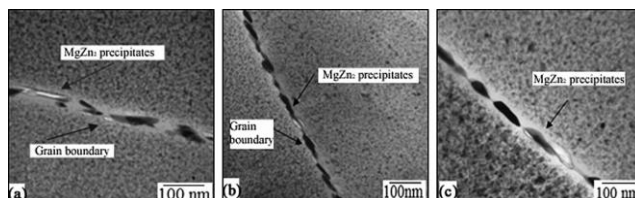


Figure 2.35 TEM images of 7075 alloy (a) as-received (b) T6 treated (c) RRA [40]

2.3.5. Calculation of solid fraction for SSM process

Rheocasting method rely on the semi-solid casting of the alloys as mentioned previously. As the name 'semi-solid' suggest, a semi-solid slurry contains some amount of solid fraction in it and the rest is liquid. Determining the amount of solid fraction in the semi-solid slurry is crucial for the final forming stage of rheocasting process since fraction of solid in the slurry is significant factor for the viscosity and the castability of semi-solid alloys. Thus, many of the rheocasting studies focused on solid fraction calculation before the production of 7075 alloys by rheocasting method. Yang et al. [20] and Curle et al. [21] determined the solid-fractions before rheocasting experiments of 7075 alloy and observed that the optimum mechanical properties were obtained by using semi-solid slurry with about 0.3 solid fraction.

There are several methods for solid fraction calculation of metals and alloys in the literature. Sim et al. [44] used Thermo-Calc computer program which requires various thermodynamic properties such as latent heat of fusion and heat capacity in order to calculate solid fraction with respect to melting temperature range. Similarly, Vijayan et al. [45] calculated the solid fraction of Al-Si alloys by using JMatPro computer program. On the other hand, there are also some mathematical models based on the calculation of solid-fraction on the cooling curves of the alloys. Emadi et al. [46] summarized these models in their study and explained Newtonian and Fourier methods. These two methods include several steps in order to calculate solid fraction. First of all, thermal analysis of the alloy should be carried out by recording the temperature of fully molten alloy until solidification finishes. Afterwards, the cooling curve and the first derivative of the cooling curve should be fitted. Once the first derivative is fitted, there are two options; either Newtonian base line is fitted under the first derivative by using polynomial fit or Fourier base line is fitted under the first derivative by Fourier fit method. The comparison of two methods are shown in figure 2.36. The final step is to integrate the area between cooling curve and the base lines or zero curves according to the formula [47];

$$F S_i = \frac{\int_0^{t_i} \left[\left(\frac{dT}{dt} \right)_{cc} - \left(\frac{dT}{dt} \right)_{zc} \right] dt}{\int_0^{t_f} \left[\left(\frac{dT}{dt} \right)_{cc} - \left(\frac{dT}{dt} \right)_{zc} \right] dt}$$

Where $\left(\frac{dT}{dt} \right)_{cc}$ represents the first derivative and $\left(\frac{dT}{dt} \right)_{zc}$ represents zero curve of Newtonian or Fourier base line [47]. Comparison of solid fractions with respect to time is shown in figure 2.37 where there is no much differences.

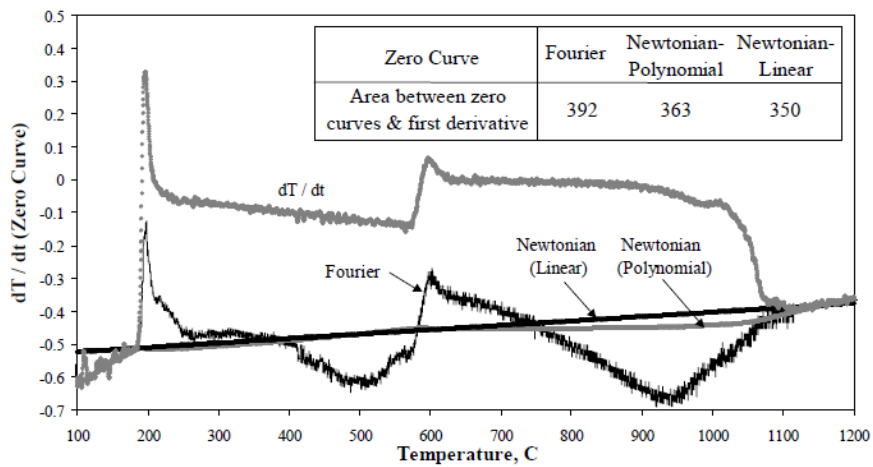


Figure 2.36 Comparison of polynomial and linear Newtonian and Fourier base lines for Al-7%Si alloy [46]

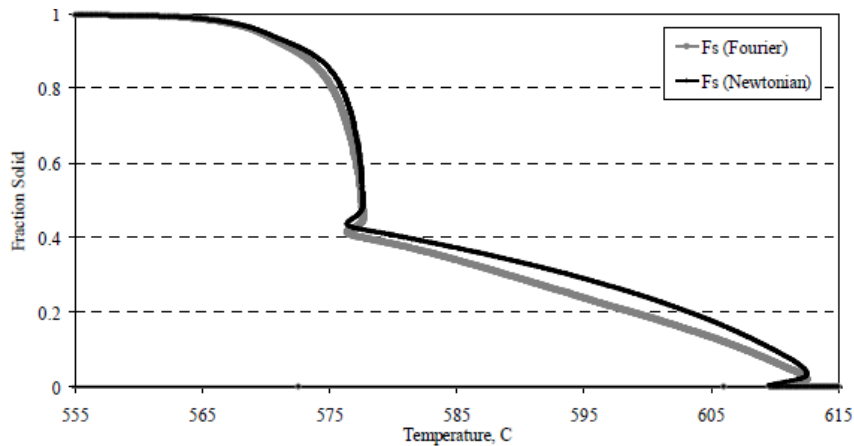


Figure 2.37 Comparison of solid fractions by Fourier and Newtonian methods [46]

CHAPTER 3

LITERATURE REVIEW

In this chapter, there will be literature studies related to rheocasting of 7075 alloys and the effect of different slurry preparation and forming techniques on the mechanical properties and the microstructure of the alloy. There are great number of researches focusing on semi-solid melting of aluminum alloys, in the literature, some of which studied the rheocasting of 7075 alloys whereas many more researchers related to thixocasting or thixoforming of 7075 alloys. On the other hand, there are many researchers mainly studied only the effect of different type of stirring or vibration on only the microstructure of rheocast 7075 alloys. Some of the researches only focused on heat treatment of 7075 rheocasting alloys. Likewise, many research has been conducted related to the effect of rheocasting on 7075 alloys in the aspect of only thermal properties or only mechanical properties.

In the scope of this thesis study, literature studies directly related to rheocasting of 7075 aluminum alloy and the mechanical, thermal and microstructural evaluation of the results of literature works will be shown. There will be four study covering mechanical and thermal property investigation of 7075 aluminum alloy produced by rheocasting whereas one study covering rheocasting of 7075 aluminum alloy matrix composite.

3.1. Rheocasting of 7075 Alloy

In a study related to rheocasting of 7075 alloy, Yang et al. [20] used inverted cone shape pouring channel which they called as ICSPC method to obtain the semi-solid slurry and applied high pressure die casting to their semi-solid slurries with different pouring temperatures and die pressures, schematic illustration of ISPC and HPDC system used in the study is seen in figure. In this study, the variables that were changed are SSM temperatures and injection pressure of HPDC machine. The objective was the observation of the effect of SSM temperature or simply solid fraction and the pressure on the microstructure and the mechanical properties of rheocast 7075 alloy. Schematic illustration of ISPC process for semi-solid slurry preparation and following HPDC for the forming of the slurry are shown in figure 3.1. The chemical composition of commercial 7075 alloy is in the standard ranges; 5.9% Zn, 2.2% Mg, 1.7% Cu, 0.35% Fe, 0.1% Si and balance aluminum by weight. After preparation of semi-solid slurry in ICSPC slurry maker, the slurry was transferred to temperature controlled crucible in which casting (SSM) temperature is adjusted. Then, the semi-solid slurry at desired casting temperature is poured into shot chamber of HPDC machine followed by injection of the slurry. Four different temperatures which were 630, 628, 626 and 624°C with three different injection pressure 60, 90 and 120 MPa were the variables in the study as seen in table 3.1. The final samples are the tensile test specimens in plate form. They applied T6 heat treatment to the tensile test specimens which is composed of simply solution treatment at 470°C for 1 hour followed by quenching and aging at 120°C for 24 hours.

Table 3-1 Rheocasting casting temperature and injection pressure information [20]

Process	Pouring Temp (°C)	Casting Temp (°C)	Injection Pressure (MPa)
Conventional HPDC	660	630	60
ICSPC		628	60
(Rheocasting)	660	626	60
		626	90
		626	120
		624	60

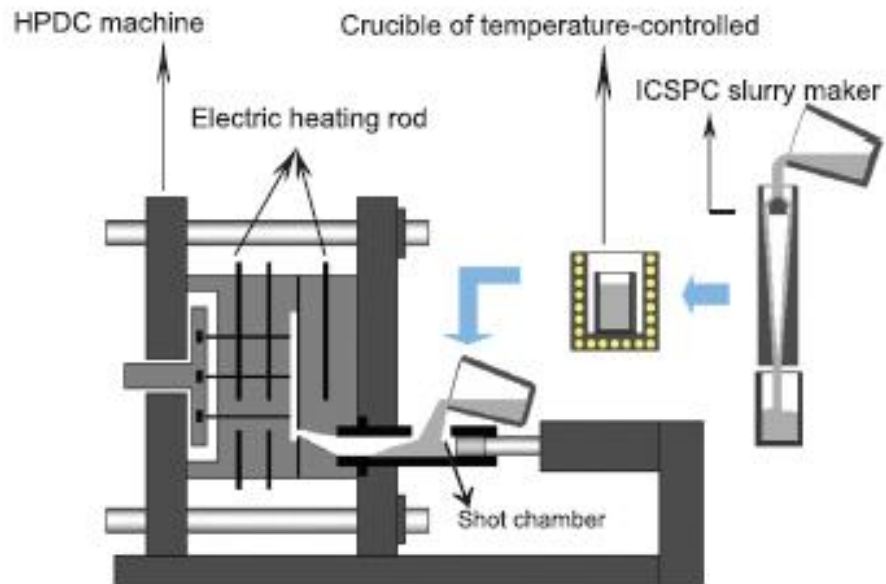


Figure 3.1 Schematic illustration of ISPC process followed by HPDC [20]

As cast microstructures of rheocast samples are seen in figure 3.2. The first image corresponds to the microstructure of conventional HPDC which has no semi-solid slurry were prepared. The others are the microstructures of rheocast samples with different casting temperatures and injection pressures. The important conclusion is that by decreasing casting temperature or increasing solid fraction at the same time resulted in successful transformation of dendritic morphology in conventional HPDC (see in figure 3.2 a) into globular grain structure (see in figure 3.2 g). Similarly, increasing pressure above from 60 MPa to 120 MPa also favored the globular grain formation.

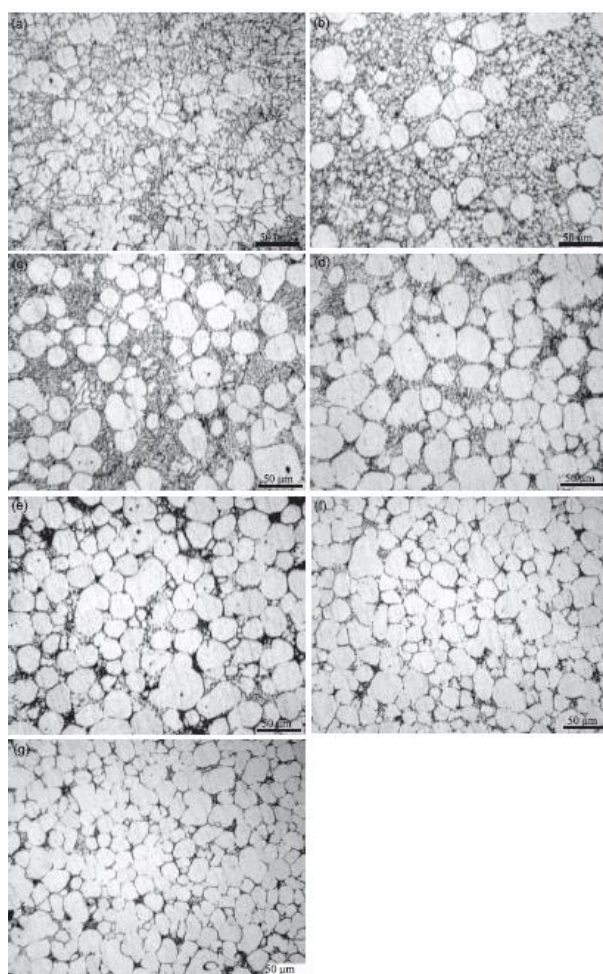


Figure 3.2 As cast microstructure of 7075 alloy produced by; (a) conventional HPDC, (b) ISPC process with 630°C casting temperature and 60 MPa injection pressure, (c) ISPC process with 628°C casting temperature and 60 MPa injection pressure, (d) ISPC process with 626°C casting temperature and 60 MPa injection pressure, (e) ISPC process with 624°C casting temperature and 60 MPa injection pressure, (f) ISPC process with 626°C casting temperature and 90 MPa injection pressure, (g) ISPC process with 626°C casting temperature and 120 MPa injection pressure [20]

Tensile test results of conventional high pressure die cast and rheocast samples, which were produced by 120 MPa injection pressure, are shown in table 3.2. The conclusion of the tensile test was that by decreasing casting temperature to a limit tensile strength shows increasing behavior whereas elongation has decreasing behavior. Moreover, the highest UTS values (up to 489 MPa) were obtained from the T6 heat treated samples having 626°C casting temperature. Therefore, it could be said that increasing solid fraction up to a limit gave the best results, 26.5 % solid amount in semi-solid slurry in this case.

Table 3-2 Tensile test results of as-cast and T6 heat treated 7075 alloy produced by conventional HPDC and rheocasting with different casting temperatures [20]

Process	Pouring Temp (°C)	Casting Temp (°C)	Solid fraction (%)	UTS (MPa)		Elongation (%)	
				As-cast	After T6	As-cast	After T6
Conventional HPDC	660			227.0-		5.55	
				243.3			
ICSPC (Rheocasting)	660	630	9.6	286.0-	459.9-	3.05	2.55
				297.4	474.1		
		628	17.9	288.2-	462.3-	2.85	2.20
				301.3	481.4		
626	26.5	293.1-	461.6-	1.65	1.20		
		299.5	489.5				
		624	34.6	275.9-	435.5-	1.05	0.75
				294.1	453.6		

In the study of Curle et al. [21], three different wrought aluminum alloys one of which was 7075 alloy were produced by rheocasting method. Induction stirring with simultaneous forced air cooling (CSIR-RCS) was chosen to produce semi-solid slurry and HPDC was used to form the final shape of semi-solid slurries of three different alloys. Commercial aluminum alloys of 2024, 6082 and 7075 were used, chemical compositions of the alloys are shown in table 3.3. The alloys were melted in tilting induction furnace after which they were transferred into stainless steel processing cup in which semi-solid slurry was prepared by CSIR-RCS technique. Optimum solid fraction for semi-solid slurries are determined as 0.30 and SSM temperatures of 0.30 solid fraction were found by ProCast computer program as seen in table 3.4. Liquid alloys were processed until the temperatures reached predetermined SSM temperatures which are measured by thermocouples. Then, the semi-solid slurries were transferred into the cavity of HPDC machine manually and forming operation were carried out to give the final shape. As cast alloys were T6 heat treated, heat treatment information is shown in table 3.5.

Table 3-3 Chemical compositions of three commercial wrought aluminum alloys (weight %) [21]

Alloy	Zn	Mg	Cu	Si	Mn	Cr	Fe
2024	0.06	1.07	4.14	0.07	0.60	0.01	0.15
6082	0.10	0.89	0.05	0.92	0.49	0.03	0.32
7075	5.79	2.38	1.43	0.23	0.14	0.16	0.21

Table 3-4 Calculated liquidus, solidus temperatures and deduced rheocasting parameters for three wrought aluminum alloys [21]

Alloy	Temperature (°C)			
	Liquidus	Solidus	Pouring	SSM
2024	644	500	680	636.5
6082	649	553	690	645.3
7075	635	486	670	622.8

Table 3-5 T6 heat treatment parameters for rheocast aluminum alloys [21]

Alloy	Solution Heat Treatment		Artificial Aging	
	Temperature (°C)	Time (hours)	Temperature (°C)	Time (hours)
2024	480	14	190	12
6082	540	2	177	10
7075	475	4	120	24

Microstructure of rheocast 7075 alloy is seen in figure 38. As cast microstructure (figure 3.3-a) shows that rheocasting successfully transformed the microstructure into globular grains and some amount of eutectic phase (seen as black dots). These finely distributed black dots corresponds to eutectic regions as seen in figure 3.3-c, and by solution heat treatment finely distributed eutectic phases could lead to incipient melting and formation of local porosities around eutectic phases. Table 3.6 shows the tensile test results of rheocast alloys, the highest tensile strength was achieved by rheocasting of 7075 allow which is 513 MPa. Poor elongation values are directly associated with local porosity due to solution treatment in the study. [21]

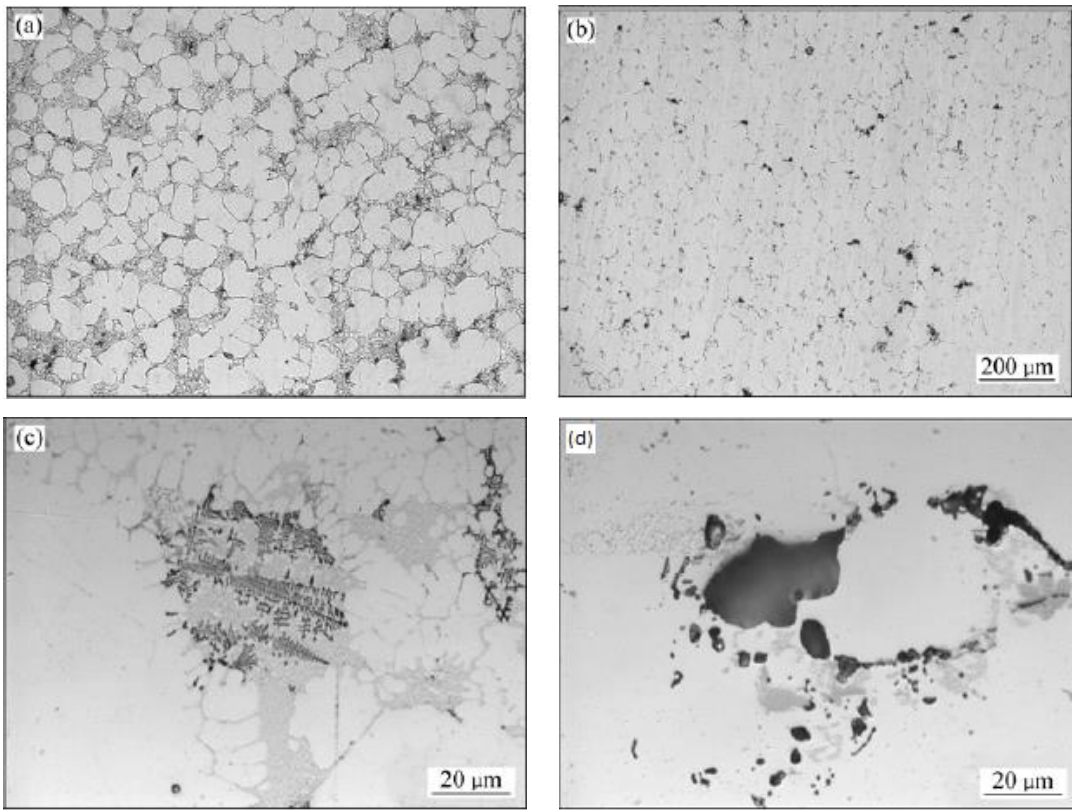


Figure 3.3 Optical micrographs of 7075 alloy; (a) as-cast F-condition, (b) T6 heat treated, (c) eutectic area in F condition, (d) eutectic area in T6 condition [21]

Table 3-6 Tensile properties of rheocast and T6 heat treated alloys [21]

Alloy	Yield Strength (MPa)	UTS (MPa)	Elongation (%)
2024 T6	351	385	5.1
6082 T6	341	365	3.6
7275 T6	467	513	3.2

In another study of Curle et al. [42], 7075 alloys were rheocast by again induction stirring (CSIR-RCS) in order to prepare semi-solid slurry followed by HPDC of the slurries. Chemical composition of three different batch of 7075 alloy is seen in table 3.7. In this study, the effect of Al-5%Ti-1%B master alloy addition on the microstructure and the mechanical properties of rheocast 7075 alloys were investigated. 622.8°C was chosen as SSM temperature which corresponds to 0.30 solid fraction in the slurry. T6 heat treatment was applied to each rheocast samples which was consist of solution treatment at 475°C for 4 hours followed by artificial aging at 120°C for 24 hours.

Table 3-7 Chemical composition of each batch of grain refined 7075 alloys [42]

Alloy	Zn	Mg	Cu	Cr	Ti	B
1	5.79	2.38	1.43	0.16	0.03	0.0015
2	5.68	2.36	1.44	0.17	0.13	0.0141
3	5.42	2.23	1.34	0.16	0.29	0.0417

Microstructures of rheocast samples with different grain refinement (Al-5Ti-1B master alloy) additions are shown in figure 3.4. As seen in the figure, the grain refinement was successfully achieved by increasing the amount of Al-5Ti-1B master alloy addition and the finest globular grain structure was obtained in rheocast 7075 alloy sample with 0.29% Ti in the microstructure. The ultimate tensile strength values of rheocast samples in T6-condition were quite close to each other which was around 516 MPa. However, increasing behaviour of elongation percent of the samples were observed as the amount of grain refinement increases, the highest elongation was obtained from the samples having 0.29% Ti addition. The reason for an increase in elongation was directly addressed to lower amount of pores with smaller in size in the eutectic regions.

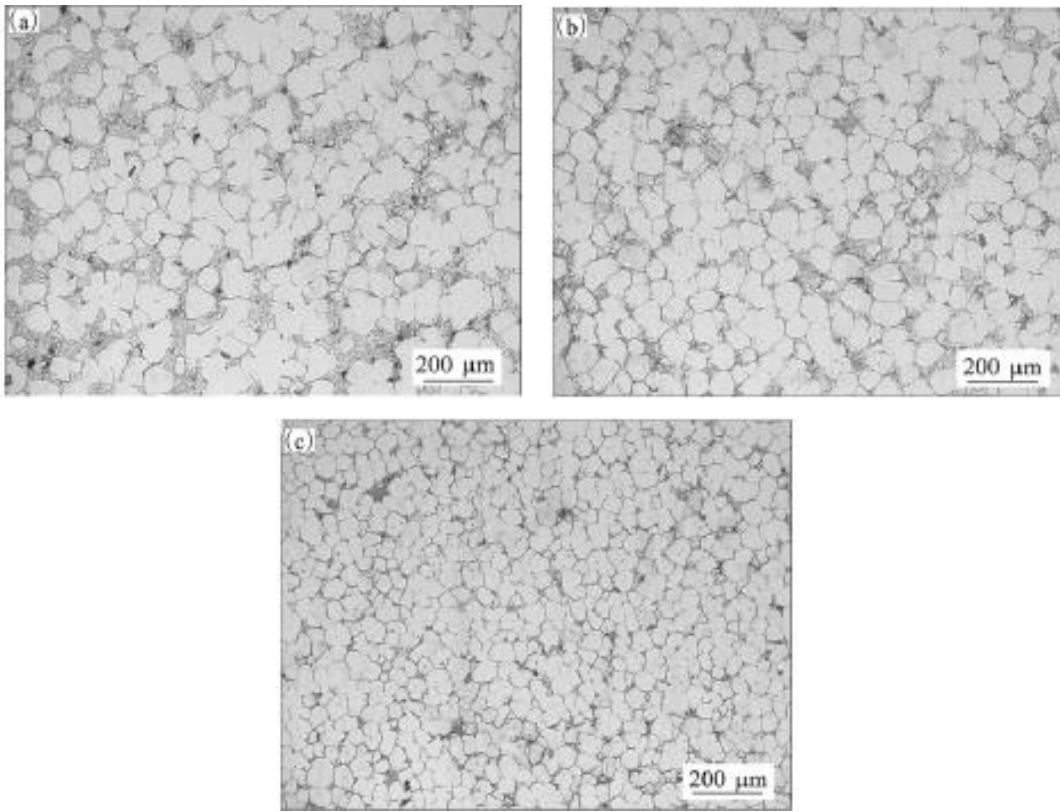


Figure 3.4 Optical micrographs of rheocast 7075 alloys in F-condition with grain refinement value of (a) 0.03% Ti, (b) 0.13% Ti, (c) 0.29% Ti [42]

Table 3-8 Tensile properties of rheocast 7075 alloys with different grade of grain refinement in T6 condition [42]

Alloy	Yield Strength (0.2% offset-MPa)	UTS (MPa)	Elongation (%)
1	467	513	3.2
2	458	516	4.5
3	453	516	5.3

Mahathaninwong et al. [43] investigated the effects of T6-heat treatment parameters on the microstructure and mechanical properties of rheocast 7075 alloy. Gas induced semi-solid (GISS) technique was used to prepare semi-solid slurries which is basically blowing gas bubbles into the molten alloy, gas induced stirring was applied for 30 seconds at 643°C. After the preparation of the slurry, squeeze casting operation was carried out in order to give the final shape of the samples. Chemical composition of rheocast 7075 alloys were; 6.08% Zn, 2.5% Mg, 1.93%Cu, 0.46% Fe, 0.4%Si in weight percentage. T6 heat treatment with different parameters was applied to as-cast samples. 450°C and 480°C were chosen as two different solution treatment temperature whereas artificial aging was applied to the samples for 1, 4, 8 and 12 hour durations.

Figure 3.5 shows SEM micrographs of rheocast samples with different heat treatment procedures. As SHT time increases the amount of the eutectic phase in grain boundaries decreases (figure 40 b-e) compared to as-cast sample (figure 3.5-a).

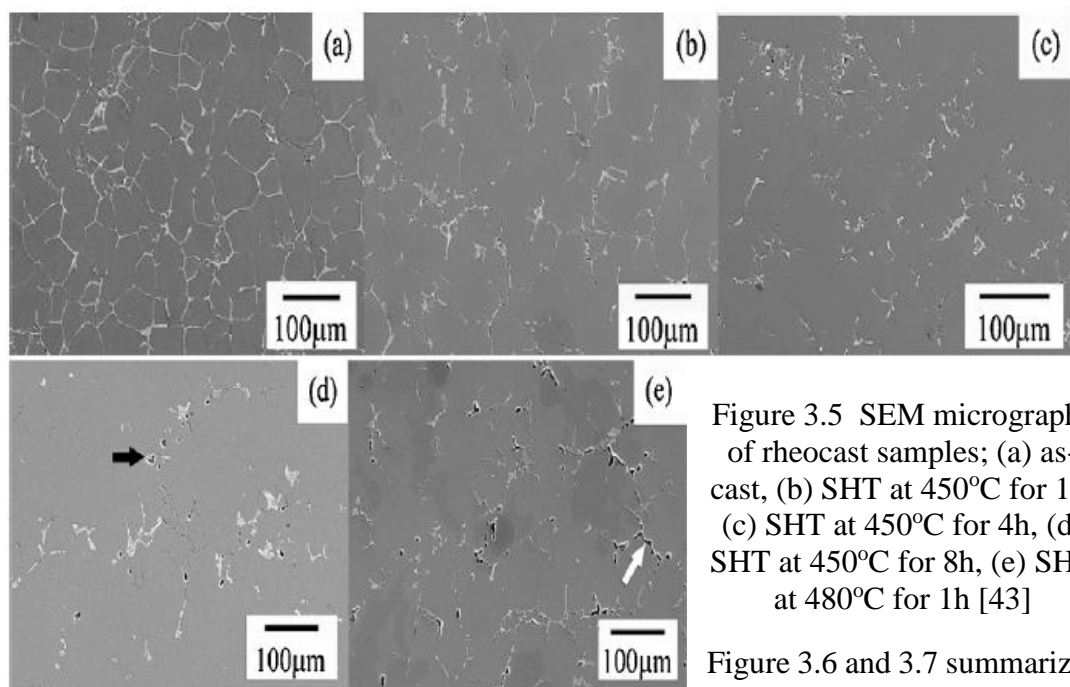


Figure 3.5 SEM micrographs of rheocast samples; (a) as-cast, (b) SHT at 450°C for 1h, (c) SHT at 450°C for 4h, (d) SHT at 450°C for 8h, (e) SHT at 480°C for 1h [43]

Figure 3.6 and 3.7 summarizes the mechanical properties of rheocast samples in the study. The highest strength, which was 486 MPa, was obtained from the sample with 120°C aging temperature and

72 hours aging time (see in figure 3.6). Similarly, highest hardness value was also obtained from the same sample (120°C for 72hours, see in figure 3.7).

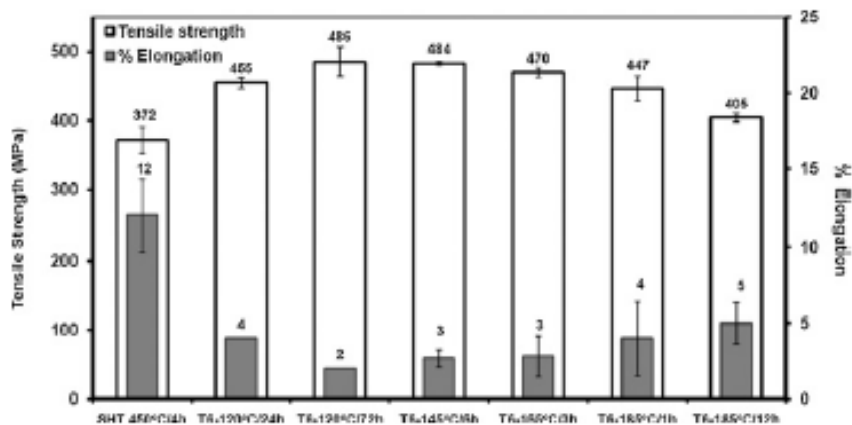


Figure 3.6 Tensile strength and elongation % of rheocast 7075 alloys in T6-condition with different aging temperatures and times [43]

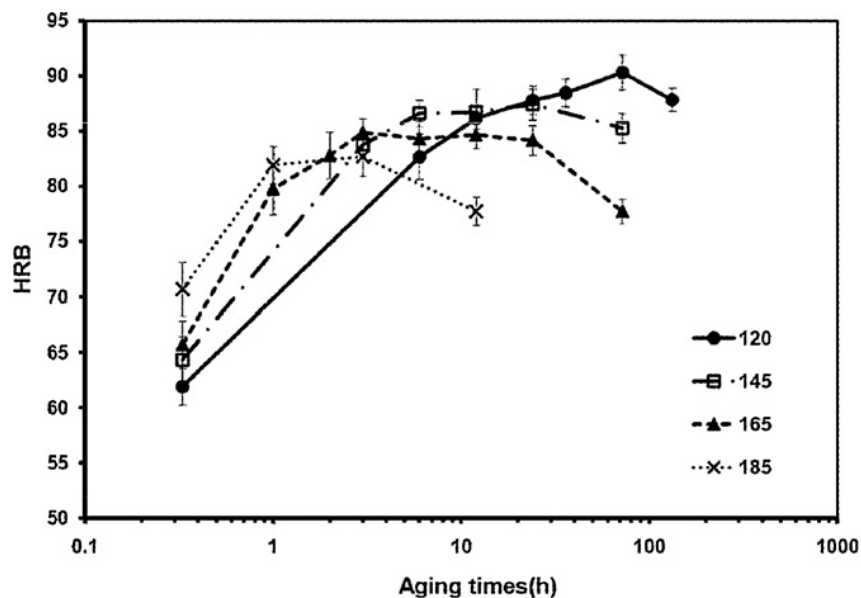


Figure 3.7 Hardness vs time graph for different aging temperatures [43]

3.2. Rheocasting of 7075 Matrix Composite

There are several studies related to rheocasting of aluminum matrix composites in the literature. The reinforcements used in the studies for aluminum matrix composites were mostly in the form of particulate such as Silicon-Carbide [50] [51], Alumina [53] and Magnesium-Silicide [54]. Most of these studies have mainly focused on the effect of particulate reinforcement addition on the wear properties of aluminum matrix composites. The information related to rheocasting of 7075 matrix composites produced by semi-solid melting method and the effect of reinforcement addition on the microstructure and the mechanical properties of 7075 matrix composites were limited for this reason.

In a study related to rheocasting of nano Silicon-carbide (SiC) reinforced 7075 aluminum matrix composite, Jiang et al. [50] have investigated the effect of nano size SiC particulate addition on the microstructure and the mechanical properties of rheocast 7075 aluminum alloy. They used commercial 7075 aluminum alloy as matrix material which contains chemical composition as follows; 6.0 wt.% Zn, 2.3 wt.% Mg, 1.56 wt.% Cu, 0.26 wt.% Si, 0.27 wt.% Mn, 0.17 wt.% Cr and balance Al. The particle size of nano SiC were 80nm. 7075 alloy was melt at 650°C in a resistance furnace and nano SiC powder was added and mixed by 2kW ultrasonic mixer for 20min at that temperature. Then, the mixture was exposed to mechanical stirring down to predetermined SSM temperature which was 620°C. After the preparation of semi-solid slurry at 620°C for various stirring time, SiC_p/Al composites were transferred to hydraulic press and squeezed into the final shape. Production route of whole rheocasting process was summarized in figure 3.8. There were three parameters altered in this study which were stirring time, the value of hydraulic pressure and the amount of nano SiC addition (in vol.%). For 1 vol. % SiC composite six different stirring time were tested; 5, 10, 15, 20, 25 and 30 minutes. Again for 1 vol. % SiC composite 5 different hydraulic press value were tested; 119, 199, 279, 338 and 398 MPa. For 20 minutes stirring time and 398 hydraulic pressure value 6 different amount of SiC addition was tested; 1 %, 1.5 %, 2 %, 2.5 % and 3 vol. %. The end product of

rheocast composite parts are seen in figure 3.9. After the production of rheocast composites, T6 heat treatment was applied.

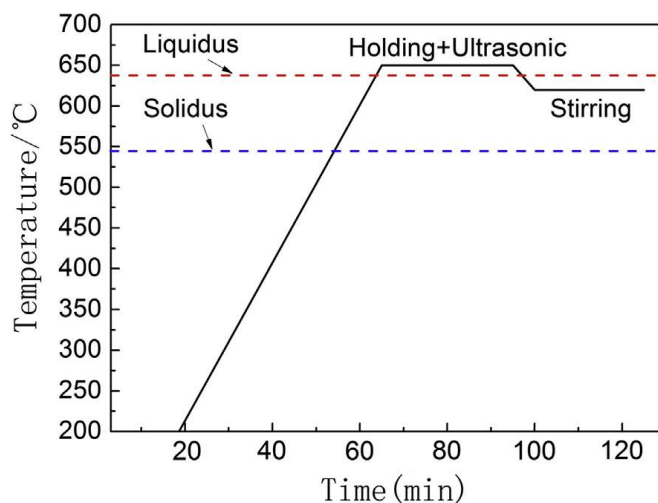


Figure 3.8 Production route of rheocast SiC_p/Al composites [50]

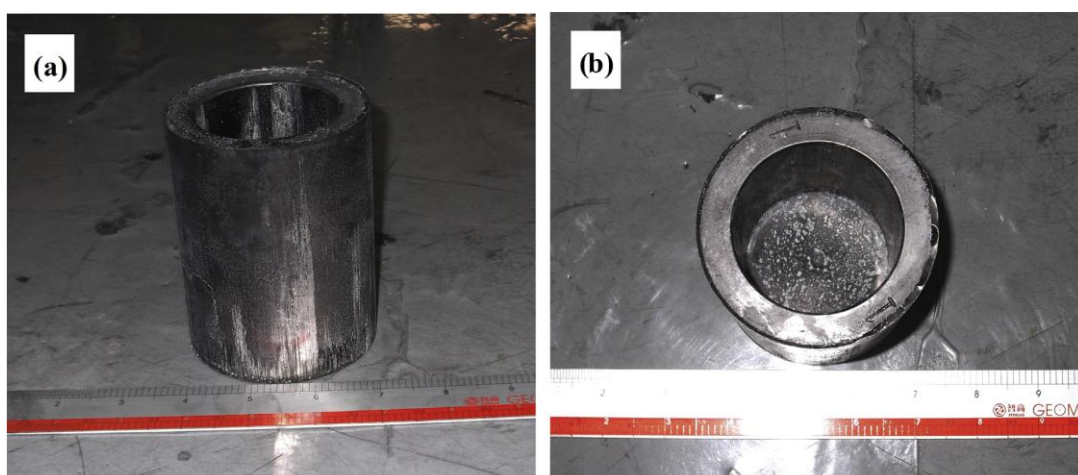


Figure 3.9 Rheocast cylindrical SiC_p/Al composite parts; a) outside surface, b) inside surface [50]

In figure 3.10, microstructures of rheocast SiC_p/7075 Al composite is shown under optical microscopy. As seen in the figure, 7075 aluminum matrix was almost completely in globular grain structure which shows that slurry forming technique and pressure assisted casting was successful. Moreover, the peaks of both aluminum and

SiC have been detected in XRD analysis as seen in figure 45-b. On the other hand, nano sized SiC particles were detected under TEM and there were also formation of some clusters which is seen under SEM image (see in figure 3.11-b).

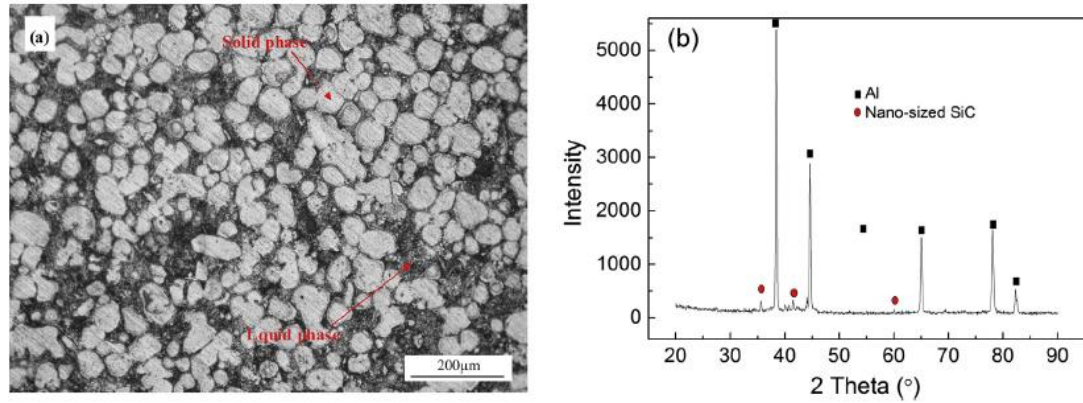


Figure 3.10 Microstructure and XRD result of ultrasonic-assisted rheocast SiC_p/Al composites; a) microstructure b) XRD pattern [50]

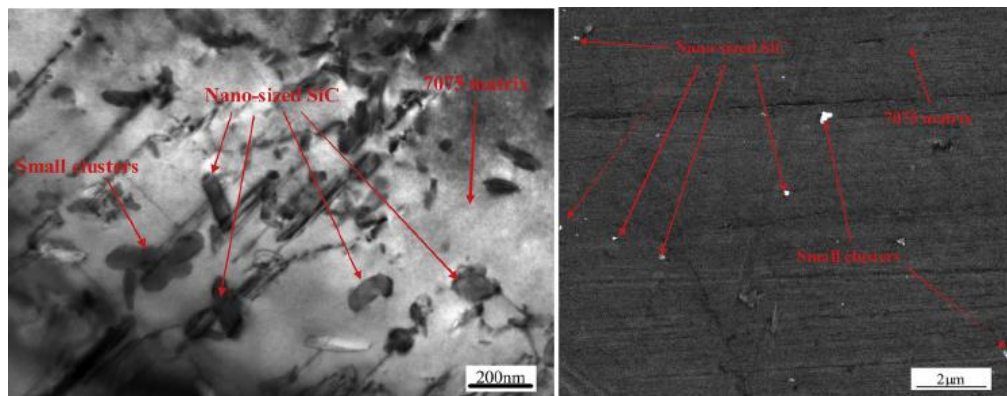


Figure 3.11 Microstructure of rheocast SiC_p/Al composite under TEM (left) and SEM (right) [50]

Mechanical test results of rheocast 7075 composites with different parameters were summarized in figure 3.12 and 3.13. As seen in figure 3.12, UTS of the composite increased by increasing applied pressure value and the maximum value of YS was 399 MPa whereas the UTS was 492 MPa. Similarly, the increase in volume percent of SiC addition raised the mechanical properties of 7075 composites up to a limit. After 2.0

vol. % SiC addition, mechanical properties started to decrease and the maximum UTS was above 450 MPa.

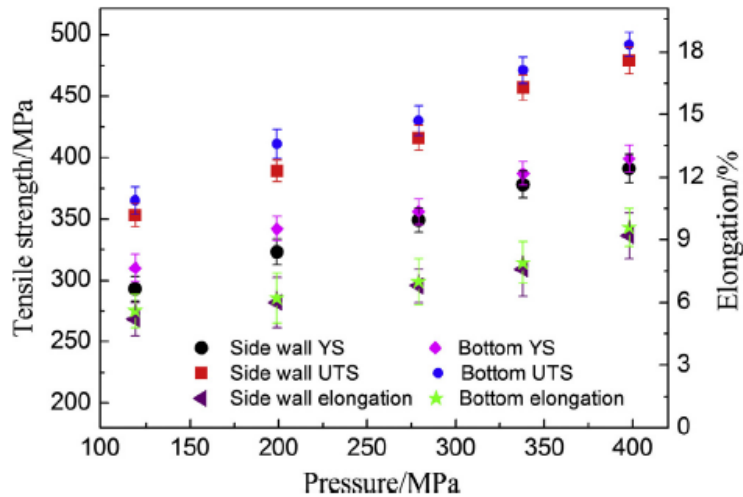


Figure 3.12 Mechanical properties of rheocast 7075 composites with different hydraulic pressure [50]

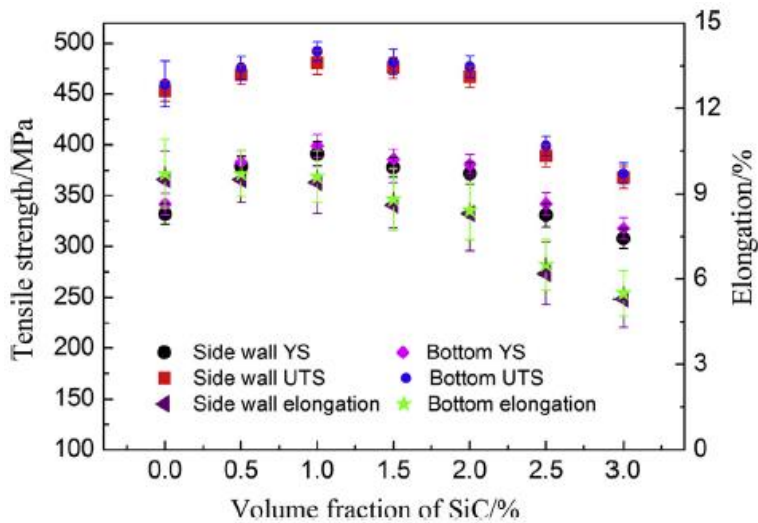


Figure 3.13 Mechanical properties of rheocast 7075 composites with different SiC vol. % [50]

CHAPTER 4

AIM OF THE STUDY

4.1. Motivation of The Study

The literature studies related to rheocasting of 7075 aluminum alloy and aluminum matrix composites showed that it is quite possible to obtain high strength values by rheocasting production method, UTS of the alloy could reach up to 510 MPa in the literature studies [21] [42] which is close to the strength of wrought 7075 alloy produced by forging, rolling, extrusion, etc. Rheocasting clearly surpass conventional casting methods and is comparable with commercial production methods for 7075 alloy such as rolling, extrusion and forging. However, the ductility values are remarkably lower than industrially used wrought aluminum alloys. The reason for that is basically referred to porosities left in the microstructure, even if the amount and the size is very limited.

The aim of this study is to observe the effect of SSM parameters on the microstructure, mechanical and thermal properties of 7075 alloys so as to find out the optimum rheocasting and heat treatment variables that yields high strength 7075 alloy comparable with commercial production method in all aspects. Therefore, by determining optimum slurry preparation variables (mechanical vibration frequency and SSM temperature) and suitable forming method the evolution of the microstructure, thermal and mechanical properties of 7075 alloy will be investigated.

After finding the optimum SSM parameters, 7075/B₄C composites were produced. The microstructure and the mechanical properties after Boron Carbide (B₄C) addition in rheocast 7075 alloys were investigated.

4.2. Main Contribution to The Literature

So far, literature studies related to rheocasting of 7075 aluminum alloy have been focused on two aspects of the effects of rheocasting process; on the microstructural and mechanical properties. In this study, the effects of rheocasting parameters on the thermal properties as well as microstructure and mechanical properties will be covered. Furthermore, many of the studies focused on different slurry preparation method; used inverted cone shape pouring channel [20], induction stirring with simultaneous forced air cooling [21] [42], gas induced stirring [43] and so on. However, the forming or shaping process right after the slurry preparation step limited to HPDC method. In this study, squeeze casting which is thought to be better candidate for shaping of semi-solid slurries was studied. More importantly, the effect of Boron Carbide addition on the microstructure and the mechanical properties of rheocast 7075 alloy was investigated for the first time.

CHAPTER 5

EXPERIMENTAL PROCEDURE

In this chapter, all the necessary information about experimental work and set-up used in this thesis study will be mentioned. In the very beginning of the thesis study, 7075 aluminum alloy for semi-solid melting method was prepared, then rheocasting experiments of 7075 alloy were carried out. After the rheocasting experiments with different parameters, relevant heat treatment procedure was applied to the samples. Characterization and the mechanical testing of both heat treated and as-cast samples were done. Various characterization methods were used in order to analyze the microstructure in detail. All the experimental steps were carried out in Metallurgical and Materials Engineering Department in Middle East Technical University.

For the rheocasting experiments, 7075 aluminum alloy was chosen due to its superior mechanical properties and suitability for semi-solid melting production method. Therefore, in the beginning of the thesis study, scrap 7075 aluminum alloy were supplied from Rutaş Co. Ltd. and the chemical composition of the scrap alloys were measured by optical emission spectroscopy.

Rheocasting experiments of 7075 alloys and 7075 alloy matrix composites were composed of basically two parts; preparation of semi-solid slurry and the shaping or forming. Mechanical vibration technique was used in order to prepare the semi-solid slurry of 7075 aluminum alloy and the composites. Besides, there are two different shaping process used in this study; sand casting (although it is not a pressure assisted casting method) and squeeze casting rather than common HPDC technique for rheocasting of 7075 alloy in the literature. Chemical composition of each rheocasting experiment was measured by optical emission spectroscopy at the end.

There are basically two variables in semi-solid rheocasting experiments which were mechanical vibration frequency and semi-solid melting (SSM) temperature. Three different vibration frequency and four different SSM temperature were determined to use. SSM temperature is the temperature at which the vibration was applied to continuously, SSM temperatures were determined by thermal analysis results which will be covered in thereafter. All in all, 15-25-35 Hertz vibration frequency values and 635-630-625-620°C SSM temperatures were used as the rheocasting parameters and twelve different castings were planned to carry out for both sand casting and squeeze casting methods.

Table 5-1 Rheocasting experiment parameters information

SSM Temperature (°C)	Vibration Frequency (hertz)		
	15	25	35
635	Casting #1	Casting #5	Casting #9
630	Casting #2	Casting #6	Casting #10
625	Casting #3	Casting #7	Casting #11
620	Casting #4	Casting #8	Casting #12

5.1. Rheocasting Experiments

Two different techniques were used for the rheocasting of partial solid slurry of 7075 alloy conditioned by mechanical vibration as given below;

1. Initial experiment was the casting into the sand mold. After the casting of liquid 7075 alloy, mechanical vibration was applied to the alloy for conditioning until the temperature reaches pre-determined SSM temperature after which solidification was completed inside the sand mold. It was aimed to see the cooling curves of mechanically vibrated 7075 alloys and determine the solidus and the liquidus temperatures.
2. The second experiment was the casting into the steel die of the squeeze casting machine. Before the casting, liquid 7075 alloy was prepared and transferred inside a ladle, mechanical vibration for conditioning was applied inside this ladle until the temperature reaches pre-determined SSM temperature. Then, the slurry of partial solid 7075 alloy was transferred by ladle into the cavity of the die and application of pressure onto the partial solid slurry was taken place. It was aimed to complete solidification under high pressure in order to eliminate pores and reach high cooling rates to get rid of dendrite morphology and produce globular structure.

Overall experimental steps were summarized in figure 5.1

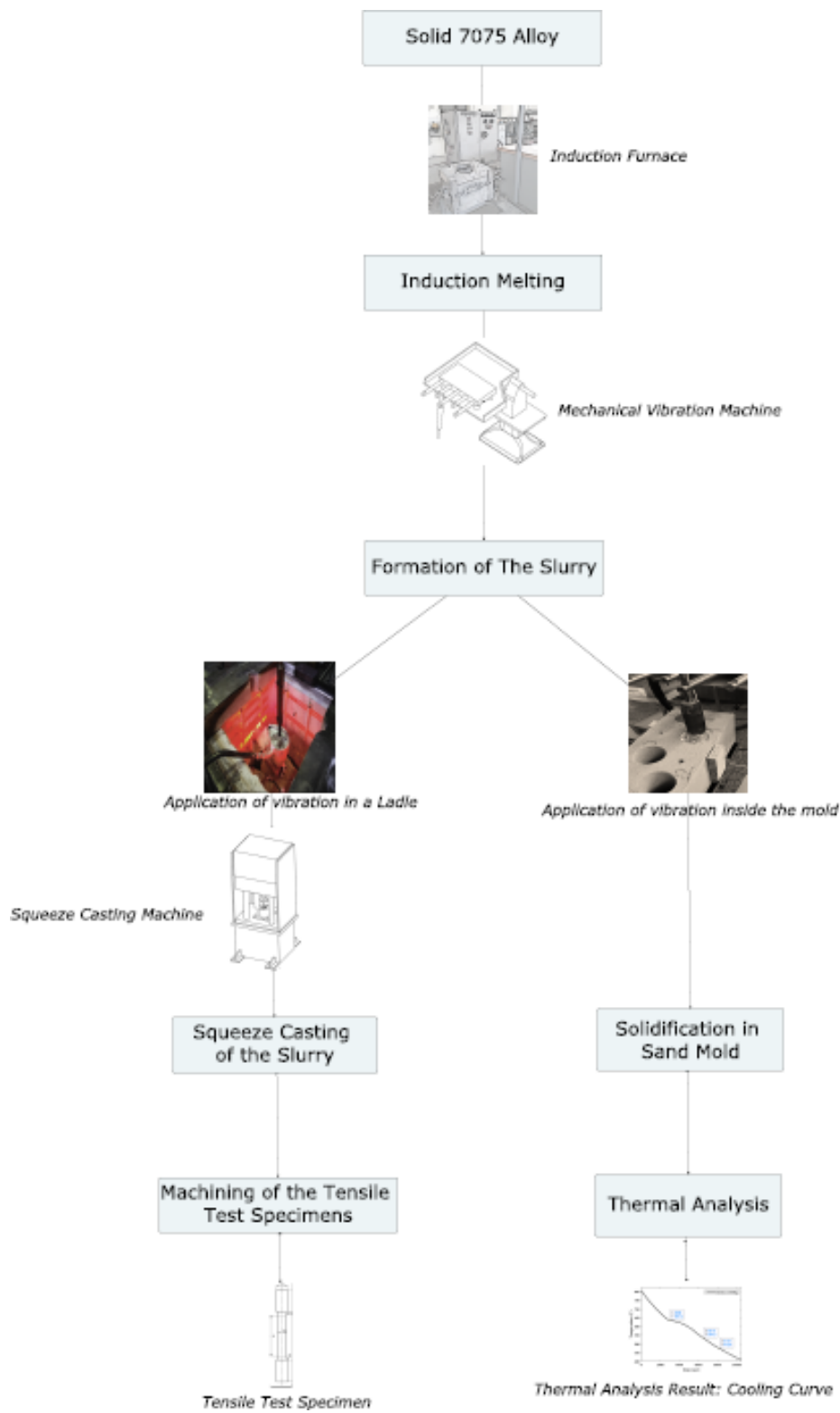


Figure 5.1 Flow chart showing overall experimental steps

5.1.1. Sand casting

The first shaping technique used was the sand casting. The initial step in sand casting experiments was the mold making. Silica sand was used as molding material and alkali phenolic resin was used as binder. Molding mixture, sand and alkali phenolic resin, was strengthened by CO₂ treatment which was simply blowing CO₂ for 3-5 minutes. Special wooden pattern has been designed in order to form a mold having 4 holes in it. Sand mold (see in figure 5.2) was prepared by using this special wooden pattern. 7075 scrap alloy was melted in the electric resistance furnace and kept at 670°C as seen in figure 5.3. Fully molten 7075 alloys were casted into the sand mold. Predetermined vibration frequency was applied to the liquid alloy by immersing graphite probe of vibratory machine into the holes of the sand mold. Liquid 7075 aluminum alloys were exposed to vibration until the temperature reached desired SSM temperatures (see in figure 5.3). In each sand casting experiment, vibration frequency was kept constant and four castings were performed at four different SSM temperatures. Therefore, three experiments were done in order to perform 12 castings with 3 different vibration frequencies. In order to carry out the thermal analysis, a thermocouple was placed at the bottom of each hole and the thermocouples were K-Type Nickel-Chromium thermocouples. Thermocouples were connected to a computer and temperature vs time data was recorded every second until the experiment completed.



Figure 5.2 Whole experimental set-up used in sand-casting experiments consisting of electrical resistance furnace, vibration machine, sand mold and thermocouple recorder

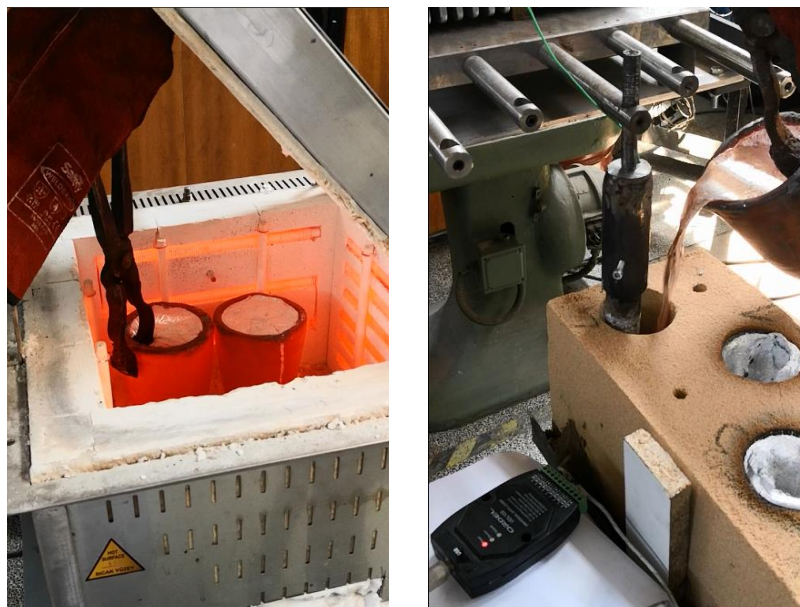


Figure 5.3 Transferring of liquid 7075 alloy and casting into the sand mold

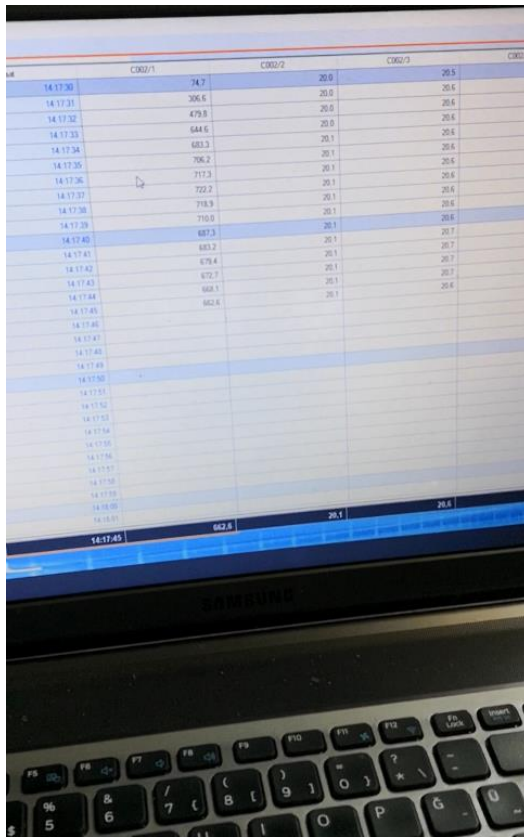


Figure 5.4 Temperature recording during solidification and the application of vibration

5.1.2. Squeeze casting

The second shaping technique used was squeeze casting. There are two type of semi-solid rheocasting were carried out by using squeeze casting as final shaping process; rheocasting of 7075 alloy and rheocasting of Boron Carbide reinforced 7075 alloy matrix composites.

5.1.2.1. Squeeze casting of 7075 alloy

The experimental set-up for squeeze casting experiments were composed of three components. Initially 7075 aluminum alloy were melted and heated up to desired temperature in in the induction furnace (25kg steel capacity Inductotherm brand furnace, see in figure 5.5). Then, semi-solid slurry preparation was carried out by applying mechanical vibration to the liquid alloy via vibration machine as seen in figure 5.6 similar to the sand casting experiments. Moreover, a K-type thermocouple was inside the graphite probe of vibratory machine which was connected to computer data logger device. By that way, it was possible to read the SSM temperatures precisely. After the preparation of semi-solid slurry, the final shaping process of pressure assisted casting was applied. For this purpose, vertical direct squeeze casting machine was made use of, there is a tool steel metal molds having rectangular cavity inside as seen in figure 5.7. The application of pressure was taken place by means of four hydraulic pistons and maximum load capacity of the machine was 100 tons. The pressure could either be applied manually or automatically.



Figure 5.5 Induction furnace (25 kg steel capacity) where 7075 alloy was prepared



Figure 5.6 Vibration machine and thermal analysis set-up connected to each other

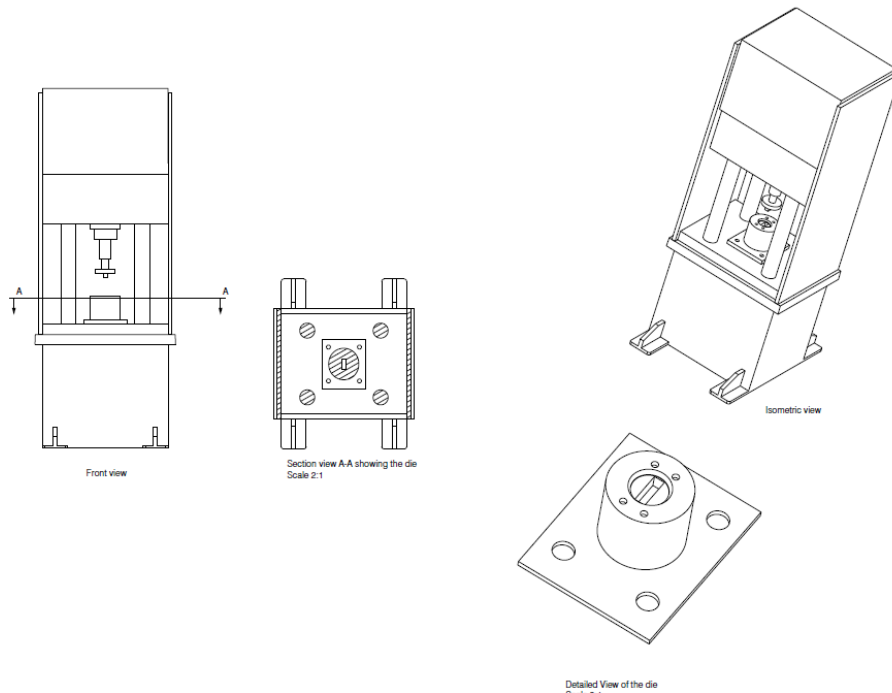


Figure 5.7 Detailed technical drawing of the squeeze casting machine and the metal die

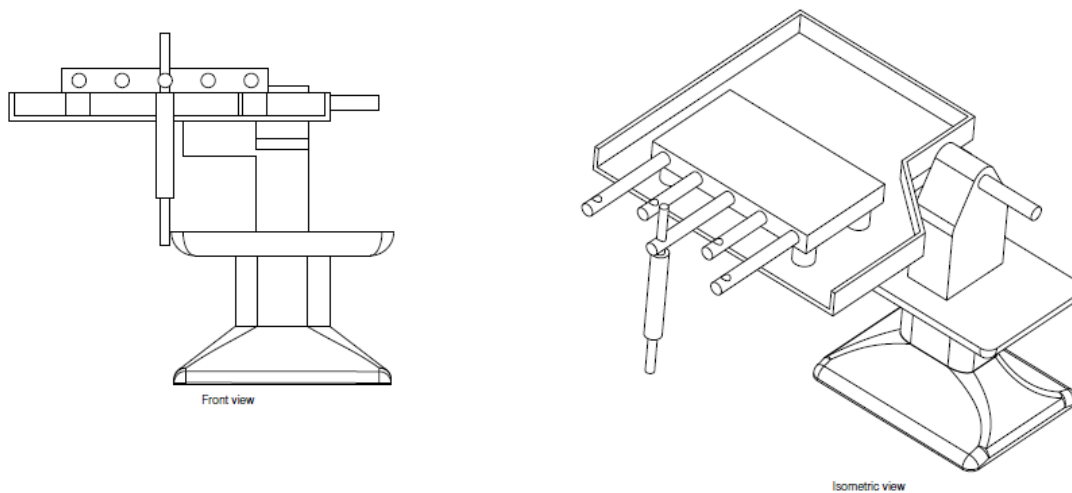


Figure 5.8 Detailed technical drawing of the mechanical vibration machine

Initially, scrap 7075 alloys were melted in the induction furnace as mentioned previously and the metal mold of squeeze casting machine was heated by torch up to 250°C (see technical drawing in figure 5.9). Then the liquid 7075 alloy at 670°C were transferred by cast iron ladle (see in figure 5.10). The ladle was placed beneath the graphite probe of vibration machine inside the electrical resistance furnace (see in figure 5.11) and the vibration was activated. The temperature of the semi-solid slurry was read and checked in every 3 seconds. Once the temperature of the semi-solid slurry reached the predetermined SSM temperature, it was transferred and poured into the die cavity of metal mold, the die cavity of the mold was 120mm in length and 40mm in width. Then the load of 100 tones which is equivalent to 204 MPa pressure for the mold cavity was applied automatically (see in figure 5.12) onto the semi-solid slurry until it was completely solidified, application of pressure was sudden until the dies contacts with metal surface after which dies pressed rather slowly. At the end of the process, rheocast product was extracted from the metal mold of squeeze casting machine by simply lifting below using hydraulic arm (see in figure 5.15). Rheocast samples were rectangular in shape and 20x40x120 mm in size approximately. The final rheocast products are shown in figure 5.16. Two samples were squeeze casted for each different parameter, i.e. vibration frequency and SSM temperature, in total 36

samples were produced by squeeze casting for 9 different casting parameters. It was not possible to perform the rheocasting experiments at 620°C SSM temperature since the excessive viscosity of semi-solid slurries did not allow to cast it into the mold.



Figure 5.9 Pre-heating of metal mold by torch



Figure 5.10 Transferring of liquid 7075 alloy and application of vibration in the ladle



Figure 5.11 The application of vibration inside the ladle for conditioning



Figure 5.12 Casting of the semi-solid slurry into the die cavity just before pressure application

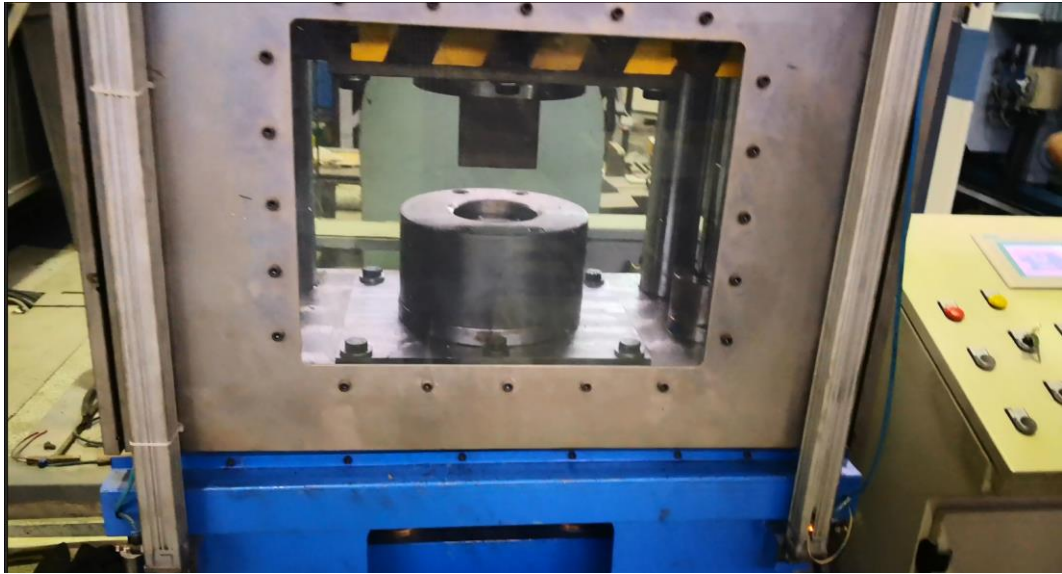


Figure 5.13 Early stage of pressure application before upper punch movement



Figure 5.14 Final stage of pressure application before ejection



Figure 5.15 The removal of the rheocast product



Figure 5.16 Semi-solid squeeze cast 7075 samples at different SSM temperatures



Figure 5.17 Single sample of 7075 alloy produced by squeeze casting

5.1.2.2. Squeeze casting of aluminum matrix composite

Aluminum matrix composite production were also carried out by semi-solid rheocasting process. 7075 aluminum alloy were used as the matrix material whereas Boron Carbide (in B_4C chemical formula) was used as reinforcement material. Boron Carbide reinforcement were in the form of powder having particle size between 1-3 μ m. In the same manner with previous rheocasting experiments, scrap 7075 alloys (supplied from Rutaş co. ltd.) were melted in the same induction furnace. After the melting of the alloy was complete, the addition of Boron Carbide was taken place. In order to provide the complete wetting condition of Boron Carbide in the liquid 7075 alloy, 2 weight % Magnesium was added stepwise into the mixture and continuous mixing was applied. Moreover, B_4C liquid 7075 alloy mixture were exposed to several heating/cooling cycle in between the melting range (475°C-650°C) in order to provide more efficient environment for complete wetting of Boron Carbide powders. Figure 5.18-a shows the initial addition of the Boron Carbide powder whereas the mixing of B_4C powders and the liquid 7075 are shown in figure 5.18-b. After 15 minutes mixing

and heating/cooling operations the mixture was quite homogenous as seen in figure 5.18-c. At the end of 30 minutes mixing, 7075/B₄C composite was quite homogenous and there were no agglomerates which could be seen by naked eye. Therefore, after 30 minutes of heating/cooling cycle and continuous mixing operation, the 7075/B₄C composite was ready to be rheocasted as seen in figure 5.18-d. The procedure was same with the squeeze casting of 7075 alloys mentioned in previous section. The liquid 7075/B₄C mixture was placed inside the electrical resistance furnace and exposed to vibration until it reaches optimum SSM temperature which was 635°C after which the squeeze casting was taken place. The composites having three different Boron Carbide amount were casted; 8wt. %, 10wt. % and 12wt. % in total.



Figure 5.18 The stages of 7075/B₄C mixture during composite making; a)initial addition of B₄C powder after mixing of; b)5 minutes; c) 15 minutes; d)30 minutes

5.1.2.3. Post processing of aluminum matrix composites

In order to enhance the homogenous particle size distribution, increase the mechanical properties of 7075/B₄C composites, hot-rolling of the composite products were carried out as post-processing. The composite products were heated up to 475°C, which is just below the solidus temperature, in an electrical resistance furnace for 1 hour while the twince rollers were pre-heated. The samples were deformed about 80% by area, the thickness of the composite samples were reduced from 9mm to 3.3mm by four pass. LAMASAN twin roll used for this process are shown in figure 5.19.



Figure 5.19 LAMASAN Twin roller which post-processing was carried out

5.2. Production of Tensile Test Specimens

After completing three different sand casting experiments, total 12 samples were rheocasted by three different vibration frequencies and four different SSM temperatures. Rheocast samples were in cylindrical in shape. Four tensile test

specimens from each of the cylinders were machined, although some specimens were broken during machining and scrapped, according to ASTM B557M-10 standards [48] (see technical drawing in figure 5.20 and standards in table 5.2). Three out of four specimens were planned to be heat treated whereas one out of four specimens was planned to be kept in as-cast form. In total, it has been planned to manufacture 36 heat treated and 12 as-cast specimens, but some of the specimens were scrapped during machining. Moreover, the rheocasting specimens with 620°C SSM temperature could not be casted in squeeze casting experiments due to their excess viscosity. Therefore, approximately 35 tensile specimens were machined from sand casting experiment samples and 40 tensile specimens were machined from squeeze casting experiment samples. An example specimen is shown in figure 5.21.

Table 5-2 Specifications of standard tensile test specimen for wrought and cast aluminum alloys [48]

Nominal Diameter	Dimensions (mm)			
	Standard Specimen	Small-Size Specimen Proportional to Standard		
	12.5	9	6	4
G-gage length	62.50 ± 0.10	45.00 ± 0.09	30.00 ± 0.06	20.00 ± 0.04
D-diameter	12.50 ± 0.25	9.00 ± 0.10	6.00 ± 0.10	4.00 ± 0.05
R-Radius of fillet	9	8	6	4
A-Length of reduced section	75	54	36	24

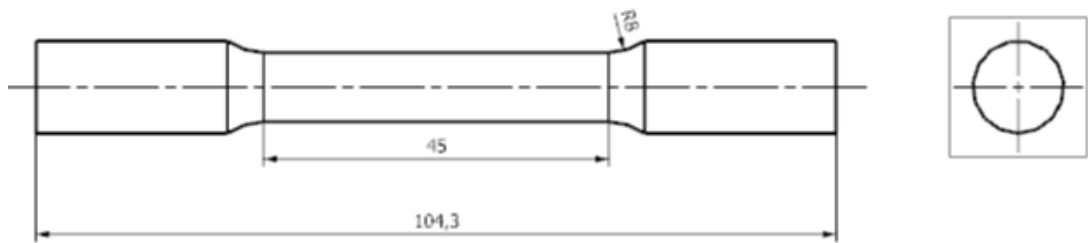


Figure 5.20 2-D Technical drawing of tensile test specimen of rheocast products



Figure 5.21 As machined tensile test specimen of squeeze casting experiment

5.3. Production of 3-Point Bending Test Specimens

After the production of B₄C particulate reinforced 7075 matrix composite by semi-solid squeeze casting method, it was almost impossible to machine tensile test specimens by turning process therefore, it was decided to machine 3-point bending test specimens by freezing process which is much more practical and could give more reliable data since the aim was to observe the mechanical properties of rheocast 7075/B₄C composites and compare them with the mechanical properties of rheocast 7075 alloy. For this reason, both the composite and 7075 alloy samples having ultimate mechanical properties were machined to obtain 3-point bending test specimens according to ASTM E290-14 standards. The specimens were rectangular in shape having about 3,5 mm thickness, 13mm width and 120mm length as seen in figure 5.22.

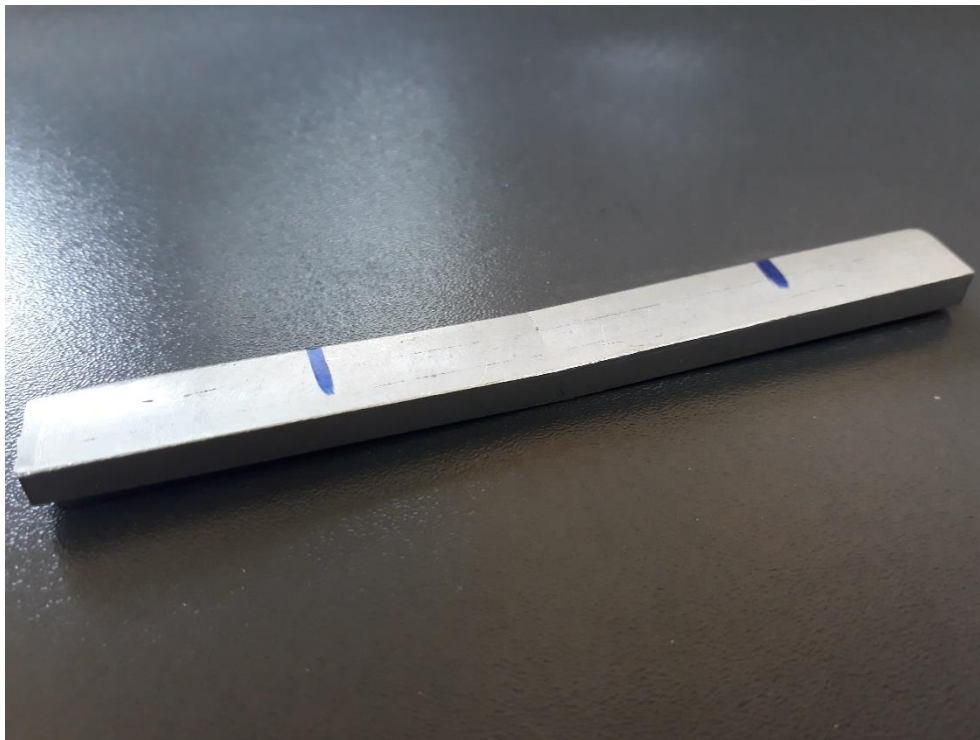


Figure 5.22 As machined 7075 alloy 3-point bending test specimen of squeeze casting experiment

5.4. Heat Treatment

T6 heat treatment is the standard heat treatment procedure generally used for 7xxx series and it consists of several stages; in the order of solution heat treatment, quenching and artificial aging. According to ASM standards [35] T6 heat treatment of 7075 alloys includes; solution heat treatment at 470-490°C (see in table 2.11) followed by water quenching at room temperature and artificial aging at 120°C for 24 hours (see in table 2.13). T6 heat treatment processes for rheocast 7075 alloys are more or less similar in most of the literature works. Therefore, based on the studies of Curle et al. [21] [42] and thesis study of Durmaz [38], optimum T6 heat treatment temperatures and times were determined. After machining of rheocast samples, tensile test specimens were categorized into two groups; one tensile specimen of each experiment was kept in as-cast form whereas three specimens of each experiment were exposed to T6 heat treatment. The details of applied T6-heat treatment process are shown in table 5.3; tensile specimens were solution heat treated at 475°C for 1.5 hours in the electrical resistance furnaces as seen in figure 5.23, then quenched in water at 25°C. After quenching, the specimens were aged at 120°C for 24 hours in the electrical resistance furnace as seen figure 5.23.

Table 5-3 T6 Heat treatment process information for rheocast 7075 alloy tensile specimens and 7075/B₄C composite 3-point bending specimens

	Temperature (°C)	Time (hours)	Medium
Solution Heat Treatment	475	1.5	Closed Furnace
Artificial Aging	120	24	Closed Furnace
Quenching	25	-	Water



Figure 5.23 Tensile test specimens' placement in the electrical resistance furnace before solutionizing

5.5. Characterization Techniques

Various material characterization methods and devices were used to examination of the samples produced by semi-solid rheocasting processes with different process parameters. In this section, chemical and thermal analysis of 7075 alloys produced and supplied will be mentioned initially. Afterwards, details of metallographic specimen preparation and use of different characterization techniques/devices; optical microscopy, SEM and X-Ray diffraction will be covered.

5.5.1. Optical emission spectroscopy

Optical emission spectroscopy is a device which is used for chemical characterization of metals and alloys. By using optical microscopy, the chemical composition of the metal could be determined precisely. The working principle is simply as follows; initially electrical energy is applied as sparks in between the electrode and the surface of the sample which leads to vaporization of the surface atoms forming ‘discharge plasma’, atoms having high energy level in this plasma emit unique spectrum specific for each element and the intensity of each spectrum emitted by the elements are measured by the detectors of the spectroscopy and therefore able to make the quantitative analysis of the elements in the metal samples [49].

In this thesis study, WAS Foundry Master optical emission spectroscopy was used to determine chemical composition of rheocast samples. The chemical analysis was performed initially for the supplied commercial alloys and chemical compositions of the alloys which were used for sand casting and squeeze casting were also measured. The optical emission spectroscopy was used under argon atmosphere by applying vacuum inside. The spectroscopy device can be seen in figure 5.24.



Figure 5.24 WAS Foundry Master optical emission spectroscopy used for chemical analysis

5.5.2. Thermal analysis

Thermal analysis of 7075 alloys are essential for the sake of this study. In order to calculate or determine the phase transformation temperatures and solid fractions, various thermal analysis of 7075 alloys produced by rheocasting were carried out. In the first stage of the thermal analysis, temperature data was collected every second during rheocasting processes by using cable and metal-casing K-Type Nickel-Chromium thermocouples which is shown in figure 5.25 and figure 5.26. The data is transferred to the computer via thermocouple data-logger which is shown in figure 5.27. After collecting temperature data for relatively long period, the data is transformed into excel file format. After this point, all the calculations were made by using computer software Math Works MATLAB program.

The very first step in the thermal analysis by MATLAB program was the plotting of cooling curves, temperature vs time graphs. The cooling curve of each rheocasting experiments with different parameters were plotted. A common cooling curve for an alloy or metal includes several turning points where the slope of the curve changes suddenly. Therefore, by taking first derivative and plotting with respect to time, it was possible to determine the solidus and the liquidus temperatures. Curve fitting tool of MATLAB program was used by plotting the cooling curves and calculating the first derivatives. Moreover, the best and almost exact results were obtained by using smoothing spline fitting which is basically generating lines in between every two points on the data. After fitting and smoothing the cooling curves precisely, the first derivatives were taken and plotted also. Phase transformation points, solidus and liquidus temperatures, were found as peak points on the first derivative curves since these points are the temperatures where the slope of the curve changes suddenly. By following these steps, thermal analysis of all rheocasting samples produced by sand casting forming method were analyzed, besides the thermal analysis of 7075 alloy which were melted and cooled in the furnace (equilibrium cooling) was done also in order to determine equilibrium solidus temperature in order to determine more reliable and safe T6 heat treatment parameters.

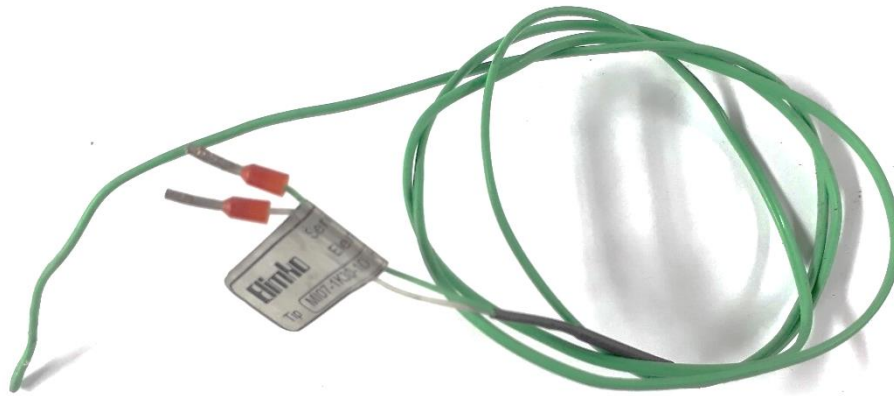


Figure 5.25 K-type cable thermocouple



Figure 5.26 K-type thermocouple with metal casing



Figure 5.27 Thermocouple data logger

5.5.3. Metallographic specimen preparation

Metallographic specimen preparation of the rheocast 7075 alloys were performed in order to examine the microstructure under optical and electron microscopy. The standard metallographic specimen preparation steps were followed for the rheocast samples. First of all, rheocast samples were cut into smaller sizes by cutter as seen in figure 5.28. The second step was the mounting of the samples using bakalite powder mixture. Then, the samples were grinded with different grades of emery papers. Grinding of the samples carried out by using emery paper grades as follows; 200-400-600-800-1200 under rotating disc grinder as seen in figure 5.29. After finishing grinding, the samples were polished by using 6 μ followed by 1 μ diamond solutions under rotating disc polishers as seen in figure 5.30. For final step, etching of the polished specimen was performed. Etching was done for 25-30 seconds with Keller's reagent.



Figure 5.28 METACUT 251 Specimen cutter (right) and the mounting device (left)



Figure 5.29 Rotating disc type grinder



Figure 5.30 Rotating disc type polisher with 6μ by 1μ diamond solutions

5.5.4. Optical microscopy

Specimens prepared by metallographic specimen preparations were examined under optical microscopy. Two types of optical microscopy were used in this study; HUVITZ and SOIF XJP-6A were used. Optical microstructure images or optical micrographs of all the specimens were taken by using HUVITZ optical microscopy as seen in figure 5.31. Micrographs were taken under different magnifications varying from 50x to 200x. Moreover, grain size measurements were done also using the same microscopy, 10 individual grains were analyzed from three different regions for each specimen, in total 30 grains. On the other hand, SOIF XJP-6A which is an inverted optical microscopy (see in figure 5.32) was used to porosity calculation of the specimens. Porosity calculation was carried out by image analysis software named DeWinter Material Plus.

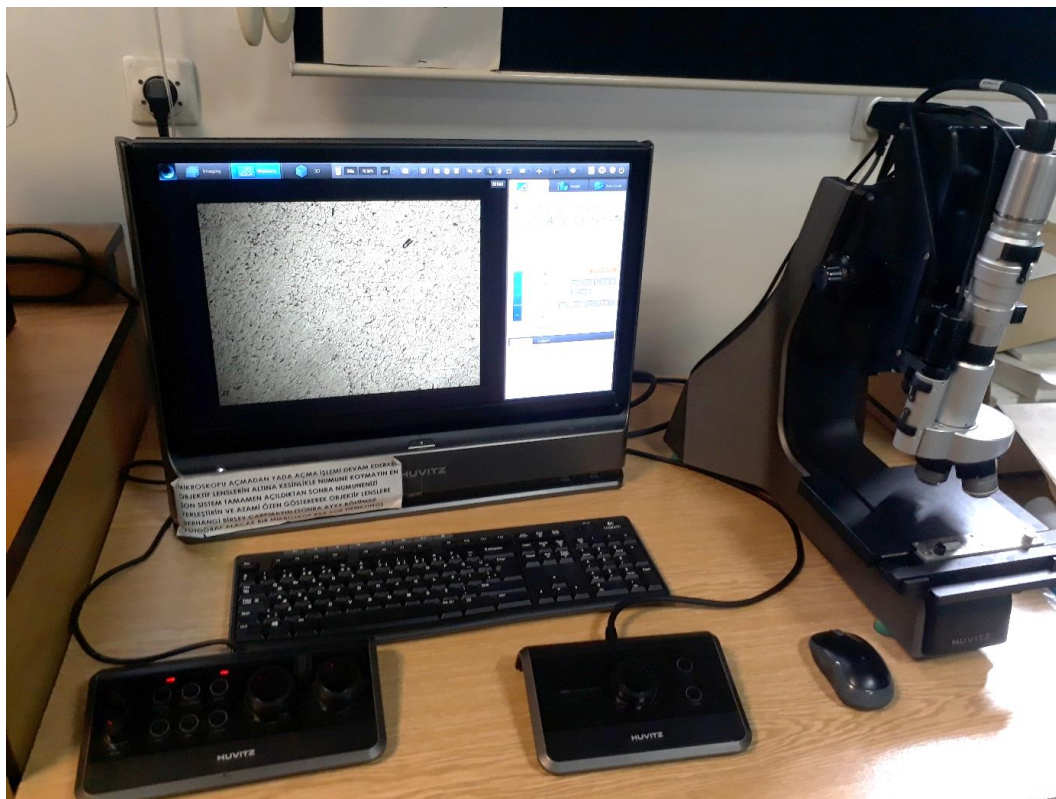


Figure 5.31 HUVITZ optical microscopy and the computer interface

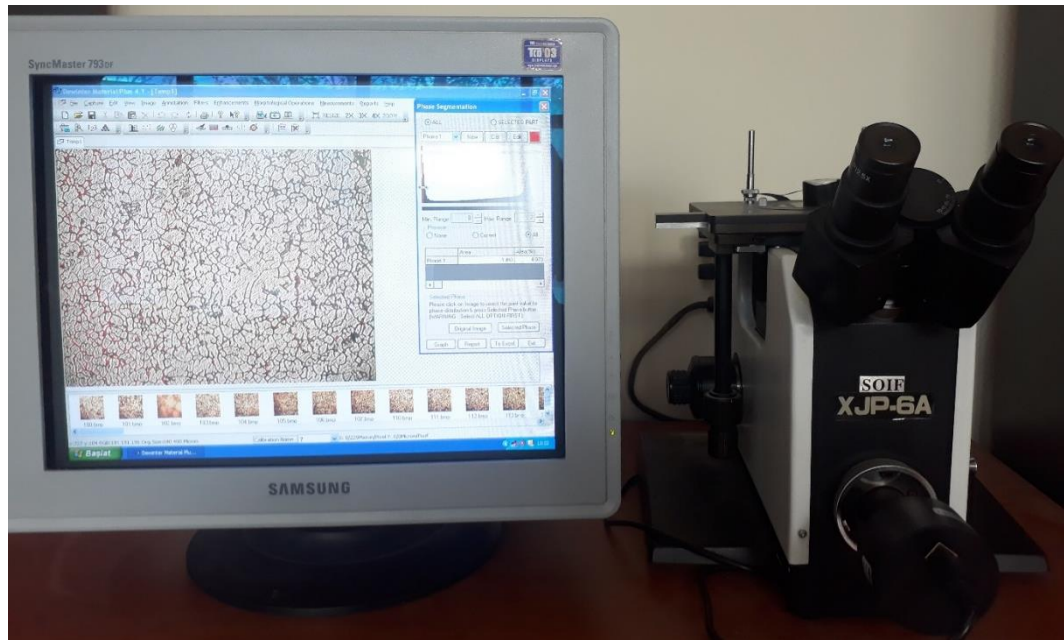


Figure 5.32 SOIF XJP-6A optical microscopy and DeWinter Material Plus

5.5.5. Scanning electron microscopy

The specimens were also examined under scanning electron microscopy in order to obtain detailed information about the microstructure, phases and chemical composition of the phases. After metallographic specimen preparation step, the specimens were coated with thin layer of silver solution in order to prevent any charging through bakelite layer of the specimens. The scanning electron microscopy used for this purpose was NOVA NANO SEM 430 as seen in figure 5.33. Microstructure images of rheocast samples were taken by using SEM as well as energy dispersive spectroscopy (EDS) analysis were performed. Field-free mode of the SEM was used for lower magnification levels whereas immersion mode of the SEM was used for higher magnifications up to x250000 levels.



Figure 5.33 NOVA NANOSEM 430 Scanning electron microscopy setup

5.5.6. X-Ray diffraction

X-ray diffraction analysis of the specimens were carried out in order to conduct the phase analysis. XRD measurements were performed within the range of $0-130^{\circ}$ scanning angle and with the scanning speed of $2^{\circ}/\text{min}$. Cu-K_{α} radiation was used. Bruker brand XRD device setup is shown in figure 5.34.



Figure 5.34 Bruker brand XRD device setup

5.6. Mechanical Testing

Mechanical testing of the rheocast 7075 alloy samples were also carried out in order to find out the effect of semi-solid melting parameters on the mechanical properties of 7075 alloy. Three type of mechanical tests were basically used which were tensile testing, hardness testing and 3-point bending testing. As stated in previous chapters, the rheocast samples had been machined to tensile test specimen shapes according to ASTM B557M-10 standards. After machining, some tensile test specimens were heat treated and the rest were kept in as-cast form as mentioned earlier. At the end, mechanical testing of both heat treated and as-cast specimens were performed. 3-Point bending test was chosen for the testing of 7075/B₄C composites since these composites are very hard and brittle to machine. It was also used for the testing of rheocast 7075 samples.

5.6.1. Tensile testing

Tensile testing was performed for all rheocast and machined specimens. The tensile test machine used for this purpose was INSTRON electromechanical testing machine as seen figure 5.35. The device was used for the purpose of both tensile and 3-point bending testings. The load was given by means of an electrical motor. The maximum load capacity of the machine was 10 tones. Tensile tests were carried out according to ASTM standards under constant strain rate of 2 mm/sec. The axial strains were measured by the optical extensometer of the device. After the testing, the stress vs strain diagrams and their plots were recorded. Tensile testing of all rheocast specimens (sand casting and squeeze casting) was done in the same manner.



Figure 5.35 Instron Electromechanical Testing Device

5.6.2. Hardness testing

Hardness which is another mechanical property were tested for all rheocast 7075 alloy specimens. Universal machine was used for hardness measurements of the specimens and Brinell hardness scale (HB 2.5) was chosen for casting aluminum alloys. The hardness machine used for this purpose can be seen in figure 5.36.



Figure 5.36 Hardness Machine used

5.6.3. 3-Point bending testing

3-point bending test was used to find out the mechanical properties (flexural strength) of 7075/B₄C composites to compare the mechanical properties of rheocast 7075 alloy and 7075 matrix composites. Since it is very difficult to machine B₄C reinforced composites in the weight percent of 8-10-12 and determination of flexural strength is more meaningful in the case of ceramic reinforced metal matrix composites, 3-point bending test was performed. In order to compare the mechanical properties of 7075 alloy and 7075 matrix composites, 3-point bending test of 7075 alloys were also carried out. For this purpose, INSTRON electromechanical testing machine with different apparatus was used (see in figure 5.37) as in the case of tensile testing. The tests were performed according to ASTM E290-14 standard test methods for bending testing of material for ductility.



Figure 5.37 3-Point Bending Test on Instron Electromechanical Testing Device

CHAPTER 6

RESULTS AND DISCUSSIONS

In this chapter, the results of each experiment will be covered and discussed in detail. The results of all casting experiments will include all the aspects such as chemical analysis, thermal analysis, mechanical tests, optical micrographs, grain size and porosity analysis. The properties of both rheocasting of 7075 metal and 7075/B₄C composites will be analyzed and discussed in order to find the best semi-solid casting parameters and observe the effect of semi-solid melting experiment parameters on the microstructure, thermal and mechanical properties of the rheocast products.

6.1. Chemical Analysis Results

As stated in previous chapters, optical spectroscopy was used in order to find the chemical composition of the rheocast products. Chemical composition of three different type of supplied scrap 7075 alloys were analyzed. Moreover, chemical composition of both sand and squeeze castings were measured for the samples produced under three different vibration frequencies. Each sample was tested three times after a calibrated/meaningful results were obtained. Spectral analysis of both sand cast and squeeze cast products showed that successfully chemical composition of rheocast 7075 products (both sand and squeeze casting) were mostly in the standard range.

Table 6-1 Spectral analysis results of different type of supplied scrap 7075 alloys

Element	Spectral Analysis Result (Element %)								
	Scrap 7075-1			Scrap 7075-2			Scrap 7075-3		
	#1	#2	#3	#1	#2	#3	#1	#2	#3
Al	90,60	90,90	91,30	87,80	87,90	87,90	89,40	88,60	89,60
Si	0,52	0,52	0,49	0,18	0,16	0,19	0,03	0,04	0,03
Fe	0,83	0,75	0,66	0,49	0,46	0,49	0,08	0,06	0,07
Cu	1,01	1,00	0,93	2,80	2,84	2,77	2,04	2,05	2,05
Mn	0,05	0,05	0,05	0,00	0,00	0,00	0,00	0,00	0,00
Mg	1,95	1,90	1,87	2,04	2,03	1,94	1,84	1,88	1,86
Zn	4,50	4,33	4,26	5,88	5,77	5,78	5,96	6,07	6,02
Cr	0,16	0,18	0,18	0,05	0,05	0,05	0,01	0,01	0,01
Ni	0,05	0,04	0,01	0,23	0,23	0,28	0,01	0,01	0,01
Ti	0,09	0,12	0,09	0,05	0,05	0,05	0,05	0,05	0,05

Table 6-2 Spectral analysis results of sand cast samples produced under three different vibration frequencies

Element	Spectral Analysis Result (Element %)								
	Under 15Hz frequency			Under 25Hz frequency			Under 35Hz frequency		
	#1	#2	#3	#1	#2	#3	#1	#2	#3
Al	89,60	90,20	89,50	88,60	88,90	81,30	87,70	89,50	89,00
Si	0,07	0,03	0,10	0,52	0,52	0,49	1,26	0,81	0,95
Fe	0,02	0,13	0,05	0,83	0,75	0,66	0,38	0,36	0,46
Cu	2,45	2,31	2,46	2,01	2,00	1,93	1,73	1,70	1,56
Mn	0,00	0,00	0,00	0,05	0,05	0,05	0,07	0,05	0,06
Mg	2,17	2,05	2,18	1,95	1,90	1,87	2,47	2,05	2,38
Zn	5,18	4,89	5,21	5,50	5,33	5,26	5,33	4,86	5,00
Cr	0,05	0,05	0,05	0,16	0,18	0,18	0,20	0,21	0,22
Ni	0,15	0,05	0,06	0,05	0,04	0,01	0,10	0,01	0,01
Ti	0,04	0,04	0,03	0,09	0,12	0,09	0,13	0,13	0,14

Table 6-3 Spectral analysis results of squeeze cast samples produced under three different vibration frequencies

Element	Spectral Analysis Result (Element %)								
	Under 15Hz frequency			Under 25Hz frequency			Under 35Hz frequency		
	#1	#2	#3	#1	#2	#3	#1	#2	#3
Al	88,40	88,50	88,50	88,50	88,70	89,00	88,00	88,30	88,10
Si	0,22	0,21	0,22	0,16	0,14	0,12	0,13	0,13	0,13
Fe	0,32	0,31	0,31	0,47	0,46	0,44	0,60	0,54	0,57
Cu	2,61	2,61	2,61	2,35	2,33	2,30	2,75	2,68	2,72
Mn	0,00	0,00	0,00	0,00	0,00	0,00	0,00	0,00	0,00
Mg	1,97	1,94	1,90	2,10	2,01	1,95	2,11	2,01	2,03
Zn	5,57	5,42	5,42	5,89	5,77	5,59	5,70	5,62	5,75
Cr	0,05	0,05	0,05	0,04	0,04	0,04	0,05	0,04	0,05
Ni	0,26	0,30	0,26	0,07	0,10	0,10	0,22	0,20	0,22
Ti	0,05	0,05	0,05	0,03	0,02	0,03	0,04	0,04	0,04

6.2. Thermal Analysis Results

Thermal analysis of rheocast 7075 alloy was done under 3 different vibration frequencies and 4 different semi-solid melting (SSM) temperatures. For this purpose, sand casting experimental set-up was constructed and carried out. There were 3 different thermal properties of rheocast 7075 alloy which was calculated; solidus temperature, liquidus temperature and solid fractions.

6.2.1. Solidus & liquidus temperature calculation

Solidus and liquidus temperatures of rheocast 7075 alloys were calculated in MATLAB program in order to derive a correlation between thermal and mechanical properties. As stated in the experimental procedure part, firstly cooling curves (Temperature vs time graphs) were plotted and their first derivatives were taken. By using proper curve fitting, dT/dt vs time graphs were plotted. The first local maximum point in these graphs corresponds to 'Liquidus Temperature' whereas the last local maximum point corresponds to 'Solidus Temperature'. The other local maximum points correspond to additional phase reactions such as formation of Mg_2Si .

Solidus/liquidus temperatures of both rheocast products and casting with non-vibration was calculated. In total, these critical temperatures of 12 different rheocast samples (with three different vibration frequency and 4 different SSM temperatures) were calculated. Example cooling curve and it's first derivative (on which critical temperatures are marked) are shown in figure 6.1 and 6.2. Detailed thermal analysis results of all rheocast samples were added in appendix part.

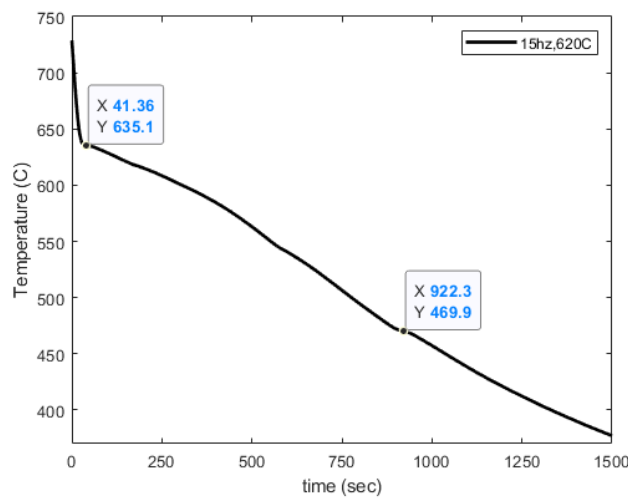


Figure 6.1 Example cooling curve with 0.25°C/sec cooling rate (15Hz frequency with 620°C SSM Temperature sample)

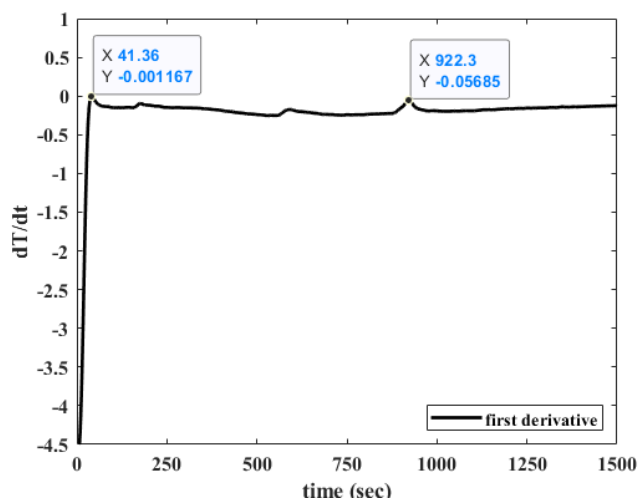


Figure 6.2 Example first derivative (15Hz frequency with 620°C SSM Temperature sample) on which local maximum points were marked

Table 6-4 Calculated solidus and liquidus temperatures of rheocast 7075 alloys produced under three different vibration frequency at four different SSM temperatures

Casting Parameters		Transformation Temperatures	
Vibration Frequency (Hz)	SSM Temperature (°C)	Solidus Temperature (°C)	Liquidus Temperature (°C)
15	635	477.9	637.3
	630	477.6	636
	625	478.1	-
	620	469.9	635.1
25	630	458.3	636.9
	625	459.0	638.6
	620	453.6	637.5
35	635	476.0	-
	630	472.9	638.3
	625	472.5	637.3
	620	471.7	637.6

Figure 6.3 and 6.4 show the variation of solidus and liquidus temperature of 7075 alloys, exposed to different vibration frequencies, with respect to SSM temperature. It can be clearly seen that the liquidus temperature of the alloy decreases as SSM temperature drops for certain regions. In the case of rheocast samples vibrated in 35 Hz, the behaviour of liquidus temperature decrease can be seen clearly (see in figure 6.4). This decreasing behavior were corrupted particularly for 15 and 25 Hz vibration frequencies. The reason for that might be there exist intense convection in the slurry at high liquid amounts and high temperatures which may cause the variations in the temperature. Whereas, solidus temperature has the behaviour of decreasing as SSM temperature decreases for all vibration frequencies (see in figure 6.3). This is clearly a evidence of hinderance of solidification or dendrite formation, therefore the decrease in the solidus and liquidus temperatures down to a point might be helpful for formation of globular grain structure and high mechanical properties of end product.

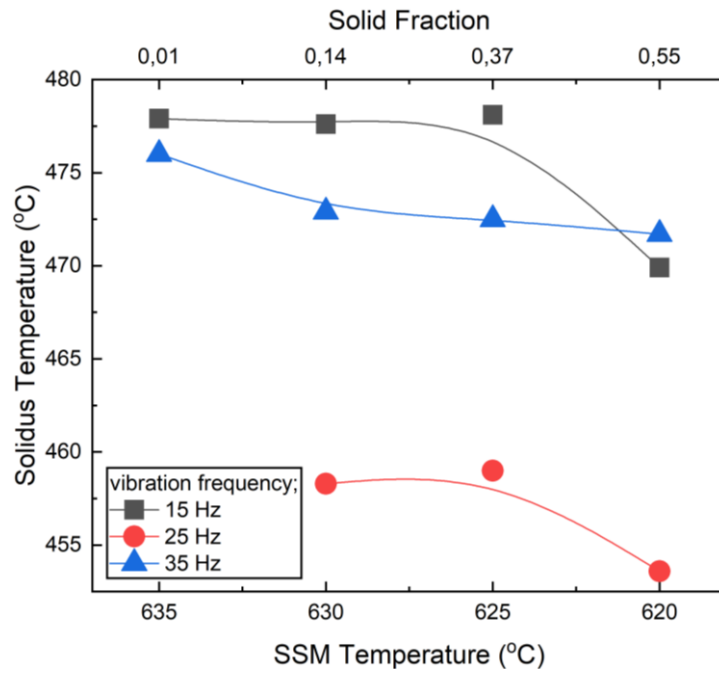


Figure 6.3 Solidus temperature variation at three different vibration frequencies (15, 25, 35 Hz) as SSM temperature decreases

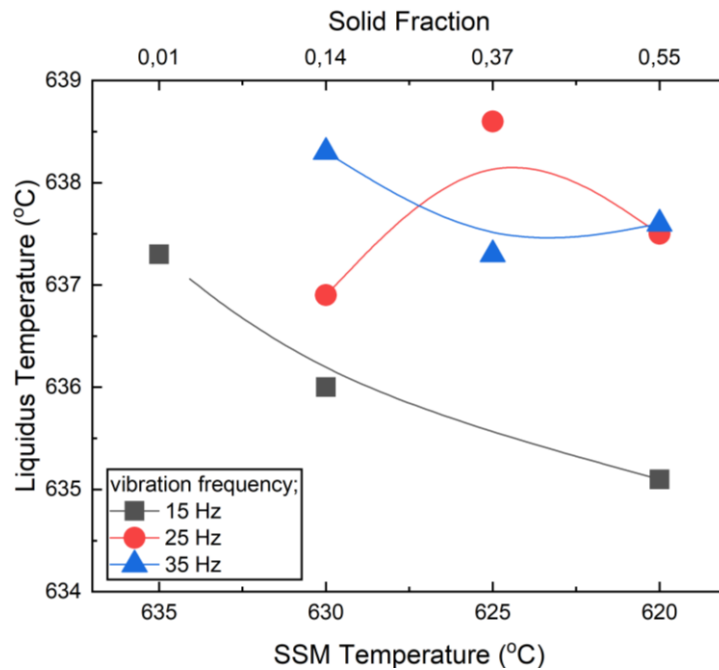


Figure 6.4 Liquidus temperature variation at three different vibration frequencies (15, 25, 35 Hz) as SSM temperature decreases

6.2.2. Calculation of solid fraction

Solid fraction of 7075 alloy in its solidification range (450-650°C) were calculated again in MATLAB. Newtonian base line method was used to calculate solid fraction. As stated in previous chapters, initially the first derivative of the cooling curve was obtained, then 4th order polynomial fitting of first derivative of cooling curve was plotted. Then, the area between the cooling curve (black curve on figure 6.5) and polynomial fit (red curve on figure 6.5) was calculated numerically which gives the solid fraction as a function of temperature.

Corresponding solid fraction vs temperature graph can be seen in figure 6.6. Solid fractions of four critical temperatures at which rheocasting was carried out (620, 625, 630 and 635°C) were also calculated, these values can be seen in table 6.5.

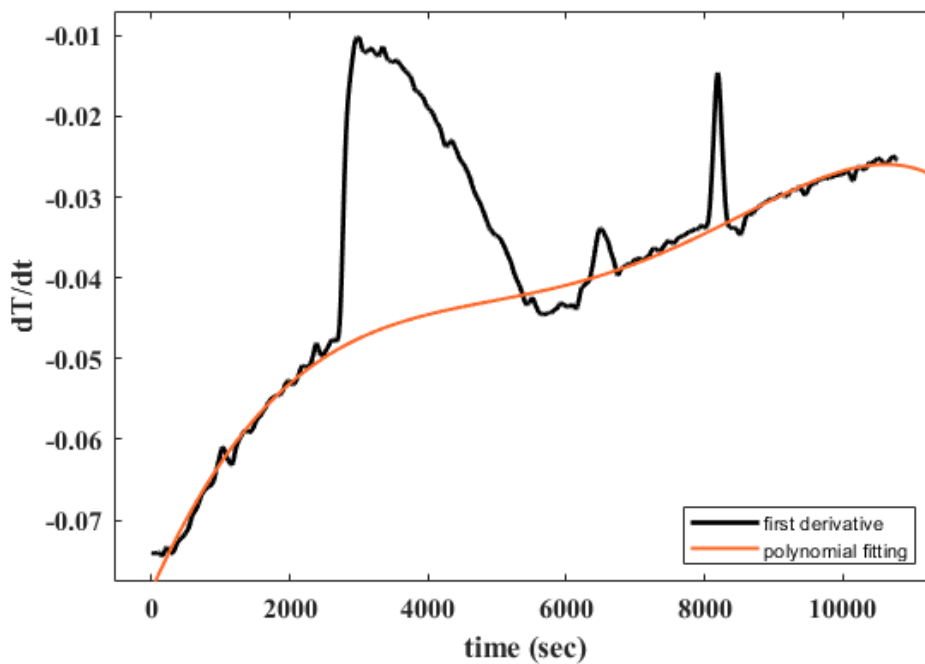


Figure 6.5 First Derivative of cooling curve of 7075 alloy with 0.05°C/sec cooling rate and its polynomial fit

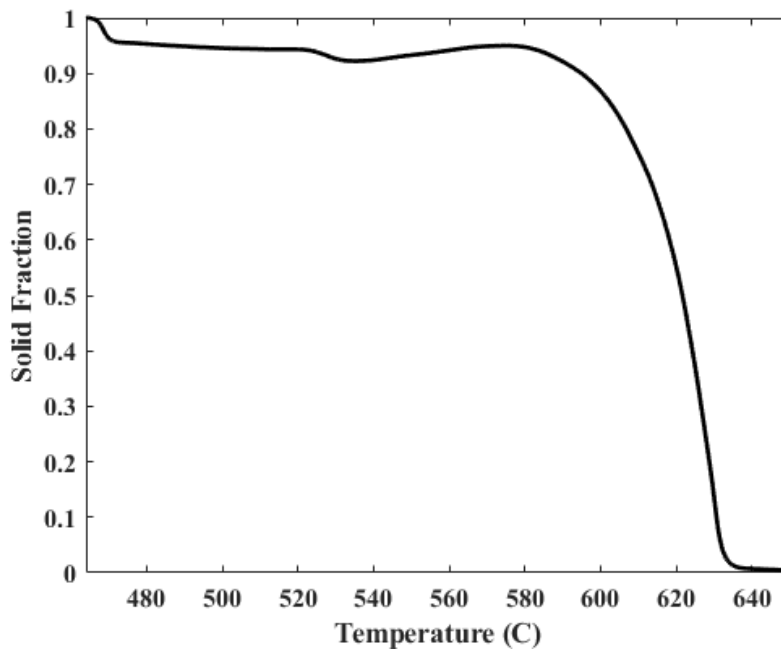


Figure 6.6 Solid fraction of 7075 alloy in the solidification temperature range (450-650°C) obtained by Newtonian method used in this study

Figure 6.7 shows the calculated solid fraction variation with respect to temperature. Solid fraction values at four critical temperatures are seen in table 6.5. The findings are quite close to the literature values. In the literature works, more or less 0.3 solid fraction amount is observed at the temperatures between 625-628°C which is consistent with the results in table 6.5. Thus, it can be said that the temperatures between 625-630°C is expected to have higher mechanical properties since most of the literature studies have concluded that 0.3 solid fraction will give the best microstructure and mechanical properties. Moreover, it will be challenging to cast 7075 alloy below 620-625°C in squeeze casting since the solid fraction reaches extremely high values like 0.5.

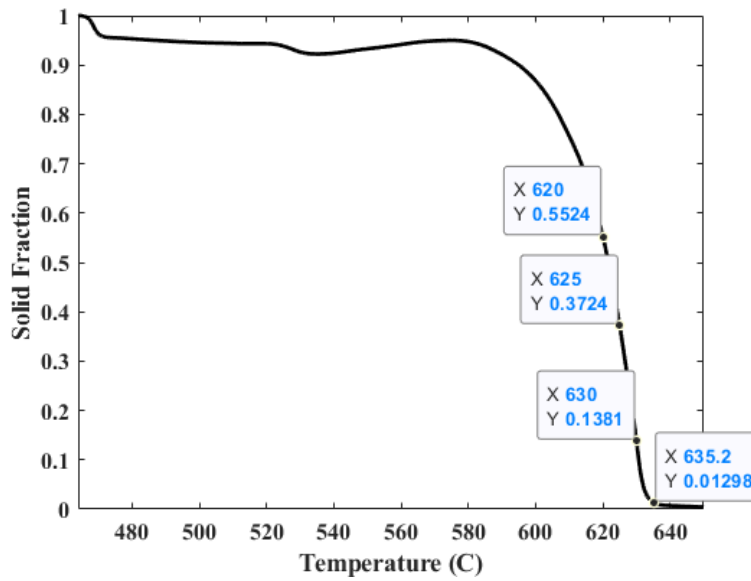


Figure 6.7 Solid fraction vs temperature graph of 7075 alloy on which four critical temperatures are marked, obtained by Newtonian method used in this study

Table 6-5 Solid fraction values of 7075 alloy at critical temperatures

Temperature (°C)	Solid Fraction
635	0.0130
630	0.1381
625	0.3724
620	0.5524

6.3. Optical Micrographs and Microstructural Analysis

In this part, three different results will be discussed; microstructures under optical microscopy, grain size measurements and porosity measurements. Microstructure evaluation of both sand and squeeze cast 7075 alloys produced with different vibration frequencies and SSM temperatures will be done. In addition, microstructures of B₄C reinforced composites and hot-rolled 7075/B₄C composites will be evaluated too.

6.3.1. Microstructure under optical microscopy

For the comparison of the microstructure results effectively, a representative set of micrographs will be evaluated and compared for both sand and squeeze casting and the rest will be mentioned in the appendix part.

6.3.1.1. Sand casting

Microstructures of the 7075 sand casting samples produced under 15Hz clearly revealed that heat-treated 7075 alloy shows more homogenous microstructure. As stated in the thermal analysis results part, the superior microstructure in terms of more globular grain structure and less defects (porosity, etc.) was expected from the samples having SSM temperatures between 625-630°C. This is somewhat the results of T6 heat treated 7075 alloys produced under 15Hz vibration frequency, the other vibration frequencies also showed the similar behaviour which can be seen in appendix B part. As seen in figure 6.8 and 6.11, 635 and 620°C SSM temperatures resulted in relatively higher and larger chunky porosity microstructure whereas 625 and 630°C SSM temperatures resulted in less and more homogenous porosity distribution. On the other hand, there is no apparent evidence of the same behaviour (minimum defects between 625-630°C SSM temperatures) for as-cast 7075 samples. For example, the highest and non-homogenous porosity distribution is seen in 625°C samples for 15Hz vibration frequency (see in figure 6.14) whereas , the highest and non-homogenous porosity distribution is seen in 630°C samples for 35Hz vibration frequency.

Therefore, it can be concluded that the elimination of the porosity in rheocasting (semi-solid melting) process is not only related to slurry formation but also strongly related to application of pressure during shape forming stage.

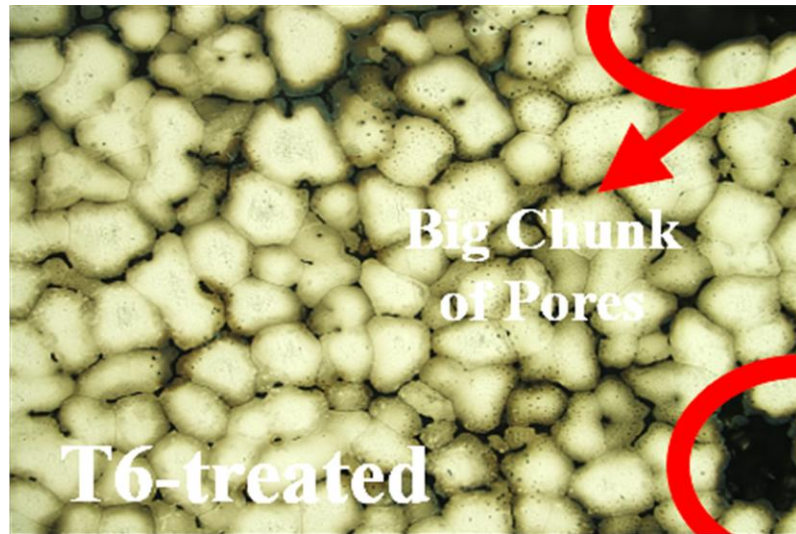


Figure 6.8 Microstructure of sand cast and T6 treated 7075 alloy produced under 15Hz frequency and 635°C SSM temperature obtained by optical microscopy (200x)



Figure 6.9 Microstructure of sand cast and T6 treated 7075 alloy produced under 15Hz frequency at 630°C SSM temperature obtained by optical microscopy (200x)



Figure 6.10 Microstructure of sand cast and T6 treated 7075 alloy produced under 15Hz frequency at 625°C SSM temperature obtained by optical microscopy (200x)

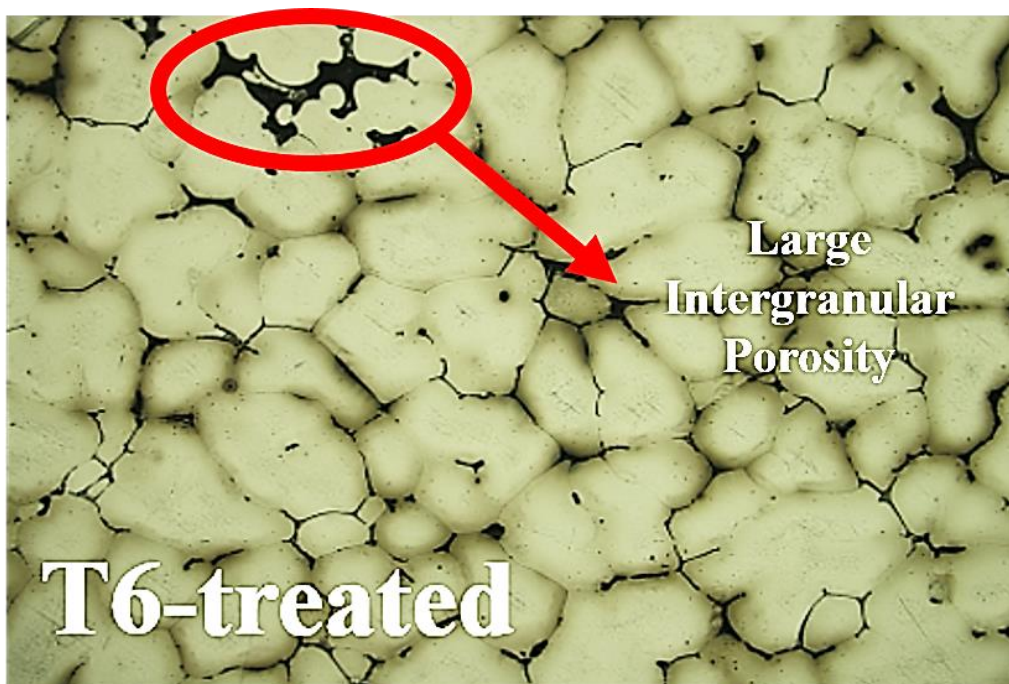


Figure 6.11 Microstructure of sand cast and T6 treated 7075 alloy produced under 15Hz frequency and 620°C SSM temperature obtained by optical microscopy (200x)



Figure 6.12 Microstructure of sand cast 7075 alloy produced under 15Hz frequency 635°C SSM temperature obtained by optical microscopy (50x)

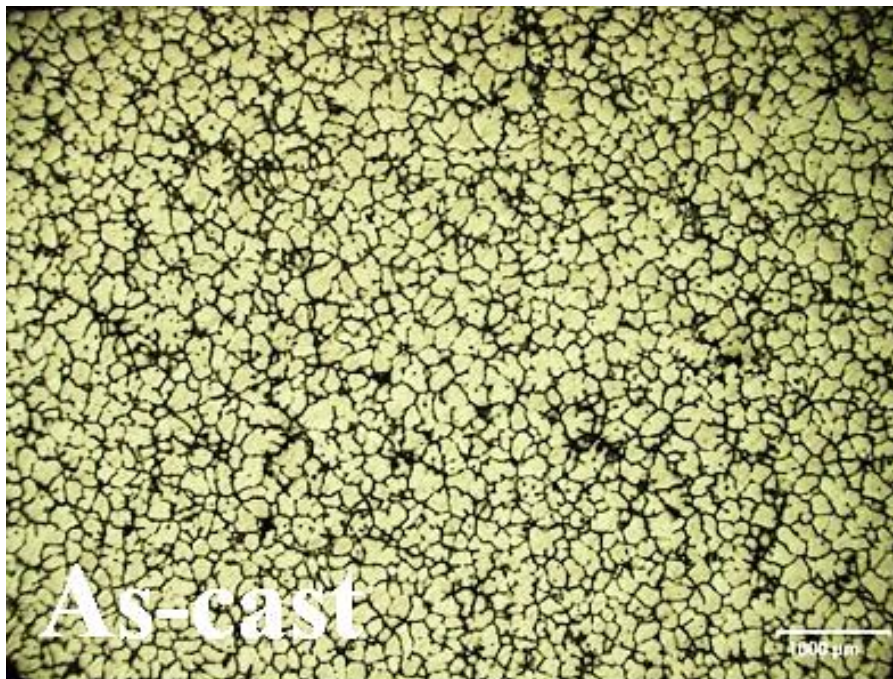


Figure 6.13 Microstructures of sand cast 7075 alloy under 15Hz frequency and 630°C SSM temperature obtained by optical microscopy (50x)



Figure 6.14 Microstructures of sand cast 7075 alloy produced under 15Hz frequency and 625°C SSM temperature obtained by optical microscopy (50x)

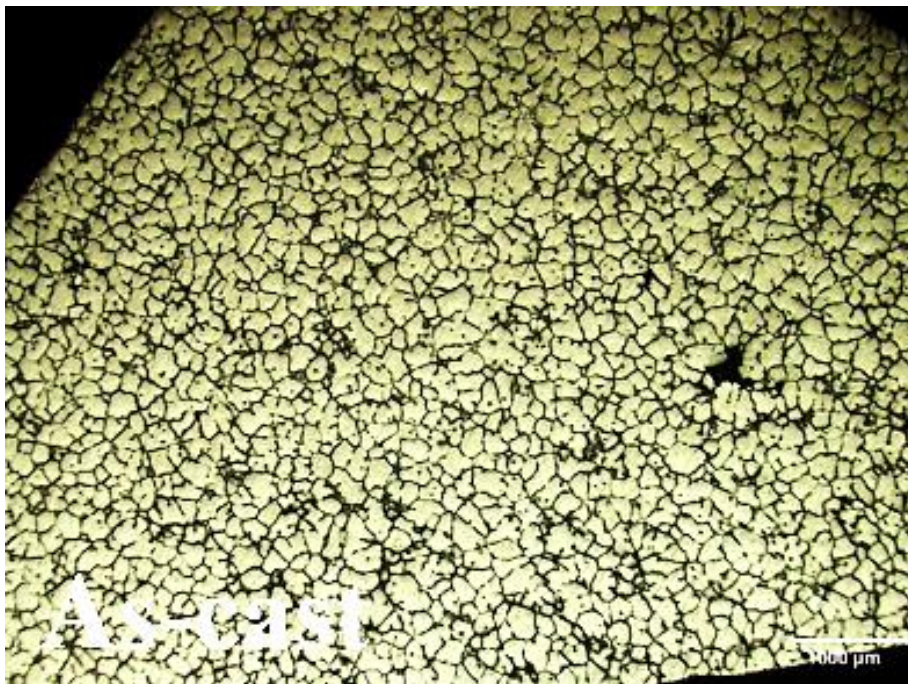


Figure 6.15 Microstructure of sand cast 7075 alloy produced under 15Hz frequency and 620°C SSM temperature obtained by optical microscopy (50x)

6.3.1.2. Squeeze casting of 7075 alloy

Microstructures of the 7075 squeeze casting samples produced under all three vibration frequencies (15, 25, 35 Hz) clearly revealed that both as-cast and heat-treated 7075 alloy shows the behaviour of high improvement of the microstructure with increasing SSM temperature up to 635°C. As seen in figure 6.16, 6.17 and 6.18, the very best globular grain structure with minimum porosity content (homogenously distributed) is seen at 635°C. The amount of porosities begins to rise with non-homogenous distribution whereas the microstructure becomes mixed with dendritic regions at 630 and 625°C SSM temperatures as seen in figure 6.17 and 6.18. Secondary dendrite arms in the microstructure can be clearly observed in figure 6.18. Microstructures of heat treated samples also supported this observation as seen in figure 6.19, 6.20 and 6.21. At first sight, this behaviour could seem to be just the opposite of the theory and thermal analysis result expectations (which were the improvement of microstructure as SSM temperature decreases to a point). However, if the time elapsing during the convey and the casting of semi-solid slurries as seen in figure 5.11 and 5.12 results in the drop of temperature at the moment when the pressure is applied. This temperature drop is measured as 5-6°C during several rheocasting experiments by K-Type thermocouple. Therefore, actual SSM°C should be 5-6°C less. For this reason, samples of rheocasting at 635°C gave the best microstructure whereas for 625°C SSM temperature the microstructure consisted of mostly dendritic structure due to time elapsing during transfer of the slurry.

Another most critical part of this microstructural evolution is seen in figure 6.22 and 6.23 which are the microstructures of squeeze cast samples with no-vibration. As-cast microstructure of 7075 alloy consists of nothing but pure dendrites having secondary arms, there is no globular grains. Porosity amount is also much higher compared to rheocast samples. Thus, the mechanical properties of rheocast alloys have higher than non-vibrated samples. In addition, there is no big difference in the microstructures of vibrated samples as the vibration frequency changes. Therefore, applying vibration at these frequency range (15-35 Hz) is enough to break dendrite arms down.

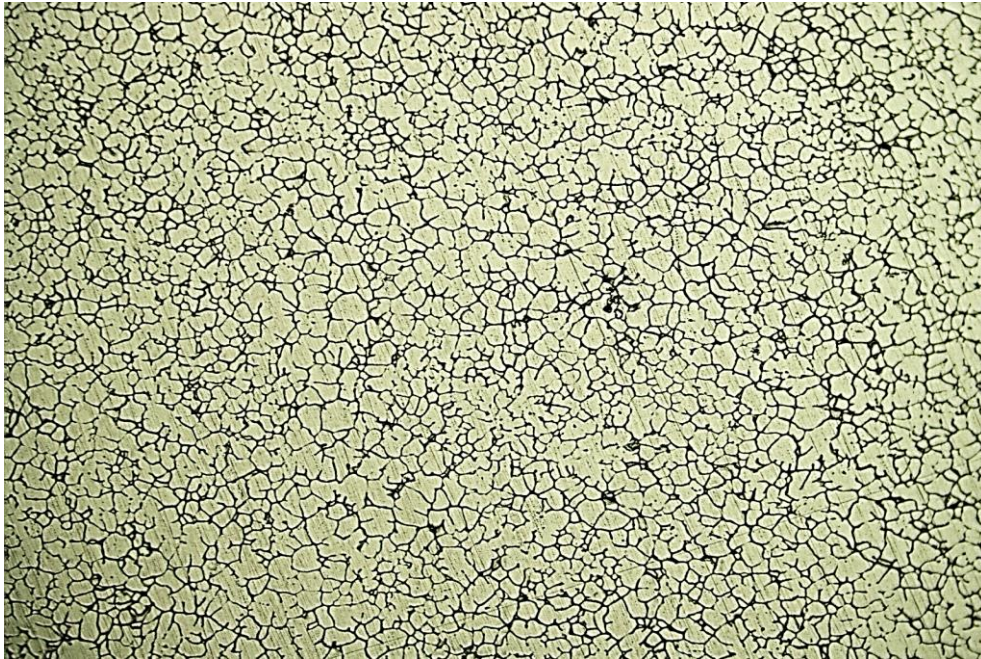


Figure 6.16 Microstructure of squeeze cast 7075 alloy produced under 25Hz frequency at 635°C SSM temperature obtained by optical microscopy (200x)

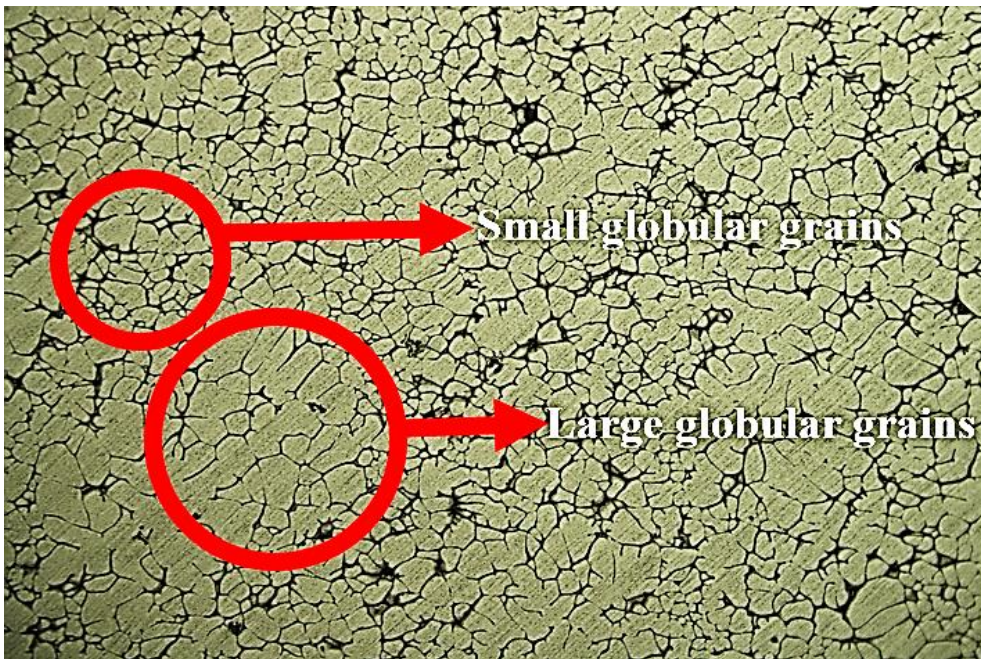


Figure 6.17 Microstructure of squeeze cast 7075 alloy under produced under 25Hz frequency at 630°C SSM temperature obtained by optical microscopy (200x)

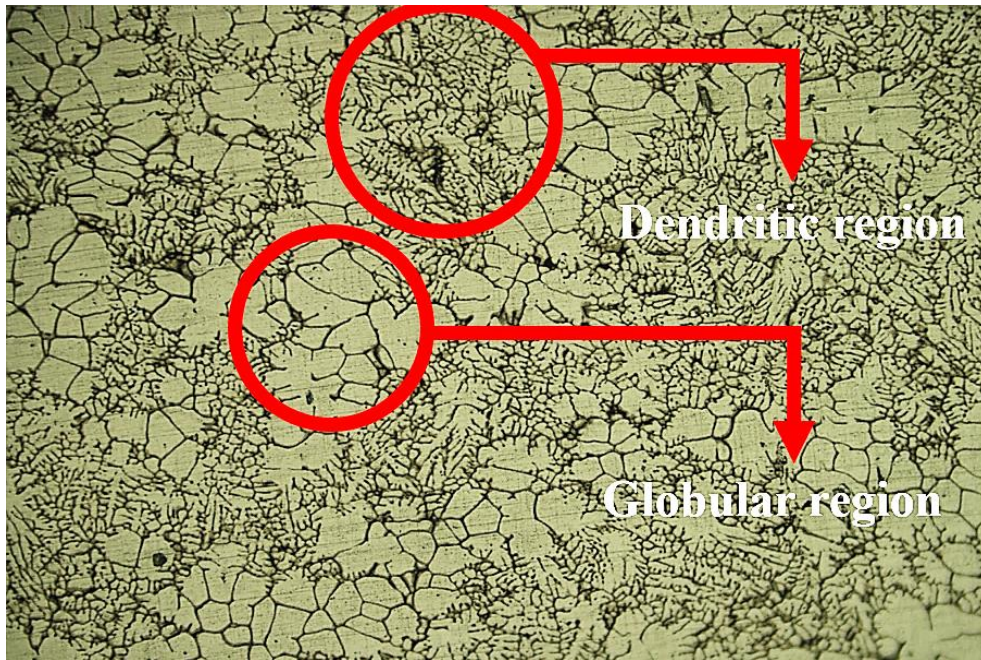


Figure 6.18 Microstructure of squeeze cast 7075 alloy under produced under 25Hz frequency at 625°C SSM temperature obtained by optical microscopy (200x)

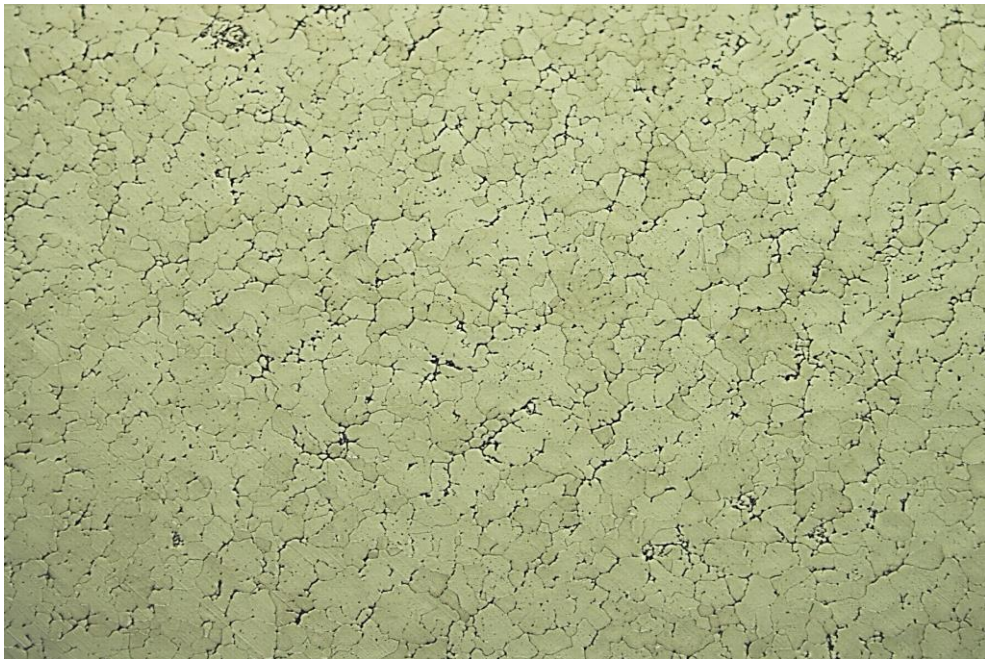


Figure 6.19 Microstructure of squeeze cast and T6-treated 7075 alloy produced under 25Hz frequency at 635°C SSM temperature obtained by optical microscopy (200x)

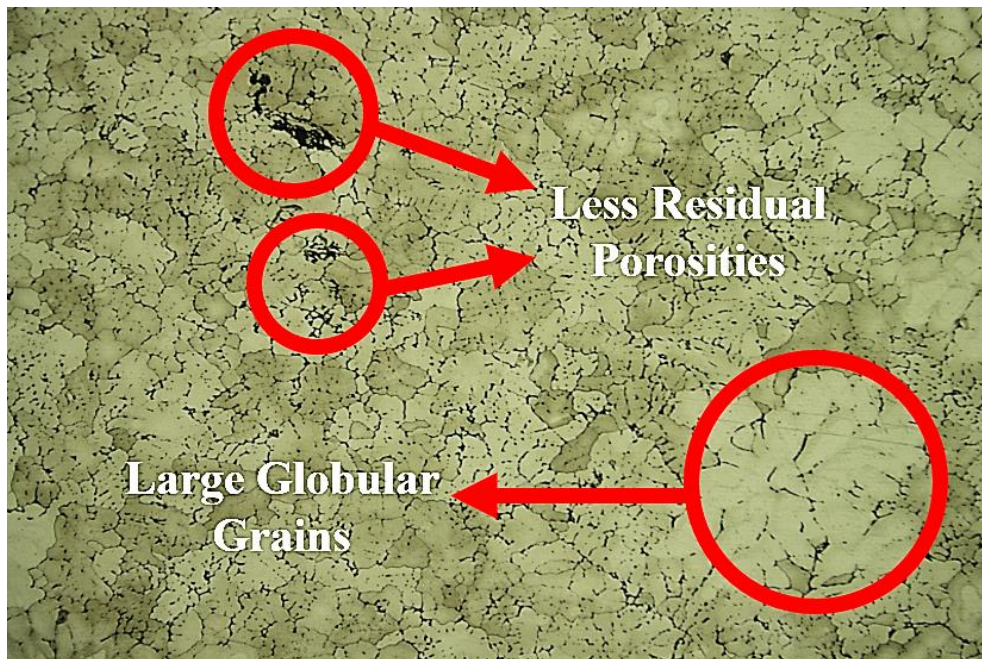


Figure 6.20 Microstructure of squeeze cast and T6-treated 7075 alloy produced under 25Hz frequency at 630°C SSM temperature obtained by optical microscopy (200x)

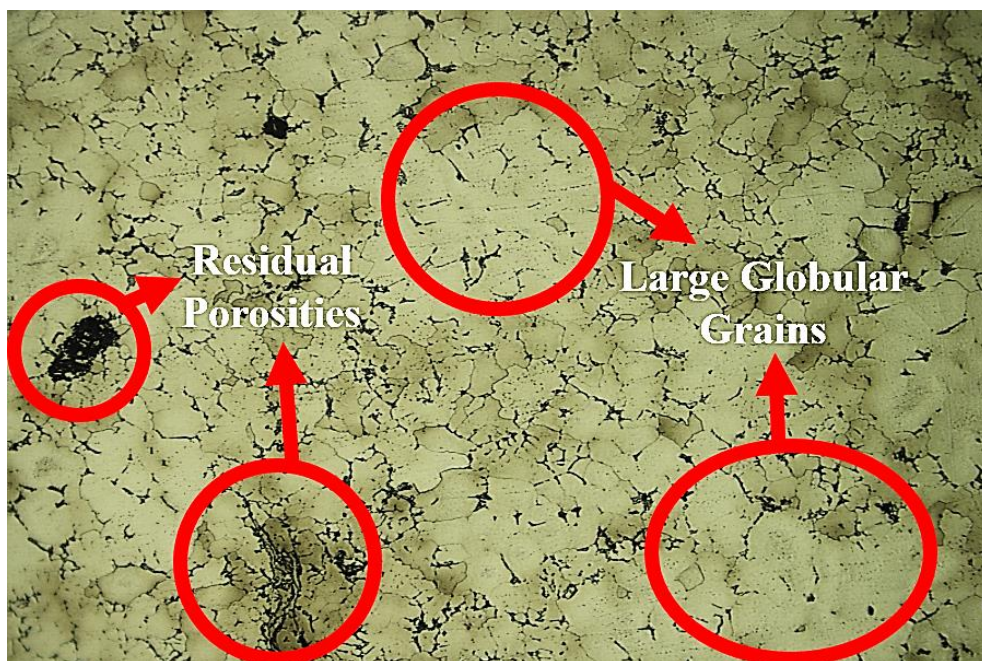


Figure 6.21 Microstructure of T6- squeeze cast and T6-treated 7075 alloy produced under 25Hz frequency at 625°C SSM temperature obtained by optical microscopy (200x)

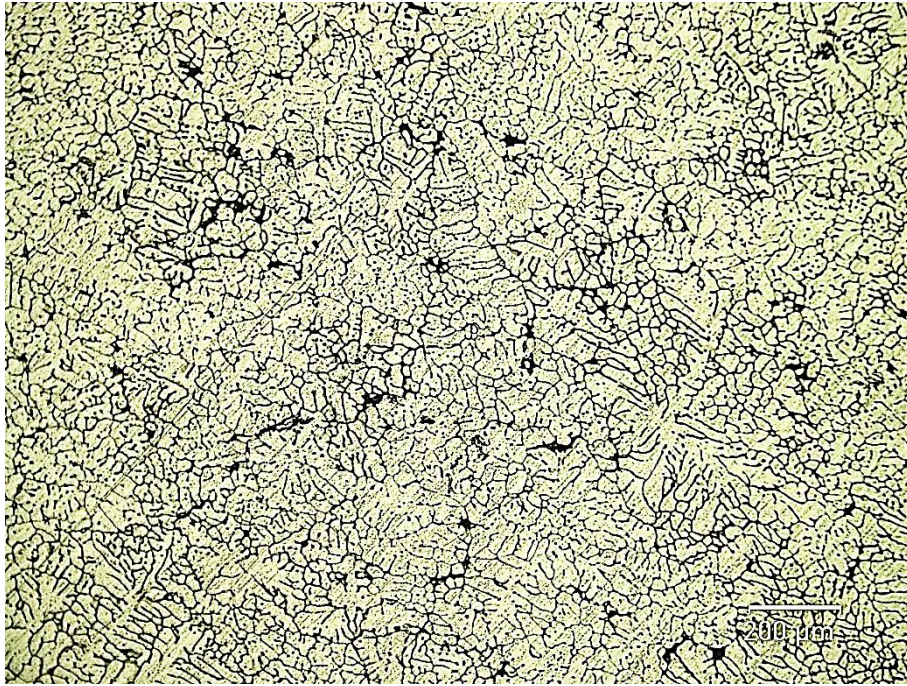


Figure 6.22 Microstructure of squeeze cast 7075 alloy produced with no-vibration at 670°C obtained by optical microscopy (200x)



Figure 6.23 Microstructures of squeeze cast and T6-treated 7075 alloy produced with no-vibration at 670°C obtained by optical microscopy (200x)

6.3.1.3. Squeeze casting of 7075/B₄C composites

In order to observe the distribution and the size of B₄C particles in various regions of the microstructure of the composites, three representative micrographs of each composite were shown in this section. Microstructures of squeeze cast 7075/B₄C composites show that the distribution of B₄C particles are considerably nonhomogenous and B₄C particles tended to form agglomerate in general. The composite having 12wt.% B₄C includes massive agglomerates of B₄C in majority of its microstructure whereas more homogenous distribution and smaller agglomerates are observed in particular regions as seen in figure 6.26. 8wt.% 7075/B₄C composite has also large agglomerates, smaller compared to 12wt.%, but the distribution is also quite nonhomogenous as 12wt.% 7075/B₄C composite. In terms of smaller agglomerate size and homogenous distribution, 10wt.% 7075/B₄C composite is the optimum and the best one, however there are also some regions where big chunk of agglomerates can be seen in its microstructure as seen in figure 6.25. In overall, the main problem for the semi-solid squeeze casting of 7075/B₄C composites is the formation of big B₄C agglomerates and non-homogenous distribution of B₄C particles. B₄C powder had the particle size of 1-3μm, however the size of B₄C agglomerates could exceed even 500μm for some composite samples which will most probably cause to fall in the mechanical properties. Among these composites, 10wt.% 7075/B₄C might have the highest mechanical properties since the microstructure has relatively uniform distribution of B₄C particles although formation of big agglomerates could be observed in particular regions.

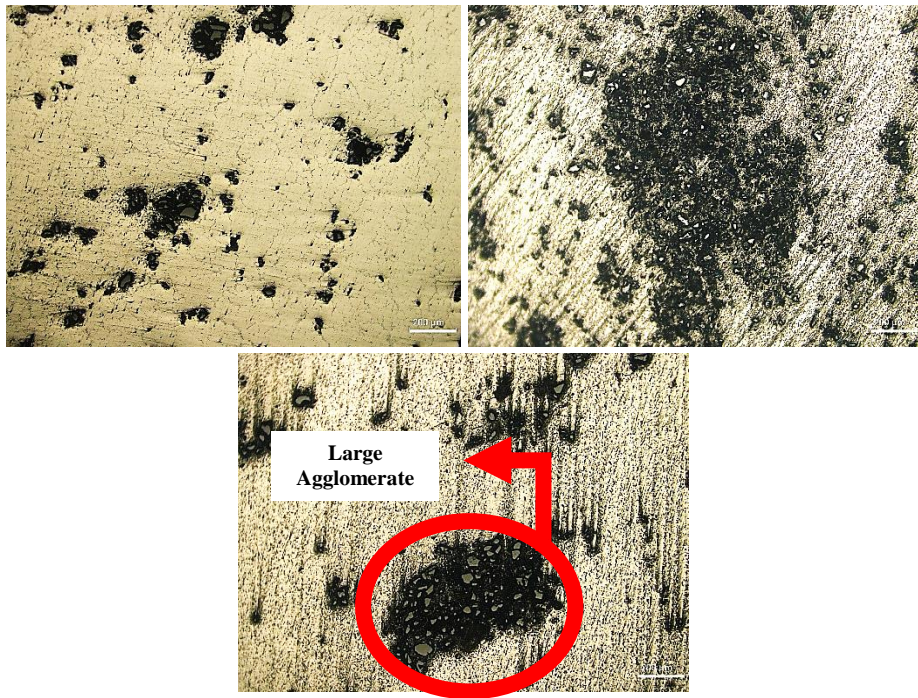


Figure 6.24 Microstructures of squeeze cast and T6-treated 8wt.% 7075/B₄C composite produced under 25Hz frequency at 635°C SSM temperature (200x)

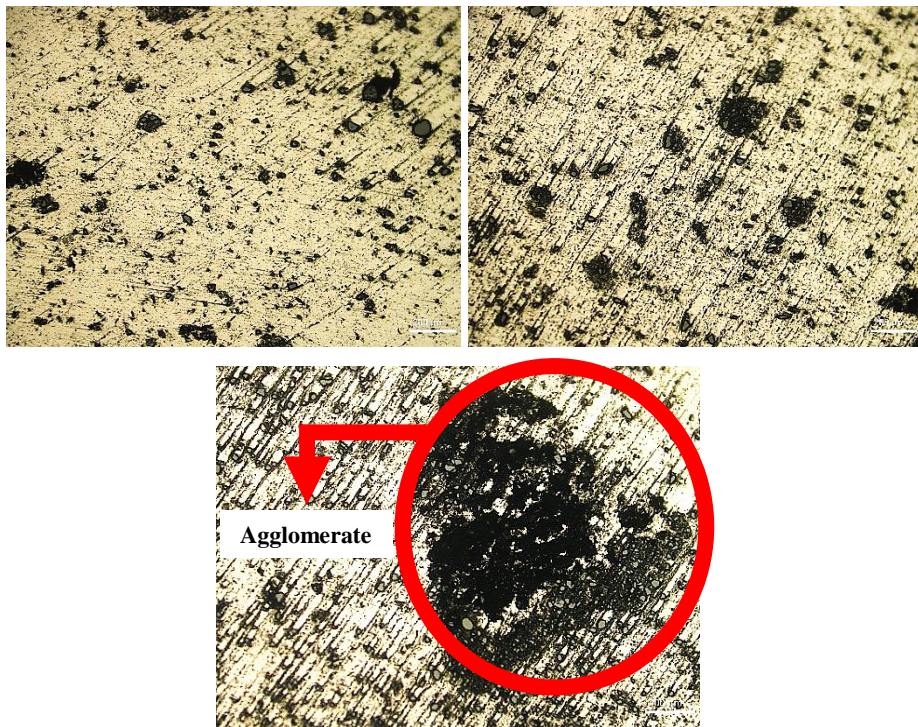


Figure 6.25 Microstructures of squeeze cast and T6-treated 10wt.% 7075/B₄C composite produced under 25Hz frequency at 635°C SSM temperature (200x)

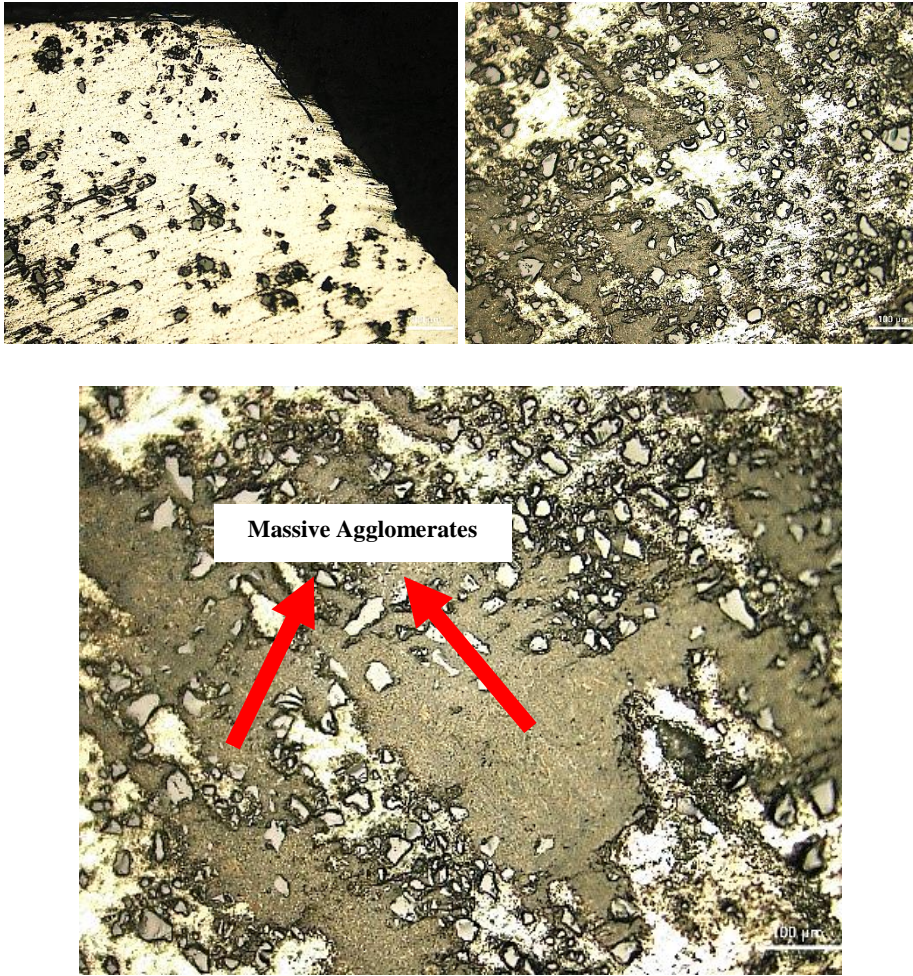


Figure 6.26 Microstructures of squeeze cast and T6-treated 10wt.% 7075/B₄C composite produced under 25Hz frequency at 635°C SSM temperature (200x)

6.3.1.4. Hot rolling of 7075/B₄C composites

In the same manner, four representative micrographs of each hot-rolled composite were shown in this section. First of all, the improvement in the distribution homogeneity and the size of the B₄C agglomerates can be clearly observed in the microstructures of all hot-rolled 7075/B₄C composites. After hot-rolling, B₄C agglomerates becomes smaller in size. The largest agglomerates were again observed

in the microstructure of 12wt.% 7075/B₄C composites having size below 200 μ m (see in figure 6.29), but the distribution of B₄C particles are much more homogenous for this composite. For 8wt.% 7075/B₄C composite, similarly distribution of B₄C particles are quite homogenous compared to squeeze casting samples. In addition to homogenous distribution, the size of the B₄C agglomerates became smaller in size for 8wt.% 7075/B₄C composites, the biggest B₄C agglomerates have the size of 50-100 μ m, but in general the size of the agglomerates is below 50 μ m as seen in figure 6.27. The best microstructure having homogenous B₄C particle distribution with minimum agglomeration belongs to 10wt.% 7075/B₄C composite. As seen in figure 6.28, B₄C particles were distributed homogeneously in the majority of the microstructure and the size of agglomerates are quite small after hot-rolling process, below 10-20 μ m in general. Therefore, it can be concluded that 10wt. % B₄C addition resulted in the optimum microstructure after hot-rolling, although there exist residual smaller agglomerates, for the semi-solid squeeze casting of 7075 alloy.

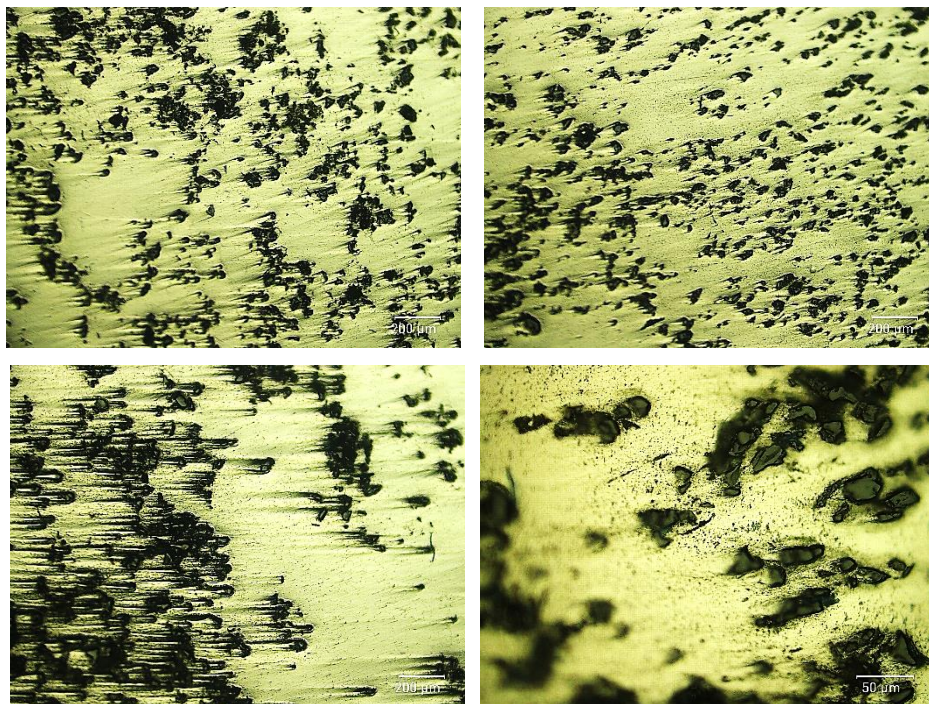


Figure 6.27 Microstructures of hot rolled and T6-treated 8wt.% 7075/B₄C composite (200x)

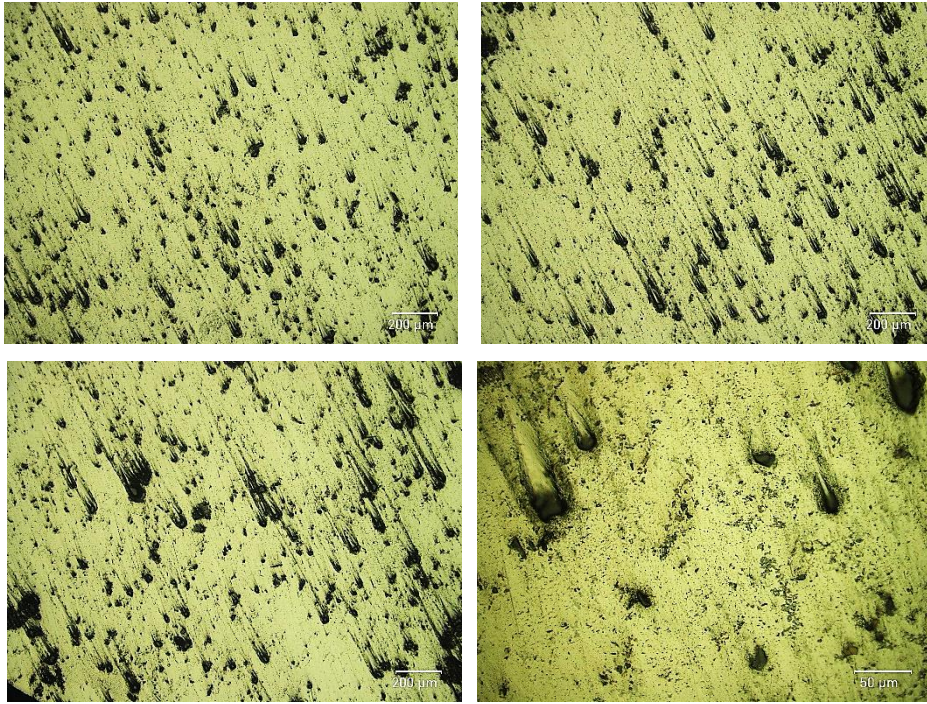


Figure 6.28 Microstructures of hot rolled and T6-treated 10wt.% 7075/B₄C composite (200x)

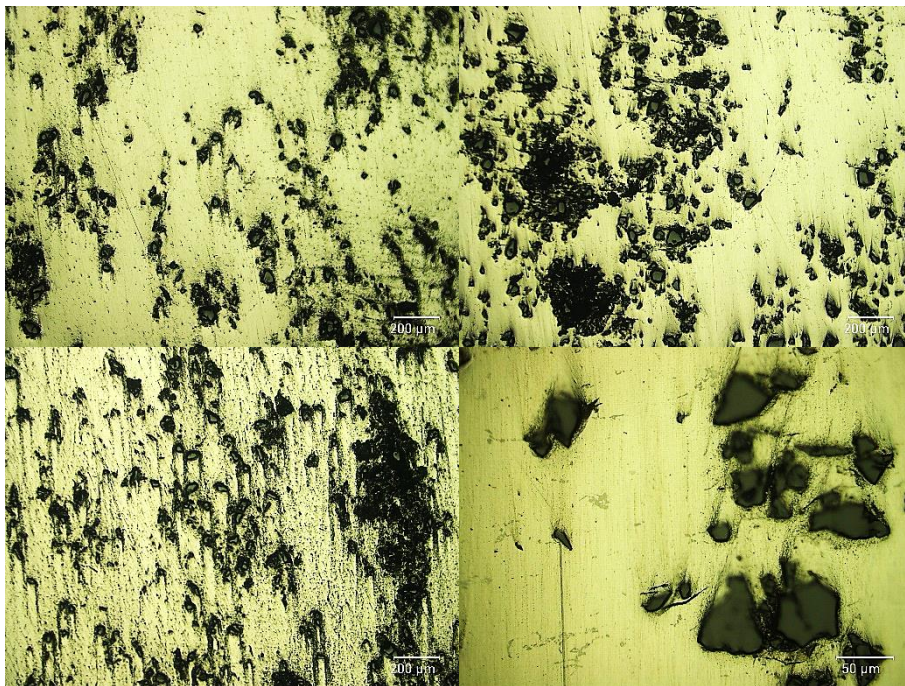


Figure 6.29 Microstructures of hot rolled and T6-treated 12wt.% 7075/B₄C composite (200x)

6.3.2. Grain size measurement

Grain size measurement of both sand and squeeze cast 7075 alloys were carried out. 10 individual grains in 3 different areas were observed, in total 30 grains were measured for each sample. Both as-cast and T6-heat treated samples were analyzed.

6.3.2.1. Sand casting

The example grain size measurements for sand castings can be seen in figure 6.30-31.

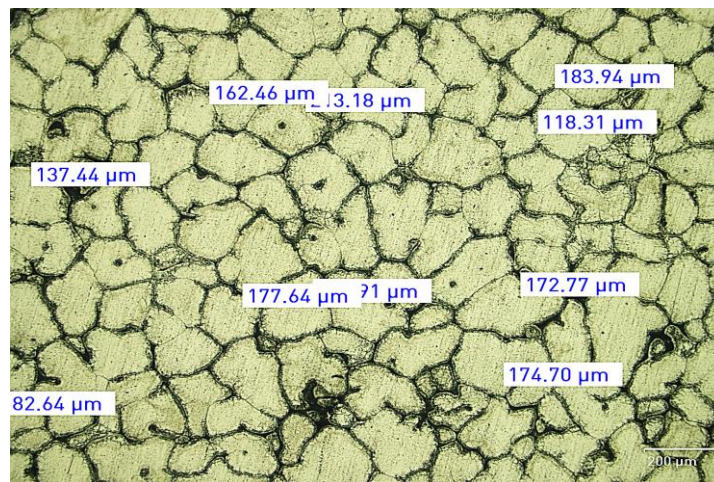


Figure 6.30 Grain size measurement on the microstructure of sand cast 7075 alloy produced under 15Hz frequency and 635°C SSM temperature (200x)

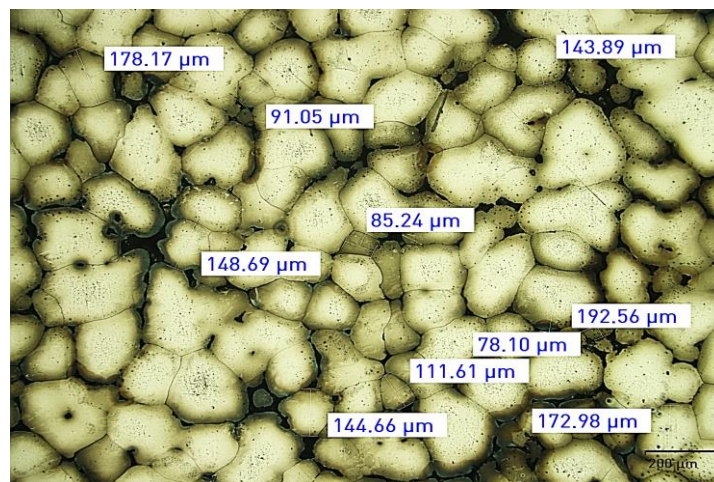


Figure 6.31 Grain size measurement on the microstructure of sand cast and T6 treated 7075 alloy under 15Hz frequency and 635°C SSM temperature (200x)

Table 6-6 Grain size measurements of sand cast 7075 alloys produced under three different vibration frequencies and four different SSM temperatures

Casting Parameters		Grain Size Measurement (Average of 10 Grains)		
Vibration Frequency (Hz)	SSM Temperature (°C)	Region #1 (µm)	Region #2 (µm)	Region #3 (µm)
15	635	125.00	124.00	128.00
	630	135.00	133.00	138.00
	625	137.00	131.00	136.00
	620	125.00	124.00	128.00
25	630	129.00	146.00	134.00
	625	119.00	128.00	109.00
	620	102.00	92.00	106.00
35	635	115.00	125.00	115.00
	630	119.00	119.00	128.00
	625	119.00	122.00	119.00
	620	127.00	126.00	122.00

Table 6-7 Grain size measurements of sand cast and T6-treated 7075 alloys produced under three different vibration frequencies and four different SSM temperatures

Casting Parameters		Grain Size Measurement (Average of 10 Grains)		
Vibration Frequency (Hz)	SSM Temperature (°C)	Region #1 (µm)	Region #2 (µm)	Region #3 (µm)
15	635	134.70	132.50	138.63
	630	145.30	128.66	132.60
	625	145.26	131.87	123.64
	620	120.40	146.21	131.68
25	630	108.00	114.00	116.00
	625	106.00	107.00	105.00
	620	112.00	105.00	99.00
35	635	136.00	138.00	140.00
	630	132.00	131.00	128.00
	625	134.00	133.00	136.00
	620	118.00	117.00	117.00

As seen in figure 6.32 and 6.33, there is a behavior of grain size decrease slightly as SSM temperature decreases although there are exceptions from place to place such as for 35Hz 620°C as-cast sample (blue line in figure 6.32). There is no clear behavior of grain refinement as SSM temperature decreases. Moreover, the fine grain structure in sand casting was above 100 μm .

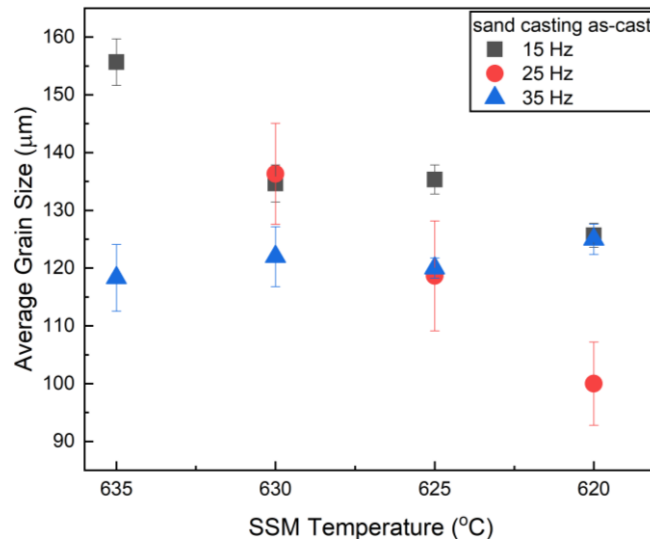


Figure 6.32 Grain size variation of sand cast 7075 alloy produced under three different vibration frequency as SSM temperature decreases

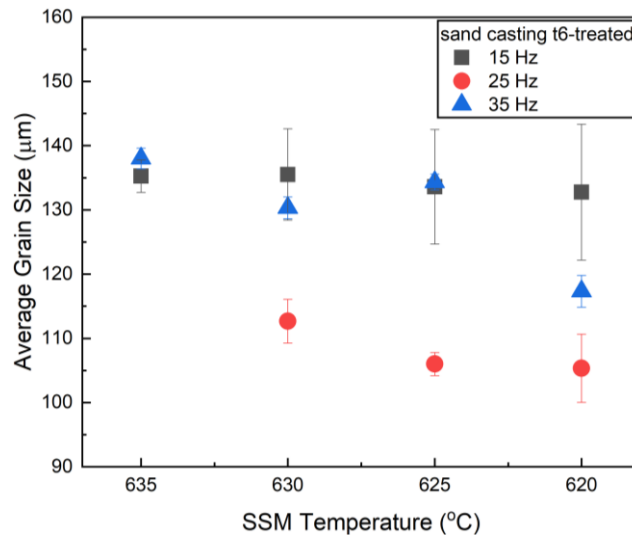


Figure 6.33 Grain size variation of sand cast and T6-treated 7075 alloy produced under three different vibration frequency as SSM temperature decreases

6.3.2.2. Squeeze casting of 7075 alloy

The example grain size measurements for squeeze casting can be seen in figure 6.34-35.

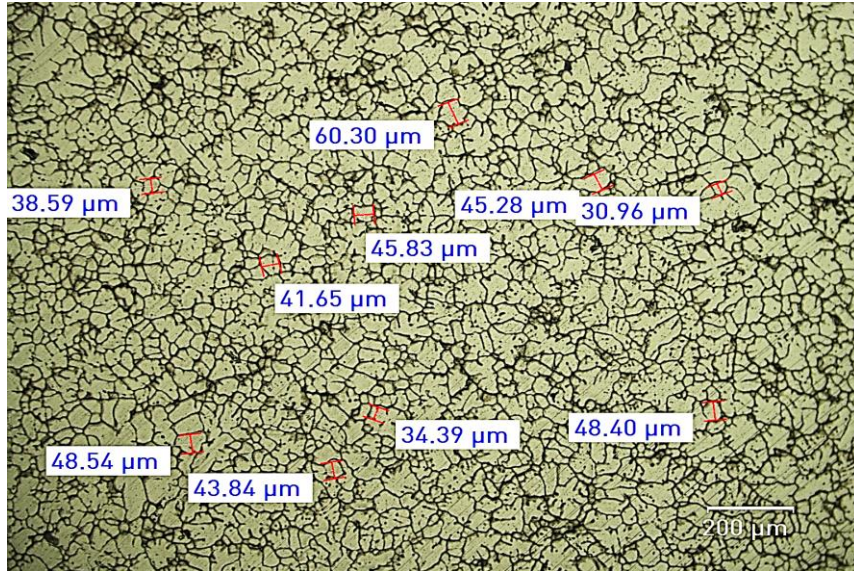


Figure 6.34 Grain size measurement on the microstructure of squeeze cast 7075 alloy produced under 15Hz frequency and 635°C SSM temperature (200x)

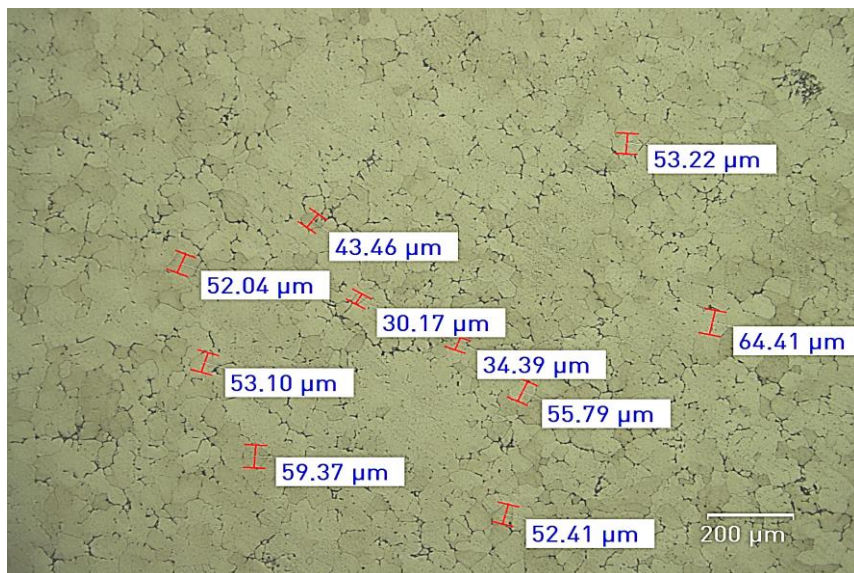


Figure 6.35 Grain size measurement on the microstructure of squeeze cast and T6 treated 7075 alloy produced under 15Hz frequency at 635°C SSM temperature (200x)

Table 6-8 Grain size measurements of squeeze cast 7075 alloys produced under three different vibration frequencies and three different SSM temperatures

Casting Parameters		Grain Size Measurement (Average of 10 Grains)		
Vibration Frequency (Hz)	SSM Temperature (oC)	Region #1 (µm)	Region #2 (µm)	Region #3 (µm)
15	635	38.85	39.88	43.78
	630	47.67	46.06	47.32
	625	55.27	53.68	58.19
25	635	41.90	34.03	42.79
	630	46.05	42.76	47.15
	625	56.56	60.03	51.38
35	635	38.27	37.54	34.95
	630	55.20	56.11	48.08
	625	56.50	51.86	50.35

Table 6-9 Grain size measurements of squeeze cast and T6 treated 7075 alloys produced under three different vibration frequencies and three SSM temperatures

Casting Parameters		Grain Size Measurement (Average of 10 Grains)		
Vibration Frequency (Hz)	SSM Temperature (oC)	Region #1 (µm)	Region #2 (µm)	Region #3 (µm)
15	635	49.84	48.35	50.74
	630	62.81	52.33	59.59
	625	66.19	59.24	76.78
25	635	43.11	41.79	40.32
	630	51.36	48.12	46.48
	625	67.89	61.89	59.85
35	635	39.57	40.45	40.34
	630	46.85	50.87	43.16
	625	68.79	64.24	64.53

As seen in figure 6.36 and 6.37, as SSM temperature decreases the average grain size increases. Undercooling (ΔT) is higher and thermal gradient ($\frac{\partial T}{\partial x}$) is lower at 625°C,

so lower grain size is expected at that temperature. Although the dendrites are so fine and dendrite arms spacings are quite small at 625°C, globular grains are quite large (see in figure 6.18) which resulted in higher average grain size at lower SSM temperatures. The finest average grain size were obtained at 635°C SSM temperature for all vibration frequencies. If 5-6°C temperature drop during semi-solid 7075 alloy delivery is taken into account, for finer average grain size, the optimum temperature of 635°C result is consistent with the solid fraction obtained by thermal analysis. The finest grain size is about 40 μm at 635°C SSM temperature.

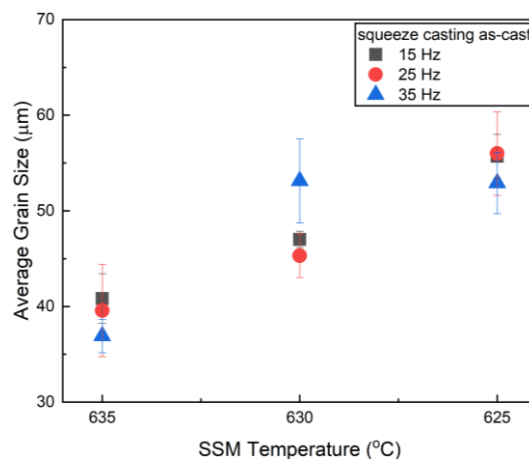


Figure 6.36 Grain size variation of squeeze cast 7075 alloy produced under three different vibration frequency as SSM temperature decreases

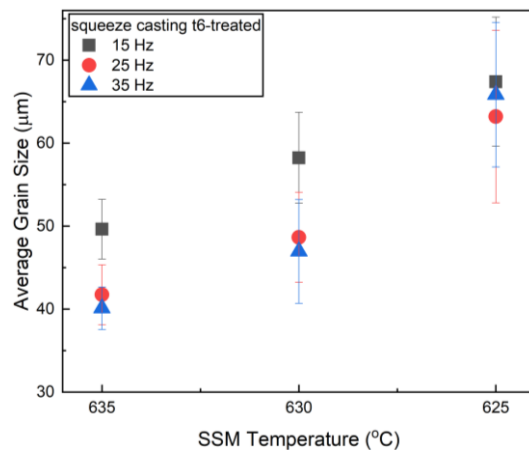


Figure 6.37 Grain size variation of squeeze cast and T6-treated 7075 alloy produced under three different vibration frequency as SSM temperature decreases

6.3.2.3. Squeeze casting and hot rolling of 7075/B₄C composite

The example grain size measurements for squeeze cast and hot-rolled 10wt.% 7075/B₄C composites can be seen in figure 6.38 and 6.39.

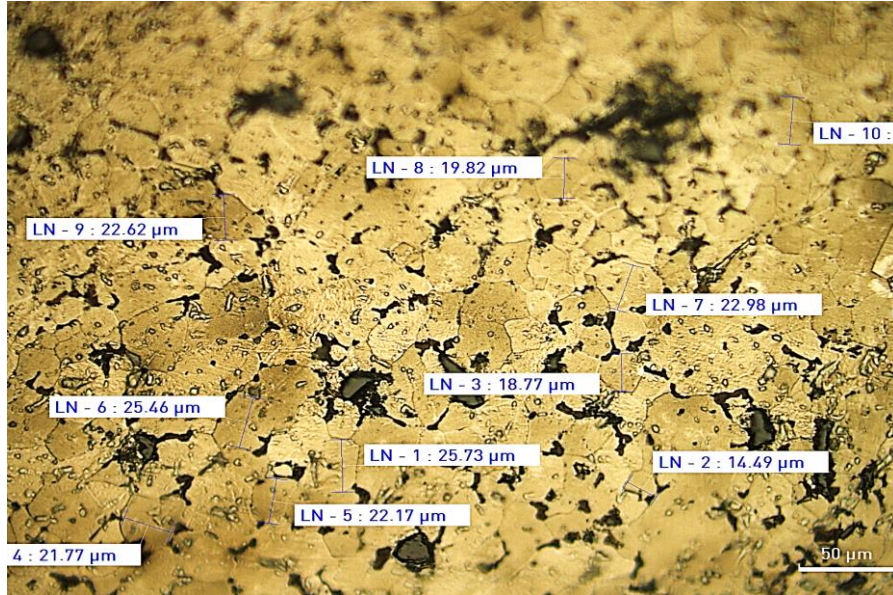


Figure 6.38 Example grain size measurement on the microstructure of T6-treated squeeze cast 10wt.% 7075/B₄C composite

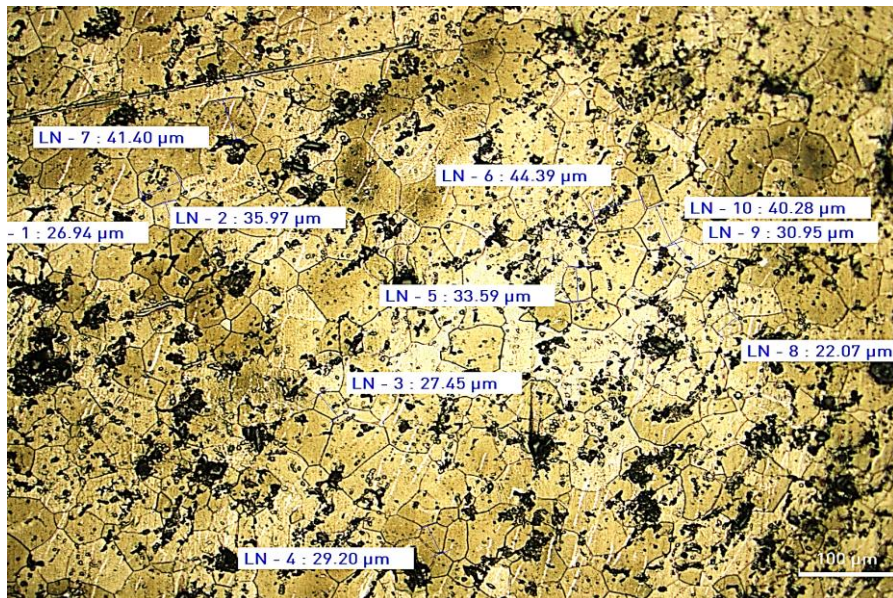


Figure 6.39 Example grain size measurement on the microstructure of T6-treated hot-rolled 10wt.% 7075/B₄C composite

Table 6-10 Grain size measurements of T6-treated squeeze cast and hot-rolled 7075/B₄C composites with different % B₄C addition

Processing	% B ₄ C Addition	Grain Size Measurement (Average of 10 Grains)		
		Region #1 (μm)	Region #2 (μm)	Region #3 (μm)
Squeeze Casting	8	32.03	23.46	26.60
	10	21.54	21.72	22.19
	12	19.94	-	-
Hot Rolling	8	38.35	39.59	38.97
	10	36.62	31.72	33.22
	12	35.58	37.80	36.30

By addition of B₄C as reinforcement to 7075 alloy, a further grain refinement was observed. For the squeeze casting samples, grain size decreased as B₄C wt.% increases and the finest average grain size was about 20 μm . On the other hand, the average grain size reaches its optimum value at 10wt.% B₄C addition for hot-rolled composites which is about 34 μm as all seen in figure 6.40.

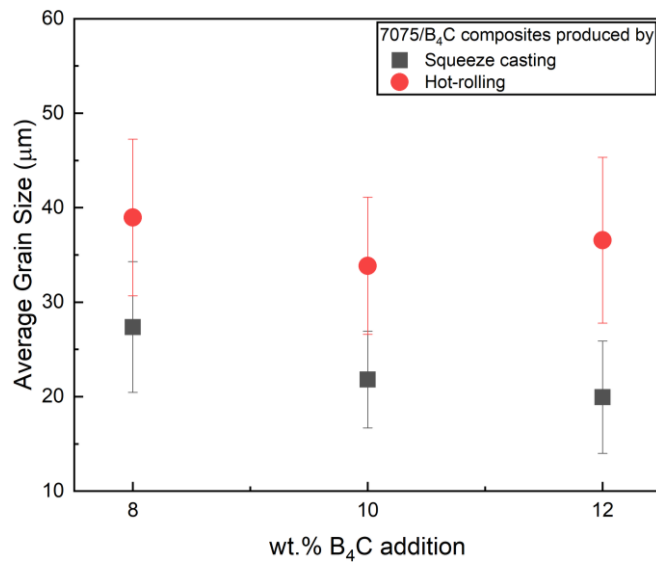


Figure 6.40 Grain size variation of T6-treated squeeze cast and hot-rolled 7075/B₄C composites as % B₄C addition

6.3.3. Porosity measurement

Porosity measurement of both sand and squeeze cast 7075 alloys were carried out. Porosity in 5 different representative areas in the microstructure of each sample were measured.

6.3.3.1. Sand casting

Example porosity calculation images on the microstructure of sand cast 7075 alloys can be seen in figure 6.41 and 6.42.



Figure 6.41 Porosity (red) in the microstructure of sand cast 7075 alloy produced under 15Hz frequency and 635°C SSM temperature (100x)



Figure 6.42 Porosity (red) in the microstructure of sand cast and T6-treated 7075 alloy produced under 15Hz frequency at 635°C SSM temperature (100x)

Table 6-11 Porosity measurement results of sand cast 7075 alloys produced under three different vibration frequencies and four different SSM temperatures

Casting Parameters		Porosity Measurement (% area)				
Vibration Frequency (Hz)	SSM Temperature (°C)	#1	#2	#3	#4	#5
15	635	5.57	3.00	5.03	10.33	3.34
	630	2.38	4.24	2.49	6.95	3.85
	625	5.44	4.90	5.50	7.17	2.29
	620	4.19	3.13	3.38	2.56	3.93
25	630	7.13	7.35	7.00	8.03	6.45
	625	5.31	4.36	4.67	4.80	7.05
	620	3.79	4.91	5.01	4.95	6.73
	635	4.50	5.33	5.97	4.26	14.61
35	630	11.65	34.61	5.04	7.47	-
	625	12.20	12.49	6.23	9.71	7.54
	620	5.18	6.19	6.09	3.75	6.61
No-vibration	670	5.07	5.42	4.59	4.01	6.79

Table 6-12 Porosity results of sand cast and T6-treated 7075 alloys produced under three different vibration frequencies and four different SSM temperatures

Casting Parameters		Porosity Measurement (% area)				
Vibration Frequency (Hz)	SSM Temperature (°C)	#1	#2	#3	#4	#5
15	635	9.81	2.94	11.42	5.08	5.11
	630	6.02	5.84	3.48	4.92	4.35
	625	5.69	6.23	6.31	4.53	8.60
	620	9.11	5.87	6.36	6.17	2.60
25	630	6.71	5.54	4.57	5.20	8.63
	625	4.61	3.32	5.09	4.33	3.82
	620	2.92	3.21	4.23	4.27	4.26
35	635	6.59	5.38	7.22	7.97	7.50
	630	8.19	6.94	6.21	4.22	7.98
	625	5.69	4.16	10.38	6.26	6.66
	620	3.96	6.30	8.41	7.55	7.34
No-vibration	670	7.42	3.32	5.54	4.25	6.10

As seen in figure 6.41 and 6.42, there are quite large chunk of pores in the microstructure of sand cast products (for the detail see appendix D). There is no exact behaviour of decrease in porosity, in some parts of figure 6.43 and 6.44. There is a decrease in porosity as SSM temperature decreases. Sand-casting properties are not parallel with the thermal analysis expectations due to the presence of non homogeneous pore distribution.

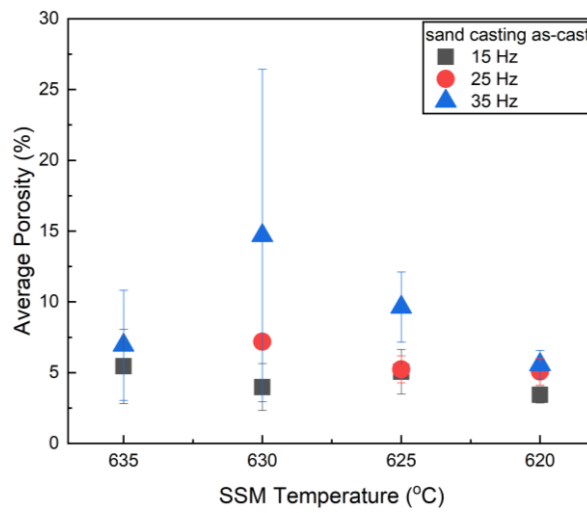


Figure 6.43 Porosity variation of sand cast 7075 alloy produced under three different vibration frequency as SSM temperature decreases

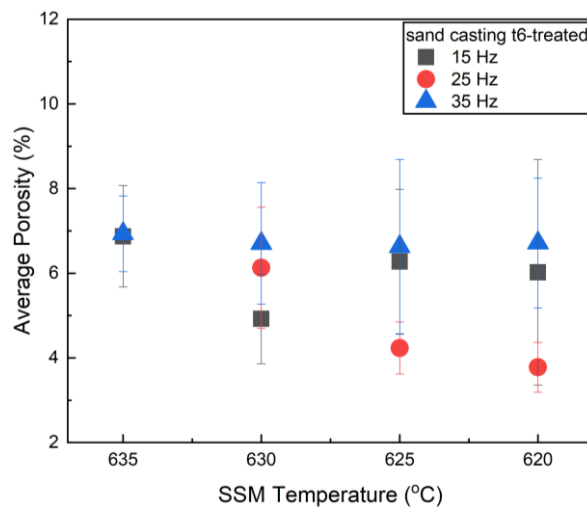


Figure 6.44 Porosity variation of sand cast and T6-treated 7075 alloy produced under three different vibration frequency as SSM temperature decreases

6.3.3.2. Squeeze casting

Image analysis of porosity distribution in the squeeze-cast 7075 alloy sample can be seen in figure 6.45 and 6.46.



Figure 6.45 Porosity (red) in the microstructure of as-squeeze cast 7075 alloy produced under 15Hz frequency at 635°C SSM temperature (100x)

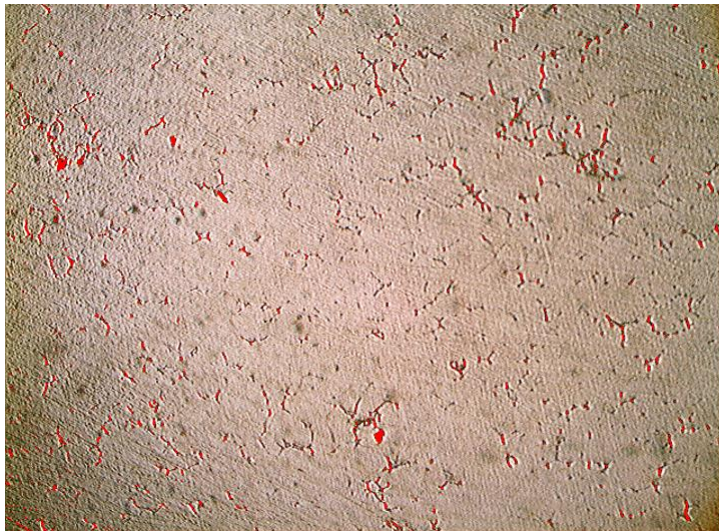


Figure 6.46 Porosity (red) in the microstructure of squeeze cast and T6-treated 7075 alloy produced by 15Hz frequency at 635°C SSM temperature (100x)

Table 6-13 Porosity results of as-squeeze cast 7075 alloys under three different vibration frequencies and four different SSM temperatures

Casting Parameters		Porosity Measurement (% area)				
Vibration Frequency (Hz)	SSM Temperature (°C)	#1	#2	#3	#4	#5
15	635	1.18	1.43	1.15	0.92	1.18
	630	1.32	1.14	1.16	1.95	1.59
	625	1.50	1.15	1.28	1.88	1.91
	635	1.44	1.54	0.82	1.56	1.44
25	630	1.61	1.89	1.66	2.23	1.78
	625	2.01	1.02	2.19	1.20	2.74
	635	0.81	0.99	0.81	1.01	0.96
35	630	1.04	1.00	1.19	1.24	1.02
	625	1.52	1.23	1.52	1.70	1.07
No-vibration	670	1.32	1.67	2.05	1.76	2.23

Table 6-14 Porosity results of as-squeeze cast and T6 treated 7075 alloys under three different vibration frequencies and four different SSM temperatures

Casting Parameters		Porosity Measurement (% area)				
Vibration Frequency (Hz)	SSM Temperature (°C)	#1	#2	#3	#4	#5
15	635	0.91	1.29	1.07	0.85	1.02
	630	0.89	1.46	1.54	1.33	1.24
	625	0.42	0.71	0.66	0.64	0.87
25	635	0.89	0.87	1.10	0.90	0.83
	630	1.05	0.85	0.76	0.79	0.88
	625	2.11	2.24	2.35	1.53	2.08
35	635	0.75	0.84	0.90	0.94	0.86
	630	0.91	1.06	1.60	1.01	1.24
	625	1.27	1.25	1.20	1.06	1.18
No-vibration	670	1.22	1.22	1.20	1.11	1.22

As seen in figure 6.45 and 6.46, the amount of average porosity in squeeze cast specimens is much less than the sand cast specimens. The size of pores are much smaller and more homogenously distributed (for the detail see appendix D). Moreover, the decreasing porosity behaviour as SSM temperature increases up to 635°C as seen in figure 6.47 and 6.48 is consistent with previous results of thermal analysis and microstructures examined. The small amount of porosity (1-2%) is evidence of the benefit and effect of semi-solid squeeze casting.

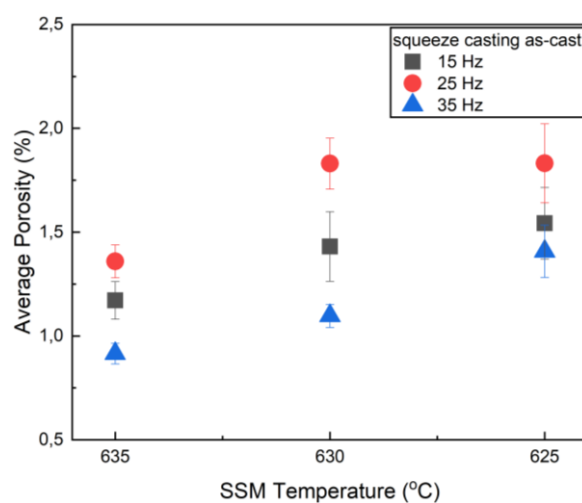


Figure 6.47 Porosity variation of squeeze cast 7075 alloy produced under three different vibration frequency as SSM temperature decreases

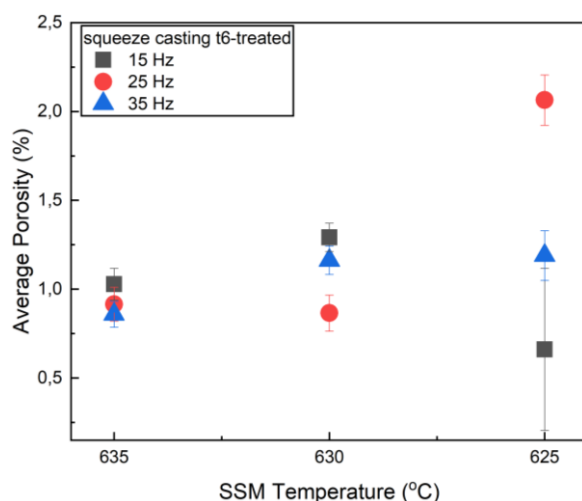


Figure 6.48 Porosity variation of squeeze cast and T6-treated 7075 alloy produced under three different vibration frequency with decreasing SSM temperature

6.4. X-Ray diffraction results

6.4.1.1. Sand casting

Sand and squeeze cast 7075 alloy samples have the XRD peaks of almost only pure Al with a little bit shifting (for detail see appendix E). Some samples have the peak of Mg_2Si phase at 40.12° angle whereas the peaks of $MgZn_2$ phase are almost invisible, this is because $MgZn_2$ precipitates are so tiny that their disturbance in aluminum crystal lattice can not be detected by XRD patterns. There are some weak peaks of $MgZn_2$ phase such as peaks at $38,62^\circ$ and $45,16^\circ$ which can be seen in figure 6.52.

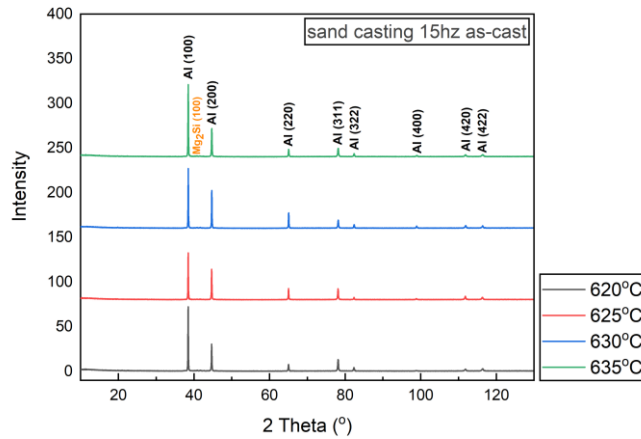


Figure 6.49 XRD Patterns of sand cast 7075 alloy produced under 15Hz vibration frequency with four different SSM temperatures

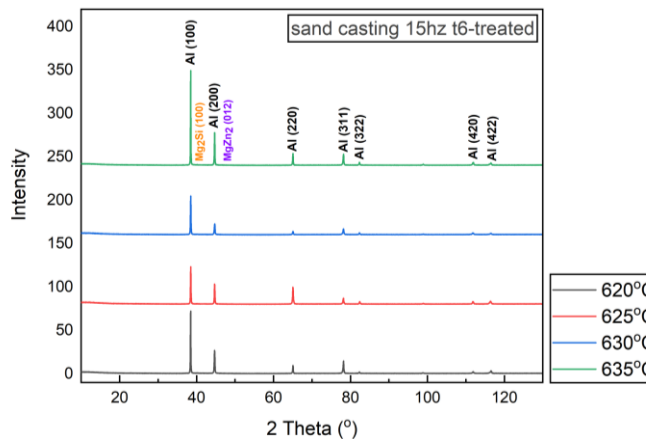


Figure 6.50 XRD Patterns of sand cast and T6-treated 7075 alloy produced under 15Hz vibration frequency with four different SSM temperatures

6.4.1.2. Squeeze casting of 7075 alloy

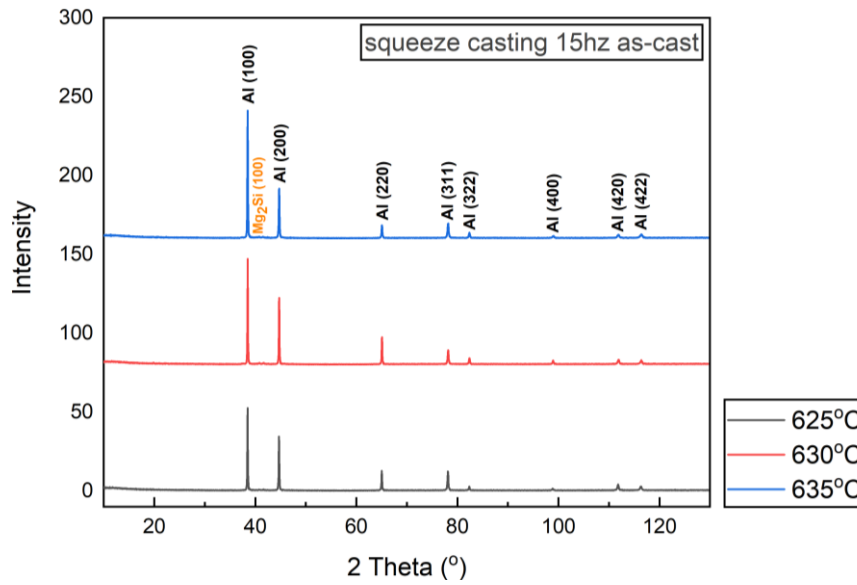


Figure 6.51 XRD Patterns of squeeze cast 7075 alloy produced under 15Hz vibration frequency with four different SSM temperatures

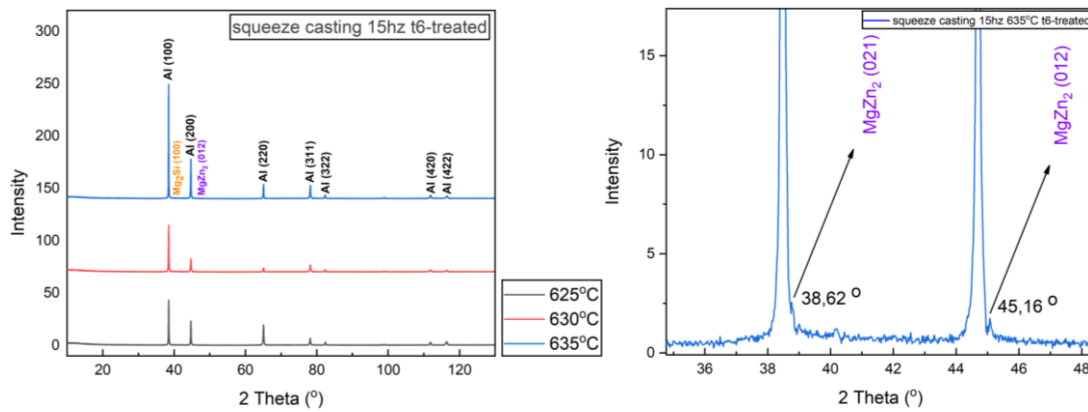


Figure 6.52 XRD Patterns of squeeze cast and T6-treated 7075 alloy produced under 15Hz vibration frequency with four different SSM temperatures (left) and focused area on the sample produced at 635°C SSM temperature (right)

6.4.1.3. Squeeze casting of 7075/B₄C composite

Figure 6.53 shows the XRD peaks of B₄C used for the production of 7075/B₄C composites, as seen in the figure the peaks corresponded to Boron Carbide (B₄C) phase. XRD patterns of squeeze cast 7075/B₄C composites are shown in figure 6.54, the peaks of aluminum phase can easily be seen but the peaks of B₄C phase are very weak. The peak of B₄C at 37.81° diffraction angle have highest intensity for 10wt.% 7075/B₄C composite which can be seen in figure 6.54.

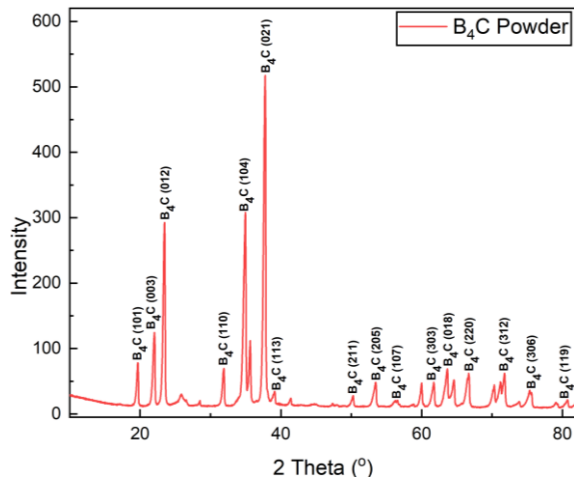


Figure 6.53 XRD Patterns of powder B₄C used for the production of 7075/B₄C

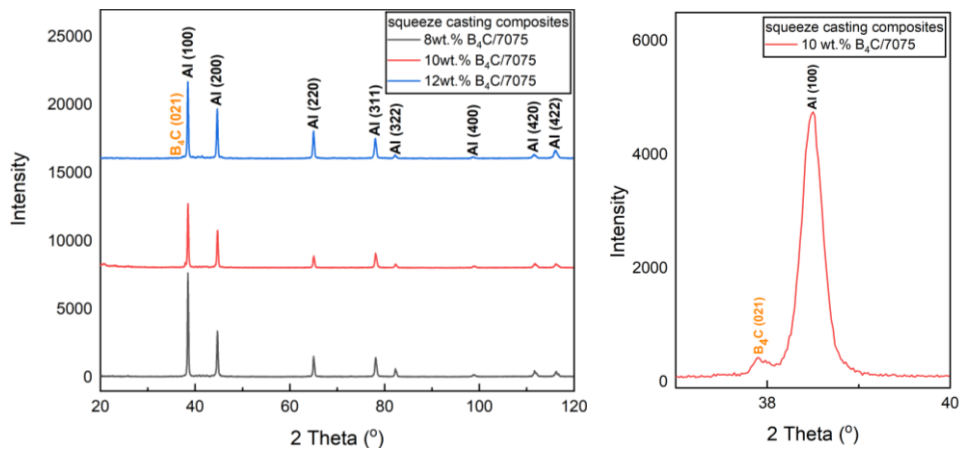


Figure 6.54 XRD Patterns of squeeze cast and T6-treated 7075/B₄C composites and peaks of 10wt.% 7075/B₄C composite between 37-40° angles

6.5. Microstructure Under Scanning Electron Microscopy

In this part, scanning electron microscopy images of various rheocast products will be shown for microstructural evaluation.

6.5.1. Sand casting

Figure 6.55 shows SEM image of homogeneously distributed fine precipitates in sand cast T6-treated 7075 alloys produced under 35Hz and 630°C SSM temperature. Figure 6.56 also shows SEM image of fine precipitates distributed in in sand cast T6-treated 7075 alloys produced under 35Hz and 635°C SSM temperature, but this time the fine precipitates cannot be formed continuously and homogeneously compared to figure 6.55. Therefore, it can be said that mechanical properties of sand castings will directly related to distribution of fine precipitates after heat treatment and the mechanical test results prove this results.

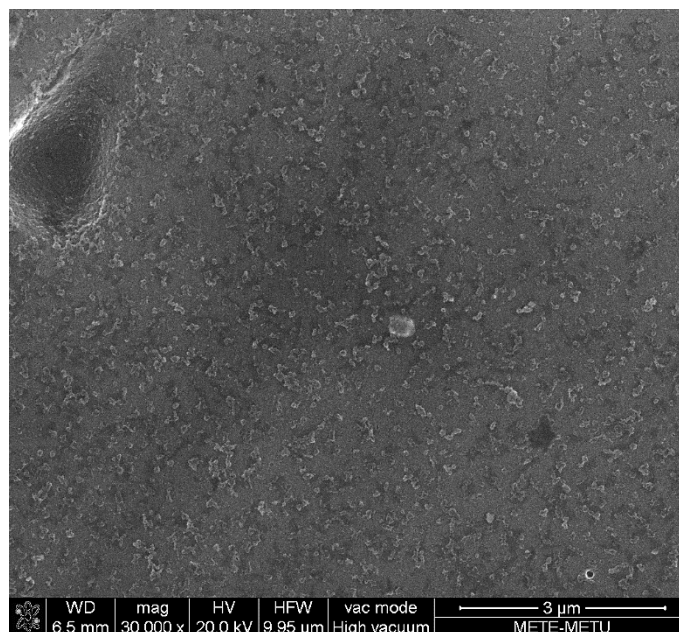


Figure 6.55 SEM image of sand cast and T6-treated 7075 alloy produced under 35Hz frequency and 630°C SSM temperature

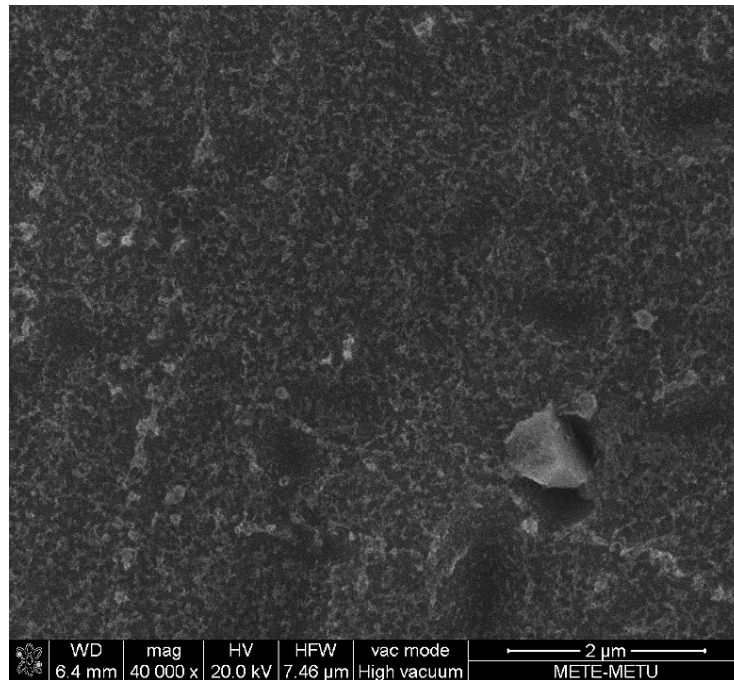


Figure 6.56 SEM image of sand cast and T6-treated 7075 alloy produced under 35Hz frequency and 635°C SSM temperature

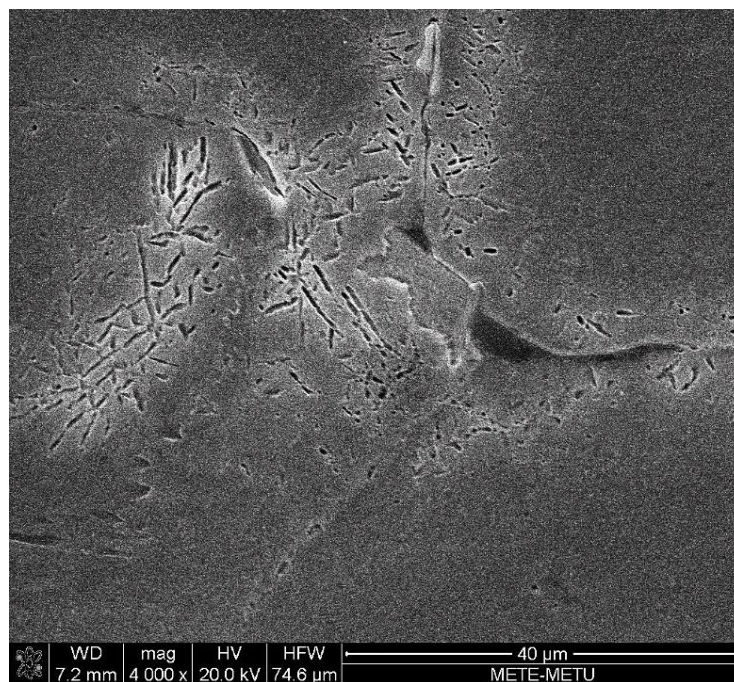


Figure 6.57 SEM image of needle-like phases in sand cast and T6-treated 7075 alloy produced under 35Hz frequency and 625°C SSM temperature

6.5.2. Squeeze casting

SEM observations in this thesis study was very crucial in terms of evaluation of microstructures. Figure 6.58 shows the mixed microstructure of dendritic and globular grains for 7075 alloy produced under 15Hz frequency and 625°C SSM temperature. As stated in optical micrographs section, squeeze cast products produced at 625°C SSM temperature consisted of mixed structure. When the grain boundary phase of dendritic structures in figure 6.59 and the grain boundary phase of globular grains in figure 6.61 were investigated, it has been revealed that the morphology and the chemistry of them are totally different from each other. This conclusion is very critical since it means that globular grains and dendrite structure actually formed in different stages of solidification or at different temperatures. Therefore, it is concluded that dendrite structure was formed in the time interval between the delivery of semi-solid slurry to squeeze casting die cavity whereas globular grains were formed during semi-solid slurry preparation. That is why, it is risky to decrease temperature below 635°C during semi-solid slurry preparation which resulted in formation of dendrite structure.

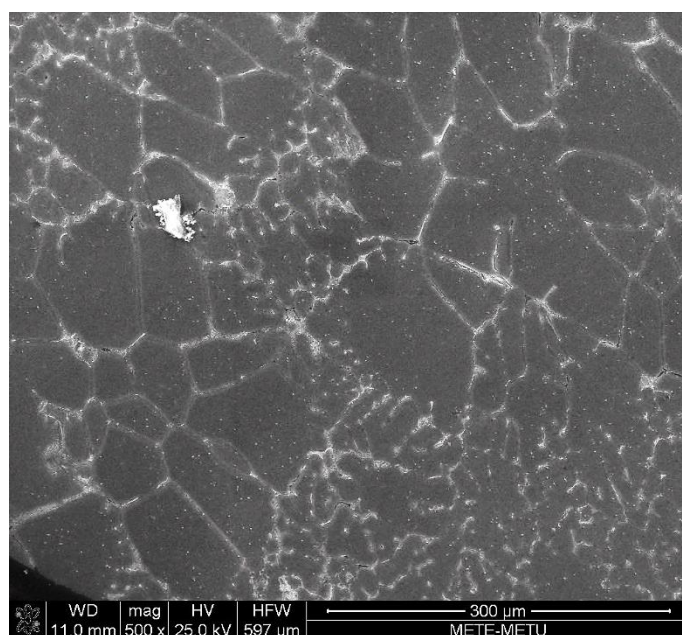


Figure 6.58 SEM image of dendrite structure mixed with globular grains in squeeze cast 7075 alloy produced under 15Hz frequency and 625°C SSM temperature

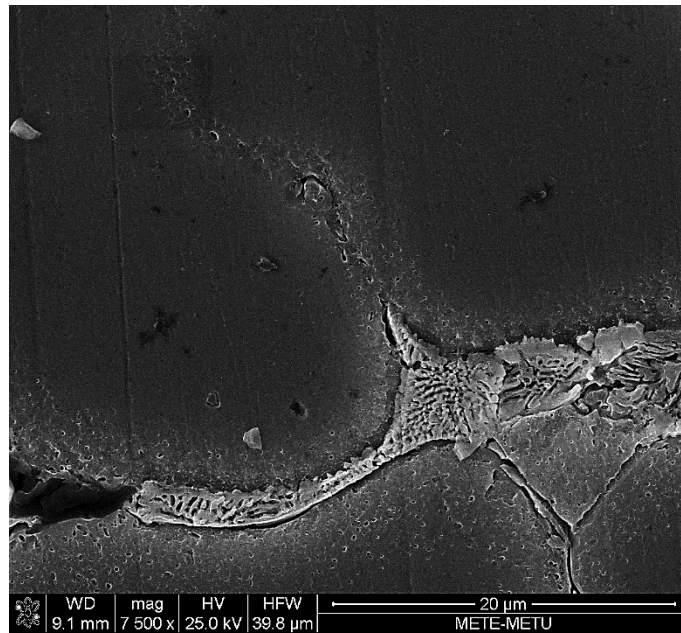


Figure 6.59 SEM image of eutectic phase in dendrite boundaries in squeeze cast 7075 alloy produced under 15Hz frequency at 625°C SSM temperature

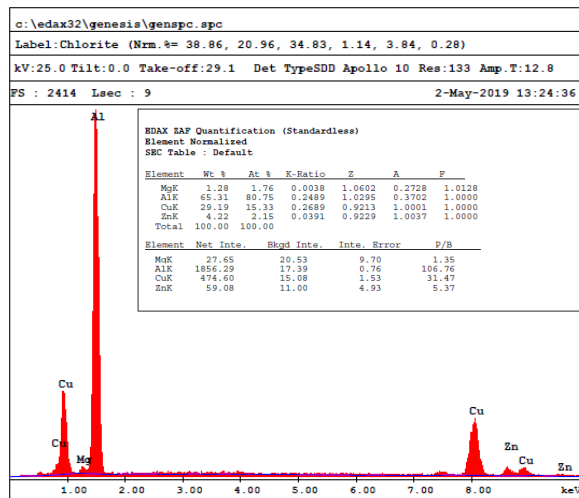


Figure 6.60 EDX analysis result of dendrite boundary phase in squeeze cast 7075 alloy produced under 15Hz frequency at 625°C SSM temperature

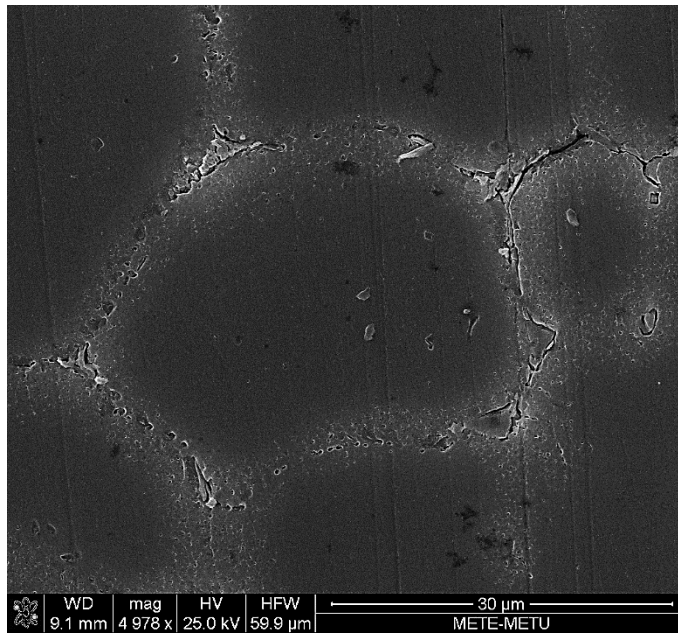


Figure 6.61 SEM image of globular alpha grains in squeeze cast 7075 alloy produced under 15Hz frequency and 635°C SSM temperature

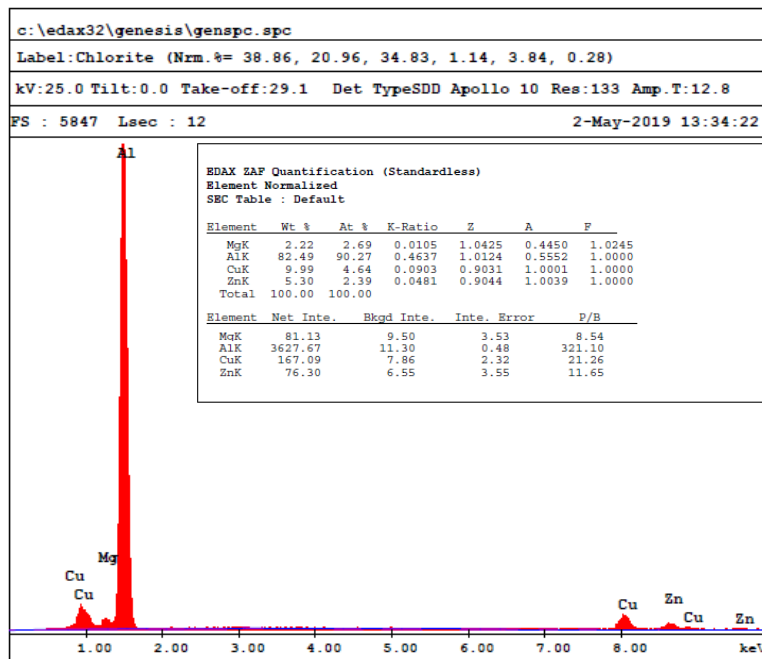


Figure 6.62 EDX analysis results of globular grain boundary in squeeze cast 7075 alloy produced under 15Hz frequency at 635°C SSM temperature

Figure 6.63 shows SEM image of white precipitates in the microstructure of squeeze cast and T6-treated 7075 alloy produced under 25Hz frequency and 635°C SSM temperature and figure 6.64 shows the EDX analysis. According to EDX result, the precipitate has 69 wt.% Al and 30 wt.% Cu. Therefore, these are most probably Al₂Cu precipitates forming in squeeze casting after heat treatment.

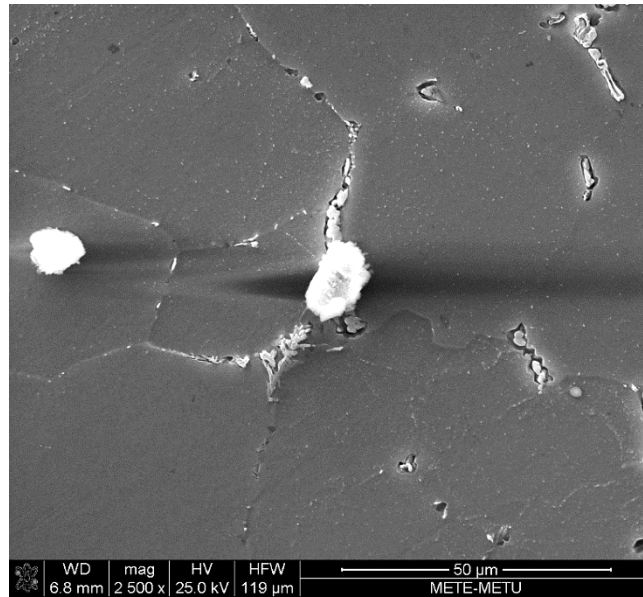


Figure 6.63 SEM image of white precipitates in squeeze cast and T6-treated 7075 alloy produced under 25Hz frequency and 635°C SSM temperature

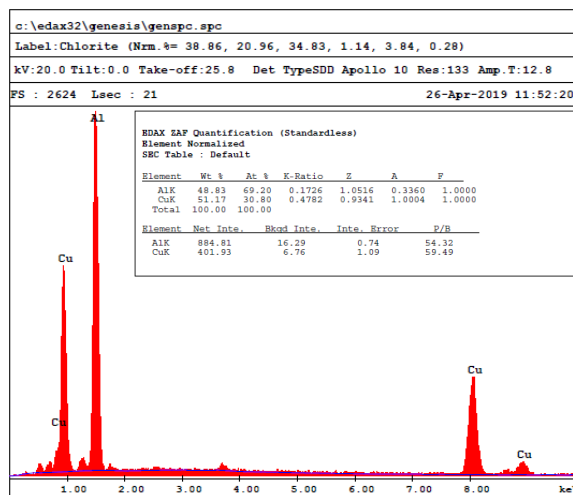


Figure 6.64 EDX analysis results of white precipitates in squeeze cast and T6-treated 7075 alloy produced under 15Hz frequency at 635°C SSM temperature

Figure 6.65 and 6.66 shows the homogeneously distributed fine precipitates in the microstructure of 7075 alloys produced at 25Hz and 35Hz frequency at 635°C SSM temperature. It is clear that these 7075 alloys have high mechanical properties due to homogenous distribution of fine precipitates.

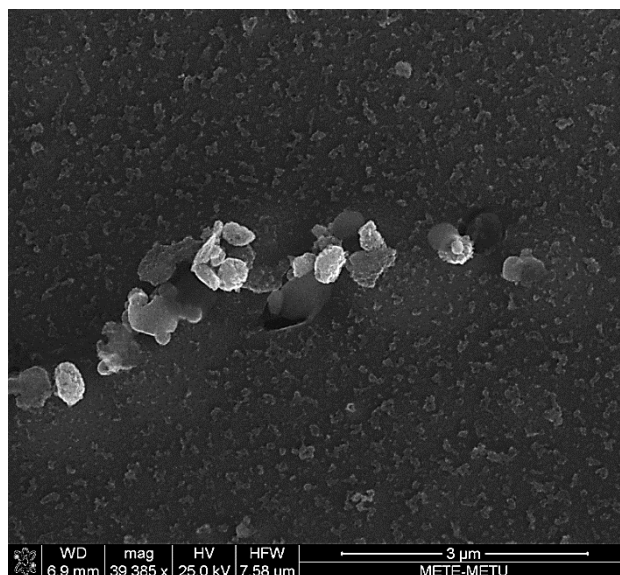


Figure 6.65 SEM image of finest precipitates in squeeze cast and T6-treated 7075 alloy produced under 25Hz frequency at 635°C SSM temperature

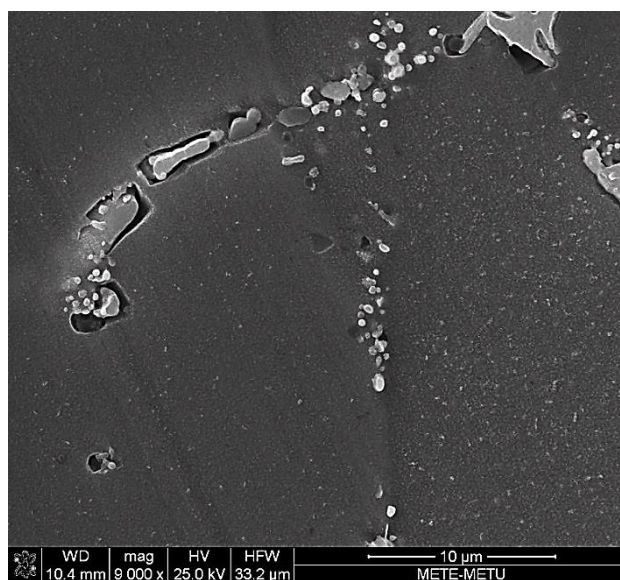


Figure 6.66 SEM image of finest precipitates in squeeze cast and T6-treated 7075 alloy produced under 35Hz frequency at 635°C SSM temperature

When these fine precipitates are investigated under higher magnifications in SEM as seen in figure 6.67, it is clear that the particles are in hundreds of nano meter in size. The EDX analysis of these precipitates could not give meaningful results since they are in a chemically undetectable size. However, it is obvious that these precipitates are most probably $MgZn_2$ precipitates giving high strength to 7075 alloy which will be consistent with the mechanical properties of squeeze cast 7075 alloys.

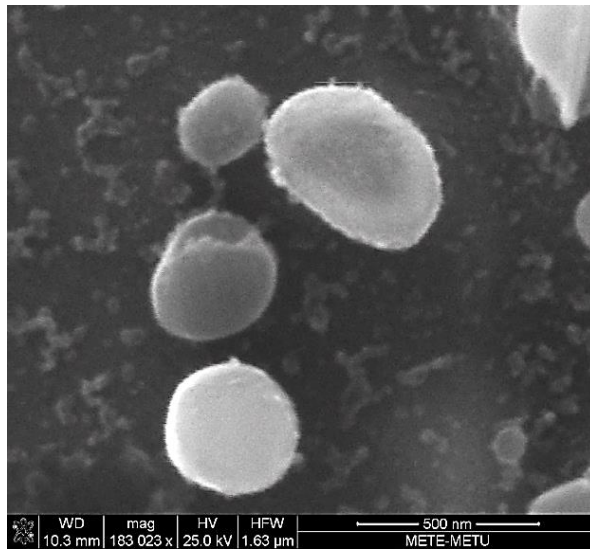


Figure 6.67 SEM image of finest precipitates in squeeze cast and T6-treated 7075 alloy produced under 35Hz frequency at 635°C SSM temperature

Figure 6.68 shows SEM image of the cleavage plane in the fracture surface of squeeze cast and T6 heat treated 7075 alloy produced under 25Hz frequency at 625°C SSM temperature and figure 6.68 shows the propagated crack of the same sample. Clear cleavage planes of the fracture surface of squeeze cast products are the sign of brittle fracture and the crack propagation seems to throughout the grain boundaries. Therefore, it was assumed that even by rhecasting of 7075 alloy at relatively low temperatures (620-630°C), it was difficult to achieve final products with high ductility. Rheocast 7075 alloys at relatively low temperatures clearly fracture in a brittle manner, porous microstructure and poor mechanical properties as will be discussed later proves this conclusion.

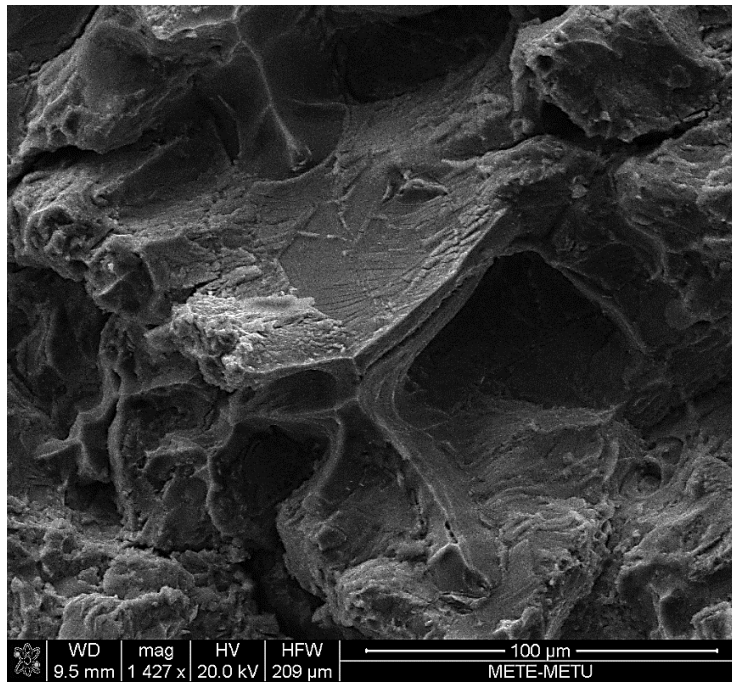


Figure 6.68 SEM image of cleavage planes in the fracture surface of squeeze cast and T6-treated 7075 alloy produced under 35Hz frequency at 625°C SSM temperature

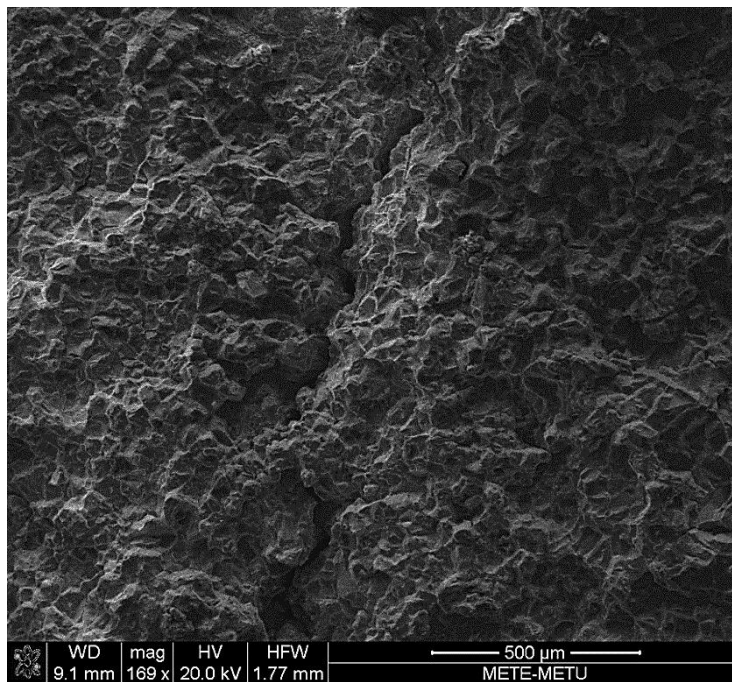


Figure 6.69 SEM image of the crack in the fracture surface of squeeze cast and T6-treated 7075 alloy produced under 35Hz frequency at 625°C SSM temperature

6.5.3. Squeeze casting and hot rolling of 7075/B₄C composite

SEM image of B₄C particules are seen in figure 6.70, the particle size of the powder was corrected as 1-3 μm in electron microscope analysis.

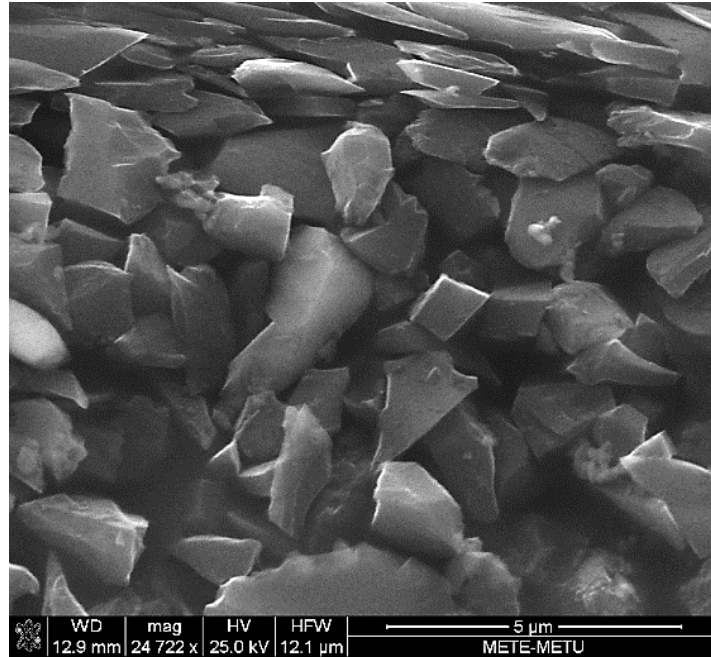


Figure 6.70 SEM image of B₄C particulate powder used for squeeze casting of 7075/B₄C composites

SEM image of big black particle in squeeze cast and T6 heat treated 8wt.% 7075/B₄C composite is shown in figure 6.71, the EDX analysis of this phase (see in figure 6.72) showed that it is certainly B₄C particle as discussed in microstructure results section. When the microstructure of hot-rolled 7075/B₄C composites are investigated, similarly black phases have been found as B₄C particles, however small white precipitates were observed all over the grain boundaries of hot-rolled 7075/B₄C composites as in the case of 10wt.% 7075/B₄C composite (see in figure 6.73). The EDX analysis of these precipitates showed that the stoichiometry of these phases belong to most probably Al₂Cu which might have additional strengthening effect on the mechanical properties of hot-rolled composites.

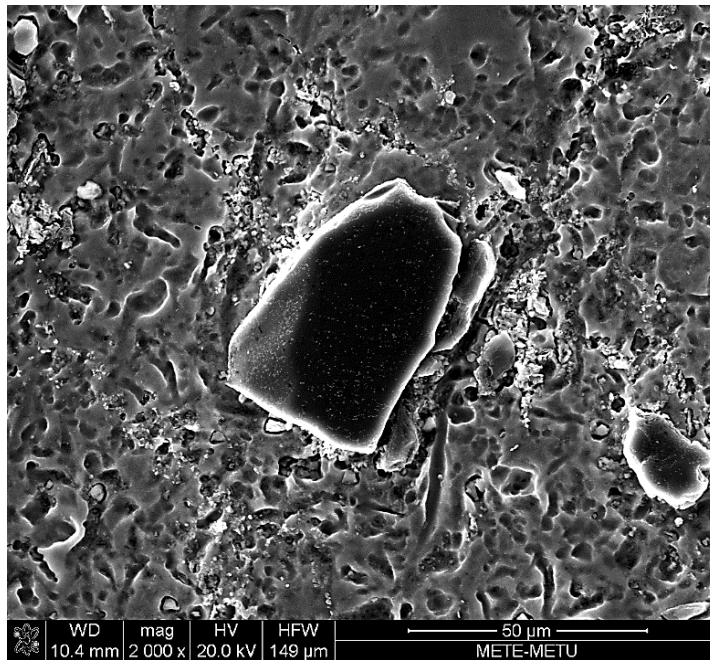


Figure 6.71 SEM image of black particle in squeeze cast 8wt.% 7075/B₄C composite

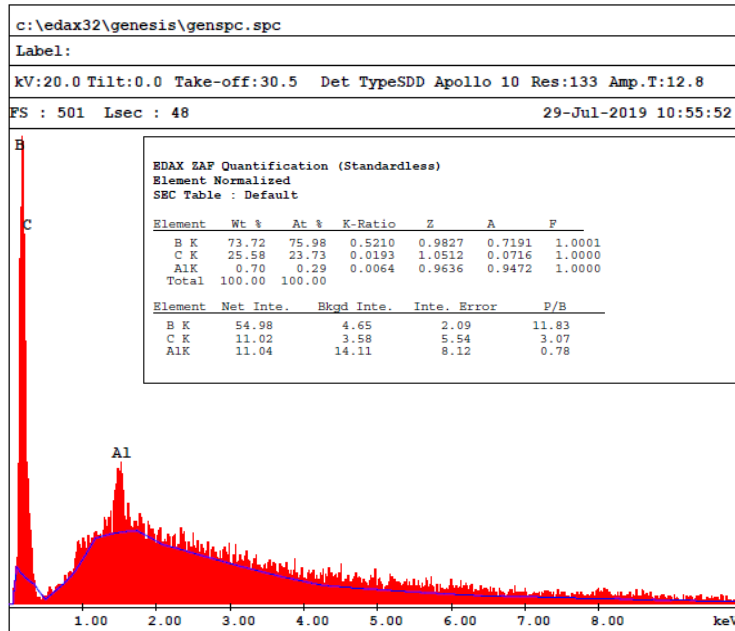


Figure 6.72 EDX analysis results of black agglomerate in squeeze cast 8wt.% 7075/B₄C composite



Figure 6.73 SEM image of white precipitates along the grain boundaries in hot-rolled 10wt.% 7075/B₄C composite

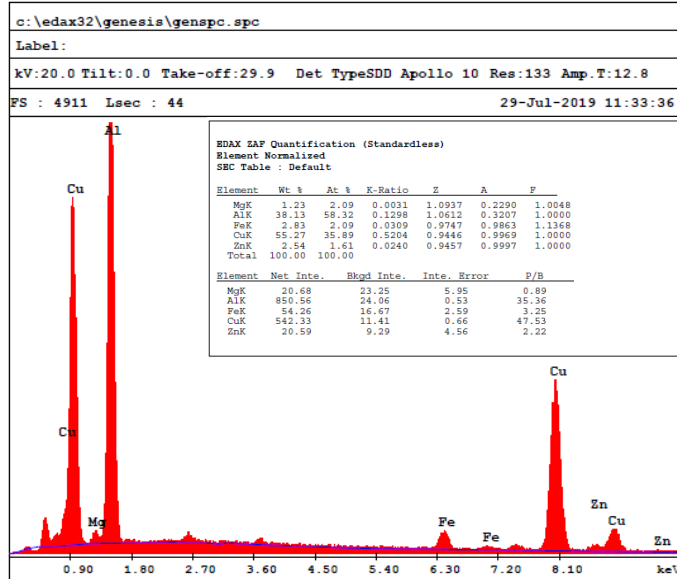


Figure 6.74 EDX analysis results of white precipitates along the grain boundaries in hot-rolled 10wt.% 7075/B₄C composite

6.6. Mechanical Testing

In this part, three different results of rheocasting experiments will be shown; hardness test results, tensile test results and 3-point bending test results.

6.6.1. Hardness test

Brinell hardness scale is used for both sand and squeeze cast samples and 5 individual hardness were taken from each sample.

6.6.1.1. Sand casting

Hardness test results of sand cast samples are shown in table 6.14 and 6.15.

Table 6-15 Hardness test results of sand cast 7075 alloys produced under three different vibration frequencies and four different SSM temperatures

Casting Parameters		Hardness Measurement (HB 2.5)				
Vibration Frequency (Hz)	SSM Temperature (°C)	#1	#2	#3	#4	#5
15	635	123.00	120.00	116.00	117.00	119.00
	630	121.00	123.00	124.00	120.00	118.00
	625	122.00	120.00	122.00	128.00	124.00
	620	126.00	123.00	122.00	119.00	120.00
25	630	111.00	107.00	110.00	109.00	106.00
	625	110.00	111.00	112.00	113.00	110.00
	620	114.00	115.00	113.00	112.00	114.00
35	635	90.00	106.00	102.00	98.00	104.00
	630	103.00	104.00	108.00	110.00	102.00
	625	123.00	120.00	116.00	112.00	118.00
	620	95.00	98.00	100.00	110.00	108.00
Non-Vibr.	670	106.00	113.00	105.00	108.00	110.00

Table 6-16 Hardness test results of sand cast and T6-treated 7075 alloys produced under three different vibration frequencies and four different SSM temperatures

Casting Parameters		Hardness Measurement (HB 2.5)				
Vibration Frequency (Hz)	SSM Temperature (°C)	#1	#2	#3	#4	#5
15	635	152.00	117.00	141.00	125.00	135.00
	630	138.00	127.00	143.00	142.00	136.00
	625	139.00	143.00	149.00	152.00	138.00
	620	137.00	145.00	140.00	145.00	139.00
25	630	118.00	121.00	120.00	119.00	122.00
	625	128.00	112.00	124.00	125.00	126.00
	620	125.00	124.00	118.00	122.00	120.00
35	635	122.00	123.00	125.00	122.00	124.00
	630	132.00	129.00	131.00	126.00	128.00
	625	129.00	126.00	131.00	130.00	132.00
	620	128.00	128.00	130.00	119.00	128.00
Non-Vibr.	670	106.00	115.00	118.00	114.00	109.00

As seen in figure 6.75 and 6.76 there is a tendency to increase of hardness as SSM temperature decreases to a limiting point. There are some exceptions but the behavior is somewhat consistent with the thermal analysis results. SSM temperature of 625°C seems to be optimum point for highest hardness and maximum 120 HB hardness value was increased to 145 HB by T6 heat treatment. It can be clearly seen that without any significant differences, 15Hz vibration resulted in highest hardness values.

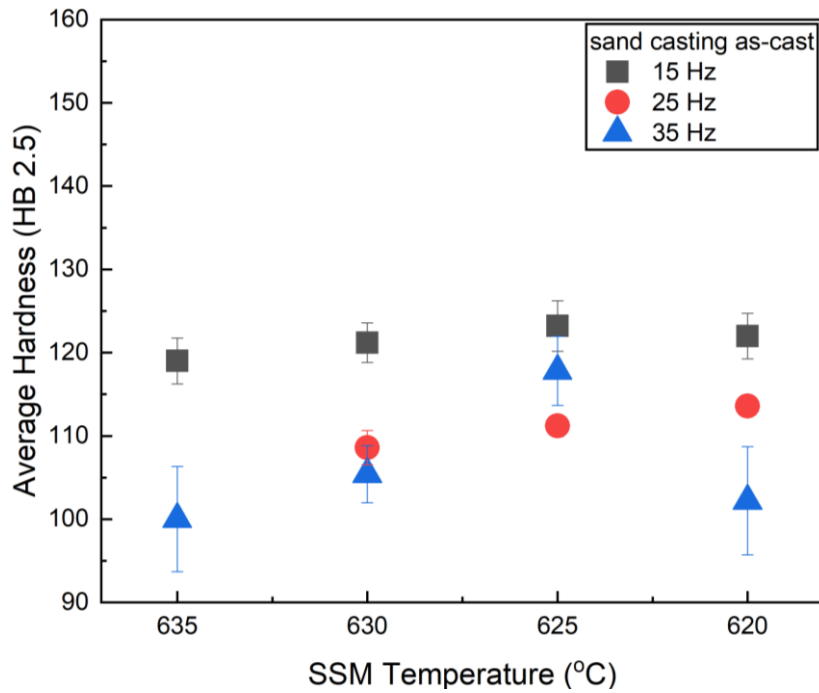


Figure 6.75 Hardness variation of sand cast 7075 alloy produced under three different vibration frequency as SSM temperature decreases

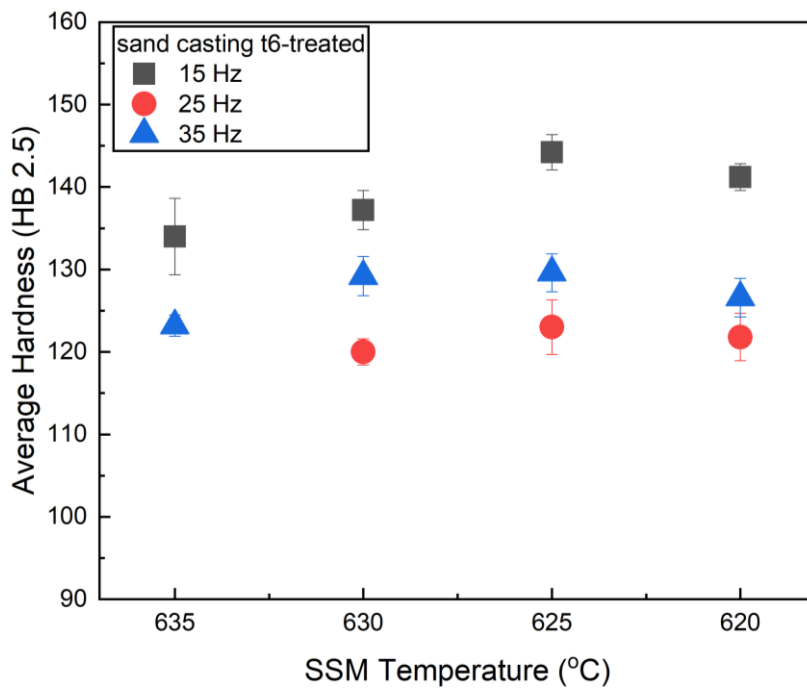


Figure 6.76 Hardness variation of sand cast and T6-treated 7075 alloy produced under three different vibration frequency as SSM temperature decreases

6.6.1.2. Squeeze casting of 7075 alloy

Table 6-17 Hardness test results of squeeze cast 7075 alloys produced under three different vibration frequencies and three different SSM temperatures

Casting Parameters		Hardness Measurement (HB 2.5)				
Vibration Frequency (Hz)	SSM Temperature (°C)	#1	#2	#3	#4	#5
15	635	93.90	101.00	107.00	98.10	103.00
	630	87.20	91.00	93.10	92.00	94.10
	625	93.10	98.20	96.40	93.20	95.60
25	635	107.00	106.00	105.00	107.00	106.00
	630	87.20	87.00	86.80	87.00	88.00
	625	95.30	87.20	90.20	87.00	89.80
35	635	104.00	101.00	105.00	103.00	105.00
	630	101.00	106.00	105.00	101.00	104.00
	625	94.30	97.00	94.50	93.00	96.70
Non-Vibr.	670	104.00	101.00	105.00	101.00	102.00

Table 6-18 Hardness test results of squeeze cast and T6-treated 7075 alloys produced under three different vibration frequencies and three different SSM temperatures

Casting Parameters		Hardness Measurement (HB 2.5)				
Vibration Frequency (Hz)	SSM Temperature (°C)	#1	#2	#3	#4	#5
15	635	147.00	147.00	141.00	146.00	145.00
	630	141.00	143.00	146.00	144.40	141.80
	625	121.00	119.00	110.00	112.00	120.00
25	635	147.00	147.00	145.00	146.00	148.00
	630	138.00	121.00	132.00	131.50	130.00
	625	116.00	113.00	128.00	118.00	121.00
35	635	149.00	147.00	152.00	151.00	151.00
	630	153.00	150.00	144.00	146.00	150.00
	625	118.00	121.00	119.00	121.00	120.00
Non-Vibr.	670	149.00	150.00	151.00	150.00	149.00

The hardness test results of squeeze castings are also quite compatible with previous results. The highest hardness values are obtained at 635°C SSM temperatures and there is an observable loose in hardness as SSM temperature decreases as seen in figure 6.77 and 6.78. The highest hardness value obtained for T6-treated samples are slight higher compared to sand castings but the hardness values are quite close to each other.

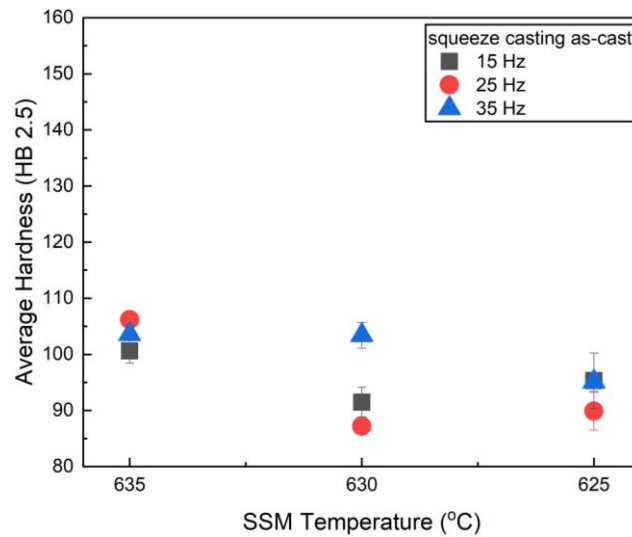


Figure 6.77 Hardness variation of squeeze cast 7075 alloy produced under three different vibration frequency as SSM temperature decreases

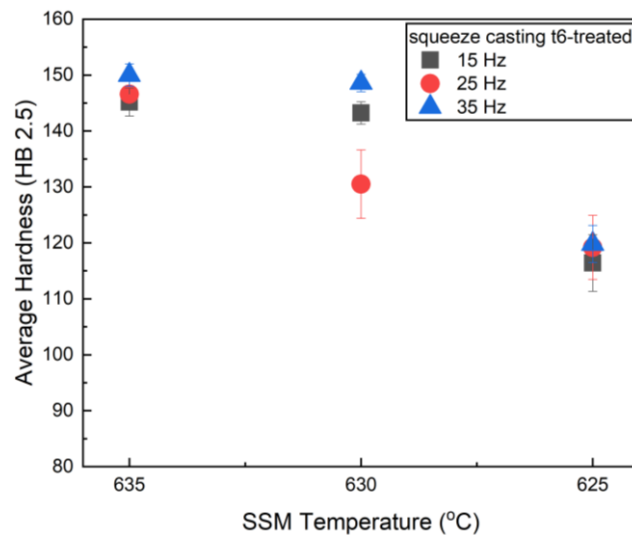


Figure 6.78 Hardness variation of squeeze cast and T6-treated 7075 alloy produced under three different vibration frequency as SSM temperature decreases

Figure 6.79 and 6.80 show the comparison of highest hardness values for as-cast and T6-treated samples. It can be clearly seen that there is actually no significant difference in maximum hardness values.

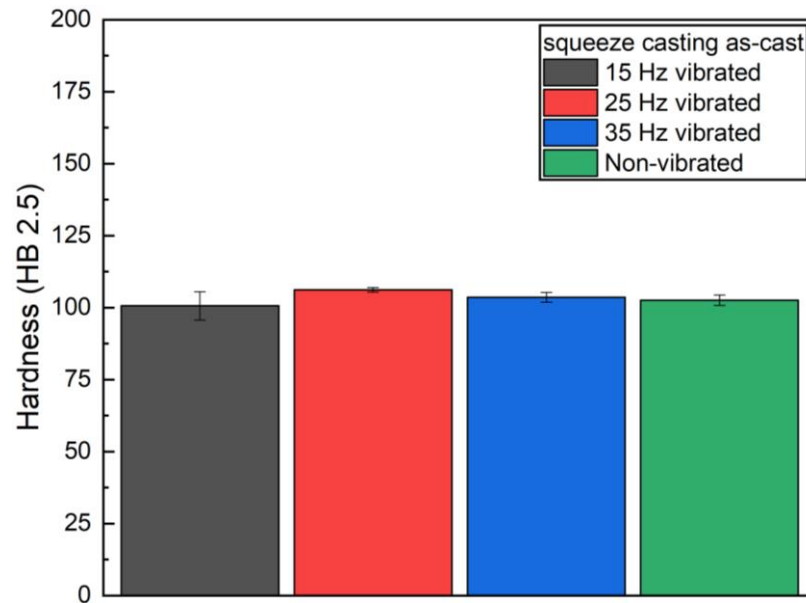


Figure 6.79 Comparison of average hardness values of squeeze cast 7075 alloy produced under different vibration frequencies at 635°C

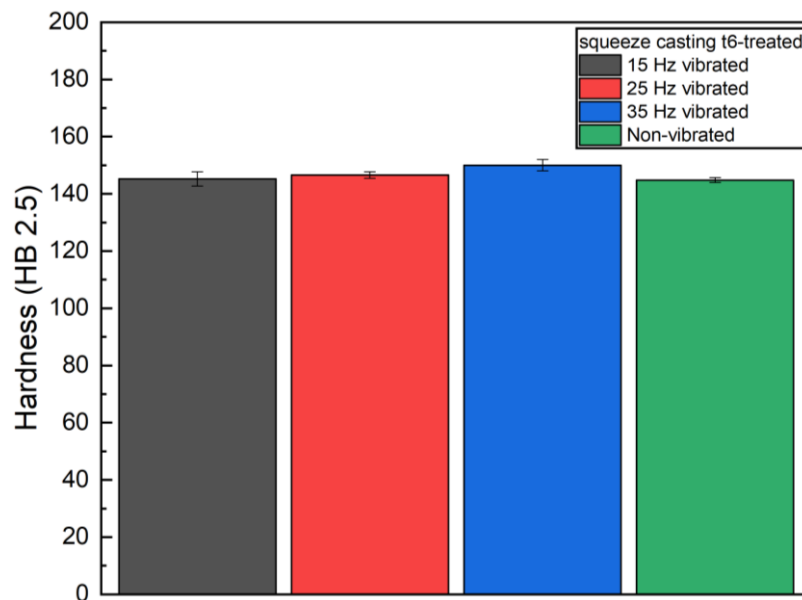


Figure 6.80 Comparison of average hardness values of squeeze cast and T6-treated 7075 alloy produced under different vibration frequencies at 635°C

6.6.1.3. Squeeze casting and hot rolling of 7075/B₄C composites

Table 6-19 Hardness test results of T6-treated squeeze cast and hot rolled 7075/B₄C composites with different % B₄C addition

Processing	% B ₄ C Addition	Hardness Measurement (HV 30)				
		#1	#2	#3	#4	#5
Squeeze Casting	8	165.00	135.00	155.00	160.00	158.00
	10	164.00	164.00	172.00	170.00	168.00
	12	183.00	174.00	207.00	178.00	180.00
Hot Rolling	8	192.00	201.00	195.00	192.00	200.00
	10	198.00	209.00	207.00	194.00	188.00
	12	180.00	207.00	201.00	206.00	189.00

Figure 6.81 shows the variation of average hardness values of squeeze cast and hot-rolled 7075/B₄C composites as wt.% B₄C addition increases. It was expected to see a clear increase in the hardness as % B₄C increases since B₄C is known to be one of the hardest material. For squeeze cast 7075/B₄C composites, the behaviour is as expected whereas the behaviour of hot-rolled 7075/B₄C composite is somewhat different. There is an improvement in the hardness as B₄C% increases up to 10%, then slight decrease in the average hardness was observed. The reason might be due to some agglomeration problem in 12wt.% 7075/B₄C composites. In overall, maximum hardness of semi-solid squeeze cast 7075 alloy which was about 150 HB2.5 was successfully improved up to 190 HB2.5 hardness value as seen in figure 6.82.

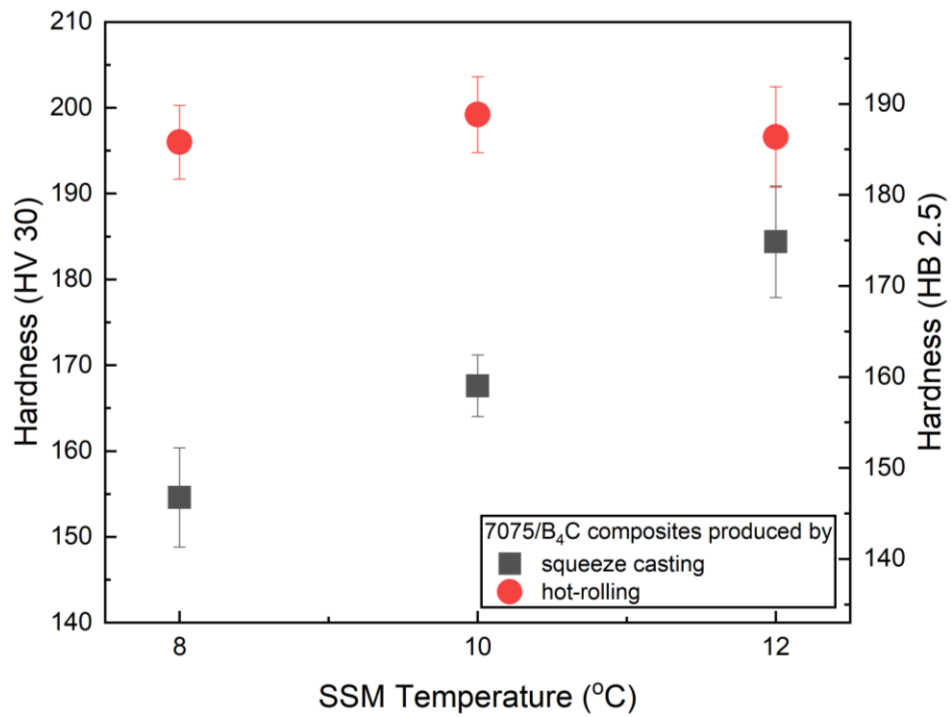


Figure 6.81 Hardness variation of T6 treated squeeze cast and hot-rolled 7075/B₄C composites as % B₄C addition

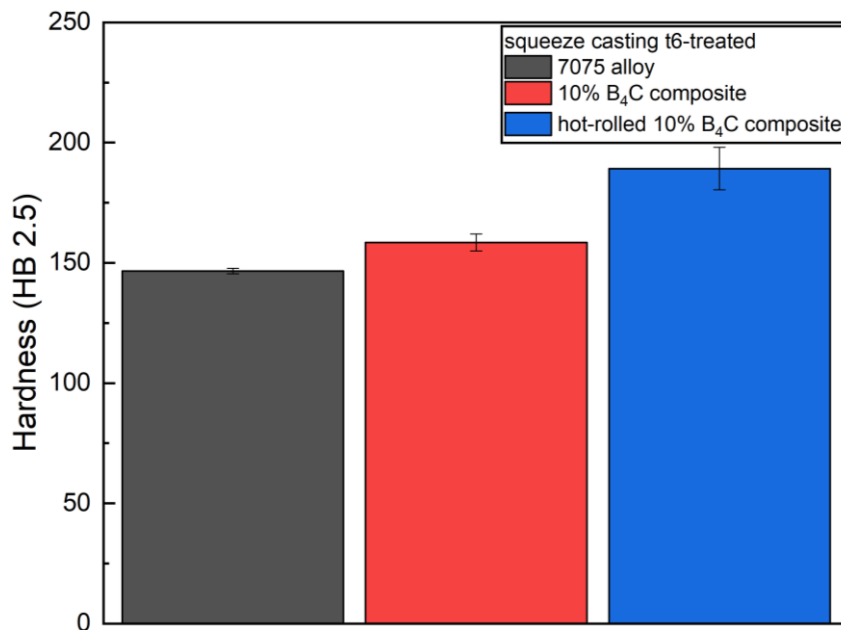


Figure 6.82 Comparison of average hardness values of T6-treated squeeze cast 7075 alloy, squeeze cast 10wt.% 7075/B₄C composite and hot-rolled 10wt.% 7075/B₄C

6.6.2. Tensile Test

For some exceptions, 3 samples were tested for T6-treated samples whereas only 1 sample were tested for the tensile test of as-cast 7075 alloys.

6.6.2.1. Sand casting

Example result of tensile stress vs tensile strain curve of 7075 alloy produced under 15 Hz vibration frequency and 635°C SSM temperature is shown in figure 6.83 (For the details, see appendix part F)

Table 6-20 Fracture stress values of tensile test results of sand cast as-cast and T6-treated 7075 alloys produced under three different vibration frequencies and four different SSM temperatures

Casting Parameters		Stress at Fracture (MPa)			
Vibration Frequency (Hz)	SSM Temperature (°C)	As-cast #1	T6-treated #1	T6-treated #2	T6-treated #3
15	635	156.03	192.64	171.06	-
	630	164.27	256.76	289.60	267.37
	625	149.88	265.85	268.15	238.28
	620	106.19	205.67	242.70	248.18
25	630	177.29	211.45	-	-
	620	131.34	240.91	-	-
35	635	111.36	181.34	178.15	184.58
	630	94.33	300.17	306.83	204.97
	625	159.63	241.65	290.12	255.27
	620	102.29	234.97	284.93	282.38

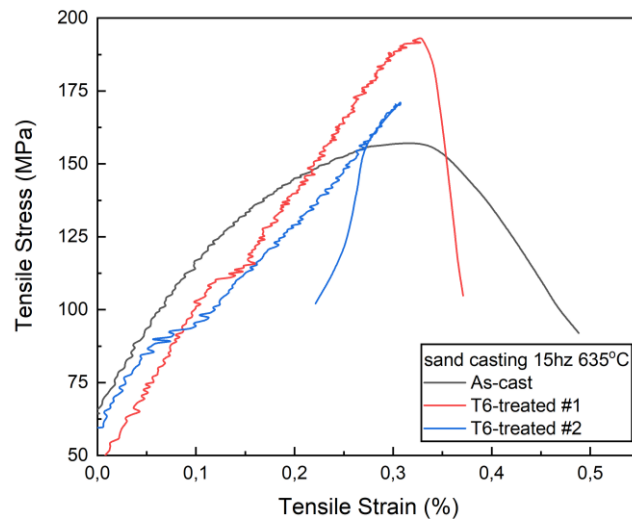


Figure 6.83 Tensile stress vs tensile strain curves for as-cast and T6-treated sand cast 7075 alloy produced under 15Hz frequency at 635°C SSM temperature

First of all, sand casting resulted in mechanically poor samples. The specimens were fractured even before yielding. Therefore, instead of ultimate tensile strength, the term ‘stress at fracture’ was used to define the maximum strength reached.

Figure 6.84 shows the stress at fracture variation of as-cast sand cast 7075 alloys as SSM temperature decreases. There is no exact behaviour of increasing or decreasing of fracture stress as SSM temperature decreases as expected. It is clear that the strength is not directly related with the vibration frequency and the temperature, this might be because of the lack of pressure application which eliminates most of the pores or during the removal of vibration probe the low viscosity at high SSM temperatures such as 635°C (see in figure 6.85) could lead to uneven flow of remaining liquid which increases porosity content. All in all, sand casting (especially as-cast samples) were not consistent with the thermal analysis results and did not give good results. On the other hand, heat treated samples were somewhat more consistent, that is, the behaviour of stress at fracture is increasing as SSM temperature decreases to a limiting point as seen in figure 6.85. The fracture stress values are significantly much lower than those in the literature studies due to the lack of pressure application during shaping of semi-solid slurries which resulted in highly porous and detrimental microstructure.

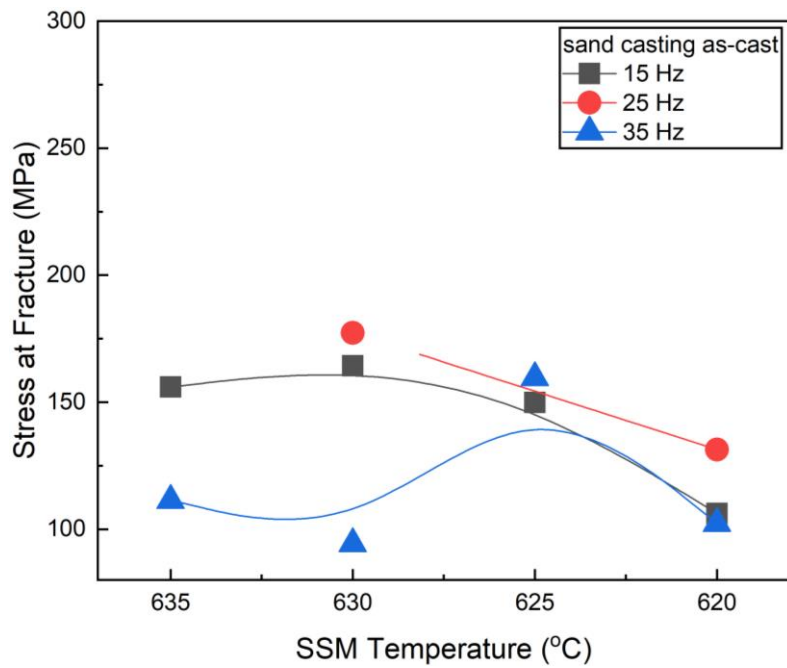


Figure 6.84 Stress at fracture variation of sand cast 7075 alloy produced under three different vibration frequency as SSM temperature decreases

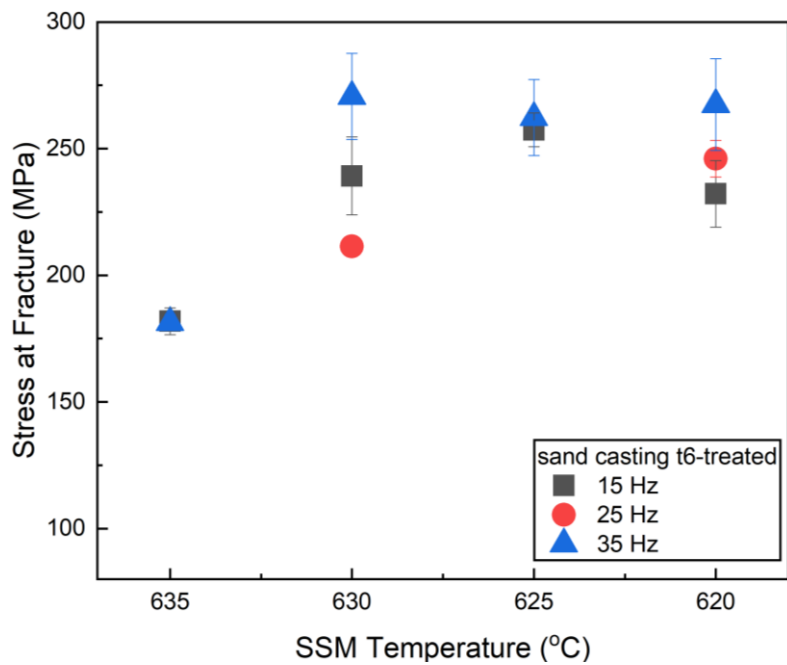


Figure 6.85 Stress at fracture variation of sand cast and T6-treated 7075 alloy produced under three different vibration frequency as SSM temperature decreases

6.6.2.2. Squeeze casting

Example result of tensile stress vs tensile strain curve of squeeze cast 7075 alloy produced under 15Hz vibration frequency and 635°C SSM temperature is shown in figure 6.86 (For the details, see appendix part G).

Table 6-21 UTS values of tensile test results of squeeze cast and T6-treated 7075 alloys produced under three different vibration frequencies and three different SSM temperatures

Casting Parameters		Ultimate Tensile Strength (MPa)			
Vibration Frequency (Hz)	SSM Temperature (°C)	As-cast #1	T6-treated #1	T6-treated #2	T6-treated #3
15	635	239.97	471.52	464.87	456.94
	630	179.89	420.58	419.31	445.21
	625	161.06	258.49	311.55	-
25	635	245.35	483.82	474.82	-
	630	184.25	416.18	436.34	419.93
	625	169.70	296.27	273.17	307.16
35	635	247.70	469.05	477.92	476.35
	630	236.31	420.85	440.54	404.56
	625	206.59	312.44	413.03	342.75
Non-Vibr.	670	206.48	428.81	444.95	434.30

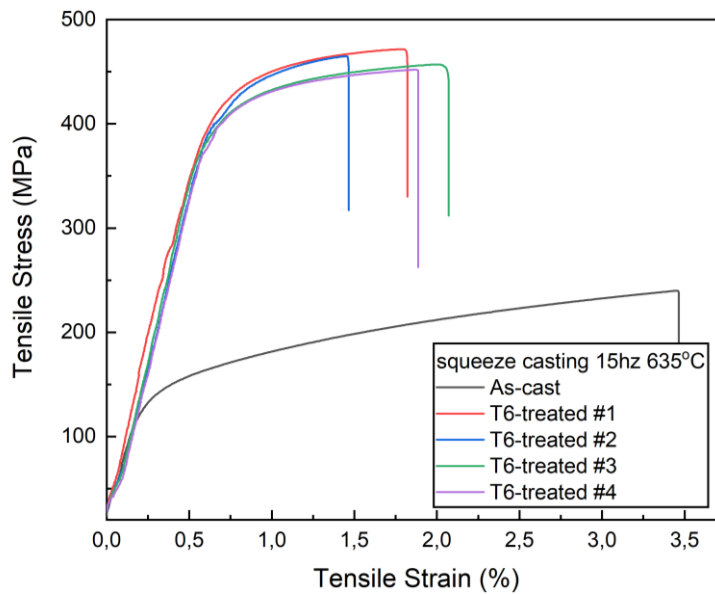


Figure 6.86 Tensile stress vs tensile strain curves for as-cast and T6 treated squeeze cast 7075 alloy produced under 15Hz frequency at 635°C SSM temperature

Figure 6.87 and 6.88 show the ultimate tensile strength variation of as-cast and T6-treated squeeze cast 7075 alloy as SSM temperature decreases. The behaviour of UTS as SSM temperature decreases is precisely decreasing trend as expected. Highest mechanical properties (UTS) was obtained for 635°C SSM temperature. The results are exactly coherent with microstructures, grain size measurements, porosity measurements and hardness test data. First of all, the best microstructure of complete globular grains were achieved at 635°C, secondly finest grain size and least porosity amounts were achieved also at 635°C. Moreover, highest hardness were obtained at 635°C SSM temperature also. The reason why the best results were shown at 635°C instead of 625-630°C which were expected in thermal analysis results have been already pointed out, i.e. it was because of the temperature drop during transportation of semi-solid 7075 alloy and so actual SSM temperature is 5-6°C was less than the determined temperatures. Figure 6.89 and 6.90 show the comparison of highest UTS obtained from vibrated (at 635°C SSM temperatures) and non vibrated (at 670°C casting temperatures) samples. It can be clearly understood that, mechanically

vibrated 7075 alloys (T6-treated) until 635°C resulted in almost 500 MPa (483 MPa for 25Hz and 635°C) which is very close to maximum literature value and 40-50 MPa higher than non-vibrated samples (see in figure 6.90). In addition, it becomes crystal clear that the effect of semi-solid melting temperature affects more in microstructure and mechanical properties compared to mechanical vibration.

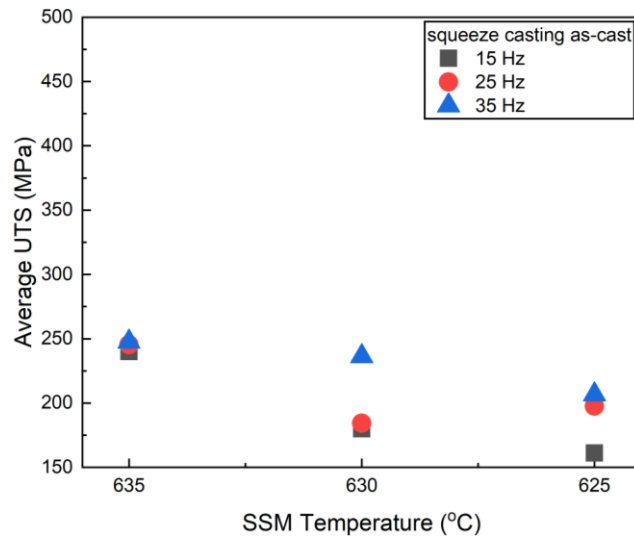


Figure 6.87 UTS variation of squeeze cast 7075 alloy produced under three different vibration frequency as SSM temperature decreases

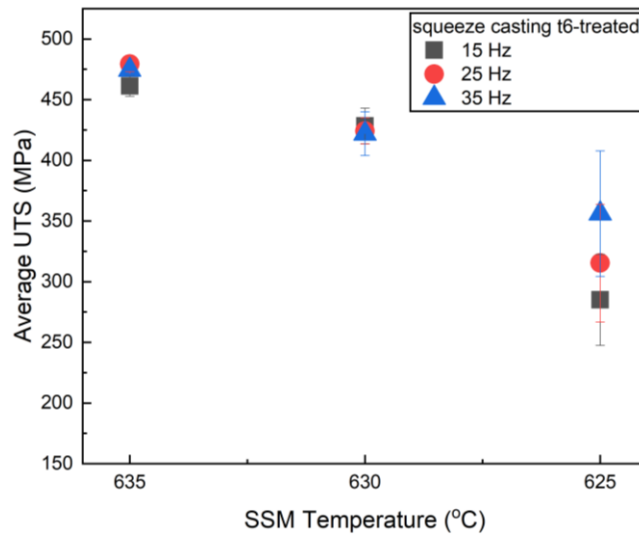


Figure 6.88 UTS variation of squeeze cast and T6-treated 7075 alloy produced under three different vibration frequency as SSM temperature decreases

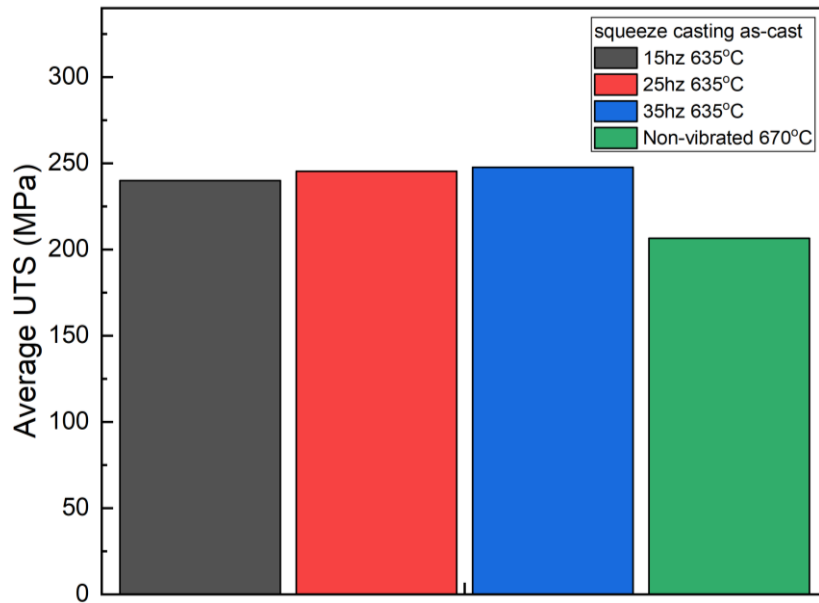


Figure 6.89 Comparison of average UTS values of squeeze cast 7075 alloy produced under different vibration frequencies at 635°C and with non-vibrated sample at 670°C

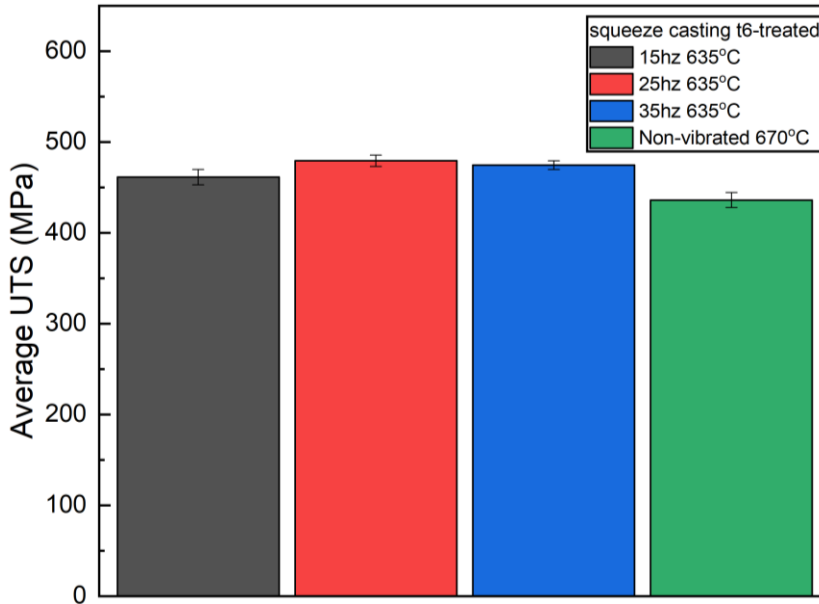


Figure 6.90 Comparison of average UTS values of squeeze cast and T6-treated 7075 alloy produced under different vibration frequencies at 635°C and with non-vibrated sample at 670°C

6.6.3. 3-Point bending test

3-Point bending test of both squeeze cast 7075 alloy and 7075 matrix composites at 635°C SSM temperature were carried out for the effective comparison of mechanical properties of 7075 alloy and 7075/B₄C composites. In order to see the effect of SSM temperature in flexural strength, 7075 alloys produced under 25Hz frequency at 630°C and 625°C were also tested.

6.6.3.1. Squeeze casting of 7075 alloy

For some exceptions, 2 samples were tested for T6-treated samples whereas only 1 sample were tested for the 3-point bending test of as-cast 7075 alloys. Example result of flexural stress vs flexural strain curve of 7075 alloy produced under 15Hz vibration frequency and 635°C SSM temperature is shown in figure 6.91 (For the details, see appendix part G).

Table 6-22 Flexural strength values of 3-point bending test results of squeeze cast as-cast and T6-treated 7075 alloys produced under three different vibration frequencies

Casting Parameters		Flexural Strength (MPa)		
Vibration Frequency (Hz)	SSM Temperature (°C)	As-cast #1	T6-treated #1	T6-treated #2
15	635	523.37	930.87	-
25	635	591.12	1020.69	932.40
	630	469.61	876.622	725.53
	625	407.15	527.91	692.55
35	635	328.72	914.39	-
No-vibration	670	513.43	915.97	940.94

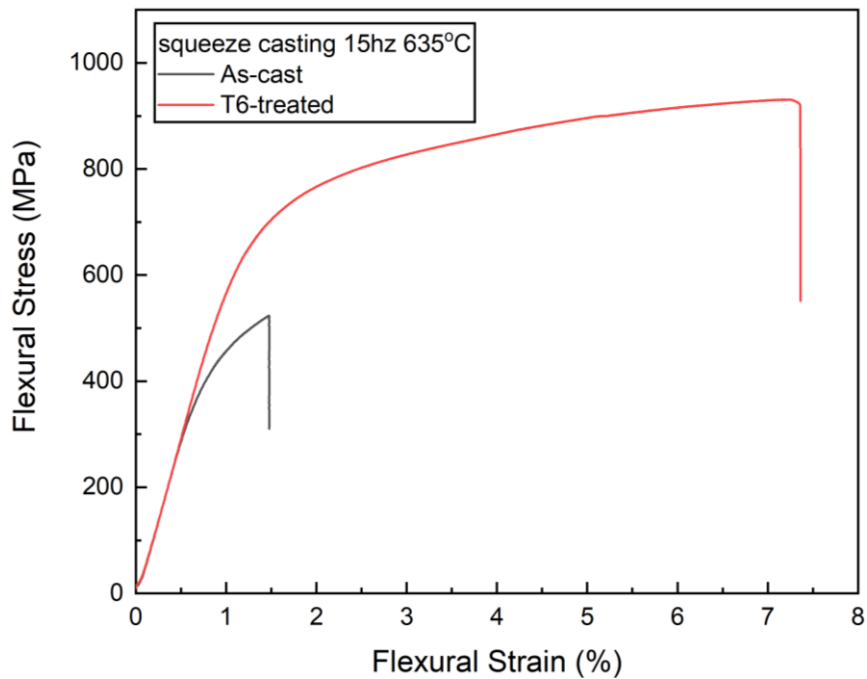


Figure 6.91 Flexural stress vs flexural strain curves for as-cast and Sand cast and T6 treated 7075 alloy produced under 15Hz frequency and 635°C SSM temperature

Figure 6.92 shows the flexural strength variation of as-cast and T6-treated squeeze cast 7075 alloy as SSM temperature decreases. There is also the behaviour of decreasing flexural strength as SSM temperature decreases as in the case of tensile test results (see in figure 6.87 and 6.88). The maximum flexural strength obtained from 25Hz vibrated sample at 635°C SSM temperature is 1020 MPa. Figure 6.93 shows the comparison of flexural strength of vibrated (at 635°C SSM temperature) and non-vibrated sample (at 670°C casting temperature). Flexural strength of vibrated samples are also mostly higher than non-vibrated samples.

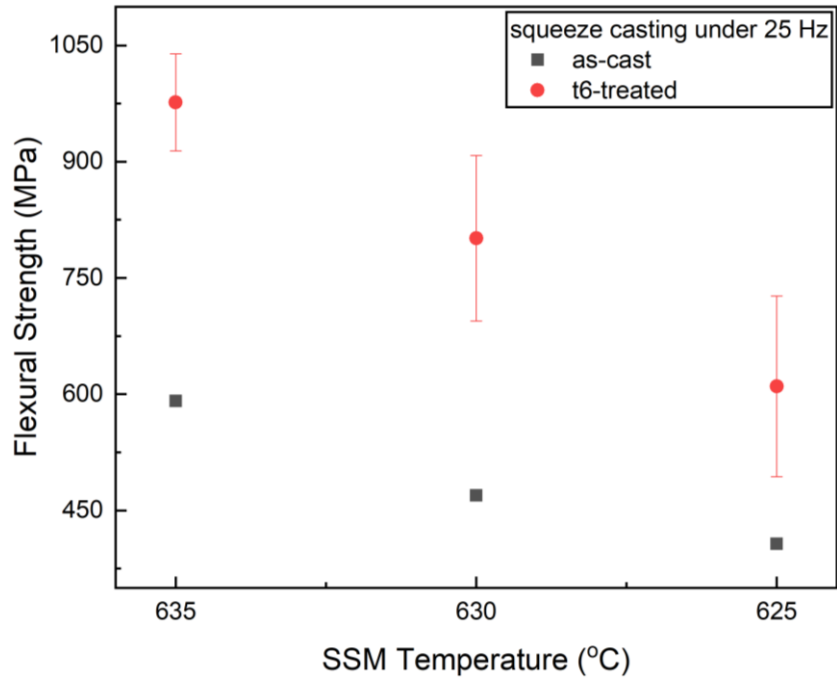


Figure 6.92 Flexural strength variation of squeeze cast T6-treated and as-cast 7075 alloy produced under three different vibration frequency as SSM temperature decreases

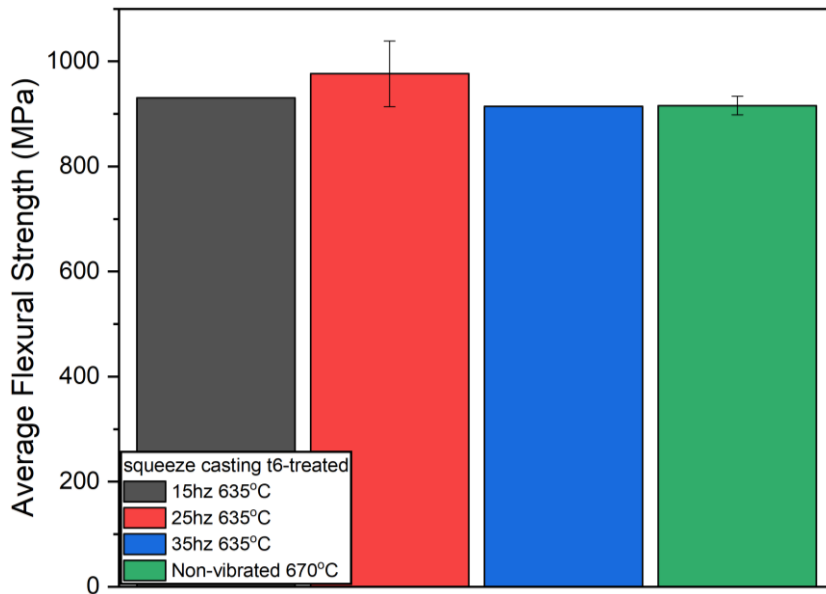


Figure 6.93 Comparison of average flexural strength values of squeeze cast and T6-treated 7075 alloy produced under different vibration frequencies at 635°C and with non-vibrated sample at 670°C

6.6.3.2. Squeeze casting of 7075/B₄C composite

For some exceptions, three samples were tested for T6-treated samples whereas only one sample were tested for the 3-point bending test of as-cast 7075/B₄C composites. Example result of flexural stress vs flexural strain curves of T6-treated 7075/B₄C composites alloy produced under 25Hz vibration frequency and 635°C SSM temperature are shown in figure 6.94.

Table 6-23 Flexural strength values of 3-point bending test results of squeeze cast and T6-treated 7075/B₄C composites produced 25Hz and 635°C

B4C Addition (%)	Flexural Strength (MPa)			
	As-cast #1	T6-treated #1	T6-treated #2	T6-treated #3
8	304.40	811.63	590.22	720.55
10	291.49	806.64	820.71	-
12	-	589.68	500.05	512.1

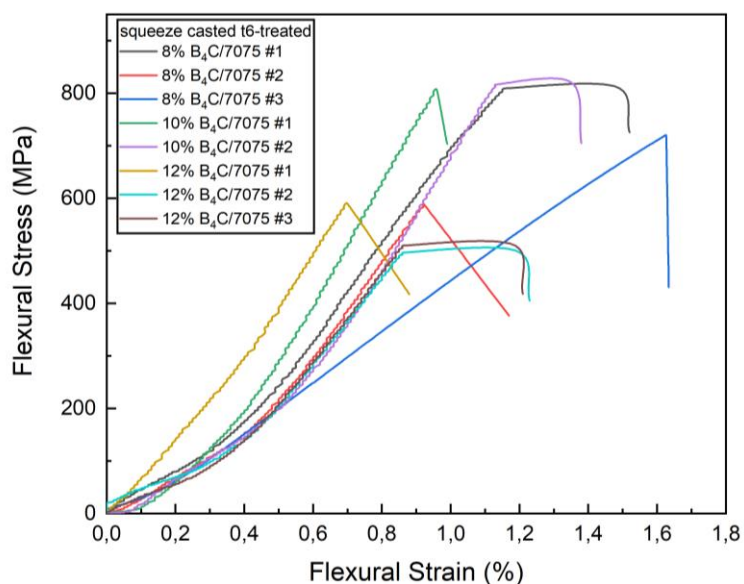


Figure 6.94 Flexural stress vs flexural strain curves of T6-treated squeeze cast 7075/B₄C composites produced under 25Hz frequency at 635°C SSM temperature

Figure 6.95 shows the comparison of flexural strength of 7075/B₄C composites having 8, 10 and 12 weight % B₄C addition. The highest flexural strength was obtained by 10% 7075/B₄C composite which is 811 MPa which is actually way lower than that of squeeze cast 7075 alloys at 635°C. The main reason for this strength drop was addressed to agglomeration of small B₄C particles in microstructure evaluation.

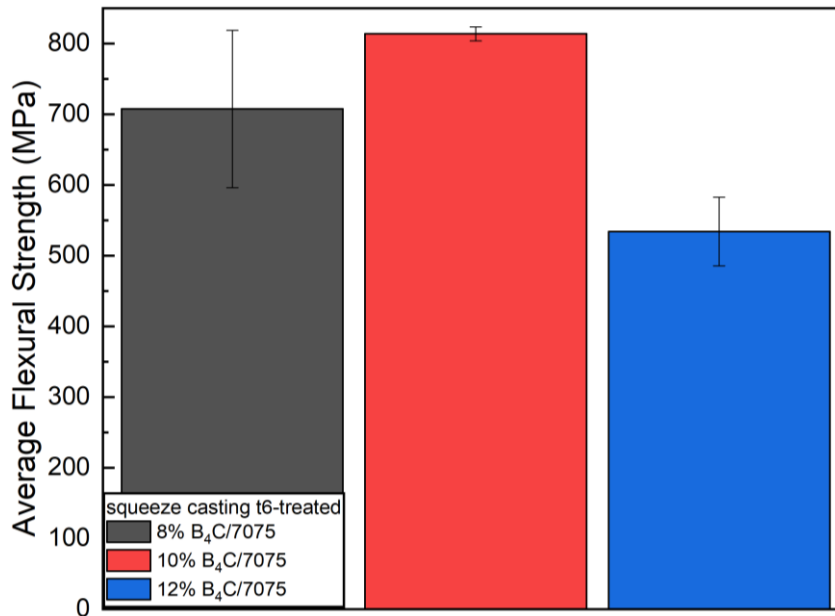


Figure 6.95 Comparison of average flexural strength values of squeeze cast and T6-treated 7075/B₄C composites produced under 25Hz vibration frequencies at 635°C

6.6.3.3. Hot rolled 7075/B₄C composite

In order to compare the mechanical properties of T6-treated squeeze castings, two samples were tested for hot rolled B₄C composites for the 3-point bending test. Example result of flexural stress vs flexural strain curves of hot-rolled 7075/B₄C composites are shown in figure 6.96.

Table 6-24 Flexural strength values of 3-point bending test results of hot-rolled and T6-treated 7075/B₄C composites

B ₄ C Addition (%)	Flexural Strength (MPa)	
	T6-treated #1	T6-treated #2
8	929.31	654.20
10	1036.61	973.55
12	816.90	-

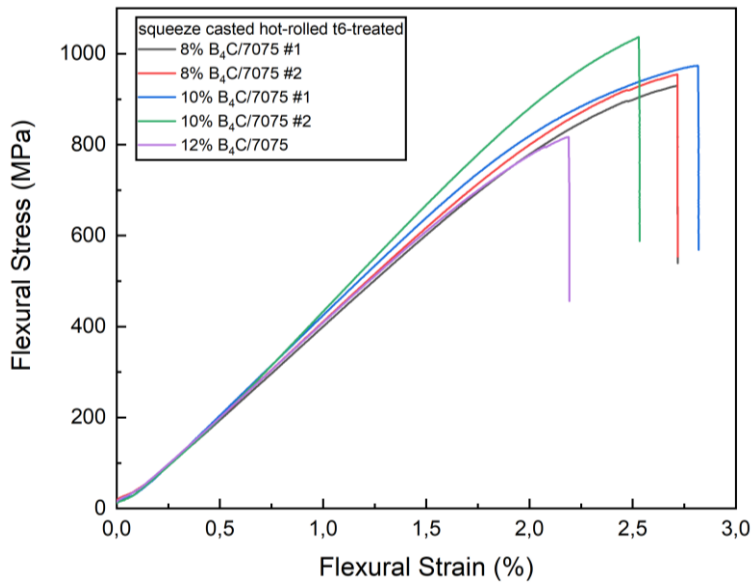


Figure 6.96 Flexural stress vs flexural strain curves of hot-rolled and T6-treated 7075/B₄C composites produced under 25Hz frequency at 635°C SSM temperature

Figure 6.97 shows the comparison of average flexural strength of hot-rolled 7075/B₄C composites having 8, 10 and 12 weight % Boron Carbide addition. The highest flexural strength was obtained by 10% 7075/B₄C composite which is 1036 MPa. Figure 6.98 shows briefly the highest mechanical properties reached for different processes in this thesis study. Although there is a fair amount of loss in flexural strength in 7075 alloy by B₄C addition, by applying post-treatment to semi-solid

squeeze cast 7075/B₄C composites, it has been apparent that mechanical properties can be further improved. If the agglomeration problem is successfully solved, the improvement in mechanical properties can even reach to higher values.

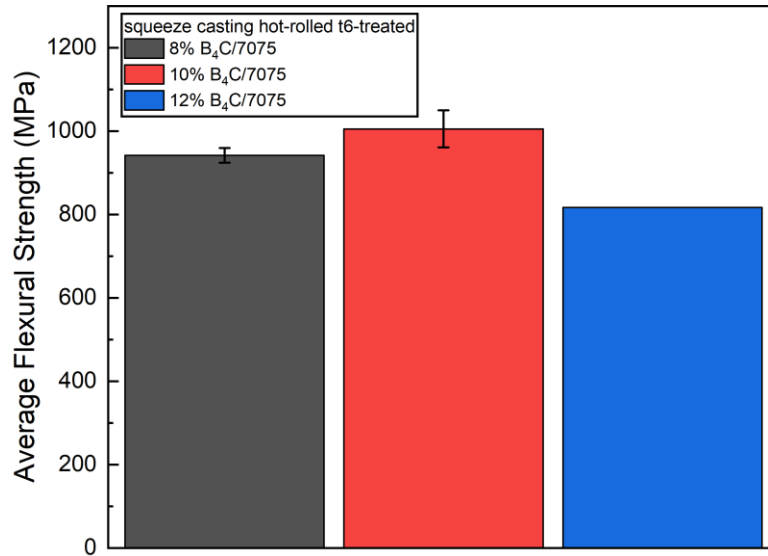


Figure 6.97 Comparison of average flexural strength values of hot-rolled and T6-treated 7075/B₄C composites

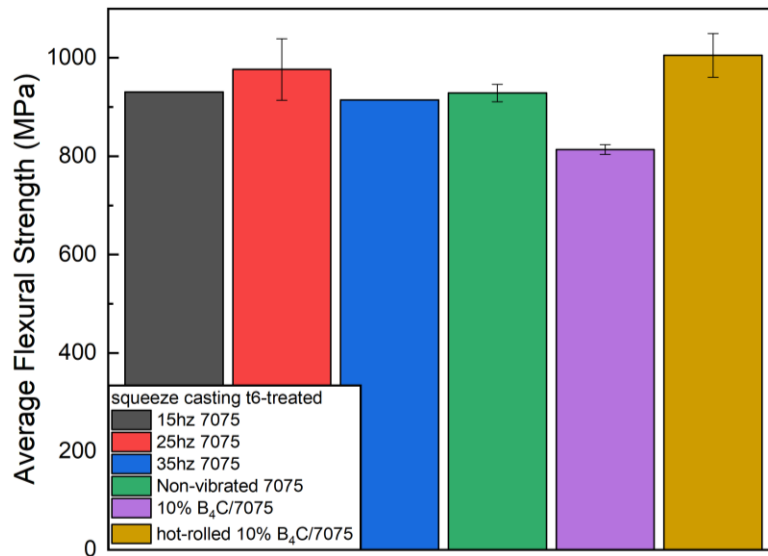


Figure 6.98 Overall comparison of average flexural strength values of T6-treated squeeze cast 7075 alloys, squeeze cast 7075/B₄C composite and hot-rolled 7075/B₄C composites

It was expected to observe decreasing of solidus and liquidus temperatures as the mechanical vibration time increases or SSM temperature decreases because of the suppression of dendritic solidification. When figure 6.3 and 6.4 is investigated, expected behavior in liquidus could not be apparent as in the case of solidus. The reason might be the lack of temperature data, since only four SSM temperature was tested, or some measurement problems of temperature data recording during sand casting experiments such as thermocouple movement, fast/slow pouring, etc.

In overall, sand casting did not result in high mechanical properties and expected behavior of optimum microstructure and mechanical properties at the temperature interval between 625-630°C. It is because of the non-homogenous distribution of the porosities in the microstructure. Without the solidification under high pressure, the effect of mechanical vibration during semi-solid processing could not be seen, i.e. fine globular grains, low porosity amount, high mechanical properties. Therefore, stress at fracture of sand cast 7075 alloys were below 300 MPa, even below the yield strength.

The best globular grain microstructure was observed at 635°C SSM temperature but there was a temperature drop of 5-6°C during the transfer of the slurry. Therefore, actual optimum SSM temperature values (<630°C) were consistent with thermal analysis results. It has been shown that mechanical vibration at frequency range of 15-35 Hz. successfully break down the dendrite arms and transformed the microstructure into globular grains (see in figure 6.16 and 6.22) but increasing frequency in this range did not show significant improvement in the microstructure and the mechanical properties. In order to complete understanding of the effect of vibration frequency wider range of frequency should be investigated.

Below 630°C SSM temperature, because of the sudden increase in solid fraction, the dendritic solidification was favored during the transfer of the slurry. Therefore, dendrite formation was observed at 625°C SSM temperature. Samples produced at this temperature had dendritic regions in the microstructure with high porosity content (see in figure 6.18 and 6.21) and the mechanical properties of them were also weaker.

CHAPTER 7

CONCLUSIONS

Thermal analysis results revealed that by decreasing SSM temperature liquidus but more apparently solidus temperature was lowered too. The decrease in solidus/liquidus temperature was considered to have beneficial effect on final globular microstructure and high mechanical properties. Optimum solid fraction and solidus/liquidus temperature was obtained under 25 Hz frequency at the temperature in between 630-625°C.

Squeeze casting experiment results showed that under 25 Hz frequency at 635°C SSM temperature gives optimum globular microstructure with highest mechanical properties. Lowering SSM temperature resulted in formation of dendrites having secondary arms which deteriorates the microstructure and the mechanical properties. There is a temperature drop during the transfer of the slurry (measured as 5-6°C) so the exact SSM temperature is less than determined ones which is consistent with thermal analysis results.

The smallest grain size of 40 μm and lowest porosity content of 1% were observed in the microstructure of rheocast alloy produced at 635°C SSM temperature. SEM and XRD results showed that the most important tiny precipitate MgZn_2 were hardly observed in XRD peaks of squeeze cast and heat treated 7075 alloys, for example at the diffraction angle of 38.62° and 45.16° of 7075 alloy produced at 15 Hz vibration frequency at 635°C SSM temperature.

Mechanical test results showed that highest UTS and hardness were obtained from the rheocast alloy produced at 635°C SSM temperature and 25 Hz frequency. Maximum hardness reached was 150 HB and maximum UTS was 483 MPa. It was apparent that by applying vibration UTS of 7075 alloy was increased about 50 MPa for T6 heat

treated samples. Similarly, flexural strength of rheocast samples produced at 635°C SSM temperature under 25 Hz frequency were the highest, the maximum flexural strength was 1020 MPa.

Addition of B₄C particles resulted in finer grain size of minimum 20 μm and improvement in the hardness (maximum 180 HB) but the flexural strength was reduced to lower values because of the main problem of agglomeration. After post treatment of hot-rolling, agglomeration problem was more or less solved and further improvement in the flexural strength of 7075 alloy was observed. The highest flexural strength for 7075/10wt.%B₄C composite was 1036 MPa. 10wt.% B₄C addition resulted in the best microstructure and mechanical properties which is similar to a squeeze casting study of 7075/SiC composites by Sencer et al. [54]

The complete globular microstructure with fine grains, homogenously distributed tiny precipitates and low porosity were achieved for the semi-solid squeeze casting of 7075 alloys developed in this work. The best microstructure and mechanical properties were obtained at 635°C SSM temperature and 25Hz vibration frequency which were the optimum processing parameters.

REFERENCES

- [1] Bauccio, M. (1994). *ASM engineered materials reference book*. ASM International.
- [2] Ivanchev, L. (2005). Near Net Shape Forming Using Semi - Solid Metal Forming.
- [3] Flemings, M. C. (1974). Solidification processing. *Metallurgical Transactions*.
<https://doi.org/10.1007/BF02643923>
- [4] Brody, H. D., & Flemings, M. C. (1966). Solute redistribution in dendritic solidification. *Transactions of the Metallurgical Society of AIME*.
<https://doi.org/10.1016/j.pain.2005.02.027>
- [5] Flemings, M. C. (1991). Behavior of metal alloys in the semisolid state. *Metallurgical Transactions B*. <https://doi.org/10.1007/BF02651227>
- [6] S.A. Metz and M.C. Flemings: *Trans. Am. Foundry men's Soc*, 1969, vol. 77
- [7] Spencer, D. B. (1971). *Ph. D Thesis*. Massachusetts Institute of Technology.
- [8] Rosenberg R. A. , Flemings M. C., T. H. F. (1960). Nonferrous binary alloys hot tearing. *AFS Trans.*, 28.
- [9] Richards R.S., R. W. (1956). The influence of vibration on the solidification of an aluminum alloy. *ASM-Trans* 48:885-901, 46.
- [10] Fan, Z. (2002). Semisolid metal processing. *International Materials Reviews*.
<https://doi.org/10.1179/095066001225001076>
- [11] Midson, S. P., & Jackson, A. (2006). A Comparison of Thixocasting and Rheocasting. In *World Foundry Congress*.
- [12] Wannasin, J., Janudom, S., Rattanochaikul, T., Canyook, R., Burapa, R., Chucheep, T., & Thanabumrunikul, S. (2010). Research and development of gas induced semi-solid process for industrial applications. *Transactions of*

Nonferrous Metals Society of China (English Edition).
[https://doi.org/10.1016/S1003-6326\(10\)60622-X](https://doi.org/10.1016/S1003-6326(10)60622-X)

- [13] Thanabumrungskul, S., Janudom, S., Burapa, R., Dulyapraphant, P., & Wannasin, J. (2010). Industrial development of gas induced semi-solid process. *Transactions of Nonferrous Metals Society of China (English Edition)*.
[https://doi.org/10.1016/S1003-6326\(10\)60623-1](https://doi.org/10.1016/S1003-6326(10)60623-1)
- [14] Yurko, J. A., Martinez, R. A., & Flemings, M. C. (2003). Commercial development of the Semi-Solid Rheocasting (SSR) process. *Metallurgical Science and Technology*, 21(1), 39.
- [15] Staley, J. T., & Tiryakioglu, M. (2001). The use of TTP curves and quench factor analysis for property prediction in aluminum alloys. *Advances in the Metallurgy of aluminum Alloys, Proceedings from Materials Solutions Conference, the James T. Staley Honorary Symposium on aluminum Alloys, Indianapolis, IN, United States, Nov. 5-8, 2001*. <https://doi.org/10.1049/iet-cta.2015.0024>
- [16] Astm Norma B 209-07. (2007). Standard Specification for aluminum and aluminum-Alloy Sheet and Plate (metric). *Standards*.
<https://doi.org/10.1520/B0209-10.2>
- [17] Wanhill, R. J. H., Prasad, N. E., & Gokhale, A. A. (2013). aluminum-*Lithium Alloys: Processing, Properties, and Applications*. aluminum-*Lithium Alloys: Processing, Properties, and Applications*. <https://doi.org/10.1016/C2012-0-00394-8>
- [18] ASM International Handbook, V. 2. (1990). ASM Handbook Vol. 2: Properties and selection: Nonferrous alloys and special-purpose materials. *ASM Metals Handbook*. [https://doi.org/10.1016/S0026-0576\(03\)90166-8](https://doi.org/10.1016/S0026-0576(03)90166-8)
- [19] Rambabu, P., Prasad, N. E., & Kutumbarao, V. V. (2017). Aerospace Materials and Material Technologies, Indian Institute of Metals Series. *Springer Science*.
<https://doi.org/10.1007/978-981-10-2143-5>

- [20] Yang, B., Mao, W., & Song, X. (2013). Microstructure characteristics and mechanical properties of rheocasting 7075 aluminum alloy. *China Foundry*. <https://doi.org/10.1103/PhysRevB.75.041303>
- [21] Curle, U. A. (2010). Semi-solid near-net shape rheocasting of heat treatable wrought aluminum alloys. *Transactions of Nonferrous Metals Society of China (English Edition)*. [https://doi.org/10.1016/S1003-6326\(09\)60364-2](https://doi.org/10.1016/S1003-6326(09)60364-2)
- [22] Fang, H. C., Chao, H., & Chen, K. H. (2014). Effect of Zr, Er and Cr additions on microstructures and properties of Al-Zn-Mg-Cu alloys. *Materials Science and Engineering A*. <https://doi.org/10.1016/j.msea.2014.05.021>
- [23] Du, Z. M., Liu, J., Chen, G., Qin, J., & Xie, S. S. (2010). Investigation of semi-solid aluminum alloy filling-plastic flowing in thixoforging. *Transactions of Nonferrous Metals Society of China (English Edition)*. [https://doi.org/10.1016/S1003-6326\(10\)60602-4](https://doi.org/10.1016/S1003-6326(10)60602-4)
- [24] Ghomashchi M.R., & Vikhrov A. (2000). Squeeze casting: an overview. *Journal of Materials Processing Technology*. <https://doi.org/10.1542/neo.6-1-e32>
- [25] Denise, B., Alberto, B., Girolamo, C., Elisa, T. M., Fabrizio, Q., & Loredana, S. (1994). Squeeze Casting of Al-Si Alloys. <https://doi.org/10.5772/32591>
- [26] Bonollo, F., Gramegna, N., & Timelli, G. (2015). High-pressure die-casting: Contradictions and challenges. *JOM*. <https://doi.org/10.1007/s11837-015-1333>
- [27] Podprocká, R., Malik, J., & Bolibruchová, D. (2015). Defects in high pressure die casting process. *Manufacturing Technology*.
- [28] Romuald Laqua, A., & V., A. (2012). Simulation of High Pressure Die Casting (HPDC) via STAR-Cast.
- [29] How Do Pressure Die Casting and Gravity Diecasting Differ? (n.d.). Retrieved from <https://www.lupton-place.co.uk/how-do-pressure-diecasting-and-gravity-diecasting-differ/>

- [30] Hot Chamber Vs. Cold Chamber Die Casting. (n.d.). Retrieved from <https://diecasting.com/blog/2016/03/23/hot-chamber-vs-cold-chamber-die-casting/>
- [31] Lumley, R. N. (2010). Progress on the heat treatment of high pressure die castings. In *Fundamentals of Aluminium Metallurgy: Production, Processing and Applications*. <https://doi.org/10.1533/9780857090256.1.262>
- [32] aluminium cylinder head automotive square silver. (n.d.). Retrieved from <http://www.buykorea.org/main/BKBMMA010M.html>
- [33] Squeeze Casting Parts. (n.d.). Retrieved from <https://www.globalsources.com/>
- [34] Callister, W. D. . J., & Rethwisch, D. G. (2007). *Materials Science and Engineering: An Introduction Seventh Edition*. Wiley (8th ed.). [https://doi.org/10.1016/0025-5416\(87\)90343-0](https://doi.org/10.1016/0025-5416(87)90343-0)
- [35] Asm International. (2001). ASM Handbook Vol.4 Heat Treating. *Technology*. [https://doi.org/10.1016/S0026-0576\(03\)90166-8](https://doi.org/10.1016/S0026-0576(03)90166-8)
- [36] Atkinson, H. V., Burke, K., & Vaneetveld, G. (2008). Recrystallisation in the Semi-Solid State in 7075 Aluminium Alloy. *International Journal of Material Forming*. <https://doi.org/10.1007/s12289-008-0220-z>
- [37] Backerud, L., Chai, G., & Tamminen, J. (1990). *Solidification Characteristics of aluminum Alloys. Vol. 2. Foundry Alloys. AFS/SkanAluminum*. <https://doi.org/10.1007/s13398-014-0173-7.2>
- [38] Tayfun Durmaz. (2017). *DEVELOPMENT OF HIGH STRENGTH aluminum MATRIX COMPOSITE BACKING PLATES FOR BALLISTIC ARMOR*. (Middle East Technical University).
- [39] Aoba, T., Kobayashi, M., & Miura, H. (2017). Effects of aging on mechanical properties and microstructure of multi-directionally forged 7075 aluminum alloy. *Materials Science and Engineering A*.

<https://doi.org/10.1016/j.msea.2017.06.017>

- [40] Kumar, P. V., Reddy, G. M., & Rao, K. S. (2015). Microstructure, mechanical and corrosion behavior of high strength AA7075 aluminium alloy friction stir welds – Effect of post weld heat treatment. *Defence Technology*. <https://doi.org/10.1016/j.dt.2015.04.003>
- [41] BOLOURI, A., SHAHMIRI, M., & CHESHMEH, E. N. H. (2010). Microstructural evolution during semisolid state strain induced melt activation process of aluminum 7075 alloy. *Transactions of Nonferrous Metals Society of China (English Edition)*. [https://doi.org/10.1016/S1003-6326\(09\)60355-1](https://doi.org/10.1016/S1003-6326(09)60355-1)
- [42] Curle, U. A., & Govender, G. (2010). Semi-solid rheocasting of grain refined aluminum alloy 7075. *Transactions of Nonferrous Metals Society of China (English Edition)*. [https://doi.org/10.1016/S1003-6326\(10\)60590-0](https://doi.org/10.1016/S1003-6326(10)60590-0)
- [43] Mahathaninwong, N., Plookphol, T., Wannasin, J., & Wisutmethangoon, S. (2012). T6 heat treatment of rheocasting 7075 Al alloy. *Materials Science and Engineering A*. <https://doi.org/10.1016/j.msea.2011.10.068>
- [44] Sim, J. G., Choi, B. H., Jang, Y. S., Kim, J. M., & Hong, C. P. (2010). Development of a Nucleation-Accelerated-Semisolid-Slurry-Making Method and its Application to Rheo-diecasting of ADC10 Alloy. *ISIJ International*, 50(8), 1165–1174. <https://doi.org/10.2355/isijinternational.50.1165>
- [45] Vijayan, V., & Prabhu, K. N. (2015). Assessment of Latent Heat and Solid Fraction of Al-22Si Alloy Using Newtonian and Fourier Analysis Techniques. *Materials Science Forum*, 830–831, 321–324. <https://doi.org/10.4028/www.scientific.net/MSF.830-831.321>
- [46] EMADI, D., V. WHITING, L., DJURDJEVIC, M., T. KIERKUS, W., & SOKOLOWSKI, J. (2004). Comparison of Newtonian and Fourier thermal analysis techniques for calculation of latent heat and solid fraction of aluminum alloys. *Metalurgija-Journal of Metallurgy*. <https://doi.org/10.30544/379>

- [47] Güngör, A. U. (2015). *DEVELOPMENT OF CAST AND HEAT TREATED 7075 ALLOY RIFLE RECEIVER*. Middle East Technical University.
- [48] ASTM Int. (2009). Standard Test Methods for Tension Testing Wrought and Cast aluminum- and Magnesium-Alloy Products (Metric)1. *Journal of Minerals & Materials Characterization & Engineering*. <https://doi.org/10.1520/B0557M-15.2>
- [49] Principle of Optical Emission Spectrometry. (2018). Retrieved from <https://www.shimadzu.com/an/elemental/oes/oes.html>
- [50] Jiang, J., & Wang, Y. (2015). Microstructure and mechanical properties of the rheocast cylindrical part of 7075 aluminum matrix composite reinforced with nano-sized SiC particles. *Materials and Design*. <https://doi.org/10.1016/j.matdes.2015.04.040>
- [51] Curle, U. A., & Ivanchev, L. (2010). Wear of semi-solid rheocast SiCp/Al metal matrix composites. *Transactions of Nonferrous Metals Society of China (English Edition)*. [https://doi.org/10.1016/S1003-6326\(10\)60594-8](https://doi.org/10.1016/S1003-6326(10)60594-8)
- [52] Qin, Q. D., Zhao, Y. G., Liu, C., Cong, P. J., Zhou, W., & Liang, Y. H. (2006). Effect of holding temperature on semisolid microstructure of Mg2Si/Al composite. *Journal of Alloys and Compounds*. <https://doi.org/10.1016/j.jallcom.2005.08.057>
- [53] Alhawari, K. S., Omar, M. Z., Ghazali, M. J., Salleh, M. S., & Mohammed, M. N. (2013). Wear Properties of A356/Al2O3 metal matrix composites produced by semisolid processing. In *Procedia Engineering*. <https://doi.org/10.1016/j.proeng.2013.12.166>
- [54] Kalkanli A, Yilmaz S, "Synthesis and characterization of aluminum alloy 7075 reinforced with silicon carbide particulates" *MATERIALS & DESIGN* Volume: 29 Issue: 4 Pages: 775-780 Published:2008

APPENDICES

A. Thermal Analysis

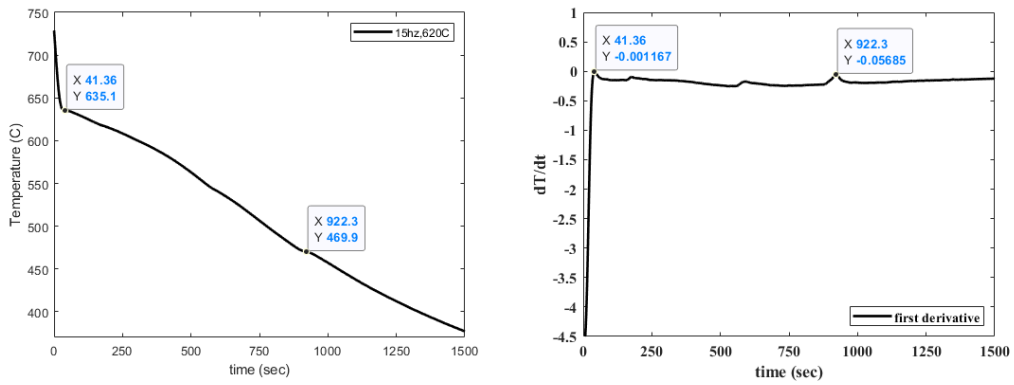


Figure A. 1 Cooling curve and its first derivative of rheocast 7075 alloy produced under 15Hz frequency at 620°C SSM temperature

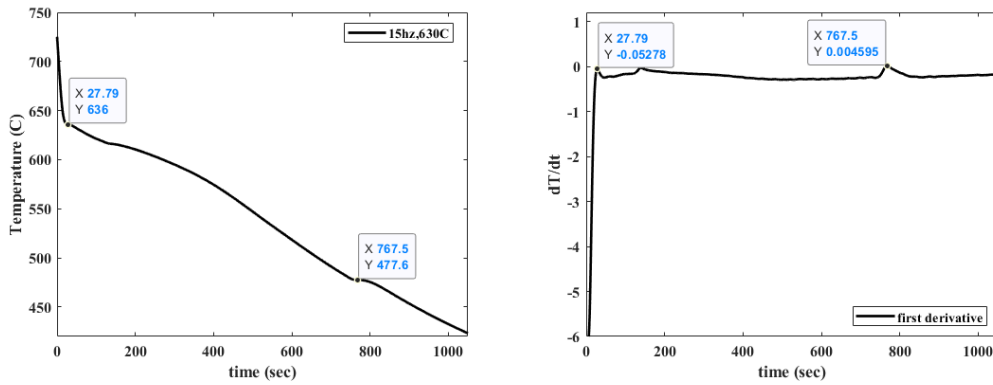


Figure A. 2 Cooling curve and its first derivative of rheocast 7075 alloy produced under 15Hz frequency at 630°C SSM temperature

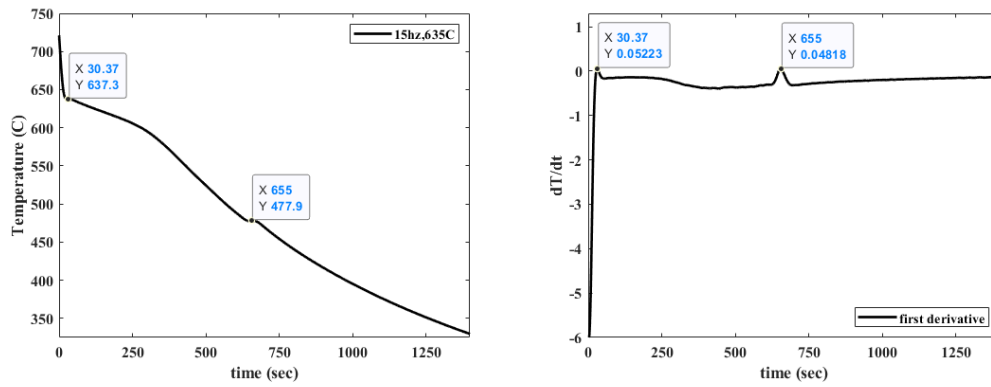


Figure A. 3 Cooling curve and its first derivative of rheocast 7075 alloy produced under 15Hz frequency at 635°C SSM temperature

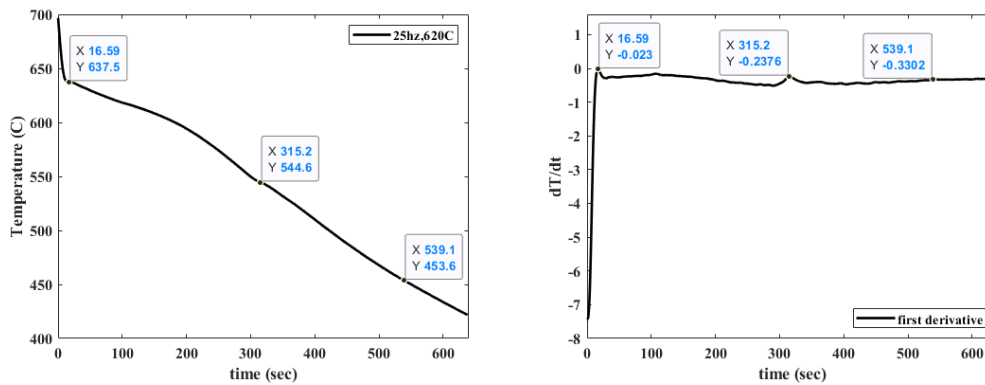


Figure A. 4 Cooling curve and its first derivative of rheocast 7075 alloy produced under 25Hz frequency at 620°C SSM temperature

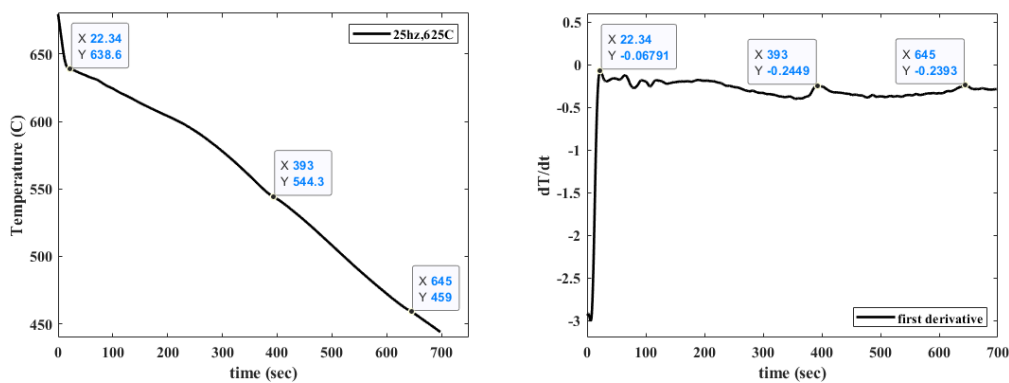


Figure A. 5 Cooling curve and its first derivative of rheocast 7075 alloy produced under 25Hz frequency at 625°C SSM temperature

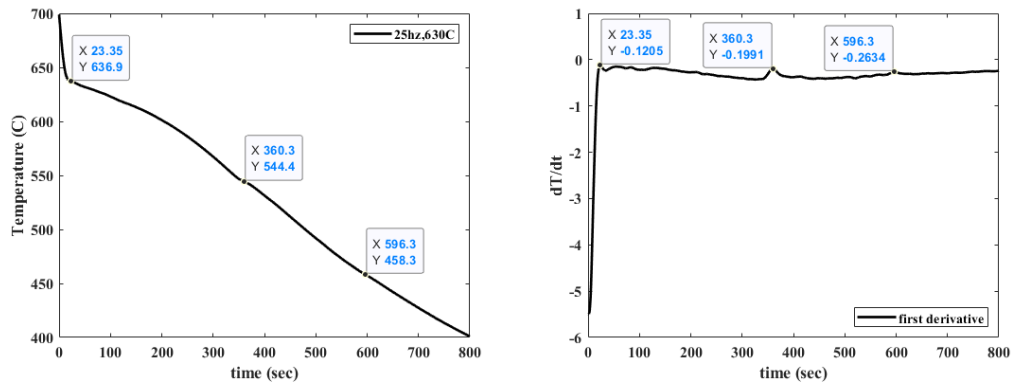


Figure A. 6 Cooling curve and its first derivative of rheocast 7075 alloy produced under 25Hz frequency at 630°C SSM temperature

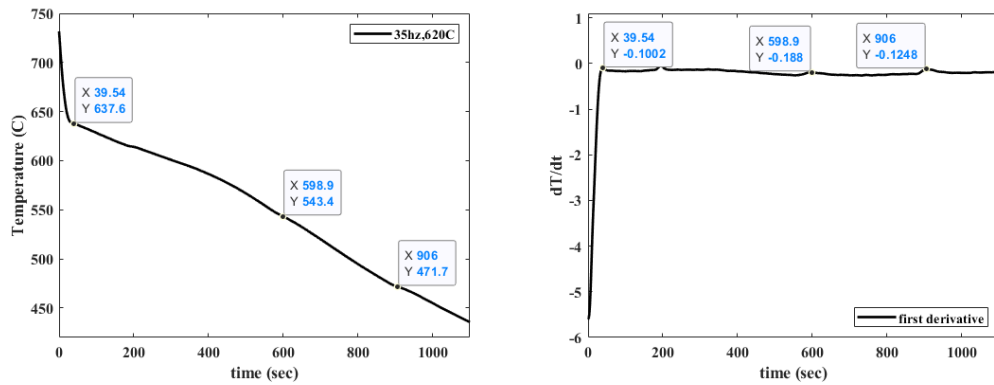


Figure A. 7 Cooling curve and its first derivative of rheocast 7075 alloy produced under 35Hz frequency at 620°C SSM temperature

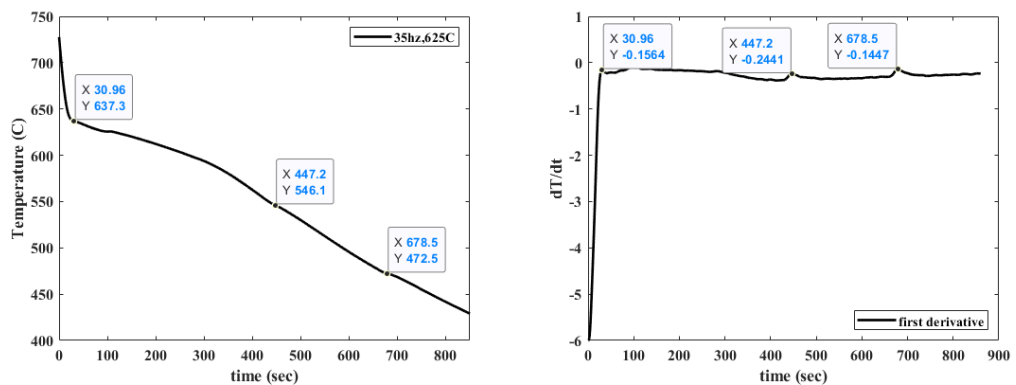


Figure A. 8 Cooling curve and its first derivative of rheocast 7075 alloy produced under 35Hz frequency at 625°C SSM temperature

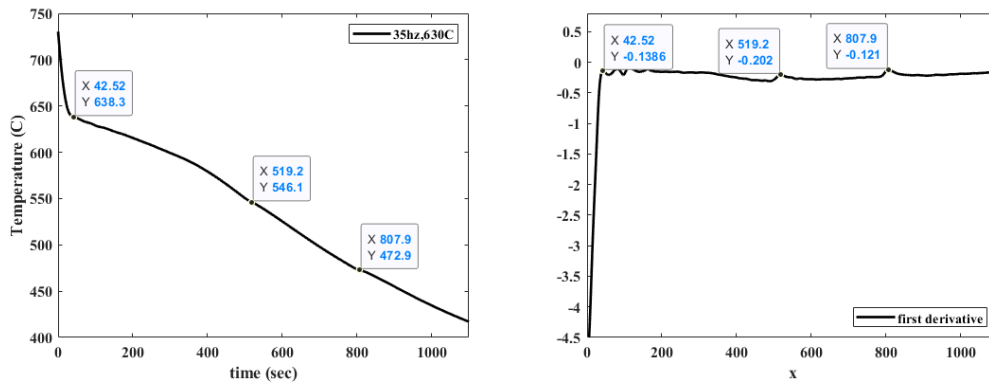


Figure A. 9 Cooling curve and its first derivative of rheocast 7075 alloy produced under 35Hz frequency at 630°C SSM temperature

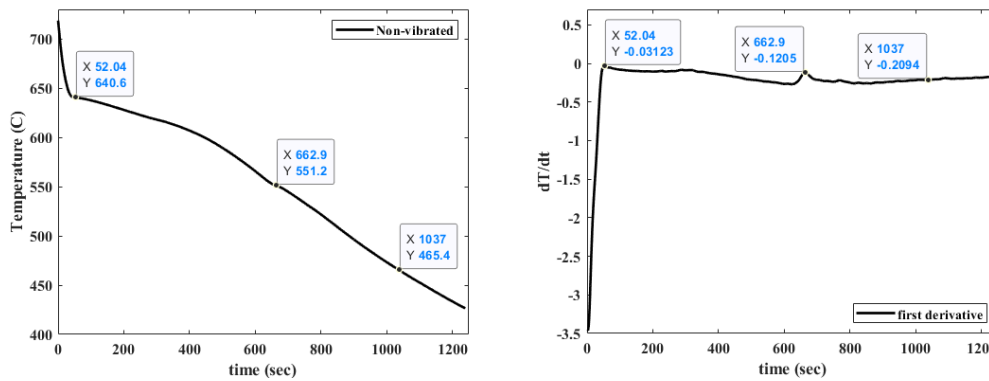


Figure A. 10 Cooling curve and its first derivative of rheocast 7075 alloy produced with no-vibration at 670°C

B. Microstructures

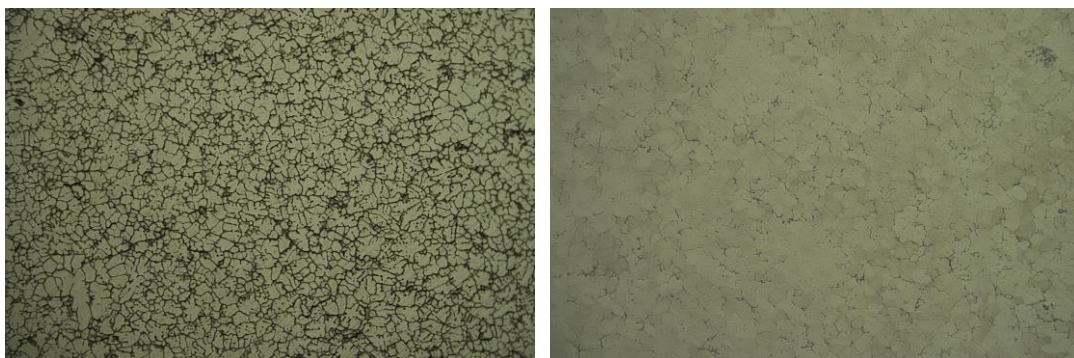


Figure B. 1 Microstructures of as-cast and T6-treated squeeze cast 7075 alloy produced under 15Hz frequency at 635°C SSM Temperature under optical microscopy

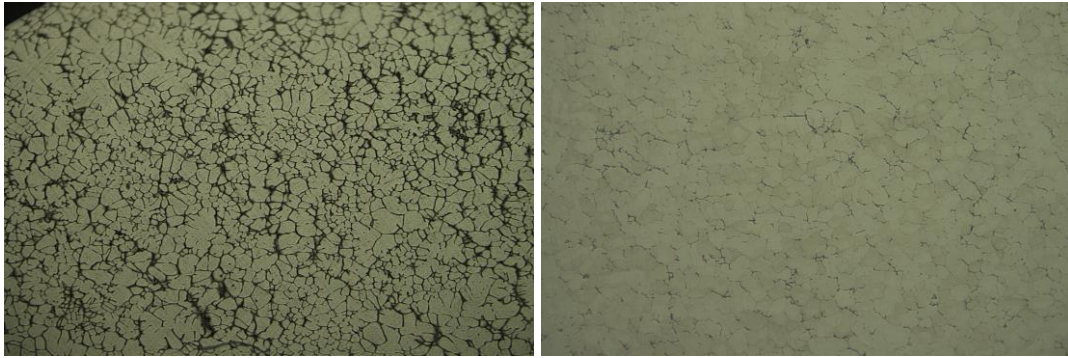


Figure B. 2 Microstructures of as-cast and T6-treated squeeze cast 7075 alloy produced under 15Hz frequency at 630°C SSM temperature under optical microscopy

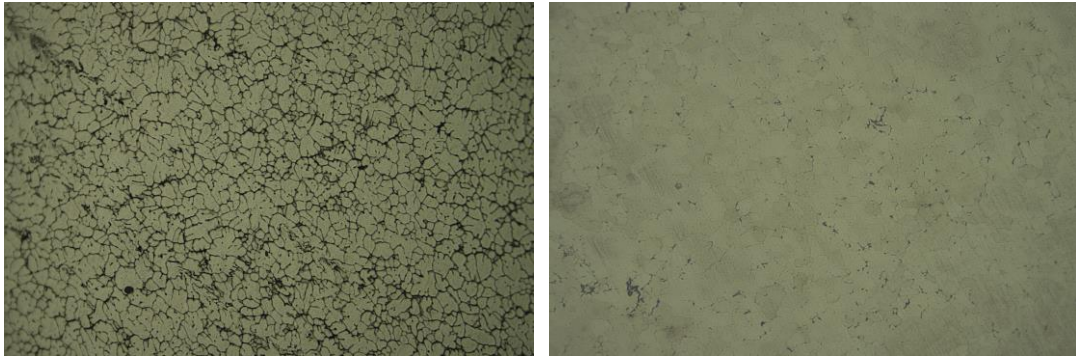


Figure B. 3 Microstructures of as-cast and T6-treated squeeze cast 7075 alloy produced under 15Hz frequency at 625°C SSM temperature under optical microscopy

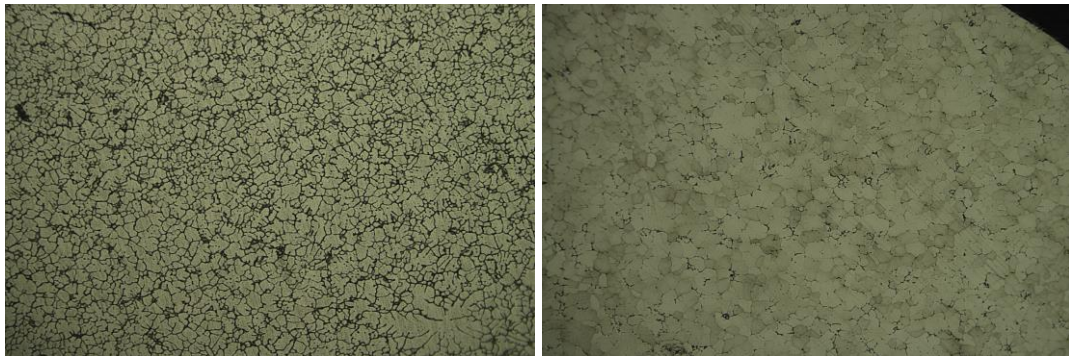


Figure B. 4 Microstructures of as-cast and T6-treated squeeze cast 7075 alloy produced under 35Hz frequency at 635°C SSM temperature under optical microscopy

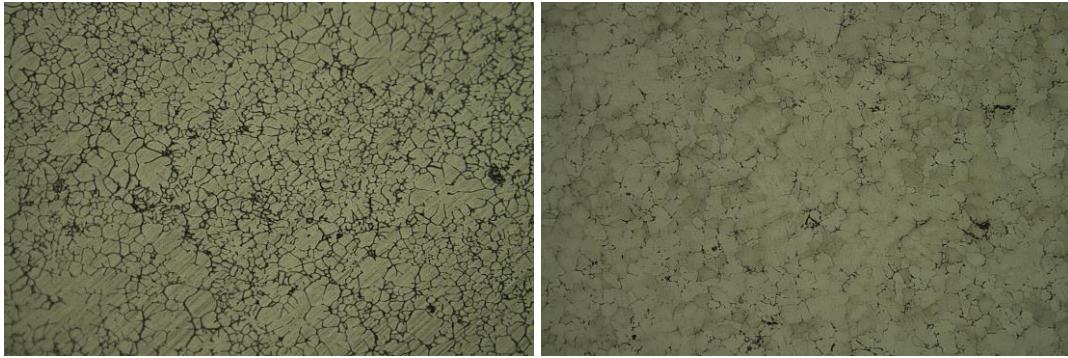


Figure B. 5 Microstructures of as-cast and T6-treated squeeze cast 7075 alloy produced under 35Hz frequency at 630°C SSM temperature under optical microscopy

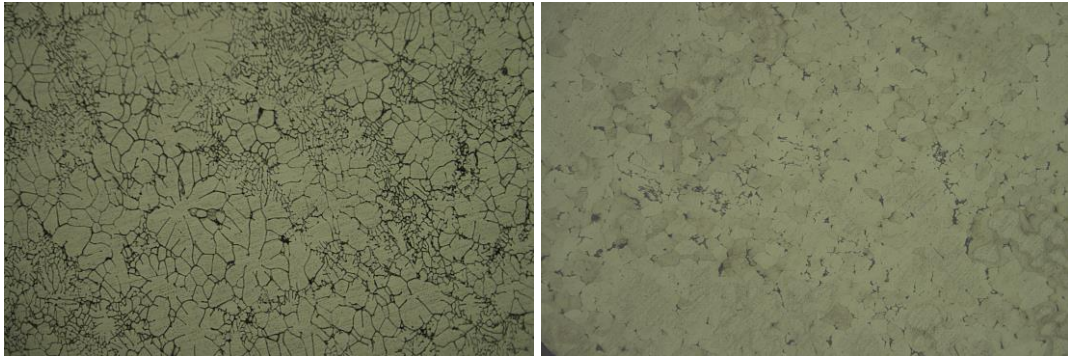


Figure B. 6 Microstructures of as-cast and T6-treated squeeze cast 7075 alloy produced under 35Hz frequency at 625°C SSM temperature under optical microscopy

C. Grain Size Measurements

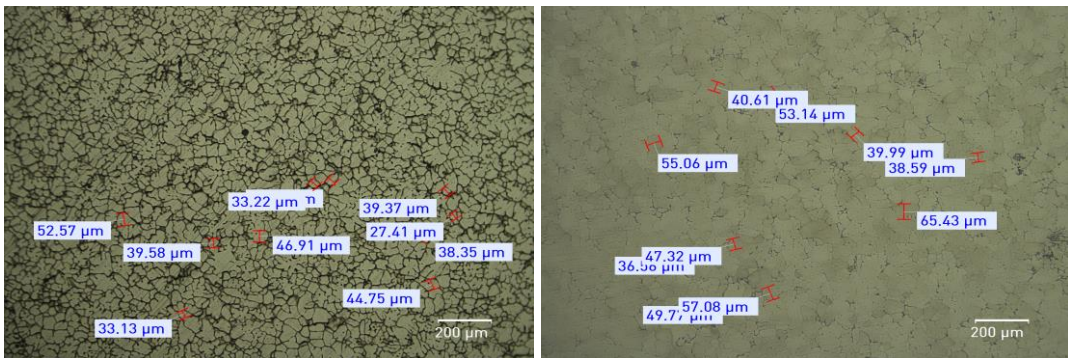


Figure C. 1 Grain size measurement of as-cast and T6-treated squeeze cast 7075 alloy produced under 15Hz frequency at 635°C SSM temperature

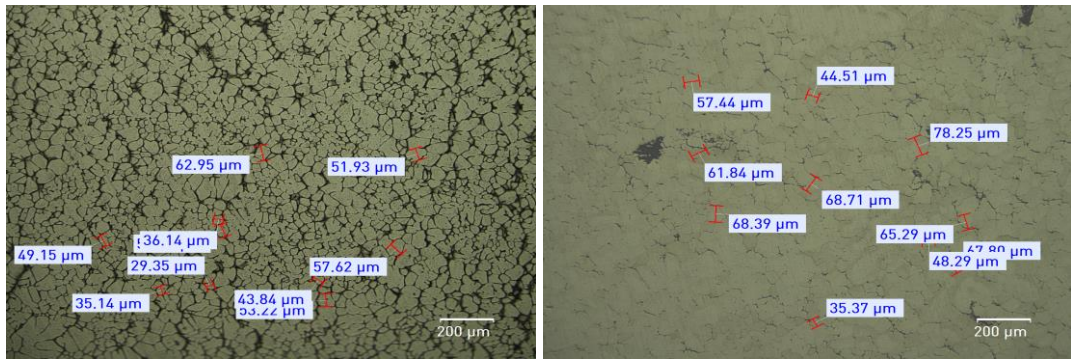


Figure C. 2 Grain size measurement of as-cast and T6-treated squeeze cast 7075 alloy produced under 15Hz frequency at 630°C SSM temperature

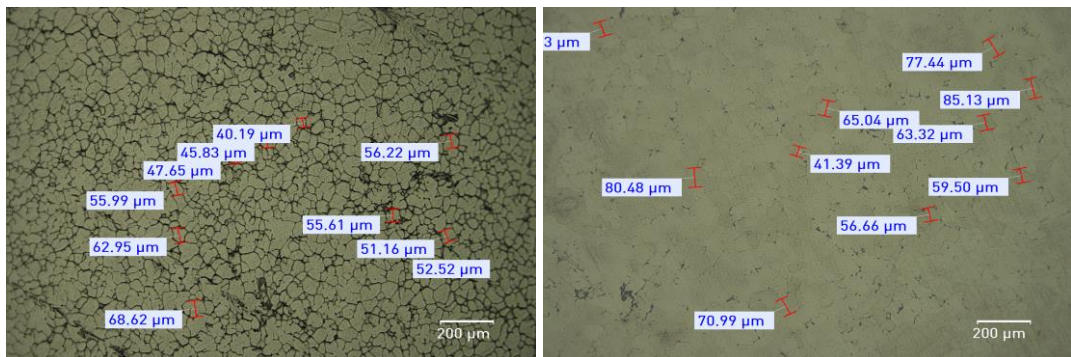


Figure C. 3 Grain size measurement of as-cast and T6-treated squeeze cast 7075 alloy produced under 15Hz frequency at 625°C SSM temperature

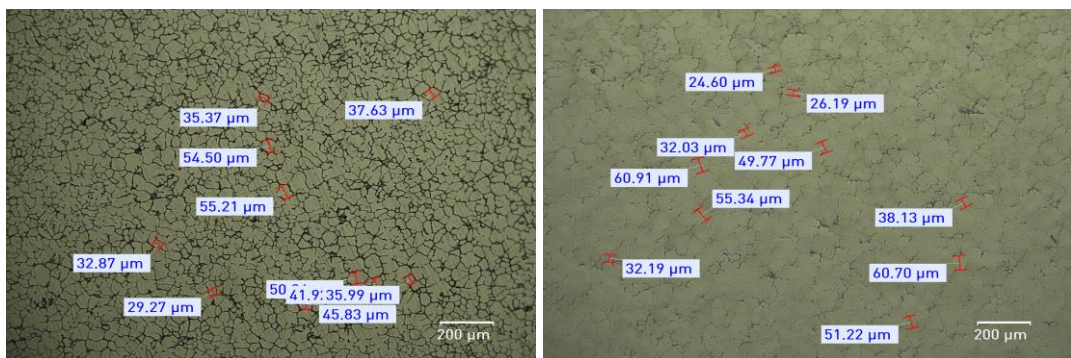


Figure C. 4 Grain size measurement of as-cast and T6-treated squeeze cast 7075 alloy produced under 25Hz frequency at 635°C SSM temperature

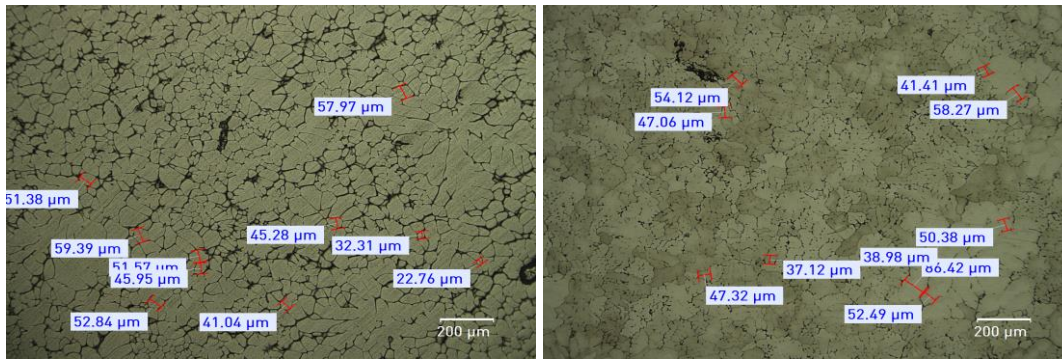


Figure C. 5 Grain size measurement of as-cast and T6-treated squeeze cast 7075 alloy produced under 25Hz frequency at 630°C SSM temperature

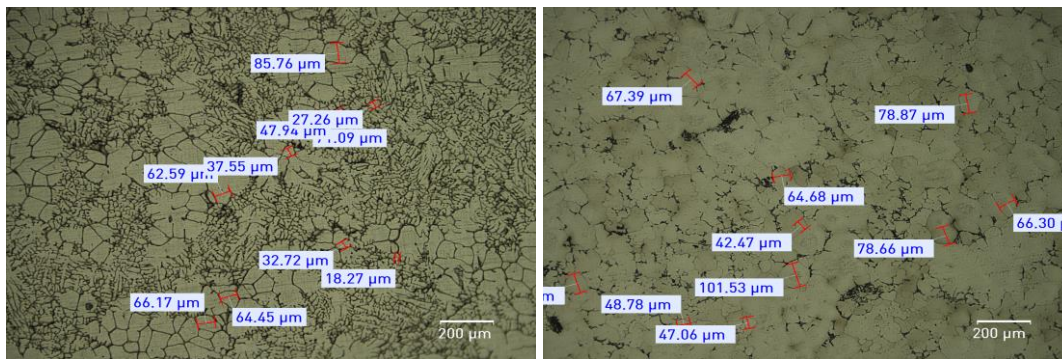


Figure C. 6 Grain size measurement of as-cast and T6-treated squeeze cast 7075 alloy produced under 25Hz frequency at 625°C SSM temperature

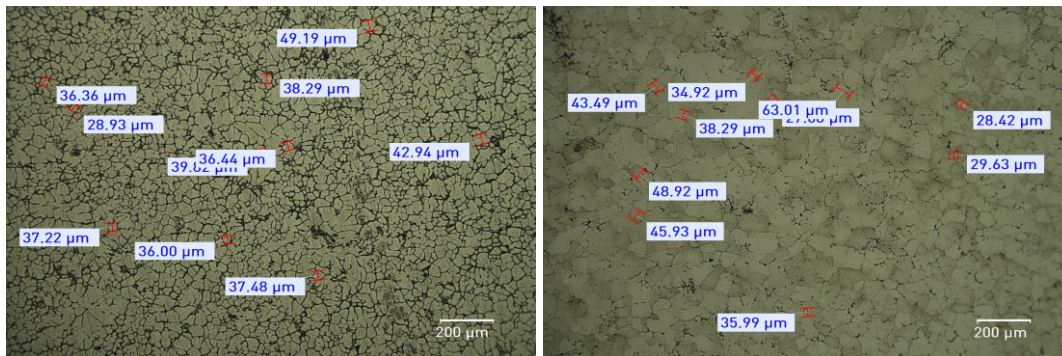


Figure C. 7 Grain size measurement of as-cast and T6-treated squeeze cast 7075 alloy produced under 35Hz frequency at 635°C SSM temperature

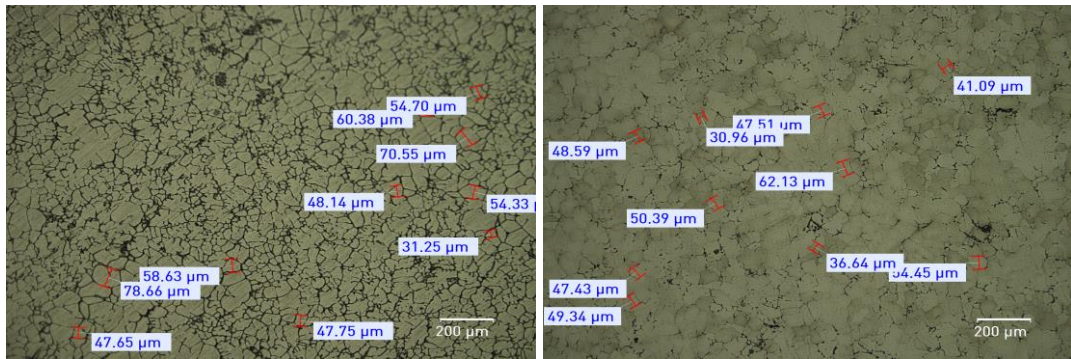


Figure C. 8 Grain size measurement of as-cast and T6-treated squeeze cast 7075 alloy produced under 35Hz frequency at 630°C SSM temperature

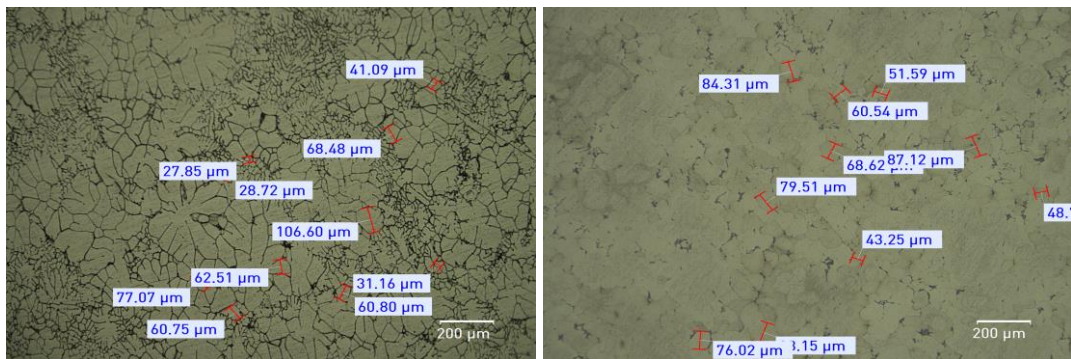


Figure C. 9 Grain size measurement of as-cast and T6-treated squeeze cast 7075 alloy produced under 35Hz frequency at 625°C SSM temperature

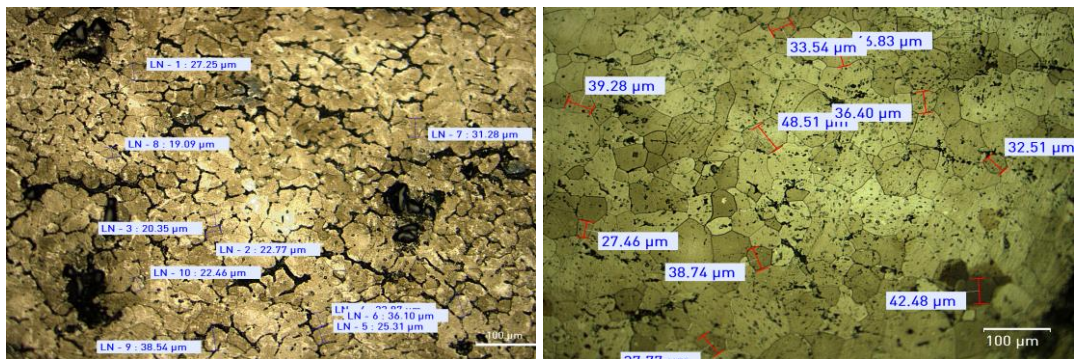


Figure C. 10 Grain size measurement of T6-treated squeeze cast (left) and hot-rolled (right) 8wt.% 7075/B₄C composite

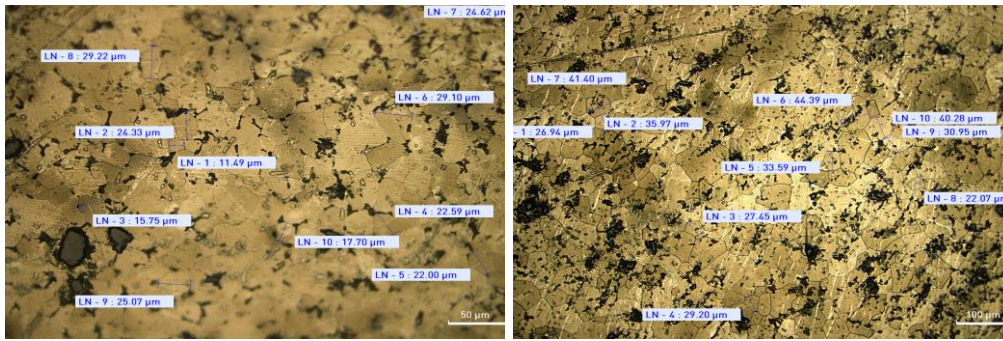


Figure C. 11 Grain size measurement of T6-treated squeeze cast (left) and hot-rolled (right) 10wt.% 7075/B₄C composite

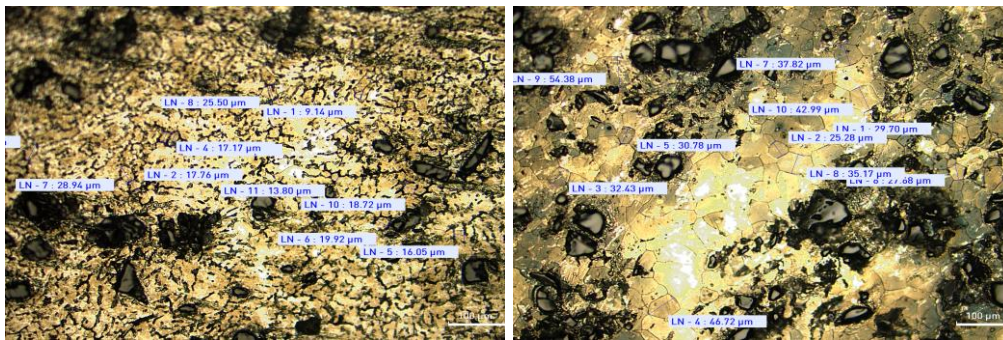


Figure C. 12 Grain size measurement of T6-treated squeeze cast (left) and hot-rolled (right) 12wt.% 7075/B₄C composite

D. XRD Results

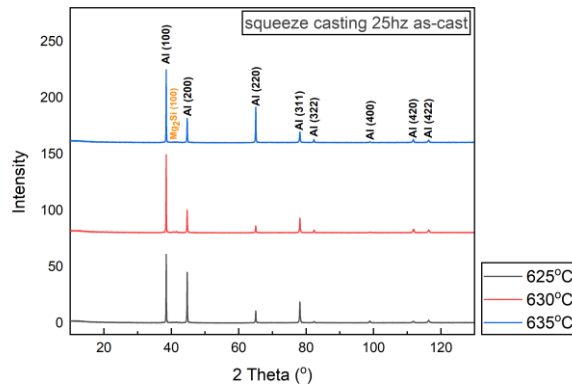


Figure D. 1 XRD patterns of squeeze cast 7075 alloys produced under 25Hz vibration frequency

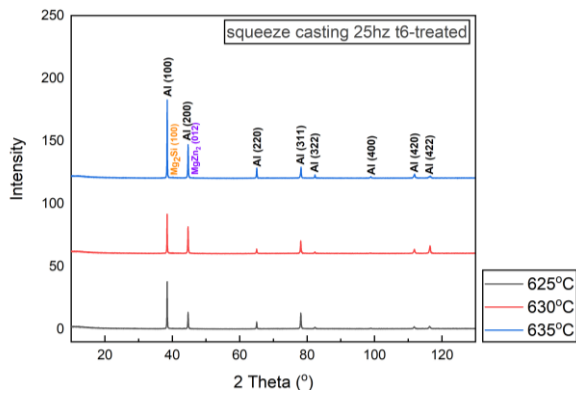


Figure D. 2 XRD patterns of T6-treated squeeze cast 7075 alloys produced under 25Hz vibration frequency

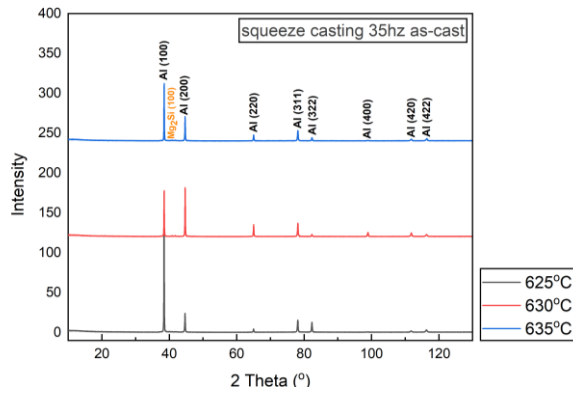


Figure D. 3 XRD patterns of squeeze cast 7075 alloys under 35Hz vibration frequency

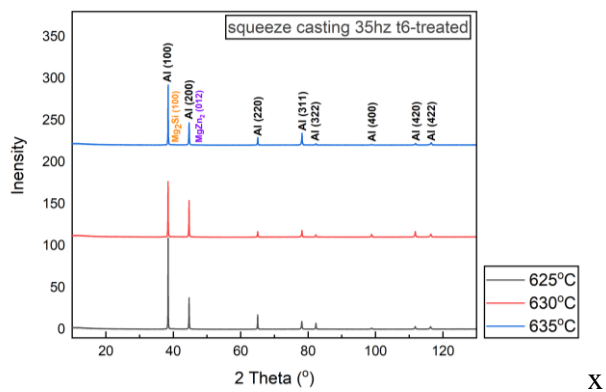


Figure D. 4 XRD patterns of T6-treated squeeze cast 7075 alloys produced under 35Hz vibration frequency

E. Tensile Test Results

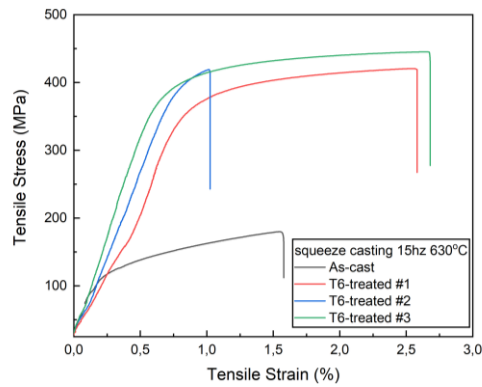


Figure E. 1 Tensile Stress vs. tensile strain curves for as-cast and T6 treated squeeze cast 7075 alloy produced under 15Hz at 630°C SSM temperature

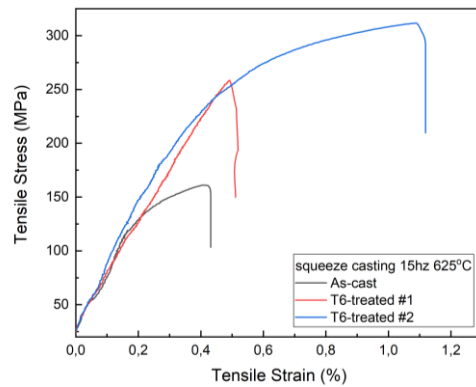


Figure E. 2 Tensile Stress vs. tensile strain curves for as-cast and T6 treated squeeze cast 7075 alloy produced under 15Hz at 625°C SSM temperature

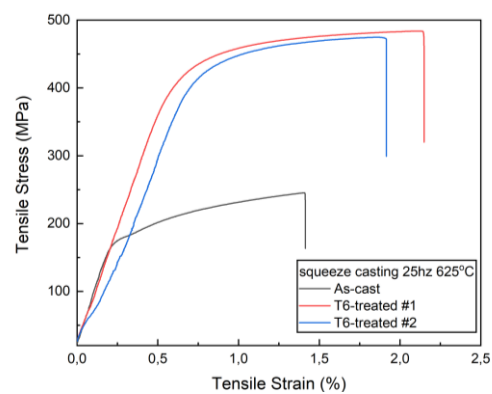


Figure E. 3 Tensile Stress vs. tensile strain curves for as-cast and T6 treated squeeze cast 7075 alloy produced under 25Hz at 635°C SSM temperature

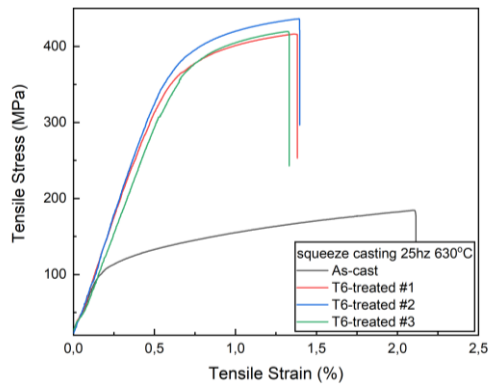


Figure E. 4 Tensile Stress vs. tensile strain curves for as-cast and T6 treated squeeze cast 7075 alloy produced under 25Hz at 630°C SSM temperature

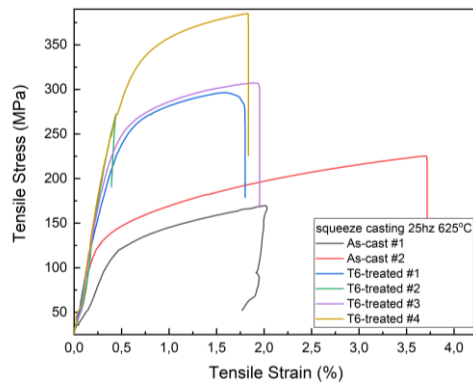


Figure E. 5 Tensile Stress vs. tensile strain curves for as-cast and T6 treated squeeze cast 7075 alloy produced under 25Hz at 625°C SSM temperature

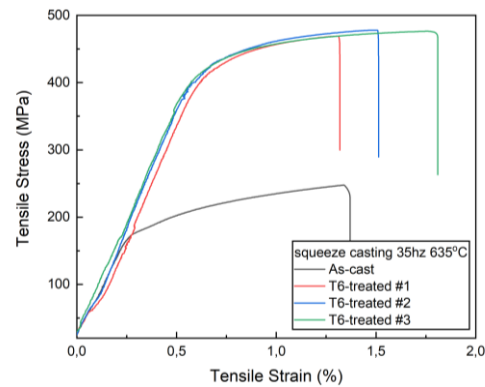


Figure E. 6 Tensile Stress vs. tensile strain curves for as-cast and T6 treated squeeze cast 7075 alloy produced under 35Hz at 635°C SSM temperature

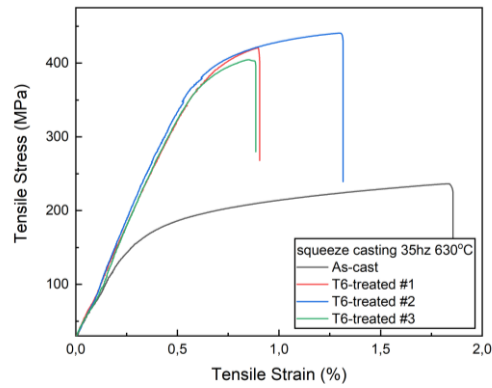


Figure E. 7 Tensile Stress vs. tensile strain curves for as-cast and T6 treated squeeze cast 7075 alloy produced under 35Hz at 630°C SSM temperature

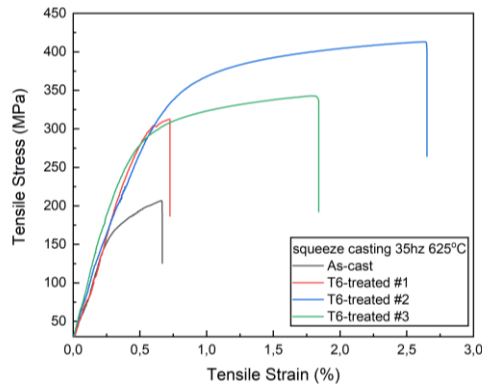


Figure E. 8 Tensile Stress vs. tensile strain curves for as-cast and T6 treated squeeze cast 7075 alloy produced under 35Hz at 625°C SSM temperature

F. 3- Point Bending Test Results

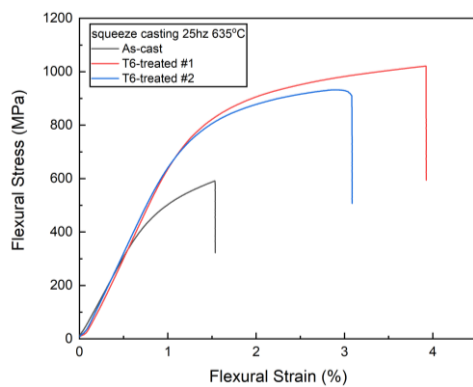


Figure F. 1 Flexure stress vs. flexure strain curves for as-cast and T6-treated squeeze cast 7075 alloy produced under 25Hz at 635°C SSM temperature

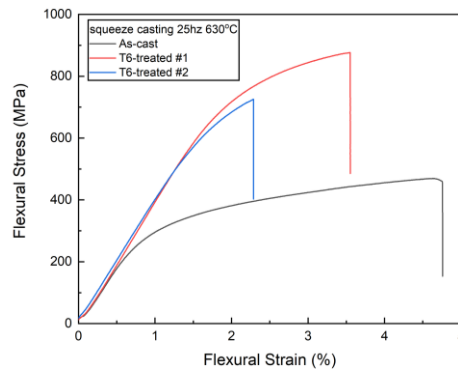


Figure F. 2 Flexure stress vs. flexure strain curves for as-cast and T6-treated squeeze cast 7075 alloy produced under 25Hz at 630°C SSM temperature

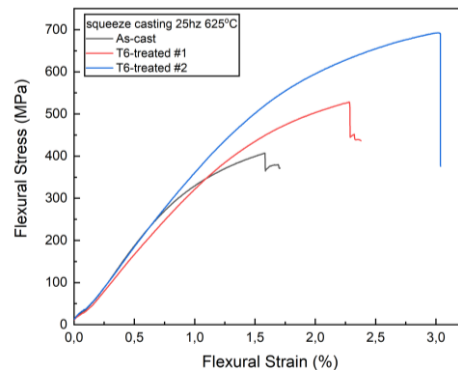


Figure F. 3 Flexure stress vs. flexure strain curves for as-cast and T6-treated squeeze cast 7075 alloy produced under 25Hz at 625°C SSM temperature

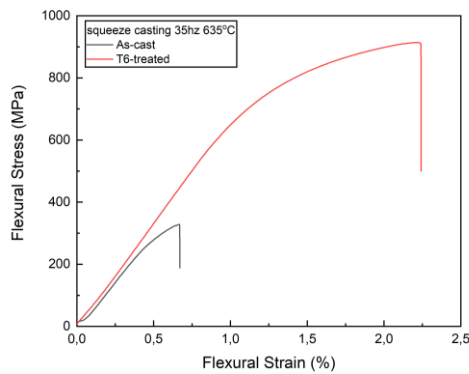


Figure F. 4 Flexure stress vs. flexure strain curves for as-cast and T6-treated squeeze cast 7075 alloy produced under 35Hz at 635°C SSM temperature